Field Computation by Moment Methods

ROGER F. HARRINGTON

IEEE

IEEE PRESS Series on Electromagnetic Waves

The IEEE PRESS Series on Electromagnetic Waves consists of new titles as well as reprints and revisions of recognized classics that maintain long-term archival significance in electromagnetic waves and applications.

Series Books Published

Collin, R. E., *Field Theory of Guided Waves*, 2d. rev. ed., 1991
Tai, C. T., *Generalized Vector and Dyadic Analysis: Applied Mathematics in Field Theory*, 1991
Elliott, R. S., *Electromagnetics: History, Theory, and Applications*, 1993
Harrington, R. F., *Field Computation by Moment Methods*, 1993

Future Series Titles

Tai, C. T., *Dyadic Green's Function in Electromagnetic Theory*
Dudley, D. G., *Mathematical Foundations of Electromagnetic Theory*

Field Computation by Moment Methods

Roger F. Harrington
Syracuse University

IEEE PRESS

IEEE PRESS Series on Electromagnetic Waves
Donald G. Dudley, Series Editor

IEEE Antennas and Propagation Society, *Sponsor*

The Institute of Electrical and Electronics Engineers, Inc., New York

445 Hoes Lane, PO Box 1331
Piscataway, NJ 08855-1331

This book may be purchased at a discount from the publisher when ordered in bulk quantities. For more information contact:

IEEE PRESS Marketing
Attn: Special Sales
PO Box 1331
445 Hoes Lane
Piscataway, NJ 08855-1331
Fax: (908) 981-8062

This is the IEEE edition of a book originally published by Macmillan Publishing Company, and subsequently kept in print by Krieger Publishing Company under the title *Field Computation by Moment Methods*.

Printed in the United States of America
10 9 8 7 6 5 4 3 2 1

ISBN 0-7803-1014-4
IEEE Order Number: PC0363-2

Library of Congress-Cataloging-in-Publication Data
Harrington, Roger F.
Field computation by moment methods / by Roger F. Harrington.
p. cm.
"IEEE Antennas and Propagation Society, sponsor."
Originally published: Malabar, Fla. : R.E. Krieger, 1968.
Includes bibliographical references and index.
ISBN 0-7803-1014-4
1. Physics—Data processing. 2. Electromagnetic theory—Data processing. 3. Unified field theory—Data processing. I. IEEE Antennas and Propagation Society. II. Title.
QC52.H37 1993
530.1'41'0285—dc20 93-7060
CIP

Contents

CHAPTER 4

CHAPTER 5

CHAPTER 6

CHAPTER 7

CHAPTER 8

CHAPTER 9

CHAPTER 10

Preface

Before the advent of high speed computers, it was advantageous to expend considerable effort to manipulate solutions analytically into a form which minimized the subsequent computational effort. It is now often more convenient to use methods which are analytically simple, but require large amounts of computation. Furthermore, many problems of practical interest can be solved only by the use of such methods. Because of the fantastic speed and storage capabilities of modern computers, almost any problem of linear analysis can be solved to some degree of accuracy. In fact, computer programs can be written for entire classes of problems, as, for example, wires of arbitrary shape with arbitrary excitation and loading (Chapter 4).

This monograph attempts to present a unified approach to the solution of field problems using computers. The methods are general, applying to fields of any type, but the examples are taken from electromagnetic theory. The material is introduced primarily by application of the theory, and the reader should not expect to find rigorous proofs and theorems. References to other literature are provided for that purpose. It is hoped that this approach will enable the reader to learn the various techniques in minimum time. Furthermore, since the details of solution vary greatly from problem to problem, only by many examples can one gain the insight needed to treat new problems. There is an art to choosing a good solution, and this art is learned through experience.

The unifying concept for this text is the *method of moments*. This is a very general concept, and almost any solution, analytical or numerical, can be interpreted by it. For example, the classical eigenfunction approach corresponds to the particular choice of eigenfunctions for expansion and testing. The Rayleigh-Ritz variational method and Galerkin's method are closely related to it, and so on. It is the author's conviction that the moment method, approached from the standpoint of function spaces and linear operators, is the best way to present the general theory. Particular cases are then interpreted within this general framework.

The text is divided into two main parts, one on *deterministic problems* and the other on *eigenvalue problems*. Chapter 1 gives a discussion of the method of moments and of the various approximations that are applicable. Chapter 2 uses some of these for electrostatic problems, Chapter 3 for some two-dimensional field problems, and Chapter 4 for three-dimensional problems of wire antennas and scatterers. Chapter 5 discusses the general formulation of electromagnetic

problems in terms of *generalized network parameters*. This approach should appeal to electrical engineers because of their familiarity with network theory. Chapter 6 considers the multiport problem, that is, structures having several ports for excitation, measurement, and loading. Chapter 7 discusses the eigenvalue problem according to the method of moments, using the nonuniform transmission line as an example. Chapter 8 applies these techniques to waveguides of arbitrary cross section, and Chapter 9 to resonant cavities containing arbitrary media. The final chapter considers the problem of optimization, and shows that it reduces to an eigenvalue problem.

The theory is best expressed in the language of linear function spaces, but an attempt has been made to minimize its use. The concepts that are needed are defined and illustrated when they are introduced. A summary of the general structure of linear spaces is given in Appendix A. A computational algorithm for the inversion of matrices is given in Appendix B, and one for the evaluation of matrix eigenvalues and eigenvectors is given in Appendix C. For a better understanding of this appended material the reader is advised to consult additional references.

Much of the material of this monograph has resulted from work performed at Syracuse University by the author and his students. The following were major contributors: Joseph Mautz, Radha Gupta, Thomas Bristol, and Robert Wallenberg. Discussions with various faculty colleagues were also most helpful. The manuscript was typed by two very efficient secretaries, Mary Jo Fairbanks and Louise Capra. Research support was provided by several contracts and grants from the Rome Air Development Center and the National Science Foundation. The author expresses his sincere thanks to everyone who has aided in the development of this book.

Roger F. Harrington

CHAPTER

1

Deterministic Problems

1-1. Introduction

The use of high-speed digital computers not only allows more computations to be made than ever before, it makes practicable methods of solution too repetitious for hand calculation. In the past much effort was expended to analytically manipulate solutions into forms which minimized the computational effort. It is now often more convenient to use computer time to reduce the analytical effort. Approximation techniques, once considered a last resort, can be carried to such high orders on computers that they are for most purposes as good as exact answers. They also permit treatment of problems not solvable by exact methods.

This text has been written to provide a unified treatment of matrix methods for computing the solutions to field problems. The basic idea is to reduce a functional equation to a matrix equation, and then solve the matrix equation by known techniques. These concepts are best expressed in the language of linear spaces and operators. However, it is not necessary that the reader have prior knowledge of this theory, because we shall define and illustrate the concepts as they are introduced. A brief summary of linear spaces and operators is given in Appendix A. Detailed expositions may be found in many textbooks [1–3].[1]

In this chapter we consider equations of the inhomogeneous type

$$L(f) = g \tag{1-1}$$

[1] Bracketed numbers refer to the References at the end of each chapter.

where L is an *operator*, g is the *source* or *excitation* (known function), and f is the *field* or *response* (unknown function to be determined). By the term *deterministic* we mean that the solution to (1-1) is unique; that is, only one f is associated with a given g. A problem of *analysis* involves the determination of f when L and g are given. A problem of *synthesis* involves a determination of L when f and g are specified. In this text we consider only the analysis problem.

This chapter presents the basic mathematical techniques for reducing functional equations to matrix equations. A unifying principle for such techniques is found in the general *method of moments*, in terms of which most specific solutions can be interpreted. We shall consider a deterministic problem solved once it is reduced to a suitable matrix equation, since the solution is then given by matrix inversion. Most computers have subroutines available for matrix inversion, which is a relatively simple operation. For reference, the widely used Gauss-Jordan method is given in Appendix B.

The examples of this chapter are simple, chosen to illustrate the theory without clouding the picture with physical concepts or complicated mathematics. However, when these methods are applied to problems of practical interest the procedures are not so simple. The details vary according to the type of problem, and can be illustrated only by treating a variety of problems. For this reason we treat many specific problems in the subsequent chapters. It is hoped that these examples will not only allow the reader to solve similar problems, but will suggest extensions and modifications to treat other types. Although most of the examples are taken from electromagnetic theory, the procedures are general and apply to field problems of any kind.

1-2. Formulation of Problems

The general methods of solution will be discussed in the notation of linear spaces and operators, and hence specific problems should be put into this notation. Given a deterministic problem of the form $L(f) = g$, we must identify the operator L, its domain (the functions f on which it operates), and its range (the functions g resulting from the operation). Furthermore, we usually need an *inner product* $\langle f, g \rangle$, which is a scalar defined to satisfy[2]

$$\langle f, g \rangle = \langle g, f \rangle \tag{1-2}$$

$$\langle \alpha f + \beta g, h \rangle = \alpha \langle f, h \rangle + \beta \langle g, h \rangle \tag{1-3}$$

$$\begin{aligned} \langle f^*, f \rangle &> 0 \qquad \text{if } f \neq 0 \\ &= 0 \qquad \text{if } f = 0 \end{aligned} \tag{1-4}$$

[2] The usual definition of inner product in Hilbert space corresponds to $\langle f^*, g \rangle$ in our notation. For this text it is more convenient to show the conjugate operation explicity wherever it occurs, and to define the adjoint operator without conjugation.

where α and β are scalars and * denotes a complex conjugate. We sometimes need the *adjoint operator* L^a and its domain, defined by

$$\langle Lf, g\rangle = \langle f, L^a g\rangle \tag{1-5}$$

for all f in the domain of L. An operator is *self-adjoint* if $L^a = L$ and the domain of L^a is that of L.

Properties of the solution depend upon properties of the operator. An operator is *real* if Lf is real whenever f is real. An operator is *positive definite* if

$$\langle f^*, Lf\rangle > 0 \tag{1-6}$$

for all $f \neq 0$ in its domain. It is *positive semidefinite* if $>$ is replaced by $\geq$ in (1-6), *negative definite* if $>$ is replaced by $<$ in (1-6), etc. We shall identify other properties of operators as they are needed.

If the solution to $L(f) = g$ exists and is unique for all g, then the *inverse operator* L^{-1} exists such that

$$f = L^{-1}(g) \tag{1-7}$$

If g is known, then (1-7) represents the solution to the original problem. However, (1-7) is itself an inhomogeneous equation for g if f is known, and its solution is $L(f) = g$. Hence L and L^{-1} form a pair of operators, each of which is the inverse of the other.

Facility in formulating problems using the concepts of linear spaces comes only with practice, which will be provided by the many examples in the following chapters. For the present, let us consider a simple abstract example so that mathematical concepts may be illustrated without bringing physical concepts into the picture.

Example. Given $g(x)$, find $f(x)$ in the interval $0 \leq x \leq 1$ satisfying

$$-\frac{d^2 f}{dx^2} = g(x) \tag{1-8}$$

$$f(0) = f(1) = 0 \tag{1-9}$$

This is a boundary-value problem for which

$$L = -\frac{d^2}{dx^2} \tag{1-10}$$

The range of L is the space of all functions g in the interval $0 \leq x \leq 1$ that we wish to consider. The domain of L is the space of those functions f in the interval

$0 \leq x \leq 1$, satisfying the boundary conditions (1-9), and having second derivatives in the range of L. The solution to (1-8) is not unique unless appropriate boundary conditions are included. In other words, both the differential operator and its domain are required to define the operator.

A suitable inner product for this problem is

$$\langle f, g \rangle = \int_0^1 f(x)g(x)\,dx \tag{1-11}$$

It is easily shown that (1-11) satisfies the postulates (1-2) to (1-4), as required. Note that the definition (1-11) is not unique. For example,

$$\int_0^1 w(x)f(x)g(x)\,dx \tag{1-12}$$

where $w(x) > 0$ is an arbitrary weighting function, is also an acceptable inner product. However, the adjoint operator depends on the inner product, which can often be chosen to make the operator self-adjoint.

To find the adjoint of a differential operator, we form the left side of (1-5), and integrate by parts to obtain the right side. For the present problem

$$\begin{aligned}\langle Lf, g \rangle &= \int_0^1 \left(-\frac{d^2f}{dx^2}\right) g\,dx \\ &= \int_0^1 \frac{df}{dx}\frac{dg}{dx}\,dx - \left[\frac{df}{dx}\,g\right]_0^1 \\ &= \int_0^1 f\left(-\frac{d^2g}{dx^2}\right)dx + \left[f\frac{dg}{dx} - g\frac{df}{dx}\right]_0^1 \end{aligned} \tag{1-13}$$

The last terms are boundary terms, and the domain of L^a may be chosen so that these vanish. The first boundary terms vanish by (1-9), and the second vanish if

$$g(0) = g(1) = 0 \tag{1-14}$$

It is then evident that the adjoint operator to (1-10) for the inner product (1-11) is

$$L^a = L = -\frac{d^2}{dx^2} \tag{1-15}$$

Since $L^a = L$ and the domain of L^a is the same as that of L, the operator is self-adjoint.

It is also evident that L is a real operator, since Lf is real when f is real. That L is a positive definite operator is shown from (1-6) as follows:

$$\langle f^*, Lf\rangle = \int_0^1 f^*\left(-\frac{d^2f}{dx^2}\right) dx$$

$$= \int_0^1 \frac{df^*}{dx}\frac{df}{dx}\,dx - \left[f^*\frac{df}{dx}\right]_0^1$$

$$= \int_0^1 \left|\frac{df}{dx}\right|^2 dx \tag{1-16}$$

Note that L is a positive definite operator even if f is complex.

The inverse operator to L can be obtained by standard Green's function techniques.[3] It is

$$L^{-1}(g) = \int_0^1 G(x, x')g(x')\,dx' \tag{1-17}$$

where G is the Green's function

$$G(x, x') = \begin{cases} x(1-x') & x < x' \\ (1-x)x' & x > x' \end{cases} \tag{1-18}$$

We can verify that (1-17) is the inverse operator by forming $f = L^{-1}(g)$, differentiating twice, and obtaining (1-8). Note that no boundary conditions are needed on the domain of L^{-1}, which is characteristic of most integral operators. That L^{-1} is self-adjoint follows from the proof that L is self-adjoint, since

$$\langle Lf_1, f_2\rangle = \langle g_1, L^{-1}g_2\rangle \tag{1-19}$$

Of course, the self-adjointness of L^{-1} can also be proved directly. It similarly follows that L^{-1} is positive definite whenever L is positive definite, and vice versa.

1-3. Method of Moments

We now discuss a general procedure for solving linear equations, called the *method of moments* [4,5]. Consider the inhomogeneous equation

$$L(f) = g \tag{1-20}$$

---

[3] See, for example, reference [2], Chapter 3.

where L is a linear operator, g is known, and f is to be determined. Let f be expanded in a series of functions $f_1, f_2, f_3, \ldots$ in the domain of L, as

$$f = \sum_n \alpha_n f_n \tag{1-21}$$

where the α_n are constants. We shall call the f_n *expansion functions* or *basis functions*. For exact solutions, (1-21) is usually an infinite summation and the f_n form a complete set of basis functions. For approximate solutions, (1-21) is usually a finite summation. Substituting (1-21) in (1-20), and using the linearity of L, we have

$$\sum_n \alpha_n L(f_n) = g \tag{1-22}$$

It is assumed that a suitable inner product $\langle f, g \rangle$ has been determined for the problem. Now define a set of *weighting functions*, or *testing functions*, $w_1, w_2, w_3, \ldots$ in the range of L, and take the inner product of (1-22) with each w_m. The result is

$$\sum_n \alpha_n \langle w_m, Lf_n \rangle = \langle w_m, g \rangle \tag{1-23}$$

$m = 1, 2, 3, \ldots$. This set of equations can be written in matrix form as

$$[l_{mn}][\alpha_n] = [g_m] \tag{1-24}$$

where

$$[l_{mn}] = \begin{bmatrix} \langle w_1, Lf_1 \rangle & \langle w_1, Lf_2 \rangle & \cdots \\ \langle w_2, Lf_1 \rangle & \langle w_2, Lf_2 \rangle & \cdots \\ \cdots & \cdots & \cdots \end{bmatrix} \tag{1-25}$$

$$[\alpha_n] = \begin{bmatrix} \alpha_1 \\ \alpha_2 \\ \vdots \end{bmatrix} \qquad [g_m] = \begin{bmatrix} \langle w_1, g \rangle \\ \langle w_2, g \rangle \\ \vdots \end{bmatrix} \tag{1-26}$$

If the matrix $[l]$ is nonsingular its inverse $[l^{-1}]$ exists. The α_n are then given by

$$[\alpha_n] = [l^{-1}_{nm}][g_m] \tag{1-27}$$

and the solution for f is given by (1-21). For concise expression of this result, define the matrix of functions

$$[f_n] = [f_1 \quad f_2 \quad f_3 \quad \ldots] \tag{1-28}$$

and write

$$f = [\tilde{f}_n][\alpha_n] = [\tilde{f}_n][l_{mn}^{-1}][g_m] \tag{1-29}$$

This solution may be exact or approximate, depending upon the choice of the f_n and w_n. The particular choice $w_n = f_n$ is known as *Galerkin's method* [6,7].

If the matrix $[l]$ is of infinite order, it can be inverted only in special cases, for example, if it is diagonal. The classical eigenfunction method leads to a diagonal matrix, and can be thought of as a special case of the method of moments. If the sets f_n and w_n are finite, the matrix is of finite order, and can be inverted by known methods (Appendix B).

One of the main tasks in any particular problem is the choice of the f_n and w_n. The f_n should be linearly independent and chosen so that some superposition (1-21) can approximate f reasonably well. The w_n should also be linearly independent and chosen so that the products $\langle w_n, g \rangle$ depend on relatively independent properties of g. Some additional factors which affect the choice of f_n and w_n are (1) the accuracy of solution desired, (2) the ease of evaluation of the matrix elements, (3) the size of the matrix that can be inverted, and (4) the realization of a well-conditioned matrix $[l]$.

Example. Consider the same equation as in the example of Section 1-2, but with the specific source $g = 1 + 4x^2$. Hence our problem is

$$-\frac{d^2f}{dx^2} = 1 + 4x^2 \tag{1-30}$$

$$f(0) = f(1) = 0 \tag{1-31}$$

This is, of course, a simple boundary-value problem with solution

$$f(x) = \frac{5x}{6} - \frac{x^2}{2} - \frac{x^4}{3} \tag{1-32}$$

To illustrate the procedure, the problem will be reconsidered by the method of moments.

For a power-series solution, let us choose

$$f_n = x - x^{n+1} \tag{1-33}$$

$n = 1, 2, 3, \ldots, N$, so that the series (1-21) is

$$f = \sum_{n=1}^{N} \alpha_n (x - x^{n+1}) \tag{1-34}$$

Note that the term x is needed in (1-33), else the f_n will not be in the domain of L; that is, the boundary conditions will not be satisfied. For testing functions, choose

$$w_n = f_n = x - x^{n+1} \tag{1-35}$$

in which case the method is that of Galerkin. In Section 1-8 it is shown that the w_n should be in the domain of the adjoint operator. Since L is self-adjoint for this problem, the w_n should be in the domain of L, as are those of (1-35).

Evaluation of the matrices (1-25) and (1-26) for the inner product (1-11) and $L = -d^2/dx^2$ is straightforward, and results in

$$l_{mn} = \langle w_m, Lf_n \rangle = \frac{mn}{m+n+1} \tag{1-36}$$

$$g_m = \langle w_m, g \rangle = \frac{m(3m+8)}{2(m+2)(m+4)} \tag{1-37}$$

For any fixed N (number of expansion functions), the α_n are given by (1-27) and the approximation to f by (1-34).

To illustrate convergence, let us consider successive approximations as N is increased. For $N = 1$, we have $l_{11} = 1/3$, $g_1 = 11/30$, and hence from (1-24) $\alpha_1 = 11/10$. For $N = 2$, the matrix equation (1-24) becomes

$$\begin{bmatrix} \frac{1}{3} & \frac{1}{2} \\ \frac{1}{2} & \frac{4}{5} \end{bmatrix} \begin{bmatrix} \alpha_1 \\ \alpha_2 \end{bmatrix} = \begin{bmatrix} \frac{11}{30} \\ \frac{7}{12} \end{bmatrix} \tag{1-38}$$

from which the α's are found as

$$\begin{bmatrix} \alpha_1 \\ \alpha_2 \end{bmatrix} = \begin{bmatrix} \frac{1}{10} \\ \frac{2}{3} \end{bmatrix} \tag{1-39}$$

For $N = 3$, the matrix equation (1-24) becomes

$$\begin{bmatrix} \frac{1}{3} & \frac{1}{2} & \frac{3}{5} \\ \frac{1}{2} & \frac{4}{5} & 1 \\ \frac{3}{5} & 1 & \frac{9}{7} \end{bmatrix} \begin{bmatrix} \alpha_1 \\ \alpha_2 \\ \alpha_3 \end{bmatrix} = \begin{bmatrix} \frac{11}{30} \\ \frac{7}{12} \\ \frac{51}{70} \end{bmatrix} \tag{1-40}$$

from which the α's are found as

$$\begin{bmatrix} \alpha_1 \\ \alpha_2 \\ \alpha_3 \end{bmatrix} = \begin{bmatrix} \frac{1}{2} \\ 0 \\ \frac{1}{3} \end{bmatrix} \tag{1-41}$$

Note that this third-order solution is the exact solution, (1-32). For $N = 4$ we

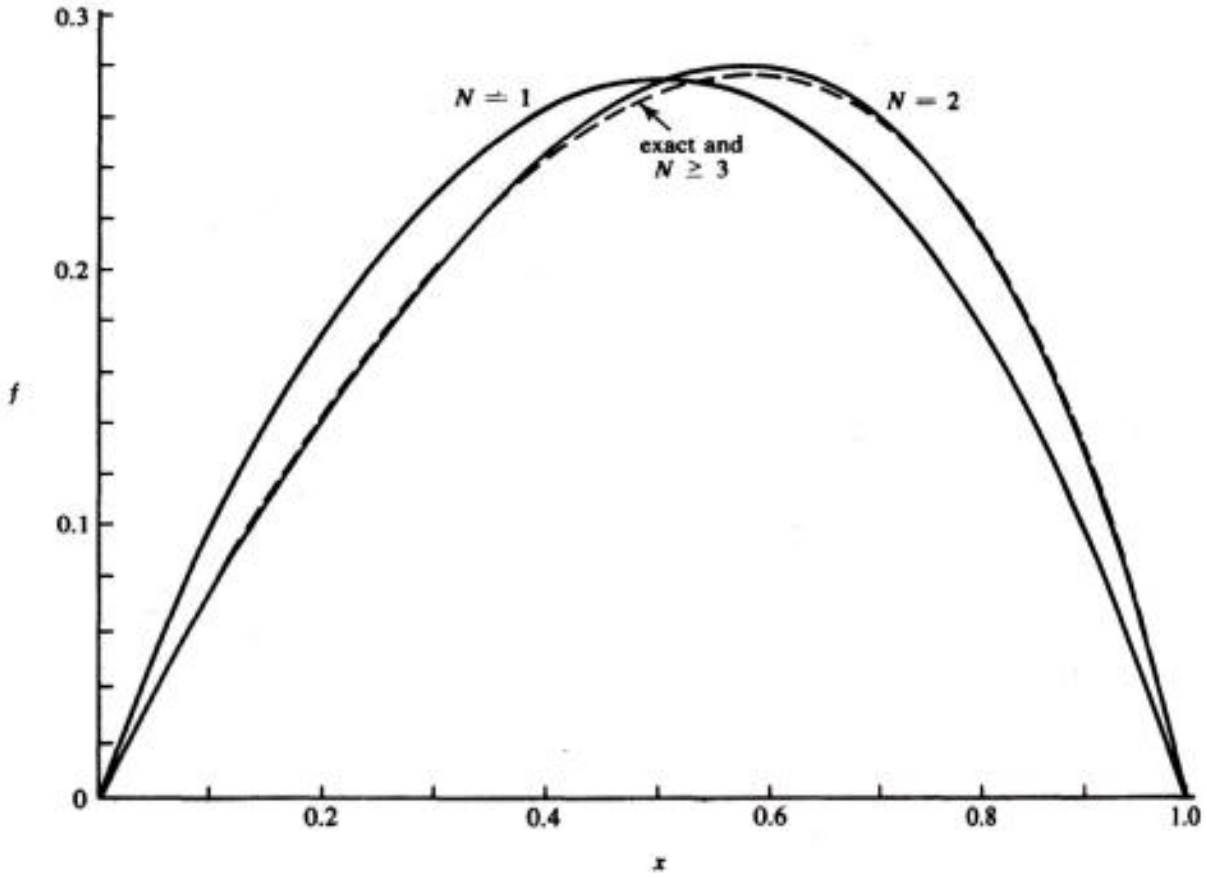

Figure 1-1. **Solutions using $f_n = x - x^{n+1}$ and Galerkin's method.**

again obtain the exact solution, and so on for higher N. Plots of the various solutions are shown in Fig. 1-1.

The reason an exact solution is obtained for this problem is that some combination of the f_n can exactly represent the solution, and any N linearly independent tests must correctly determine the coefficients. If the solution cannot be expressed as a finite series of the f_n, then we continue to obtain approximate solutions converging to the exact solution in the sense of projections, as discussed in Section 1-8.

More important than solving any particular equation, the inverse matrix $[l^{-1}]$ gives a representation of the inverse operator L^{-1}. Hence we have a solution (usually approximate) to $Lf = g$ for *any* g. In physical problems, L represents the system, g the excitation, and f the response. A determination of the $[l^{-1}]$ matrix therefore gives us a general solution for the system, that is, the response f for arbitrary excitation g, assuming that g is reasonably well behaved.

1-4. Point Matching

The integration involved in evaluating the $l_{mn} = \langle w_m, Lf_n \rangle$ of (1-25) is often difficult to perform in problems of practical interest. A simple way to obtain approximate solutions is to require that equation (1-22) be satisfied at discrete

points in the region of interest. This procedure is called a *point-matching method.* In terms of the method of moments, it is equivalent to using Dirac delta functions as testing functions. The following example illustrates this in the one-dimensional case.

Example. Reconsider the problem of Section 1-3, stated by (1-30) and (1-31). Again we choose expansion functions (1-33), so that (1-22) becomes

$$\sum_{n=1}^{N} \alpha_n \left[-\frac{d^2}{dx^2}(x - x^{n+1}) \right] = 1 + 4x^2 \tag{1-42}$$

For a point-matching solution, let us take the points

$$x_m = \frac{m}{N+1} \qquad m = 1, 2, \ldots, N \tag{1-43}$$

which are equispaced in the interval $0 \leq x \leq 1$. Requiring (1-42) to be satisfied at each x_m gives us the matrix equation (1-24), with elements

$$l_{mn} = n(n+1)\left(\frac{m}{N+1}\right)^{n-1} \tag{1-44}$$

$$g_m = 1 + 4\left(\frac{m}{N+1}\right)^2 \tag{1-45}$$

Note that this result is identical to choosing weighting functions

$$w_m = \delta(x - x_m) \tag{1-46}$$

where $\delta(x)$ is the Dirac delta function, and applying the method of moments with inner product (1-11).

To illustrate some numerical results, consider the solution as N is increased. For $N = 1$, we have $l_{11} = 2$, $g_1 = 2$, and from (1-27) $\alpha_1 = 1$. For $N = 2$, the matrix equation is

$$\begin{bmatrix} 2 & 2 \\ 2 & 4 \end{bmatrix} \begin{bmatrix} \alpha_1 \\ \alpha_2 \end{bmatrix} = \begin{bmatrix} \frac{13}{9} \\ \frac{25}{9} \end{bmatrix} \tag{1-47}$$

from which the α's are found as

$$\begin{bmatrix} \alpha_1 \\ \alpha_2 \end{bmatrix} = \begin{bmatrix} \frac{1}{18} \\ \frac{2}{3} \end{bmatrix} \tag{1-48}$$

For $N = 3$, the exact solution (1-41) must again be obtained, since the exact solution is a linear combination of the f_n's and we are applying N independent tests. Similarly, for $N > 3$ we continue to obtain the exact answer for the same reason. Plots of these solutions differ to some extent from those of Fig. 1-1 but are qualitatively similar. The point-matching solutions in this case are actually less accurate than the corresponding Galerkin approximations, but for low orders of solution they are usually sensitive to the particular points of match. For high-order solutions the use of equispaced points normally gives excellent results.

Note that even though the $[I]$ matrices of (1-36) and (1-44) are quite different in form, they give similar results. There are infinitely many possible sets of basis functions and of testing functions. Some sets may give faster convergence than others, or give matrices easier to evaluate, or give acceptable results with smaller matrices, etc. For any particular problem one of our tasks is to choose sets well suited to the problem.

1-5. Subsectional Bases

Another approximation useful for practical problems is the *method of subsections*. This involves the use of basis functions f_n each of which exists only over subsections of the domain of f. Then each α_n of the expansion (1-21) affects the approximation of f only over a subsection of the region of interest. This procedure often simplifies the evaluation and/or the form of the matrix $[I]$. Sometimes it is convenient to use the point-matching method of Section 1-4 in conjunction with the subsectional method.

Example. Again consider the problem of Section 1-3, stated by (1-30) and (1-31). N equispaced points on the interval $0 \le x \le 1$ are defined by the x_m of (1-43). A subinterval is defined to be of width $1/(N+1)$ centered on the x_m. This is shown for case $N = 5$ in Fig. 1-2(a). A function which exists over only one subinterval is the *pulse function*

$$P(x) = \begin{cases} 1 & |x| < \dfrac{1}{2(N+1)} \\ 0 & |x| > \dfrac{1}{2(N+1)} \end{cases} \tag{1-49}$$

For $N = 5$, the function $P(x - x_2)$ is shown in Fig. 1-2(b). A linear combination of $f_n = P(x - x_n)$ according to (1-21) gives a *step approximation* to f, as represented by Fig. 1-2(c). However, for $L = -d^2/dx^2$, the operation LP does not yield a function in the range of L. Hence the pulse functions cannot be used as basis functions unless we extend the operator (Section 1-7) or use an approximate operator (Section 1-6).

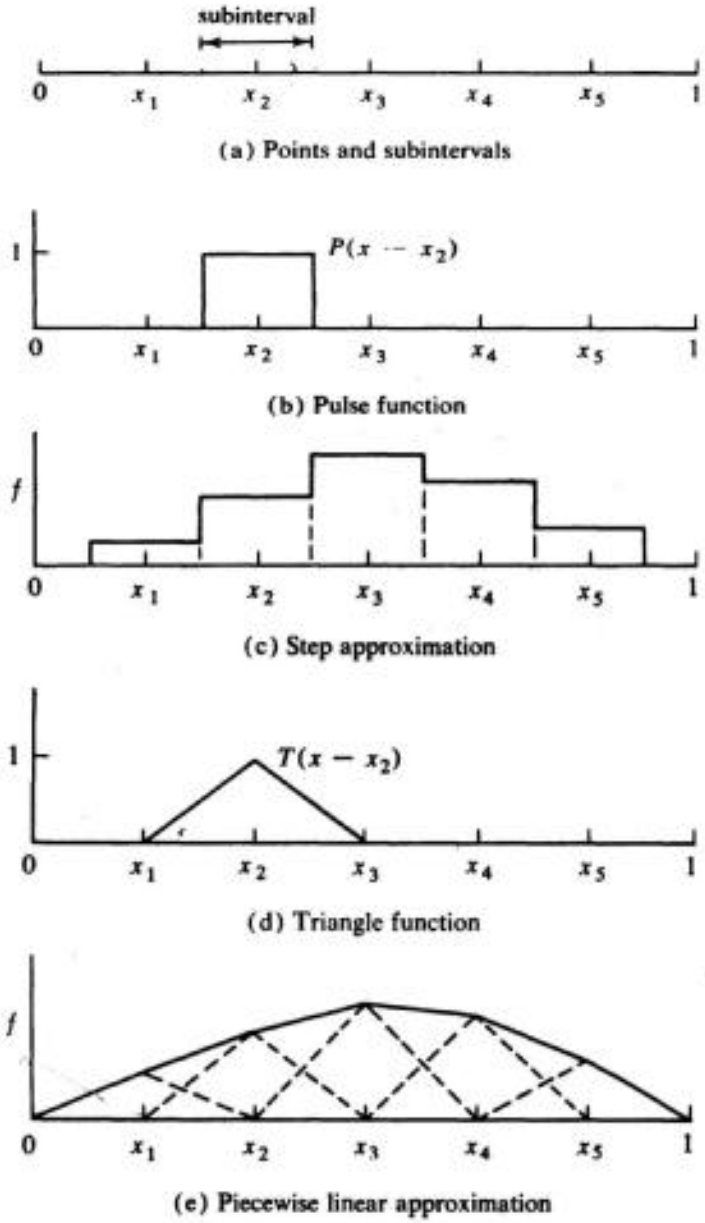

***Figure 1-2.* Subsectional bases and functional approximations.**

A better-behaved function is the *triangle function*, defined as

$$T(x) = \begin{cases} 1 - |x|(N+1) & |x| < \dfrac{1}{N+1} \\ 0 & |x| > \dfrac{1}{N+1} \end{cases} \tag{1-50}$$

For the case $N = 5$ the function $T(x - x_2)$ is shown in Fig. 1-2(d). A linear

combination of triangle functions of the form

$$f = \sum_{n=1}^{N} \alpha_n T(x - x_n) \tag{1-51}$$

gives a *piecewise linear approximation* to f, as represented by Fig. 1-2(e). For $L = -d^2/dx^2$, the operation LT gives the symbolic function

$$LT(x - x_n) = (N + 1)[-\delta(x - x_{n-1}) + 2\delta(x - x_n) - \delta(x - x_{n+1})] \tag{1-52}$$

where $\delta(x)$ is the Dirac delta function. We can use this result in the method of moments as long as the w_n are not also symbolic functions. We cannot use a point-matching procedure in this case.

To follow through the method of moments, let $f_n = T(x - x_n)$, that is, use the expansion (1-51). As testing functions, choose $w_m = P(x - x_m)$. For inner product (1-11), the matrix elements of (1-25) and (1-26) are easily evaluated as

$$l_{mn} = \begin{cases} 2(N+1) & m = n \\ -(N+1) & |m-n| = 1 \\ 0 & |m-n| > 1 \end{cases} \tag{1-53}$$

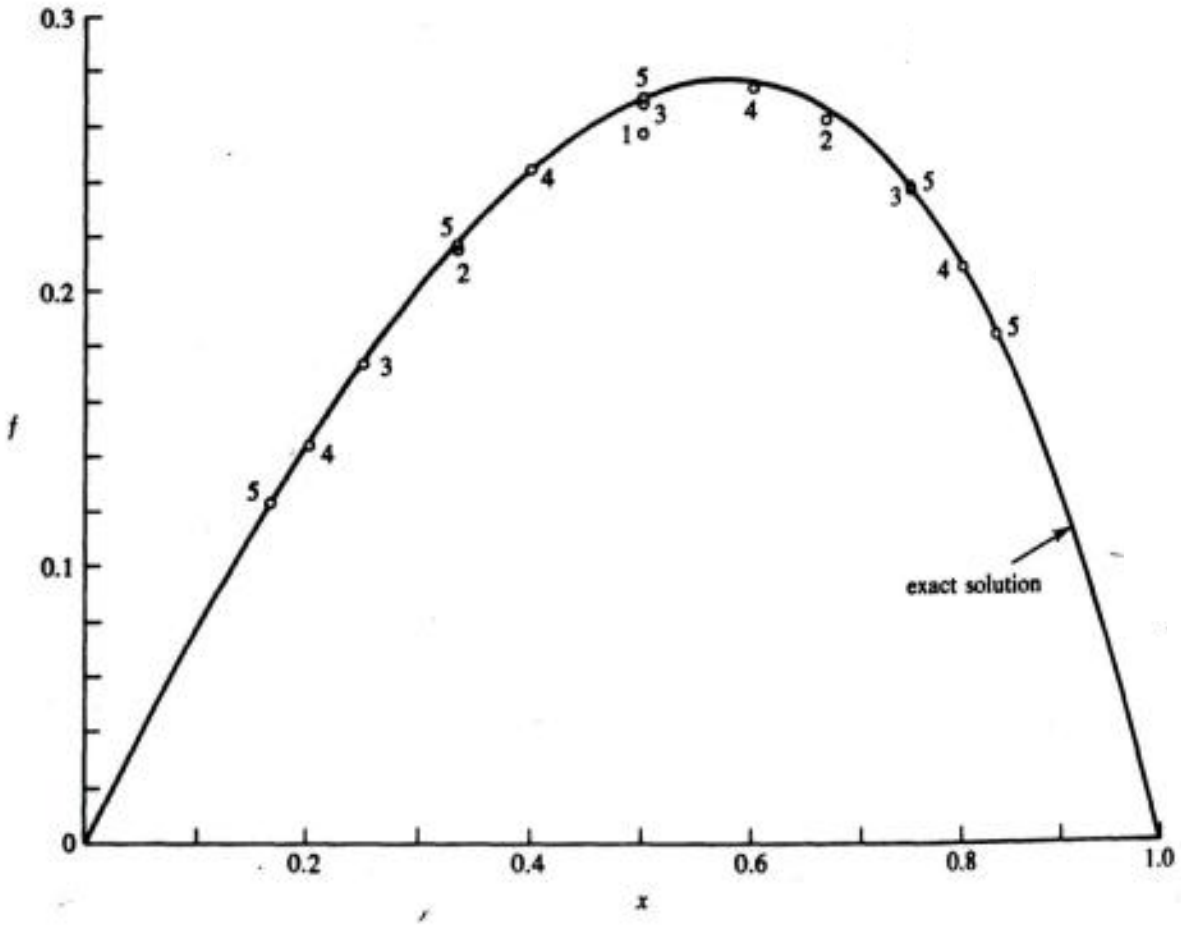

Figure 1-3. **Moment solutions using triangles for expansion and pulses for testing. Numbers adjacent to points denote order of solution.**

$$g_m = \frac{1}{N+1}\left[1 + \frac{4m^2 + (1/3)}{(N+1)^2}\right] \tag{1-54}$$

Note the particularly simple form of [*I*]. We shall encounter this form again in connection with difference equations (Section 1-6).

Figure 1-3 illustrates the convergence of the above solution as N (number of subsections) is increased. Only the break points of the piecewise linear solution are shown; the functional approximation is given by straight lines joining these points. The break points are, of course, also the α_n, since they are the peaks of the triangle-function components.

1-6. Approximate Operators

In complex problems it is sometimes convenient to approximate the operator to obtain approximate solutions. For differential operators, the finite-difference approximation has been widely used [8]. For integral operators, an approximate operator can be obtained by approximating the kernel of the integral operator [6]. Any method whereby a functional equation is reduced to a matrix equation can be interpreted in terms of the method of moments. Hence for any matrix solution using approximation of the operator there will be a corresponding moment solution using approximation of the function.

Example. Let us consider the problem (1-30) and (1-31) by a finite-difference approximation. This involves replacing all derivatives by finite differences; that is, for a given Δx,

$$\frac{df}{dx} \approx \frac{1}{\Delta x}\left[f\left(x + \frac{\Delta x}{2}\right) - f\left(x - \frac{\Delta x}{2}\right)\right]$$

$$\frac{d^2f}{dx^2} \approx \frac{1}{\Delta x}\left[f'\left(x + \frac{\Delta x}{2}\right) - f'\left(x - \frac{\Delta x}{2}\right)\right] \tag{1-55}$$

$$\approx \frac{1}{(\Delta x)^2}\left[f(x - \Delta x) - 2f(x) + f(x + \Delta x)\right]$$

For our present problem, consider the interval $0 \le x \le 1$ divided into $N + 1$ segments, with end points x_n, as depicted in Fig. 1-2(a). For Δx equal to one segment, $\Delta x = 1/(N + 1)$, and a finite-difference approximation to $L = -d^2/dx^2$ is

$$L^d f = (N+1)^2\left[-f\left(x - \frac{1}{N+1}\right) + 2f(x) - f\left(x + \frac{1}{N+1}\right)\right] \tag{1-56}$$

Note that $L^d \to L$ as $N \to \infty$ for all f in the domain of L.

We can now apply the method of moments to the approximate equation

$$L^d f = 1 + 4x^2 \tag{1-57}$$

subject to boundary conditions $f(0) = f(1) = 0$. Most commonly this is done by a point-matching procedure at the x_m. The result is a matrix equation of the form (1-24), where the α_n correspond to $f(x_n)$,

$$l_{mn} = \begin{cases} 2(N+1)^2 & m = n \\ -(N+1)^2 & |m-n| = 1 \\ 0 & |m-n| > 1 \end{cases} \tag{1-58}$$

$$g_m = 1 + 4\left(\frac{m}{N+1}\right)^2 \tag{1-59}$$

Note that the $[l]$ matrix of (1-58) is the same form as that of (1-53) obtained from a subsectional basis. [The trivial difference in the position of $N + 1$ can be taken care of by choosing $w_m = (N + 1)\,P(x - x_m)$ in the solution of Section 1-5.] The g_m of (1-59) and (1-54) are slightly different, and hence the two solutions will be slightly different. However, as N becomes larger the two g_m approach one another, so the rates of convergence of the two solutions are about the same.

Numerical results for the above solution are similar to those of Fig. 1-3. Iterative procedures are sometimes used to solve the matrix equations obtained by difference approximations [9]. However, iterative procedures usually converge slowly, and with high-speed large-memory computers it is often simpler to invert the matrix. Because of the tridiagonal form of $[l]$, special techniques can be used to invert it [10].

1-7. Extended Operators

As noted earlier, an operator is defined by an operation (for example, $L = -d^2/dx^2$) plus a domain (space of functions to which the operation may be applied). We can *extend the domain* of an operator by redefining the operation to apply to new functions (not in the original domain) as long as this extended operation does not change the original operation in its domain. If the original operator is self-adjoint, it is desirable to make the extended operator self-adjoint also. By this procedure we can use a wider class of functions for solution by the method of moments. This becomes particularly important in multivariable problems (fields in multidimensional space), where it is not always easy to find simple functions in the domain of the original operator.

Example A. Suppose we wish to use pulse functions for an expansion of f in a moment solution for the operator $L = -d^2/dx^2$. As noted in Section 1-5, these are not in the original domain of L. However, for any functions w and f in the original domain,

$$\langle w, Lf \rangle = \int_0^1 \frac{dw}{dx}\frac{df}{dx}\,dx \tag{1-60}$$

obtained from (1-11) by integration by parts. If Lf does not exist, but df/dx does exist, (1-60) can be used to define an extended operator. This extends the domain of L to include functions f whose second derivatives do not exist, but whose first derivatives do exist. It is still assumed that $f(0) = f(1) = 0$. Actually, the type of extension represented here is precisely that which gives rise to the theory of symbolic functions. By using Dirac delta functions in earlier sections we anticipated this concept of extending the domain of a differential operator.

To apply the method of moments using pulse functions and the extended operator, let

$$f = \sum_{n=1}^{N} \alpha_n P(x - x_n) \tag{1-61}$$

where P are the pulse functions defined by (1-49). For testing functions, let $w_m = T(x - x_m)$, where T are the triangle functions defined by (1-50). The elements of the $[l]$ matrix are found using (1-60) as

$$l_{mn} = \langle w_m, Lf_n \rangle = \begin{cases} 2(N+1) & m = n \\ -(N+1) & |m-n| = 1 \\ 0 & |m-n| > 1 \end{cases} \tag{1-62}$$

Note that these are identical to the elements (1-53), which were for f_n and w_m reversed from those of the present solution. We could have anticipated this result because L is self-adjoint. The elements of the $[g]$ matrix are now given by

$$g_m = \int_0^1 T(x - x_m)(1 + 4x^2)\,dx \tag{1-63}$$

which yields a result slightly different from (1-54). However, the two g_m approach each other as N becomes large, and the convergence of the two solutions is about the same.

Numerical results for the above example are similar to those of Fig. 1-3 for various N. However, the functional approximation in this case is a step approximation; that is, the points are midpoints of steps, instead of break points of a piecewise linear approximation as in Fig. 1-3.

Example B. As a second example, let us extend the original domain of $L = -d^2/dx^2$ to apply to functions not satisfying the boundary conditions $f(0) = f(1) = 0$. Referring to (1-13), we note that boundary terms appear if the functions do not obey the given boundary conditions. However, if an extended operator L^e is defined by

$$\langle w, L^e f\rangle = \int_0^1 wLf\,dx - \left[f\frac{dw}{dx}\right]_0^1 \tag{1-64}$$

we have $\langle w, L^e f\rangle = \langle f, L^e w\rangle$ even if the original boundary conditions are not met. Hence the extended operator is self-adjoint regardless of boundary conditions. A method-of-moments solution therefore proceeds in this extended domain in the same manner as for the original domain, except that the expansion and testing functions need not satisfy boundary conditions.

To illustrate the procedure, consider the choice

$$f_n = w_n = x^n \qquad n = 1, 2, \ldots, N \tag{1-65}$$

For $N \geq 4$ these functions form a basis for the exact solution (1-32), and hence the exact solution should be obtained. Evaluating the matrices in the usual way, using the extended operator for $l_{mn} = \langle w_m, L^e f_n\rangle$, for $N = 4$ we obtain the matrix equation

$$\begin{bmatrix} -1 & -2 & -3 & -4 \\ -2 & -\frac{8}{3} & -\frac{7}{2} & -\frac{22}{5} \\ -3 & -\frac{7}{2} & -\frac{21}{5} & -5 \\ -4 & -\frac{22}{5} & -5 & -\frac{40}{7} \end{bmatrix} \begin{bmatrix} \alpha_1 \\ \alpha_2 \\ \alpha_3 \\ \alpha_4 \end{bmatrix} = \begin{bmatrix} \frac{3}{2} \\ \frac{17}{15} \\ \frac{11}{12} \\ \frac{27}{35} \end{bmatrix} \tag{1-66}$$

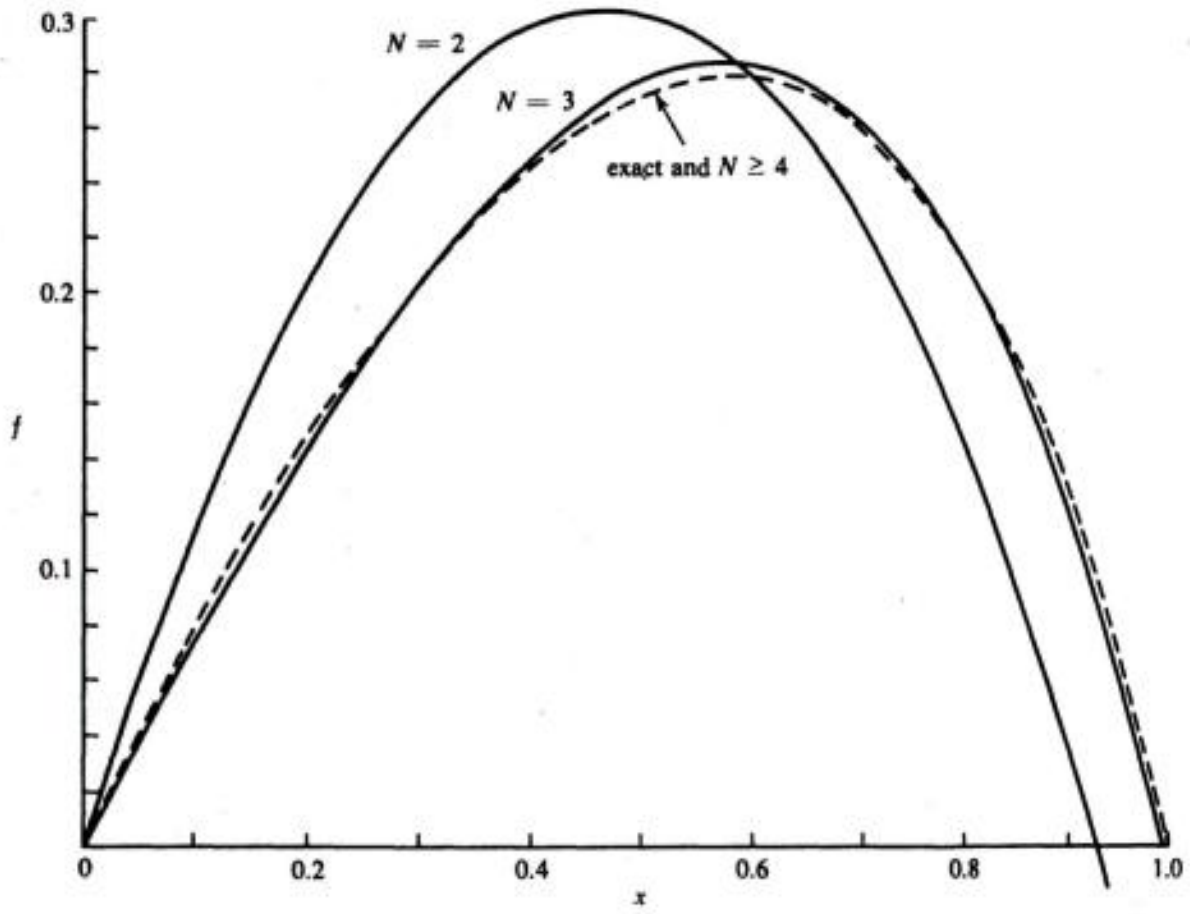

Figure 1-4. **Extended operator moment solutions using powers of x for expansion and testing.**

This may be solved for the α's to obtain

$$\begin{bmatrix} \alpha_1 \\ \alpha_2 \\ \alpha_3 \\ \alpha_4 \end{bmatrix} = \begin{bmatrix} \frac{5}{6} \\ -\frac{1}{2} \\ 0 \\ -\frac{1}{3} \end{bmatrix} \tag{1-67}$$

which is indeed the exact solution. Note that if (1-65) are used with the original operator $L = -d^2/dx^2$ a singular $[l]$ matrix results, and hence no solution is obtained. To illustrate convergence using the extended operator, Fig. 1-4 shows plots of the cases $N = 2$ and $N = 3$, plus the exact solution ($N \geq 4$).

1-8. Variational Interpretation

It is well known that Galerkin's method ($w_n = f_n$) is equivalent to the Rayleigh-Ritz variational method [6,7]. That the general method of moments is also a variational method is usually not noted, but the proof is essentially the same as for Galerkin's method [7].

Let us first interpret the method of moments according to the concepts of linear spaces. Let $\mathcal{S}(Lf)$ denote the range of L, $\mathcal{S}(Lf_n)$ denote the space spanned by the Lf_n, and $\mathcal{S}(w_n)$ denote the space spanned by the w_n. The method of moments (1-23) then equates the projection of Lf onto $\mathcal{S}(w_n)$ to the projection of the approximate Lf onto $\mathcal{S}(w_n)$. Figure 1-5 represents this pictorially. In the

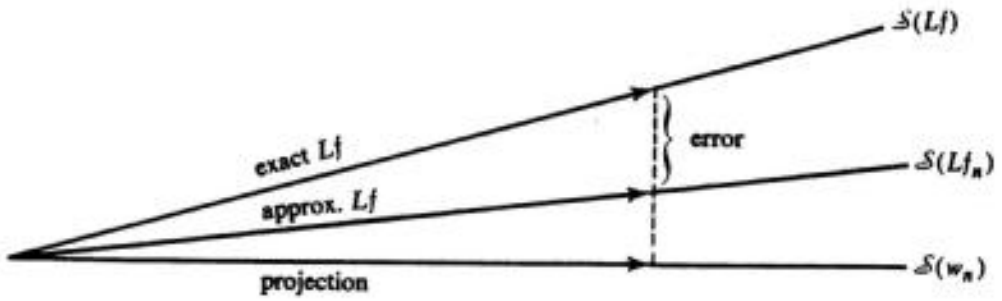

Figure 1-5. **Pictorial representation of the method of moments in function space.**

special case of Galerkin's method, $\mathcal{S}(w_n) = \mathcal{S}(f_n)$. Because the process of obtaining projections minimizes an error, the method of moments is an error-minimizing procedure. Because the error is orthogonal to the projections, it is of second order. This same conclusion is obtained from the calculus of variations [7]. The derivation of the variational results will not be given here, but we shall summarize the conclusions.

Given an operator equation $Lf = g$, it is desired to determine a functional of f (number depending on f)

$$\rho(f) = \langle f, h \rangle \tag{1-68}$$

where h is a given function. If h is a continuous function, then $\rho(f)$ is a *continuous linear functional*. The functional ρ may be f itself if h is an impulse function, but then ρ is no longer a continuous functional. Now let L^a be the adjoint operator to L, and define an adjoint function f^a (adjoint field) by

$$L^a f^a = h \tag{1-69}$$

By the calculus of variations, it can then be shown that [7]

$$\rho = \frac{\langle f, h \rangle \langle f^a, g \rangle}{\langle Lf, f^a \rangle} \tag{1-70}$$

is a variational formula for ρ with stationary point (1-68) when f is the solution to $Lf = g$ and f^a the solution to (1-69). For an approximate evaluation of ρ, let

$$f = \sum_n \alpha_n f_n \qquad f^a = \sum_m \beta_m w_m \tag{1-71}$$

Substitute these in (1-70), and apply the Rayleigh-Ritz conditions $\partial\rho/\partial\alpha_i = \partial\rho/\partial\beta_i = 0$ for all i. The result is that the necessary and sufficient conditions for ρ to be a stationary point are equations (1-23). Hence the method of moments is equivalent to the Rayleigh-Ritz variational method [7]. The method of moments is closely related to the direct methods of the calculus of variations, so called because they yield a solution to the variational problem without recourse to the associated differential equation.

The above variational interpretation can be used to give additional insight into how to choose the testing functions. It is evident from (1-69) and (1-71) that the w_n should be chosen so that some linear combination of them can closely represent the adjoint field f^a. When we calculate f itself by the method of moments, h of (1-68) is a Dirac delta function and f^a of (1-69) is a Green's function. This implies that some combination of the w_n should be able to approximate the Green's function. Since a Green's function is usually poorly behaved, we should expect computation of a field by the method of moments to converge less slowly than computation of a continuous linear functional. This is found actually to be the case.

1-9. Perturbation Solutions

Sometimes the problem under consideration is only slightly different (perturbed) from a problem which can be solved exactly (the unperturbed problem). A first-order solution to the perturbed problem can then be obtained by using the solution to the unperturbed problem as a basis for the method of moments. This procedure is called a *perturbation method*. Higher-order perturbation solutions

can be obtained by using the unperturbed solution plus correction terms in the method of moments. Sometimes this is done as successive approximations by including one correction term at a time, but for machine computations it is usually easier to include all correction terms at once.

To express these concepts in equation form, let

$$L_0(f_0) = g \tag{1-72}$$

represent the unperturbed problem for which the solution f_0 is known. Let $M = L - L_0$ be the difference operator, and hence

$$L(f) = (L_0 + M)(f) = g \tag{1-73}$$

represents the perturbed problem for which the solution f is desired. For a first-order perturbation solution, let

$$f = \alpha f_0 \tag{1-74}$$

and apply the method of moments. If L is self-adjoint, the testing function $w = f_0$ may be chosen; otherwise we should choose $w = f_0^a$, the solution to the unperturbed adjoint problem. An application of the method of moments to this one-term expansion yields

$$(\langle f_0, L_0 f_0 \rangle + \langle f_0, M f_0 \rangle)\alpha = \langle f_0, g \rangle \tag{1-75}$$

Now, by (1-72), $\langle f_0, L_0 f_0 \rangle = \langle f_0, g \rangle$, and the above equation can be written

$$\alpha = 1 - \frac{\langle f_0, M f_0 \rangle}{\langle f_0, g \rangle + \langle f_0, M f_0 \rangle} \tag{1-76}$$

If the perturbation is truly small, the second term in the denominator of (1-76) will be small compared to the first term, and from (1-74) and (1-76)

$$f \approx \left(1 - \frac{\langle f_0, M f_0 \rangle}{\langle f_0, g \rangle}\right) f_0 \tag{1-77}$$

This is the first-order perturbation solution.

For higher-order solutions, we merely choose $f_1 = f_0$ in the general method of moments (Section 1-3) and $f_2, f_3, \ldots$ serve as correction terms. For self-adjoint operators, choose $w_1 = f_0$; otherwise choose $w_1 = f_0^a$. The advantage of a perturbation approach over other moment solutions rests primarily in the faster convergence of the perturbation solution.

References

[1] B. Z. Vulikh, *Introduction to Functional Analysis for Scientists and Technologists*, translated by I. N. Sneddon, Pergamon Press, Oxford, 1963.

[2] B. Friedman, *Principles and Techniques of Applied Mathematics*, John Wiley & Sons, Inc., New York, 1956.

[3] J. W. Dettman, *Mathematical Methods in Physics and Engineering*, McGraw-Hill Book Co., New York, 1962.

[4] L. V. Kantorovich and G. P. Akilov, *Functional Analysis in Normed Spaces*, translated by D. E. Brown, Pergamon Press, Oxford, 1964, pp. 586–587.

[5] R. F. Harrington, "Matrix Methods for Field Problems," *Proc. IEEE*, Vol. **55**, No. 2, Feb. 1967, pp. 136–149.

[6] L. V. Kantorovich and V. I. Krylov, *Approximate Methods of Higher Analysis*, 4th ed., translated by C. D. Benster, John Wiley & Sons, Inc., New York, 1959, Chap. IV.

[7] D. S. Jones, "A Critique of the Variational Method in Scattering Problems," *IRE Trans.*, Vol. **AP-4**, No. 3, 1956, pp. 297–301.

[8] G. E. Forsythe and W. R. Wasow, *Finite-Difference Methods for Partial Differential Equations*, John Wiley & Sons, Inc., New York, 1960.

[9] R. V. Southwell, *Relaxation Methods in Theoretical Physics*, Vol. **1**, Oxford University Press, London, 1946.

[10] P. Henrici, *Discrete Variable Methods in Ordinary Differential Equations*, John Wiley & Sons, Inc., New York, 1962, pp. 350–355.

CHAPTER

2

Electrostatic Fields

2-1. Operator Formulation

The static electric intensity **E** is conveniently found from an electrostatic potential ϕ according to

$$\mathbf{E} = -\nabla\phi \tag{2-1}$$

where ∇ is the gradient operator. In a region of constant permittivity ε and volume charge density ρ, the electrostatic potential satisfies the *Poisson equation*

$$-\varepsilon\nabla^2\phi = \rho \tag{2-2}$$

where ∇^2 is the Laplacian operator. For unique solutions, boundary conditions on ϕ are needed. In other words, the domain of the operator must be specified.

For now, consider fields from charges in unbounded space, in which case

$$r\phi \to \text{constant as } r \to \infty \tag{2-3}$$

where r is the distance from the coordinate origin, for every ρ of finite extent. Now the differential operator formulation is

$$L\phi = \rho \tag{2-4}$$

where

$$L = -\varepsilon\nabla^2 \tag{2-5}$$

and the domain of L is those functions ϕ whose Laplacian exists and have $r\phi$ bounded at infinity according to (2-3). The well-known solution to this problem is

$$\phi(x, y, z) = \iiint \frac{\rho(x', y', z')}{4\pi\varepsilon R}\, dx'\, dy'\, dz' \tag{2-6}$$

where $R = \sqrt{(x - x')^2 + (y - y')^2 + (z - z')^2}$ is the distance from a source point (x', y', z') to a field point (x, y, z). Hence the inverse operator to L is

$$L^{-1} = \iiint dx'\, dy'\, dz' \frac{1}{4\pi\varepsilon R} \tag{2-7}$$

It is important to keep in mind that (2-7) is inverse to (2-5) only for the boundary conditions (2-3). If the boundary conditions are changed, L^{-1} changes. Also, the designation of (2-5) as L and (2-7) as L^{-1} is arbitrary, and we could reverse the notation if desired.

A suitable inner product for electrostatic problems (ε constant) is[1]

$$\langle \phi, \psi \rangle = \iiint \phi(x, y, z)\psi(x, y, z)\, dx\, dy\, dz \tag{2-8}$$

where the integration is over all space. That (2-8) satisfies the required postulates (1-2), (1-3), and (1-4) is easily verified. We now wish to show that L is self-adjoint for this inner product. For this, form the left side of (1-5),

$$\langle L\phi, \psi \rangle = \iiint (-\varepsilon\nabla^2\phi)\psi\, d\tau \tag{2-9}$$

where $d\tau = dx\, dy\, dz$. Green's identity is

$$\iiint_V (\psi\nabla^2\phi - \phi\nabla^2\psi)\, d\tau = \oiint_S \left(\psi \frac{\partial\phi}{\partial n} - \phi \frac{\partial\psi}{\partial n}\right) ds \tag{2-10}$$

where S is the surface bounding the volume V and n is the outward direction normal to S. Let S be a sphere of radius r, so that in the limit $r \to \infty$ the volume V includes all space. For ϕ and ψ satisfying boundary conditions (2-3), $\psi \to C_1/r$ and $\partial\phi/\partial n \to C_2/r^2$ as $r \to \infty$. Hence $\psi\, \partial\phi/\partial n \to C/r^3$ as $r \to \infty$, and similarly for $\phi\, \partial\psi/dn$. Since $ds = r^2 \sin\theta\, d\theta\, d\phi$ increases only as r^2, the right side of (2-10) vanishes as $r \to \infty$. Equation (2-10) then reduces to

$$\iiint \psi\nabla^2\phi\, d\tau = \iiint \phi\nabla^2\psi\, d\tau \tag{2-11}$$

---

[1] For ε a function of position, the differential operator (2-5) is changed to $-\nabla\cdot(\varepsilon\nabla)$, and ε should be included in (2-8) as a weight function to make this new operator self-adjoint.

from which it is evident that the adjoint operator L^a is

$$L^a = L = -\varepsilon\nabla^2 \tag{2-12}$$

Since the domain of L^a is that of L, the operator L is self-adjoint. The mathematical concept of self-adjointness in this case is related to the physical concept of reciprocity [1].

It is evident from (2-5) and (2-7) that L and L^{-1} are real operators. It will now be shown that they are also positive definite; that is, they satisfy (1-6). As discussed in Section 1-2, we need only show it for either L or L^{-1}. For L, form

$$\langle \phi^*, L\phi \rangle = \iiint \phi^*(-\varepsilon\nabla^2\phi)\, d\tau \tag{2-13}$$

and use the vector identity $\phi\nabla^2\phi = \nabla\cdot(\phi\nabla\phi) - \nabla\phi\cdot\nabla\phi$ plus the divergence theorem. The result is

$$\langle \phi^*, L\phi \rangle = \iiint_V \varepsilon\nabla\phi^*\cdot\nabla\phi\, d\tau - \oiint_S \varepsilon\phi^*\nabla\phi\cdot d\mathbf{s} \tag{2-14}$$

where S bounds V. Again take S a sphere of radius r. For ϕ satisfying (2-3), the last term of (2-14) vanishes as $r \to \infty$ for the same reasons as in (2-10). Then

$$\langle \phi^*, L\phi \rangle = \iiint \varepsilon|\nabla\phi|^2\, d\tau \tag{2-15}$$

and, for ε real and $\varepsilon > 0$, L is positive definite. In this case positive definiteness of L is related to the concept of electrostatic energy.

2-2. Charged Conducting Plate

Consider a square conducting plate $2a$ meters on a side and lying on the $z = 0$ plane with center at the origin, as shown in Fig. 2-1. Let $\sigma(x, y)$ represent the surface charge density on the plate, assumed to have zero thickness. The electrostatic potential at any point in space is

$$\phi(x, y, z) = \int_{-a}^{a} dx' \int_{-a}^{a} dy' \frac{\sigma(x', y')}{4\pi\varepsilon R} \tag{2-16}$$

where $R = \sqrt{(x - x')^2 + (y - y')^2 + z^2}$. The boundary condition is $\phi = V$ (constant) on the plate. The integral equation for the problem is therefore

$$V = \int_{-a}^{a} dx' \int_{-a}^{a} dy' \frac{\sigma(x', y')}{4\pi\varepsilon\sqrt{(x - x')^2 + (y - y')^2}} \tag{2-17}$$

where $|x| < a$, $|y| < a$. The unknown to be determined is the charge density $\sigma(x, y)$. A parameter of interest is the capacitance of the plate

$$C = \frac{q}{V} = \frac{1}{V}\int_{-a}^{a} dx \int_{-a}^{a} dy\, \sigma(x, y) \tag{2-18}$$

which is a continuous linear functional of σ.

Let us first go through a simple subsection and point-matching solution [2], and later interpret it in terms of more general concepts. Consider the plate divided into N square subsections, as shown in Fig. 2-1. Define functions

$$f_n = \begin{cases} 1 & \text{on } \Delta s_n \\ 0 & \text{on all other } \Delta s_m \end{cases} \tag{2-19}$$

and let the charge density be represented by

$$\sigma(x, y) \approx \sum_{n=1}^{N} \alpha_n f_n \tag{2-20}$$

Substituting (2-20) in (2-17), and satisfying the resultant equation at the midpoint (x_m, y_m) of each Δs_m, we obtain the set of equations

$$V = \sum_{n=1}^{N} l_{mn}\alpha_n \qquad m = 1, 2, \ldots, N \tag{2-21}$$

where

$$l_{mn} = \int_{\Delta x_n} dx' \int_{\Delta y_n} dy' \frac{1}{4\pi\varepsilon\sqrt{(x_m - x')^2 + (y_m - y')^2}} \tag{2-22}$$

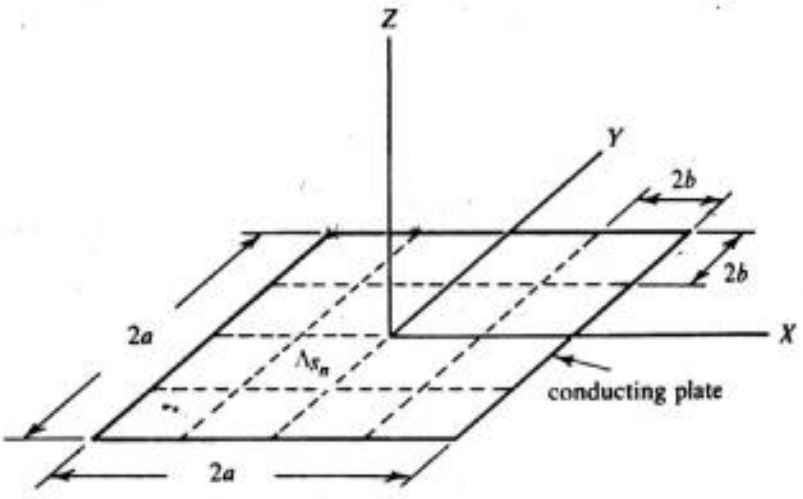

Figure 2-1. Square conducting plate and subsections.

Note that l_{mn} is the potential at the center of Δs_m due to a uniform charge density of unit amplitude over Δs_n. A solution to the set (2-21) gives the α_m, in terms of which the charge density is approximated by (2-20). The corresponding capacitance of the plate, approximating (2-18), is

$$C \approx \frac{1}{V} \sum_{n=1}^{N} \alpha_n \Delta s_n = \sum_{mn} l_{mn}^{-1} \Delta s_n \tag{2-23}$$

This result can be interpreted as stating that the capacitance of an object is the sum of the capacitances of all its subsections plus the mutual capacitances between every pair of subsections.

To translate the above results into the language of linear spaces and the method of moments, let

$$f(x, y) = \sigma(x, y) \tag{2-24}$$

$$g(x, y) = V \qquad |x| < a, |y| < a \tag{2-25}$$

$$L(f) = \int_{-a}^{a} dx' \int_{-a}^{a} dy' \frac{f(x', y')}{4\pi\varepsilon\sqrt{(x - x')^2 + (y - y')^2}} \tag{2-26}$$

Then $L(f) = g$ is equivalent to (2-17). A suitable inner product, satisfying (1-2) to (1-4), for which L is self-adjoint, is

$$\langle f, g \rangle = \int_{-a}^{a} dx \int_{-a}^{a} dy\, f(x, y) g(x, y) \tag{2-27}$$

To apply the method of moments, we use the functions (2-19) as a subsectional basis, and define testing functions

$$w_m = \delta(x - x_m)\delta(y - y_m) \tag{2-28}$$

which is the two-dimensional Dirac delta function. Now the elements of the $[l]$ matrix (1-25) are those of (2-22), and the $[g]$ matrix of (1-26) is

$$[g_m] = \begin{bmatrix} V \\ V \\ \vdots \\ V \end{bmatrix} \tag{2-29}$$

The matrix equation (1-24) is, of course, identical to the set of equations (2-21). In terms of the inner product (2-27), the capacitance (2-18) can be written

$$C = \frac{\langle \sigma, \phi \rangle}{V^2} \tag{2-30}$$

since $\phi = V$ on the plate. Equation (2-30) is the conventional stationary formula for the capacitance of a conducting body [3].

For numerical results, the l_{mn} of (2-22) must be evaluated. Let $2b = 2a/\sqrt{N}$ denote the side length of each Δs_n. The potential at the center of Δs_n due to unit charge density over its own surface is

$$l_{nn} = \int_{-b}^{b} dx \int_{-b}^{b} dy \frac{1}{4\pi\varepsilon\sqrt{x^2 + y^2}}$$

$$= \frac{2b}{\pi\varepsilon} \ln(1 + \sqrt{2}) = \frac{2b}{\pi\varepsilon}(0.8814) \tag{2-31}$$

This derivation uses Dwight [4], 200.01 and 731.2. The potential at the center of Δs_m due to unit charge over Δs_n can be similarly evaluated, but the formula is complicated. For most purposes it is sufficiently accurate to treat the charge on Δs_n as if it were a point charge, and use

$$l_{mn} \approx \frac{\Delta s_n}{4\pi\varepsilon R_{mn}} = \frac{b^2}{\pi\varepsilon\sqrt{(x_m - x_n)^2 + (y_m - y_n)^2}} \qquad m \neq n \tag{2-32}$$

This approximation is 3.8 per cent in error for adjacent subsections, and has less error for nonadjacent ones. Table 2-1 shows capacitance, calculated by (2-23) using the α's obtained from the solution of (2-21), for various numbers of subareas. The second column of Table 2-1 uses the approximation (2-32), the third

TABLE 2-1. Capacitance of a Unit Square Plate
(picofarads/meter)

No. of subareas	$C/2a$ approx. l_{mn}	$C/2a$ exact l_{mn}
1	31.5	31.5
9	37.3	36.8
16	38.2	37.7
36	39.2	38.7
100	39.8	39.5

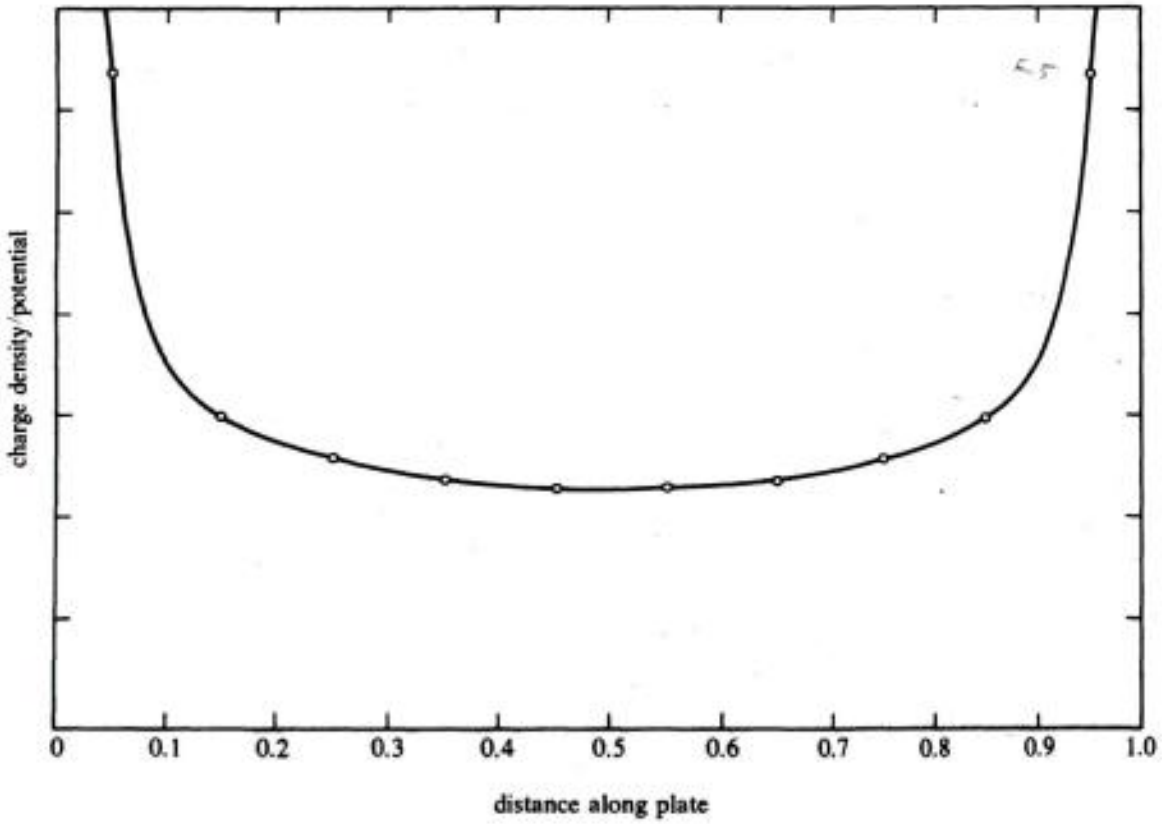

Figure 2-2. **Approximate charge density on subsections adjacent to the centerline of a square conducting plate.**

column uses an exact evaluation of the l_{mn}. A good estimate of the true capacitance is 40 picofarads. Figure 2-2 shows a plot of the approximate charge density along the subareas nearest the center line of the plate, for the case $N = 100$ subareas. Note that σ exhibits the well-known square root singularity at the edges of the plate.

Other geometries for which square subareas have been used to obtain numerical solutions are rectangular plates [2] and solid conducting cubes [5]. The related problem of a parallel-plate capacitor is treated in Section 2-4.

2-3. Conductors of Complex Shape

Often it is not possible to use square subareas for electrostatic problems. In this section we consider some simple approximations which enable almost any conducting body to be treated by subarea approximations.

First, consider the plane disk of radius r, with uniform charge density of unit amplitude. The electrostatic potential ϕ at its center is given by the simple integral

$$\phi = \int_0^{2\pi} d\theta \int_0^r \rho \, d\rho \, \frac{1}{4\pi\varepsilon\rho} = \frac{r}{2\varepsilon} \tag{2-33}$$

Let us compare this potential for a disk to that at the center of a square area with unit charge density and the same area A, given by (2-31). The result is

$$\phi_{\text{disk}} = \frac{\sqrt{A}}{\varepsilon}(0.2821)$$
$$\phi_{\text{square}} = \frac{\sqrt{A}}{\varepsilon}(0.2806) \tag{2-34}$$

There is less than 0.54 per cent difference between the two. This is because the major contribution to ϕ is due to the charge in the immediate vicinity of the field point, and this is the same in each case. Hence if a subarea is not too narrow (has a reasonably large area/perimeter ratio), a good approximation to the diagonal elements of the $[l]$ matrix is

$$l_{nn} \approx \frac{0.282}{\varepsilon}\sqrt{A_n} \tag{2-35}$$

where A_n is the area of the nth subarea. A useful approximation for the off-diagonal elements is the point-charge approximation of (2-32), which can be written in general as

$$l_{mn} \approx \frac{A_n}{4\pi\varepsilon R_{mn}} \qquad m \neq n \tag{2-36}$$

where $R_{mn} = \sqrt{(x_m - x_n)^2 + (y_m - y_n)^2 + (z_m - z_n)^2}$ is the distance between the centers of the mth and nth subareas. Approximation (2-36) cannot be used if the body has different areas very close together, as, for example, in the parallel-plate capacitor (see Section 2-4).

When the above approximations are not sufficiently accurate, the following procedure is convenient for calculating the l_{mn}. Figure 2-3 shows an elongated

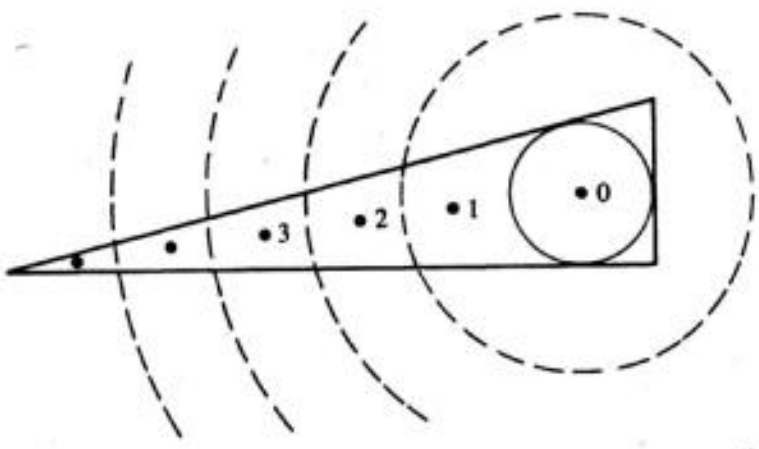

Figure 2-3. Numerical evaluation of l_{nn}.

triangular subarea. To evaluate l_{nn}, divide the area into a disk plus segments of circular annuli, as shown. Label these subsubareas 0, 1, 2,.... Then

$$l_{nn} = \frac{1}{\varepsilon}\left(0.282\sqrt{A_0} + \frac{1}{4\pi}\sum_i \frac{A_i}{R_{0i}}\right) \tag{2-37}$$

where A_0 is the area of the disk, the A_i $(i = 1, 2, \ldots)$, are the areas of the annular segments, and R_{0i} is the distance from the center of the ith annulus to the center of the disk. Equation (2-37) is basically a numerical evaluation of the integral for l_{nn}. If the subarea is not planar, the subsubareas can be taken as those lying between concentric spheres. Evaluation of l_{mn} elements for very close subareas can be accomplished in a similar manner. For problems having rotational symmetry, it is sometimes convenient to take complete annular subareas, as demonstrated by the following example.

Example. Consider a hollow conducting tube of circular cross section and length L, as shown in Fig. 2-4. We wish to determine the electrostatic capacitance.

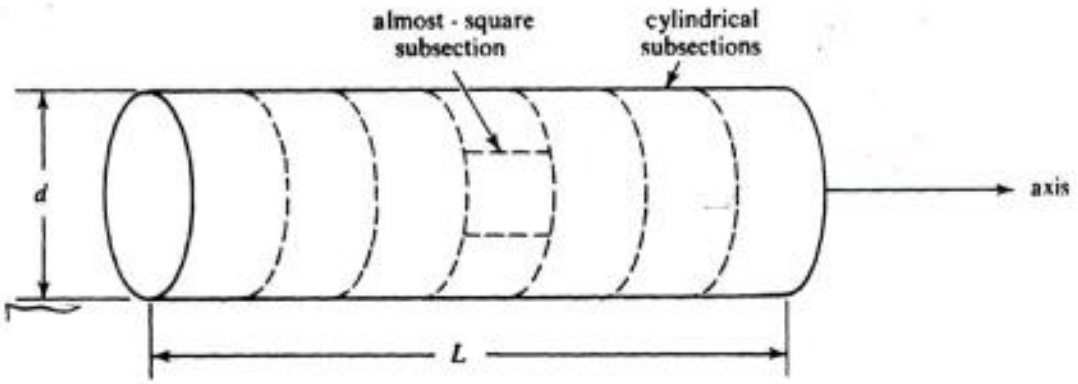

Figure 2-4. **Hollow conducting circular cylinder.**

The tube has rotational symmetry about its axis, and hence cylindrical subsections are convenient, as indicated on the figure. To evaluate the l_{mn}, each subcylinder can be further divided into smaller, almost square, subsections, as shown in Fig. 2-4. The l_{mn} for a point-matching solution are then evaluated by formulas similar to (2-37) as applied to the almost-square subsubsections. Note that for this problem all the l_{nn} are equal, and the l_{mn} depend only on $|m - n|$. Hence $[l]$ is a *Toeplitz matrix* [6].

Some numerical results are given in Table 2-2, calculated using 10 cylindrical subsections. The corresponding charge density was as expected, being almost uniform in the central region of a thin tube and singular at the ends. A similar problem, that of the capacitance of washer-type conducting plate, has been treated in the literature [7]. This latter problem was done using an analytical evaluation of the l_{mn} rather than a numerical one.

Table 2-2. Capacitance C(picofarads) for a Hollow Tube of Length 1 Meter, for Various Length/Diameter (L/d) Ratios

L/d	1	2	6	20	60
C	63	42	25	17	12

2-4. Arbitrary Excitation of Conductors

So far we have been considering only the specific problem of a charged conducting body. We now wish to take the more general viewpoint that the $[l]$ matrix characterizes the conducting body (or bodies) for any excitation. The excitation may be due to charge on the conductors or to external charges which produce an "impressed" field. The particular excitation enters only into the $[g]$ matrix of the method of moments, and hence $[l]$ depends only on the geometry of the conductors. Once the inverse matrix $[l^{-1}]$ is obtained, a specific solution is obtained by matrix multiplication according to (1-27).

To express these ideas in equation form, consider the general problem represented by Fig. 2-5. There are N conducting bodies, having net charges $q_1, q_2, \ldots, q_N$, and potentials $V_1, V_2, \ldots, V_N$. External to the conductors there may be additional sources which, in the absence of conductors, produce a potential ϕ^i (impressed field). The boundary condition is that ϕ^i plus the potential due to charges on the conductors must be constant on each conductor. In equation form, this is

$$\phi^i + \sum_{\Sigma S_n} \iint \frac{\sigma}{4\pi\varepsilon R}\, ds = \begin{cases} V_1 \text{ on } S_1 \\ V_2 \text{ on } S_2 \\ \vdots \\ V_N \text{ on } S_N \end{cases} \tag{2-38}$$

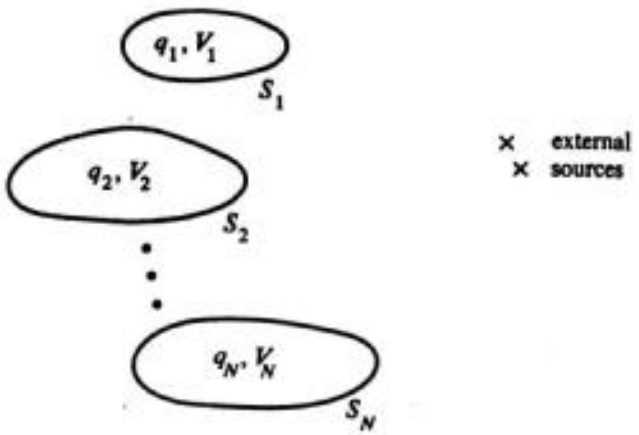

Figure 2-5. N charged conductors in the field of external sources.

where σ is the surface charge density on the conductors. The ϕ^i and V_n are assumed known, and (2-38) is an integral equation for σ. Equation (2-17) is the specialization of (2-38) to a charged conducting plate with no external sources. The total charge q_n instead of V_n may be specified on each conductor, in which case the V_n are treated as unknown constants in (2-38) to be obtained after σ is found.

Example. To illustrate these concepts, consider the two-body problem of parallel square conducting plates, as shown in Fig. 2-6. We here treat the case V_n specified on the plates but with no external sources ($\phi^i = 0$). The same plates in an impressed field are considered in Section 2-5.

Let both the top and bottom plates be divided into N square subsections, so that the total number of subsections is $2N$. The charge density is assumed constant on each subsection, and the total field is matched at the center of each subsection. The evaluation of the $[l]$ matrix follows the procedure of Section 2-2, and results in the following $2N$ by $2N$ matrix

$$[l] = \begin{bmatrix} [l^{tt}] & [l^{tb}] \\ [l^{bt}] & [l^{bb}] \end{bmatrix} \tag{2-39}$$

where t denotes "top plate" and b denotes "bottom plate." The N by N submatrices on the diagonal are single-plate matrices; hence

$$[l^{tt}] = [l^{bb}] = [l] \qquad \text{of Section 2-2} \tag{2-40}$$

The off-diagonal submatrices are the plate-to-plate matrices, which must be equal:

$$[l^{tb}] = [l^{bt}] \tag{2-41}$$

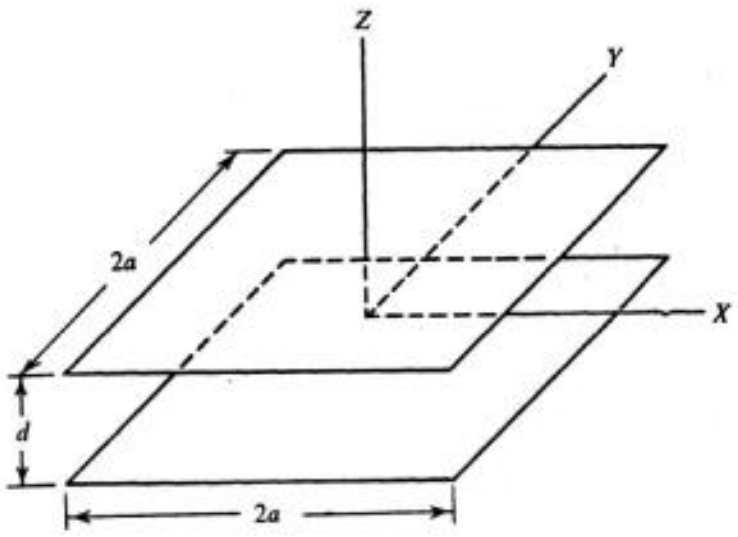

Figure 2-6. Parallel square conducting plates.

Let the elements l^{tb}_{mn} be ordered so that when $m = n$ the subareas are one on top of the other; that is, they coincide as $d \to 0$. Now if $m \neq n$, the point-charge approximation of (2-32) gives good results; that is,

$$l^{tb}_{mn} = \frac{b^2}{\pi\varepsilon\sqrt{(x_m - x_n)^2 + (y_m - y_n)^2 + d^2}} \tag{2-42}$$

When $m = n$, the square subsection can be approximated by a circular one of the same area, and the potential evaluated a distance d above it. The integration gives (2-33) with r replaced by $\sqrt{r^2 + d^2} - d$; hence the desired l^{tb}_{nn} is (2-35) modified by the ratio of these factors, or

$$l^{tb}_{nn} \approx \frac{0.282}{\varepsilon}(2b)\left[\sqrt{1 + \frac{\pi}{4}\left(\frac{d}{b}\right)^2} - \frac{\sqrt{\pi}\,d}{2b}\right] \tag{2-43}$$

This completes the evaluation of $[l]$.

Suppose we wish to evaluate the usual capacitance between the two plates. This corresponds to voltage $+V$ on the top plate and $-V$ on the bottom one. Hence the excitation matrix is

$$[g_m] = \begin{bmatrix} [g^t_m] \\ [g^b_m] \end{bmatrix} \tag{2-44}$$

where

$$[g^t_m] = -[g^b_m] = \begin{bmatrix} V \\ V \\ \vdots \\ \vdots \end{bmatrix} \tag{2-45}$$

The α_n correspond to the charge densities on each subarea and are given by (1-27). However, for this problem, it is evident from symmetry that the charge density on the top plate is minus that on the bottom plate. Hence

$$[\alpha_n] = \begin{bmatrix} [\alpha^t_n] \\ [\alpha^b_n] \end{bmatrix} = \begin{bmatrix} [\alpha^t_n] \\ -[\alpha^t_n] \end{bmatrix} \tag{2-46}$$

and we can use this to reduce $[l][\alpha] = [g]$ to

$$[l^{tt}_{mn} - l^{tb}_{mn}][\alpha^t_n] = [g^t_m] \tag{2-47}$$

which is only an N by N matrix equation. The charge densities on the top plate are now found by inversion as

$$[\alpha^t_m] = [(l^{tt} - l^{tb})^{-1}_{mn}][g^t_n] \tag{2-48}$$

where $[g^t]$ is given by (2-45). The capacitance of the parallel-plate capacitor is

$$C = \frac{\text{charge on top plate}}{V}$$

$$= \frac{1}{V} \sum_{\text{top}} \alpha_n^t \, \Delta s_n \tag{2-49}$$

Since all the $\Delta s = 4b^2$ and all elements of $[g^t] = V$, this can be written

$$C = 4b^2 \sum_{mn} (l^{tt} - l^{tb})^{-1}_{mn} \tag{2-50}$$

which is simply $4b^2$ times the sum of all elements of $[(l^{tt} - l^{tb})^{-1}]$.

Computations for this case have been made and compared with other approximate solutions [8]. When fringing is neglected, the capacity is $C \approx \varepsilon A/d$. Figure 2-7 shows the results obtained from (2-50) for the case $N = 36$, normalized to $\varepsilon A/d$. It is interesting to note that, when d is as little as $0.05a$, neglecting fringing results in 6 per cent error. The error rapidly increases as d becomes larger, becoming 100 per cent as $d \to \infty$.

Now suppose we want the capacitance of the two plates when connected together. This is obtained by keeping both plates at the same potential V. Then, instead of (2-45), we have

$$[g_m^t] = [g_m^b] = \begin{bmatrix} V \\ V \\ \vdots \\ \vdots \end{bmatrix} \tag{2-51}$$

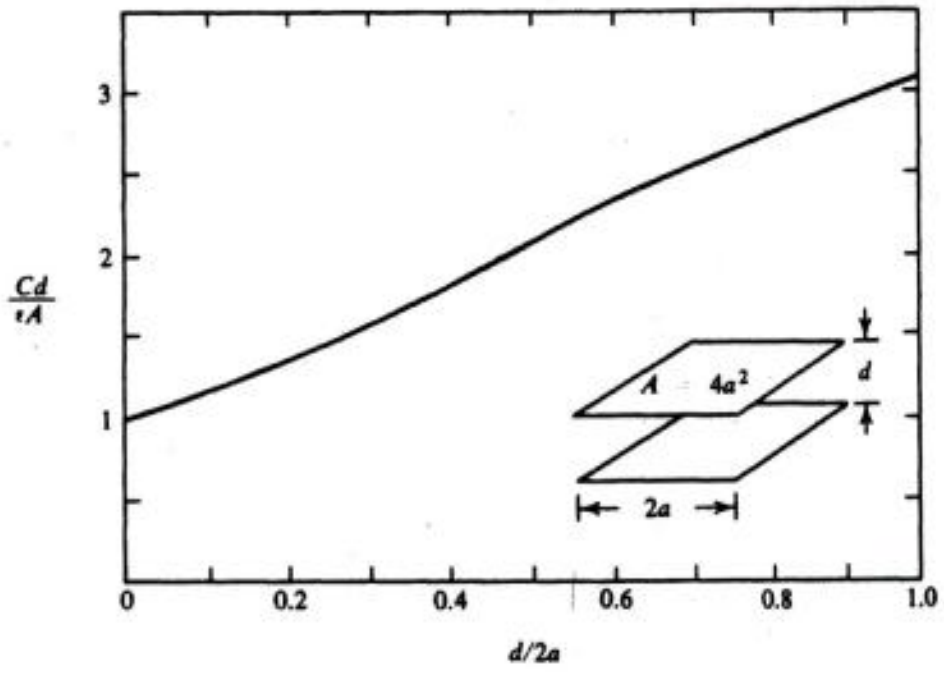

Figure 2-7. Capacitance of a square parallel-plate capacitor, normalized to $\varepsilon A/d$.

and, from symmetry, instead of (2-46),

$$[\alpha_n] = \begin{bmatrix} [\alpha_n^t] \\ [\alpha_n^t] \end{bmatrix} \tag{2-52}$$

Analogous to (2-47), the N by N matrix equation for the present excitation is

$$[l_{mn}^{tt} + l_{mn}^{tb}][\alpha_n^t] = [g_m^t] \tag{2-53}$$

and, analogous to (2-48), the solution is

$$[\alpha_m^t] = [(l^{tt} + l^{tb})_{mn}^{-1}][g_n^t] \tag{2-54}$$

The capacitance of the two plates connected together is then

$$C = \frac{\text{total charge}}{V}$$

$$= \frac{2}{V} \sum_{\text{top}} \alpha_n^t \, \Delta s_n \tag{2-55}$$

which can also be written in the form of (2-50) as

$$C = 8b^2 \sum_{mn} (l^{tt} + l^{tb})_{mn}^{-1} \tag{2-56}$$

Note that as $d \to 0$, $[l^{tt}] \to [l^{tb}]$ and C becomes the capacitance of a single plate (Section 2-2). As $d \to \infty$, $[l^{tb}] \to 0$, and C becomes twice the capacitance of a single plate.

2-5. Electric Polarizability

If a conducting body with no net charge is placed in a uniform electrostatic field, a net dipole moment $\mathbf{p}$ usually results. In general,

$$\mathbf{p} = \oiint_S \mathbf{r}\sigma \, ds \tag{2-57}$$

where $\mathbf{r} = \mathbf{u}_x x + \mathbf{u}_y y + \mathbf{u}_z z$ is the radius vector from the origin to a point on the surface S of the conductor, and $\sigma(x, y, z)$ is the surface charge density on S. The dipole moment is proportional to the impressed field $\mathbf{E}^i$ which produces σ; hence

$$\mathbf{p} = [\chi] \cdot \mathbf{E}^i \tag{2-58}$$

where $[\chi]$ is the *polarizability tensor*. Elements of $[\chi]$ may be found by applying a unit field $\mathbf{E}$ and evaluating components of $\mathbf{p}$. For example, $\chi_{xy} = p_x$ for

$\mathbf{E} = \mathbf{u}_y$, and so on. The polarizability tensor is a useful quantity for the analysis of artificial dielectrics [9] and for scattering by small objects.

The appropriate integral equation is (2-38) specialized to a single conducting body S, which is

$$\oiint_S \frac{\sigma}{4\pi\varepsilon R}\, ds = V - \phi^i \tag{2-59}$$

where ϕ^i is a potential from which the electrostatic field is determined by $\mathbf{E}^i = -\nabla\phi^i$. The constant potential V must be obtained from the condition

$$\oiint_S \sigma\, ds = 0 \tag{2-60}$$

That is, the net charge on S is zero. Whenever $\mathbf{E}^i$ is perpendicular to a plane of reflection symmetry for the conductor, we can choose $\phi^i = 0$ on that plane and $V = 0$ in (2-59), which is equivalent to satisfying condition (2-60).

Example. Consider the parallel conducting plates of Fig. 2-6. We wish to determine the polarizability tensor when they are connected together, that is, maintained at the same potential. From symmetry considerations, it is apparent that an E_x will produce only a p_x, an E_y only a p_y, and an E_z only a p_z. Hence the polarizability tensor is diagonal:

$$[\chi] = \begin{bmatrix} \chi_{xx} & 0 & 0 \\ 0 & \chi_{yy} & 0 \\ 0 & 0 & \chi_{zz} \end{bmatrix} \tag{2-61}$$

and the x, y, and z axes are principal axes of $[\chi]$. Also, from symmetry, $\chi_{xx} = \chi_{yy}$ for square plates.

To evaluate χ_{zz}, take $\mathbf{E}^i = \mathbf{u}_z$ and $\phi^i = -z$. Note that $\phi^i = 0$ on $z = 0$, the plane of symmetry, and hence (2-60) will be satisfied. Now the integral equation (2-59) becomes

$$\oiint_S \frac{\sigma}{4\pi\varepsilon R}\, ds = \begin{cases} d/2 & \text{on top plate} \\ -d/2 & \text{on bottom plate} \end{cases} \tag{2-62}$$

This is the same integral equation as for the parallel-plate capacitor, except that V is replaced by $d/2$. Hence the charge distribution is given by (2-48), where

$$[g^t] = \begin{bmatrix} \frac{d}{2} \\ \frac{d}{2} \\ \vdots \end{bmatrix} \tag{2-63}$$

The polarizability is then found by approximating (2-57) by the summation

$$\chi_{zz} = p_z = \sum_{n=1}^{N} \left(\frac{d}{2} \alpha_n \Delta s_n + \frac{d}{2} \alpha_n \Delta s_n \right)$$

$$= \frac{d^2 \Delta s}{2} \sum_{mn} (l^{tt} - l^{tb})^{-1}_{mn} \tag{2-64}$$

where $\Delta s = 4b^2$. In terms of the capacitance between the parallel plates, (2-50),

$$\chi_{zz} = \tfrac{1}{2} d^2 C \tag{2-65}$$

This relationship between polarizability and capacitance results because of the parallel-plate nature of the problem, and does not result in general. As a check on (2-65), note that $q = CV = Cd/2$, and $p_z = qd = d^2C/2$. Note that when fringing can be neglected, (2-65) becomes

$$\chi_{zz} \approx \tfrac{1}{2} \varepsilon \, dA = \frac{\varepsilon}{2} (\text{volume}) \tag{2-66}$$

where A is the area of one plate and the volume is that between the plates.

For the other two elements $\chi_{xx} = \chi_{xy}$ of (2-61), let $\mathbf{E}^i = \mathbf{u}_x$ and $\phi^i = -x$. Again $\phi^i = 0$ on a plane of symmetry, whence (2-60) is satisfied. Now, instead of (2-62), the integral equation is

$$\oint\!\!\oint \frac{\sigma}{4\pi\varepsilon R} \, ds = -x \qquad \text{on the plates} \tag{2-67}$$

It is evident that the charge distribution is the same on both plates, and hence is given by (2-54) with

$$[g_n^t] = \begin{bmatrix} x_1 \\ x_2 \\ \vdots \\ \vdots \end{bmatrix} \tag{2-68}$$

where x_n is the x coordinate of the Δs_n subarea. The approximate evaluation of (2-57) then gives

$$\chi_{xx} = p_x = \sum_{n=1}^{N} x_n 2\alpha_n \Delta s_n$$

$$= 8b^2 \sum_{mn} x_m (l^{tt} + l^{tb})^{-1}_{mn} x_n \tag{2-69}$$

Another way of writing this result is

$$\chi_{xx} = 2b^2[\tilde{g}^t_m][(l^{tt} + l^{tb})^{-1}_{mn}][g^t_n] \tag{2-70}$$

where $\sim$ denotes transpose. This is a form that we shall encounter again in subsequent chapters.

2-6. Dielectric Bodies

The electrical state of a dielectric body in an electrostatic field is characterized by its polarization,

$$\mathbf{P} = \mathbf{D} - \varepsilon_0 \mathbf{E} = (\varepsilon - \varepsilon_0)\mathbf{E} \tag{2-71}$$

where ε is the capacitivity (permittivity) of the dielectric and ε_0 that of vacuum. The electric field due to the polarization is given by [10]

$$\mathbf{E}^p = \mathscr{E}(\mathbf{P}) = -\nabla\left(\iiint \frac{\mathbf{P} \cdot \mathbf{u}_R}{4\pi\varepsilon_0 R^2}\, d\tau\right) \tag{2-72}$$

where $\mathbf{u}_R$ is the unit vector pointing from the source point to the field point. Basically (2-72) is a superposition of the fields from all dipole elements $\mathbf{P}d\tau$ of source. The total field $\mathbf{E}^i + \mathbf{E}^p$ must satisfy (2-71) in the dielectric; hence an integral equation for $\mathbf{P}$ is

$$\mathbf{E}^i + \mathscr{E}(\mathbf{P}) = \frac{1}{\Delta\varepsilon}\mathbf{P} \tag{2-73}$$

where $\mathscr{E}$ is defined by (2-72) and $\Delta\varepsilon = \varepsilon - \varepsilon_0$.

A solution may be obtained by subsection and point-matching techniques. In canonical form (2-73) is

$$L(\mathbf{P}) = \mathscr{E}(\mathbf{P}) - \frac{1}{\Delta\varepsilon}\mathbf{P} = -\mathbf{E}^i \tag{2-74}$$

The functions in (2-74) are vectors, and require three numbers to represent them at a point. Following the method of moments, we use the following subsectional basis functions:

$$f_n = \begin{cases} (\mathbf{u}_x, \mathbf{u}_y, \mathbf{u}_z) & \text{in } \Delta\tau_n \\ (0, 0, 0) & \text{elsewhere} \end{cases} \tag{2-75}$$

where the $\mathbf{u}$'s are coordinate unit vectors and $\Delta\tau_n$ is a representative volume element. The elements of the α_n coefficients of (1-21) can then be interpreted as the amplitude of the x, y, and z components of $\mathbf{P}$ in $\Delta\tau_n$; that is

$$\begin{aligned}\alpha_n &= (\alpha_{nx}, \alpha_{ny}, \alpha_{nz}) \\ &= \mathbf{P}(x_n, y_n, z_n) = \mathbf{P}_n\end{aligned} \tag{2-76}$$

where (x_n, y_n, z_n) are the coordinates of the center of $\Delta\tau_n$. Using the expansion (1-21) in (2-74), and matching the resultant equation at the centers of all $\Delta\tau_m$, we obtain the matrix equation

$$[l_{mn}][\mathbf{P}_n] = -[\mathbf{E}_m^i] \tag{2-77}$$

where $\mathbf{E}_m^i = \mathbf{E}^i(x_m, y_m, z_m)$. Each element of $[l]$ is a dyadic, of the form

$$l_{mn} = \begin{bmatrix} e_{mn}^{xx} - \dfrac{1}{\Delta\varepsilon} & e_{mn}^{xy} & e_{mn}^{xz} \\ e_{mn}^{yx} & e_{mn}^{yy} - \dfrac{1}{\Delta\varepsilon} & e_{mn}^{yz} \\ e_{mn}^{zx} & e_{mn}^{zy} & e_{mn}^{zz} - \dfrac{1}{\Delta\varepsilon} \end{bmatrix} \tag{2-78}$$

where the e_{mn} are derived from $\mathscr{E}$ in the same manner as the l_{mn} are derived from L. For a physical interpretation of the elements of (2-78), we note that e_{mn}^{xx} is the x component of $\mathbf{E}$ at (x_m, y_m, z_m) due to $\mathbf{P} = \mathbf{u}_x$ at (x_n, y_n, z_n), e_{mn}^{yx} is the y component of $\mathbf{E}$ due to the same $\mathbf{P}$, etc. The solution to (2-77) is, of course, given by

$$[\mathbf{P}_m] = -[l_{mn}^{-1}][\mathbf{E}_n^i] \tag{2-79}$$

If m and n range from 1 to N, this is a $3N$ by $3N$ matrix equation due to the vector nature of $\mathbf{P}$ and $\mathbf{E}$. Note that the e terms of (2-78) are independent of ε, which enters only into the $\Delta\varepsilon$ terms.

For crude solutions, the following approximations are often adequate. When $m \neq n$ each $\mathbf{P}_n\,\Delta\tau_n$ can be viewed as a point dipole, and $\mathbf{E}$ evaluated at $\Delta\tau_m$. The result is

$$e_{mn}^{ij} \approx \mathbf{u}_i \cdot e_{mn} \cdot \mathbf{u}_j \tag{2-80}$$

where i, j denote x, y, or z, and e_{mn} is the dyad

$$e_{mn} = -\frac{\Delta\tau_n}{4\pi\varepsilon_0} \nabla_m(\mathbf{R}/R^3) \tag{2-81}$$

where $\mathbf{R} = \mathbf{u}_x(x_m - x_n) + \mathbf{u}_y(y_m - y_n) + \mathbf{u}_z(z_m - z_n)$. When $m = n$ the field can be approximated by that at the center of a sphere having the same **P**. This results in

$$e_{nn}^{ii} \approx -\frac{1}{3\varepsilon_0} \tag{2-82}$$

and $e_{nn}^{ij} = 0$, $i \neq j$. For better results, the approximation (2-82) may be replaced by the field at the center of a spheroid or cylinder which approximates $\Delta\tau$. Still better results can be obtained by numerical integrations similar to those of Section 2-3.

The above solution remains valid for inhomogeneous dielectrics (ε a function of position), in which case the ε of each $\Delta\tau$ is taken to be that at its center. For *homogeneous* dielectrics, the problem can be formulated in terms of a surface distribution of bound charge [11], instead of a volume distribution of **P**. Since charge is a scalar quantity, this procedure materially reduces the number of unknowns in the matrix solution.

References

[1] R. F. Harrington, *Introduction to Electromagnetic Engineering*, McGraw-Hill Book Co., New York, 1958, pp. 117–120.

[2] D. Reitan and T. Higgins, "Accurate Determination of the Capacitance of a Thin Conducting Rectangular Plate," *A.I.E.E. Trans.*, Vol. **75**, Part I, Jan. 1957, pp. 761–766.

[3] J. Van Bladel, *Electromagnetic Fields*, McGraw-Hill Book Co., New York, 1964, p. 96.

[4] H. B. Dwight, *Tables of Integrals and Other Mathematical Data*, The Macmillan Co., New York, 1947.

[5] D. Reitan and T. Higgins, "Calculation of the Electrical Capacitance of a Cube," *Journ. Appl. Phys.*, Vol. **22**, No. 2, Feb. 1951, pp. 223–226.

[6] U. Grenander and G. Szegö, *Toeplitz Forms and Their Applications*, University of California Press, Berkeley, 1958.

[7] T. Higgins and D. Reitan, "Calculation of the Capacitance of a Circular Annulus by the Method of Subareas," *A.I.E.E. Trans.*, Vol. **70**, 1951, pp. 926–933.

[8] D. K. Reitan, "Accurate Determination of the Capacitance of Rectangular Parallel-Plate Capacitors," *Journ. Appl. Phys.*, Vol. **30**, No. 2, Feb. 1959, pp. 172–176.

[9] R. E. Collin, *Field Theory of Guided Waves*, McGraw-Hill Book Co., New York, 1960, Chap. 12.

[10] R. Plonsey and R. E. Collin, *Principles and Applications of Electromagnetic Fields*, McGraw-Hill Book Co., New York, 1961, p. 75.

[11] Reference [3], pp. 73–77.

CHAPTER

3

Two-dimensional Electromagnetic Fields

3-1. Transverse Magnetic Fields

To avoid unnecessary details, we start our consideration of electromagnetic fields with two-dimensional problems. These can be thought of as three-dimensional problems for which there is no variation of field quantities with respect to one cartesian coordinate, taken to be the z coordinate. We postpone a general discussion of three-dimensional fields until Chapter 5, after we have treated a number of special cases.

An arbitrary electromagnetic field can be expressed as the sum of a *transverse magnetic* (TM) part and a *transverse electric* (TE) part. The TM part has only components of magnetic field $\mathbf{H}$ transverse to z, and the TE part has only components of $\mathbf{E}$ transverse to z. For two-dimensional fields in isotropic media, the TM part has only a z component of $\mathbf{E}$ and the TE part only a z component of $\mathbf{H}$. In many cases the TM and TE parts can be treated separately, reducing the problem to a scalar problem. In this section we consider only TM fields, the TE case being considered in Section 3-4.

In general a time-harmonic electromagnetic field ($e^{j\omega t}$ time variation) satisfies the *Maxwell equations*

$$\nabla \times \mathbf{E} = -j\omega\mu\mathbf{H} \tag{3-1}$$

$$\nabla \times \mathbf{H} = j\omega\varepsilon\mathbf{E} + \mathbf{J} \tag{3-2}$$

where $\mathbf{J}$ is the volume distribution of electric currents. For TM fields, assume

that $\mathbf{E} = \mathbf{u}_z E_z(x, y)$, and similarly for $\mathbf{J}$. The Maxwell equations then lead to

$$\nabla^2 E_z + k^2 E_z = j\omega\mu J_z \tag{3-3}$$

where $k = \omega\sqrt{\varepsilon\mu} = 2\pi/\lambda$ is the wavenumber (λ = wavelength). Equation (3-3) is the two-dimensional *Helmholtz equation*. Solutions may be obtained by first finding the field from a two-dimensional point source, that is, a three-dimensional line source. The field at $\boldsymbol{\rho} = \mathbf{u}_x x + \mathbf{u}_y y$ due to a filament of current I at $\boldsymbol{\rho}' = \mathbf{u}_x x' + \mathbf{u}_y y'$ is [1]

$$E_z = \frac{-k\eta}{4} I H_0^{(2)}(k\,|\boldsymbol{\rho} - \boldsymbol{\rho}'|) \tag{3-4}$$

where $\eta = \sqrt{\mu/\varepsilon} \approx 120\pi$ is the intrinsic impedance of free space and $H_0^{(2)}$ is the Hankel function of the second kind, zero order. The E_z of (3-4) is the *Green's function* for the operator of (3-3). A general solution is then the superposition of E_z due to all elements of source $J_z\,ds$, or

$$E_z(\boldsymbol{\rho}) = \frac{-k\eta}{4} \iint J_z(\boldsymbol{\rho}') H_0^{(2)}(k\,|\boldsymbol{\rho} - \boldsymbol{\rho}'|)\,ds' \tag{3-5}$$

where the integration is over the cross section of the cylinder of currents J_z.

3-2. Conducting Cylinders, TM Case

Consider a perfectly conducting cylinder excited by an impressed electric field E_z^i, as represented by Fig. 3-1. The impressed field induces surface currents J_z on the conducting cylinder, which produce a scattered field E_z^s. The field due to J_z is given by (3-5) specialized to the cylinder surface C. The boundary condition is

$$E_z = E_z^i + E_z^s = 0 \qquad \text{on } C \tag{3-6}$$

that is, the tangential electric field vanishes on C. Hence, combining (3-5) and (3-6), we have the integral equation

$$E_z^i(\boldsymbol{\rho}) = \frac{k\eta}{4} \int_C J_z(\boldsymbol{\rho}') H_0^{(2)}(k\,|\boldsymbol{\rho} - \boldsymbol{\rho}'|)\,dl' \qquad \rho \text{ on } C \tag{3-7}$$

where $E_z^i(\boldsymbol{\rho})$ is known and J_z is the unknown to be determined.

The simplest numerical solution of (3-7) consists of using pulse functions for a basis and point matching for testing. To accomplish this, the scatterer contour C is divided into N segments ΔC_n and pulse functions defined as

$$f_n(\boldsymbol{\rho}) = \begin{cases} 1 & \text{on } \Delta C_n \\ 0 & \text{on all other } \Delta C_m \end{cases} \tag{3-8}$$

Letting $J_z = \sum \alpha_n f_n$, substituting in (3-7), and satisfying the resultant equation at the midpoint (x_m, y_m) of each ΔC_m, we obtain the matrix equation

$$[l_{mn}][\alpha_n] = [g_m] \tag{3-9}$$

where the elements of $[\alpha_n]$ are the α_n coefficients, the elements of $[g_m]$ are

$$g_m = E_z^i(x_m, y_m) \tag{3-10}$$

and the elements of $[l_{mn}]$ are

$$l_{mn} = \frac{k\eta}{4} \int_{\Delta C_n} H_0^{(2)}[k\sqrt{(x - x_m)^2 + (y - y_m)^2}]\, dl \tag{3-11}$$

A solution for the current is then given by $J_z = [f_n][l_{nm}^{-1}][g_m]$, as discussed in Section 1-3.

There is no simple analytic expression for the integral (3-11), but we can evaluate it by various approximations. The crudest approximation is to treat an element $J_z\, \Delta C_n$ as a filament of current when the field point is not on ΔC_n; that is,

$$l_{mn} \approx \frac{\eta}{4} k\, \Delta C_n H_0^{(2)}[k\sqrt{(x_n - x_m)^2 + (y_n - y_m)^2}] \tag{3-12}$$

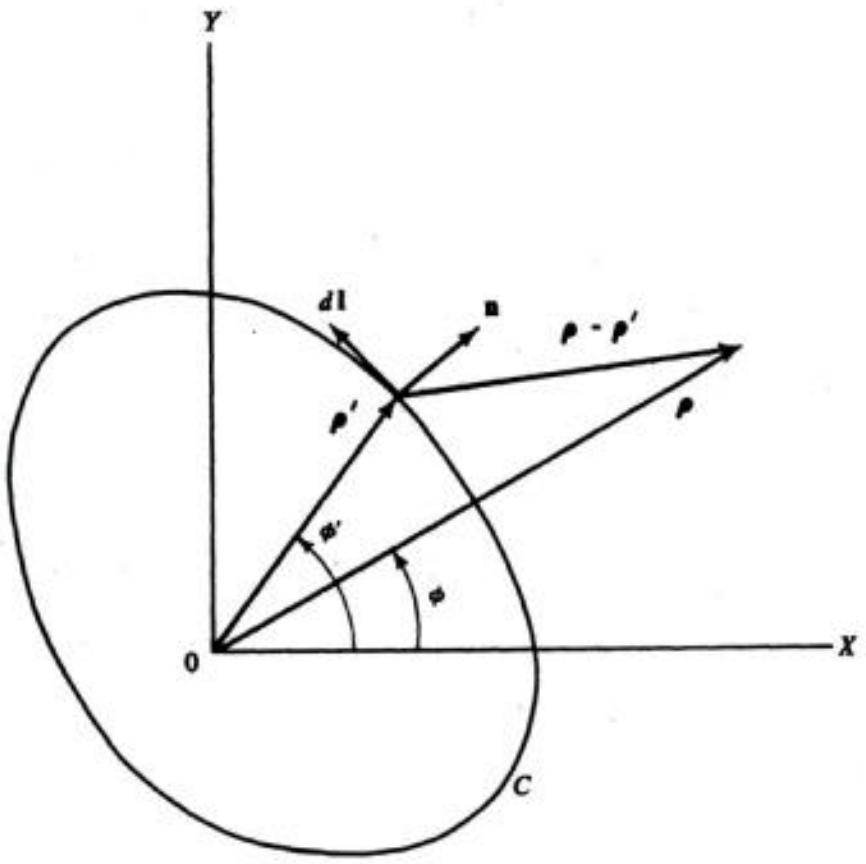

Figure 3-1. Cross section of a cylinder and coordinate system.

when $m \neq n$. For the diagonal elements l_{nn} the Hankel function has an integrable singularity, and the integral must be evaluated analytically. For this, we approximate ΔC_n by a straight line and use the small argument formula

$$H_0^{(2)}(z) \approx 1 - j\frac{2}{\pi}\log\left(\frac{\gamma z}{2}\right) \tag{3-13}$$

where $\gamma = 1.781\ldots$ is Euler's constant. An evaluation of (3-11) then gives

$$l_{nn} \approx \frac{\eta}{4} k\,\Delta C_n\left[1 - j\frac{2}{\pi}\log\left(\frac{\gamma k\,\Delta C_n}{4e}\right)\right] \tag{3-14}$$

where $e = 2.718\ldots$ The approximations (3-12) and (3-14) are analogous to those used in Section 2-2 for electrostatic problems. Better approximations for the present problem will be discussed in Section 3-3.

Example. Consider TM plane-wave scattering by conducting cylinders [2,3]. In this case the impressed field is a uniform plane wave, which, if incident from the direction ϕ_i, is given by

$$E_z^i = e^{jk(x\cos\phi_i + y\sin\phi_i)} \tag{3-15}$$

This determines the excitation $[g_m]$ according to (3-10). An approximate evaluation of $[l_{mn}]$ is given by (3-12) and (3-14). The solution for J_z is then found by matrix inversion in the usual manner.

A parameter of interest is the *scattering cross section* σ, defined as the width (area in three-dimensional problems) for which the incident wave carries sufficient power to produce, by omnidirectional radiation, the same scattered power density in a given direction. In equation form, this is

$$\sigma(\phi) = 2\pi\rho\left|\frac{E^s(\phi)}{E^i}\right|^2 \tag{3-16}$$

where $E^s(\phi)$ is the distant field from J_z. It can be found by using the asymptotic expression for $H_0^{(2)}$ in (3-5). The result is [1]

$$E^s(\phi) = \eta k K \int_C J_z(x', y')e^{jk(x'\cos\phi + y'\sin\phi)}\,dl' \tag{3-17}$$

where

$$K(\rho) = \frac{1}{\sqrt{8\pi k\rho}}\,e^{-j(k\rho + 3\pi/4)} \tag{3-18}$$

Substituting (3-15) and (3-17) in (3-16), we obtain

$$\sigma(\phi) = \frac{k\eta^2}{4}\left|\int_C J_z(x', y')e^{jk(x'\cos\phi + y'\sin\phi)}\,dl'\right|^2 \tag{3-19}$$

This can be evaluated numerically once J_z is found.

A particularly descriptive form for the evaluation of (3-19) is obtained as follows. Let the integral be approximated by a sum over all ΔC_n, with $J_z = \alpha_n$, $x = x_n$, $y = y_n$ in the integrand for each ΔC_n. The result is

$$\sigma(\phi_i, \phi_s) = \frac{k\eta^2}{4}|[V_n^s][Z_{nm}^{-1}][V_m^i]|^2 \tag{3-20}$$

where $[V_m^i]$ is an "excitation" voltage matrix

$$[V_m^i] = [\Delta C_m e^{jk(x_m\cos\phi_i + y_m\sin\phi_i)}] \tag{3-21}$$

$[Z_{mn}]$ is a scatterer "impedance" matrix

$$[Z_{mn}] = [\Delta C_m l_{mn}] \tag{3-22}$$

and $[V_n^s]$ is a "measurement" voltage matrix.

$$[V_n^s] = [\Delta C_n e^{jk(x_n\cos\phi_s + y_n\sin\phi_s)}] \tag{3-23}$$

where $\phi = \phi_s$ is the angle at which σ is evaluated. We shall encounter this form again in Section 3-6 and subsequent chapters, it being a special case of the generalized network parameters discussed in Chapter 5. Note that (3-20) obeys the reciprocity relationship $\sigma(\phi_i, \phi_s) = \sigma(\phi_s, \phi_i)$; that is, the scattering cross section is unchanged if the transmitter and receiver are interchanged.

A number of computations have been made for rectangular conducting cylinders using approximations similar to those above [2]. A more accurate numerical evaluation of the integral equation was used by Andreasen to compute solutions for cylinders of other shapes [3]. It should be pointed out that the approximations made above will not converge to the exact solution as N is increased, because the l_{mn}, $m \neq n$, are not exact in the limit. The solution will converge to the exact solution if (3-12) is replaced by a more accurate approximation. To illustrate the accuracy that can be obtained using the simple approximations of this section, Fig. 3-2 shows the magnitude of the current on an ellipse as computed by Andreasen and by the formulas of this section. It is interesting to note that if the current is calculated by $\mathbf{n} \times \mathbf{H}$ on C instead of using the α_n, a better solution is obtained, as indicated in Fig. 3-2. The scattering cross section, as computed by Andreasen and by the above formulas, is illustrated by Fig. 3-3.

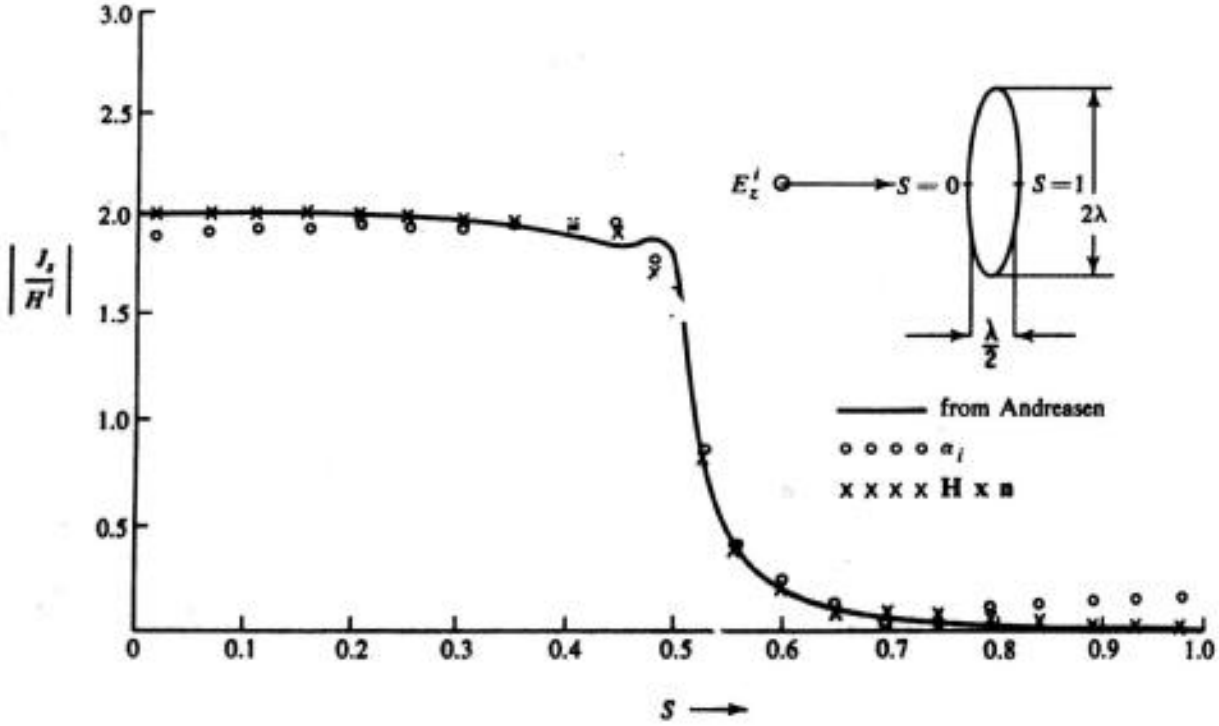

Figure 3-2. Current density on a conducting elliptic cylinder excited by a plate wave, TM case.

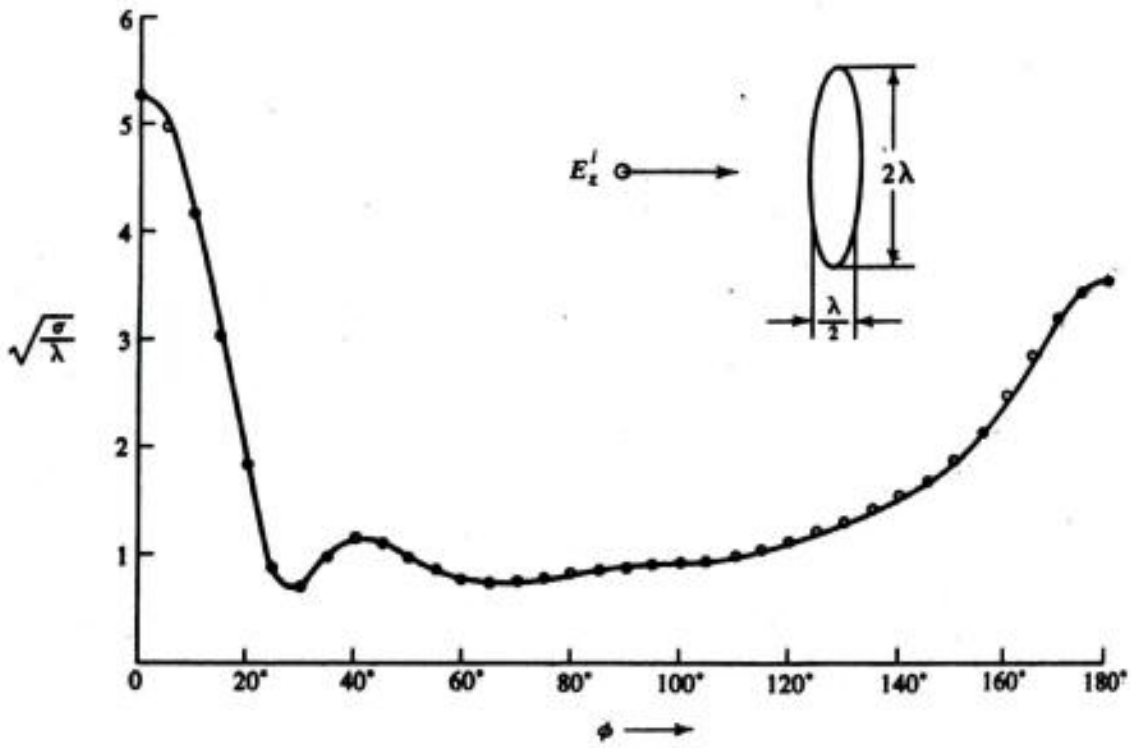

Figure 3-3. Scattered field pattern for a conducting elliptic cylinder excited by a plane wave, TM case.

Note that the two results are almost identical, even though the currents (Fig. 3-2), differ appreciably. This is because $\sqrt{\sigma}$ is a continuous linear functional of J, and hence is insensitive to small variations in J about its true value (Section 1-8).

3-3. Various Approximations

The accuracy of a solution and the rate of convergence depend upon the approximations made. The solution of Section 3-2 can be improved by more accurate evaluation of the l_{mn}, as follows. For the l_{nn}, additional terms can be included in (3-13), but this will not appreciably affect convergence, since (3-14) is exact in the limit $\Delta C_n \to 0$. For the l_{mn} terms, $m \neq n$, we can expand the integrand of (3-11) in a Taylor series about (x_n, y_n), and integrate the dominant terms analytically. This will give both improved accuracy and convergence to the exact solution as $N \to \infty$.

It has been found that the rate of convergence is almost twice as fast if a piecewise linear approximation to J_z is used instead of the step approximation. In other words, the Nth-order linear solution gives about the same accuracy as the $2N$th-order step solution. For a piecewise linear solution, instead of the steps of (3-8) we use the triangles of (1-50), as discussed in Section 1-5. The evaluation of the l_{mn} proceeds similarly to that for the pulse functions [4].

Solutions have also been obtained by Galerkin's method, using pulses for both expansion and testing functions. It was found that, for solutions of the subsectional-basis type, the accuracy and convergence of the Galerkin solution were about the same as for the point-matching solution. The Galerkin method apparently has its greatest utility in perturbational solutions, that is, when the solution is represented by only one expansion function, or by a few functions.

Perhaps the most convenient way of obtaining better approximations when using computers is to numerically evaluate the l_{mn}. For this, we divide each ΔC_n into smaller subintervals, and approximate the integral over each subinterval by (3-12) if nonsingular and by (3-14) if singular. To be explicit, let Fig. 3-4(a) represent a small section of the contour of a cylindrical conductor. Let the subintervals ΔC_{n-1}, ΔC_n, and ΔC_{n+1} be further subdivided as indicated by points a, b, c, and d. Figure 3-4(b) shows the same contour straightened out, and an expansion function constructed of three pulses. This three-stepped function approximates a triangle function, shown dashed. Now, remembering that each l_{mn} represents the field $-E_z$ at (x_m, y_m) due to expansion function f_n at (x_n, y_n), we can easily justify that, for $m = n$,

$$l_{mn} = (\tfrac{1}{2}l_{21} + l_{22} + \tfrac{1}{2}l_{23})_{mn} \tag{3-24}$$

where l_{21} and l_{23} are given by (3-12) with ΔC_n replaced by C_{ab} and C_{cd}, and l_{22} is given by (3-14) with ΔC_n replaced by C_{bc} (see Fig. 3-4). The factors 1/2 in the first and third terms of (3-24) arise from the fact that the pulses over C_{ab} and C_{cd} are one half the amplitude of the pulse over C_{bc}. For the l_{mn} elements, $m \neq n$, the

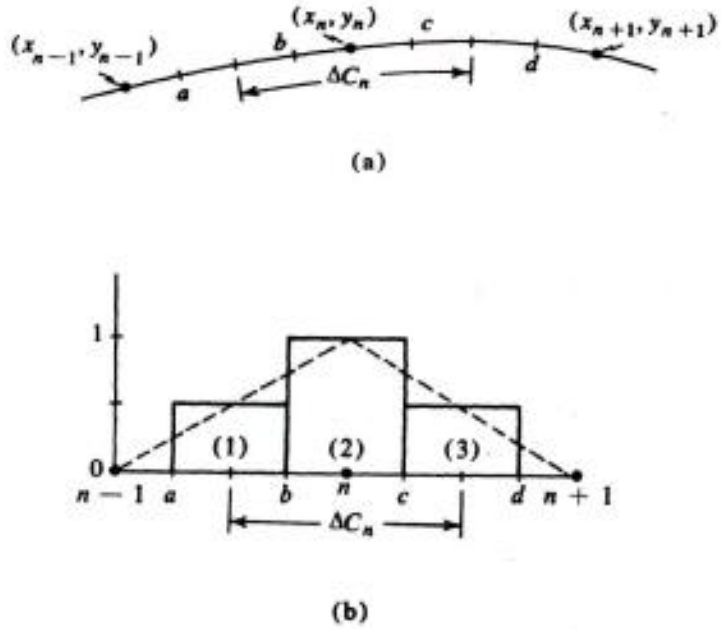

Figure 3-4. **(*a*) Section of the contour. (*b*) Expansion function consisting of three constrained pulses.**

procedure is the same, except that (3-12) is used for all l_{ij} since the field point never coincides with the source point.

To illustrate the accuracy obtainable with the above procedure, Fig. 3-5 shows the resultant current compared with Andreasen's results [3]. Note that we have taken smaller ΔC's in the region of rapid curvature on the ellipse for better accuracy. It was found that when point m was distant from point n, say

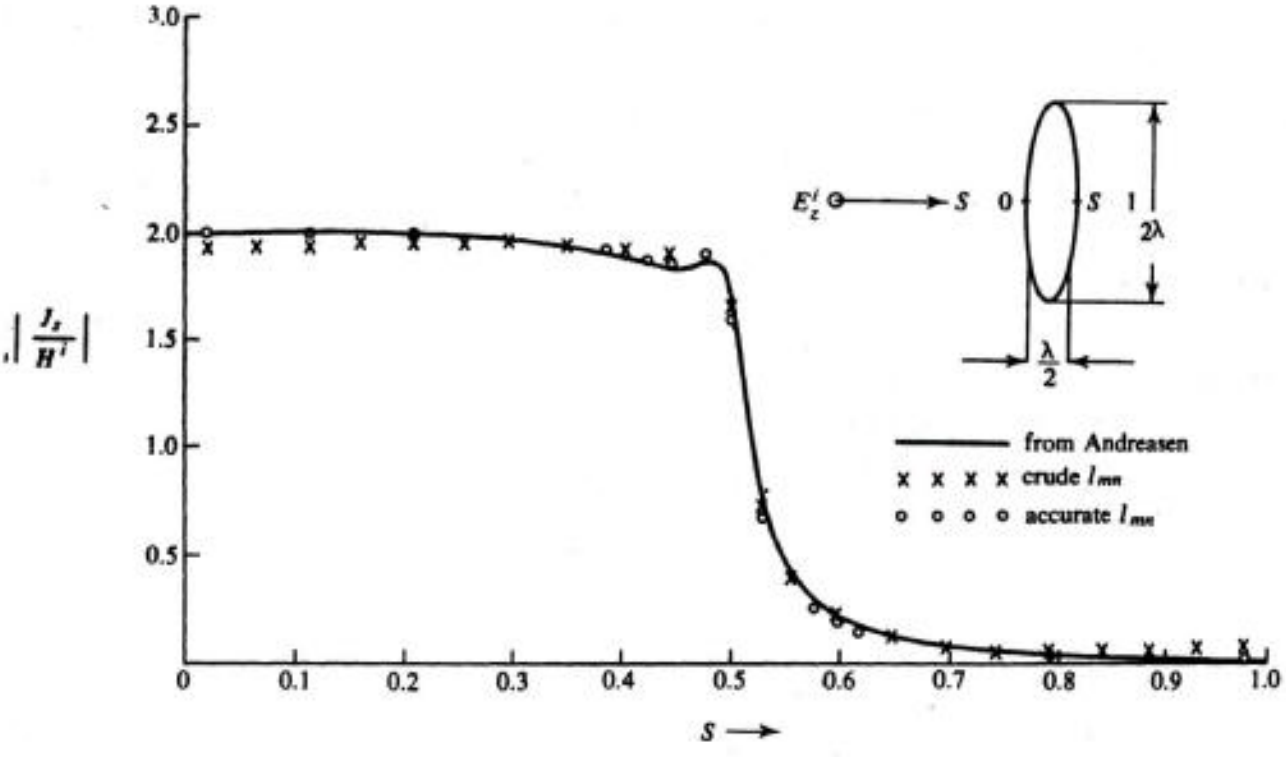

Figure 3-5. **Current density on a conducting elliptic cylinder excited by a plane wave, using constrained pulses, TM case.**

$|\rho_m - \rho_n| > \lambda/4$, we can use (3-12) instead of (3-24) with no appreciable loss in accuracy. In other words, it is more important to evaluate l_{mn} carefully for ΔC's close together than for distant ones. The use of expansion functions of the type shown in Fig. 3-4 is equivalent to dividing the conductor into $2N$ segments, and constraining every other α_n to be the average of its adjacent α_n's before inverting the $[l_{mn}]$ matrix. We can, of course, use more pulses to approximate a triangle function, but, judging from the accuracy of Fig. 3-5, this probably is unnecessary for most purposes.

If we wish an approximation to the Galerkin solution, instead of the point-matching solution, the functions of Fig. 3-4 can be used for both expansion and testing. However, instead of analytically evaluating the second integration, we can numerically evaluate it using approximations (3-12) and (3-14). The result is

$$l_{mn} = [\tfrac{1}{2}l_{22} + \tfrac{1}{4}(l_{12} + l_{21} + l_{23} + l_{32}) + \tfrac{1}{8}(l_{11} + l_{13} + l_{31} + l_{33})]_{mn} \quad (3\text{-}25)$$

where the l_{ij} are the same l_{ij} that appear in (3-24). One factor of 1/2 comes from the fact that ΔC for each component pulse is 1/2 of ΔC_n, other factors of 1/2 come from the fact that the two end pulses are 1/2 the amplitude of the central pulse (Fig. 3-4). It is apparent from the forms of (3-24) and (3-25) that there will be little difference between the two l_{mn}, and hence between the two solutions. Of course, in the Galerkin solution the g_m of (3-10) should also be modified to represent a numerical integration of E_z^i with the testing function of Fig. 3-4.

If the conductor is symmetrical about some axis, as is the ellipse, the problem can be reduced to two matrices of order $N/2$, instead of a single matrix of order N. Since the time required to invert a matrix is proportional to N^3, this reduces the matrix inversion time to one fourth the original time. The procedure is discussed in the literature [3,4]. Finally, if the incident field E_z^i is also symmetrical about the same axis as is the conductor, only a single matrix of the order $N/2$ need be inverted.

3-4. Transverse Electric Fields

A two-dimensional TE field in isotropic media has no z component of **E** and only a z component of **H**. The most convenient general expression for the field is in terms of potentials[1]

$$\mathbf{H} = \frac{1}{\mu}\nabla \times \mathbf{A} \quad (3\text{-}26)$$

$$\mathbf{E} = -j\omega\mathbf{A} - \nabla\Phi \quad (3\text{-}27)$$

[1] In reference [1] the vector potential is defined so that $\mu\mathbf{A}$ replaces **A** in (3-26) to (3-28). We denote the scalar potential by Φ and the charge density by q to avoid confusion with the polar coordinates ρ and ϕ.

where the *magnetic vector potential* **A** and the *electric scalar potential* Φ satisfy

$$\nabla^2\mathbf{A} + k^2\mathbf{A} = -\mu\mathbf{J} \tag{3-28}$$

$$\nabla^2\Phi + k^2\Phi = -\frac{q}{\varepsilon} \tag{3-29}$$

The electric charge density q is related to **J** by the *equation of continuity*

$$\nabla \cdot \mathbf{J} = -j\omega q \tag{3-30}$$

Both (3-28) and (3-29) are Helmholtz equations, the same as (3-3), and hence solutions are of the form (3-5). Defining the two-dimensional Green's function

$$G(\boldsymbol{\rho}, \boldsymbol{\rho}') = \frac{1}{4j} H_0^{(2)}(k|\boldsymbol{\rho} - \boldsymbol{\rho}'|) \tag{3-31}$$

we can express solutions to (3-28) and (3-29) in unbounded two-dimensional space as [1]

$$\mathbf{A}(\boldsymbol{\rho}) = \mu \iint \mathbf{J}(\boldsymbol{\rho}')G(\boldsymbol{\rho}, \boldsymbol{\rho}')\, ds' \tag{3-32}$$

$$\Phi(\boldsymbol{\rho}) = \frac{1}{\varepsilon} \iint q(\boldsymbol{\rho}')G(\boldsymbol{\rho}, \boldsymbol{\rho}')\, ds' \tag{3-33}$$

where the integration is over a z = constant cross section of the cylinder. In evaluating the formulas of this section it should be remembered that all quantities are independent of z; hence all z derivatives are zero.

3-5. Conducting Cylinders, TE Case

Let the conducting cylinder of Fig. 3-1 be excited by an impressed TE field. We wish to determine the current on the cylinder and the field produced by this current. This problem can be solved by enforcing the condition tangential $E = 0$ on C, as shown in Section 3-6, but first we consider the H-field formulation used in the literature [2,3].

As discussed in Section 3-4, the TE field has only a z component of **H**, and a transverse component of **J**. The total magnetic field H_z at any point is the sum of the impressed field H_z^i plus the scattered field H_z^s due to **J** on C; that is,

$$H_z = H_z^i + H_z^s \tag{3-34}$$

The scattered field is related to its source **J** by (3-26) and (3-32), or

$$H_z^s = \mathbf{u}_z \cdot \nabla \times \int_C JG \, d\mathbf{l}' \tag{3-35}$$

where the vector $d\mathbf{l}'$ designates the reference direction of J. The field H_z is finite external to C, zero internal to C, and the discontinuity of H_z on C equals the current density. If the interior of C lies on the left side of $d\mathbf{l}$ (right-hand rule), then

$$J = -[H_z]_{C_+} \tag{3-36}$$

where the C_+ denotes that H_z is evaluated just external to C. Specializing (3-34) to C_+, we have

$$J = -\left[H_z^i + \mathbf{u}_z \cdot \nabla \times \int_C JG \, d\mathbf{l}'\right]_{C_+} \tag{3-37}$$

which is an equation for the unknown current J. Equation (3-37) differs from the classical integral equation in that a derivative operator as well as an integral operator is present.

Because of the discontinuity in H_z at C we have to be particularly careful in evaluating (3-37). The Green's function G is singular, and a simple interchange of differentiation and integration is not always possible [5]. Figure 3-6 shows an expanded view of the conductor boundary to help clarify these concepts. The contour C lies on the current sheet, C_+ lies just outside, and C_- just inside. At point a on C_+, $H_z = -J$, and at point b on C_-, $H_z = 0$. If the scatterer is a conducting sheet of infinitesimal thickness, it should be treated as the limit of one of finite thickness.

We can write (3-37) in general operator notation as

$$L(J) = -H_z^i \tag{3-38}$$

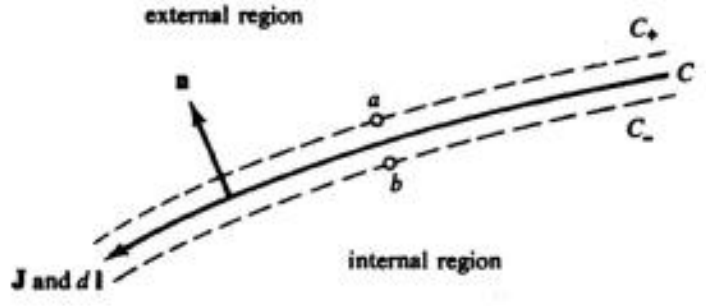

Figure 3-6. Section of cylindrical boundary.

where

$$L(J) = J + \left[\mathbf{u}_z \cdot \nabla \times \int_C JG\, d\mathbf{l}'\right]_{C_+} \tag{3-39}$$

and proceed according to the method of moments. Again the simplest approximation is to use the pulses (3-8) as basis functions, and point matching for testing. The current is then given by $J = \sum \alpha_n f_n$, and the resulting matrix equation is (3-9) with

$$g_m = -H_z^i(x_m, y_m) \tag{3-40}$$

$$l_{mn} = \delta_{mn} + H_z(m, n) \tag{3-41}$$

where δ_{mn} is the Kronecker delta and $H_z(m, n)$ denotes H_z at (x_m, y_m) on C_+ due to unit current density on ΔC_n at (x_n, y_n). Figure 3-7 represents a typical current element $J\mathbf{l} = \Delta\mathbf{C}_n$ and local coordinates (x, y). From symmetry, and the fact that the discontinuity in H_z is J, we have

$$H_z\Big|_{\substack{x=0+\\y=0}} = -H_z\Big|_{\substack{x=0-\\y=0}} = -1/2 \tag{3-42}$$

and hence, by (3-41),

$$l_{nn} \approx 1/2 \tag{3-43}$$

If $\Delta C_n \ll \lambda$ and the field point (x, y) is distant from $J\mathbf{l} = \Delta\mathbf{C}_n$, then the source

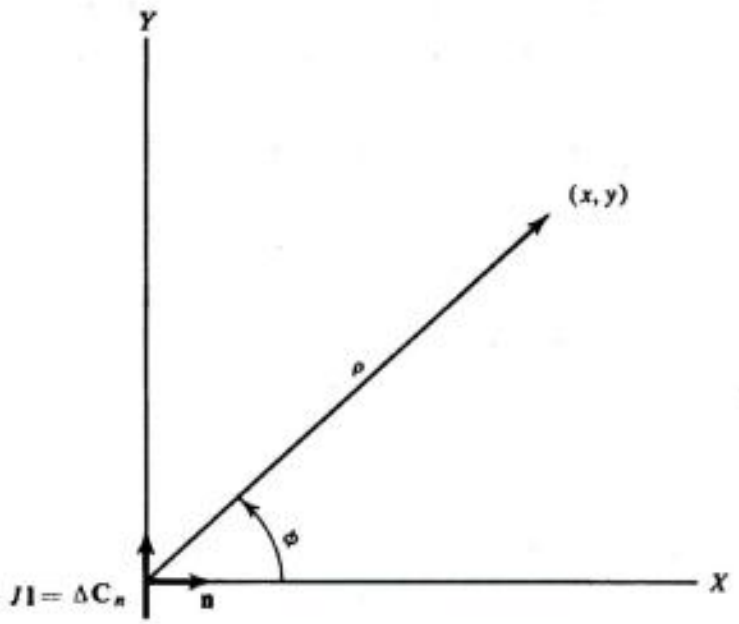

Figure 3-7. **Element of current $J\mathbf{l}$ and local coordinates.**

behaves as a point source. From (3-32)

$$A_y = \frac{\mu \, \Delta C_n}{4j} H_0^{(2)}(k\rho) \tag{3-44}$$

and from (3-26)

$$H_z = \frac{\Delta C_n}{4j} \frac{\partial}{\partial x} H_0^{(2)}(k\rho)$$

$$= \frac{j}{4} k \, \Delta C_n \cos \phi \, H_1^{(2)}(k\rho) \tag{3-45}$$

where $H_1^{(2)}$ is the Hankel function of order 1. We can translate this to an arbitrary origin by replacing ρ by $|\rho_m - \rho_n|$ and $\cos \phi$ by $\mathbf{n} \cdot \mathbf{R}$, where

$$\mathbf{R} = \frac{\boldsymbol{\rho}_m - \boldsymbol{\rho}_n}{|\boldsymbol{\rho}_m - \boldsymbol{\rho}_n|} \tag{3-46}$$

is a unit vector from the source point (x_n, y_n) to the field point (x_m, y_m). This result can be used as an approximation for all $m \neq n$. Hence (3-41) becomes, for $m \neq n$,

$$l_{mn} \approx \frac{j}{4} k \, \Delta C_n (\mathbf{n} \cdot \mathbf{R}) H_1^{(2)}(k|\boldsymbol{\rho}_m - \boldsymbol{\rho}_n|) \tag{3-47}$$

The solution is then given by $J = [\tilde{f}_n][l_{nm}^{-1}][g_m]$, as discussed in Section 1-3.

For better approximations we can use the methods of Section 3-3 to obtain more accurate l_{mn}. For example, the pulse approximation to a triangle function, Fig. 3-4, can be used, with the new l_{mn} given by (3-24). Alternatively, the approximate triangle function can be used for both expansion and testing, giving the Galerkin result (3-25). Still more accurate evaluation of the l_{mn} may be required to treat thin conducting sheets when points m and n are close together.

Example. Consider TE plane-wave scattering by conducting cylinders. An impressed uniform plane wave incident from the direction ϕ_i is given by

$$H_z^i = e^{jk(x \cos \phi_i + y \sin \phi_i)} \tag{3-48}$$

The g_m are determined from this by (3-40), and the l_{mn} are given by (3-43) and (3-47) for a first-order solution. The current is then found by matrix inversion and multiplication in the usual manner.

Again the scattering cross section σ is of interest, given by

$$\sigma(\phi) = 2\pi\rho \left| \frac{H^s(\phi)}{H^i} \right|^2 \tag{3-49}$$

analogous to (3-16). Here $H^s(\phi)$ is the distant field from J, obtainable by using the asymptotic formula for $H_1^{(2)}$ in (3-45), and summing over all elements of source. This gives [3]

$$H_z^s(\phi) = Kk \int_C J(x', y')\mathbf{n} \cdot \mathbf{R} e^{jk(x' \cos\phi + y' \sin\phi)}\, dl' \tag{3-50}$$

where K is given by (3-18). Substituting (3-48) and (3-50) in (3-49), we obtain

$$\sigma(\phi) = \frac{k}{4} \left| \int_C J(x', y')\mathbf{n} \cdot \mathbf{R} e^{jk(x' \cos\phi + y' \sin\phi)}\, dl' \right|^2 \tag{3-51}$$

which can be evaluated once J is found. The numerical evaluation of (3-51) can be put in a form similar to (3-20) for computational convenience.

To illustrate a typical result, Fig. 3-8 shows the TE solution for the current induced on the same elliptic cylinder as in Fig. 3-2 for the TM case. The computations are those of Andreasen [3], and correspond in accuracy to using

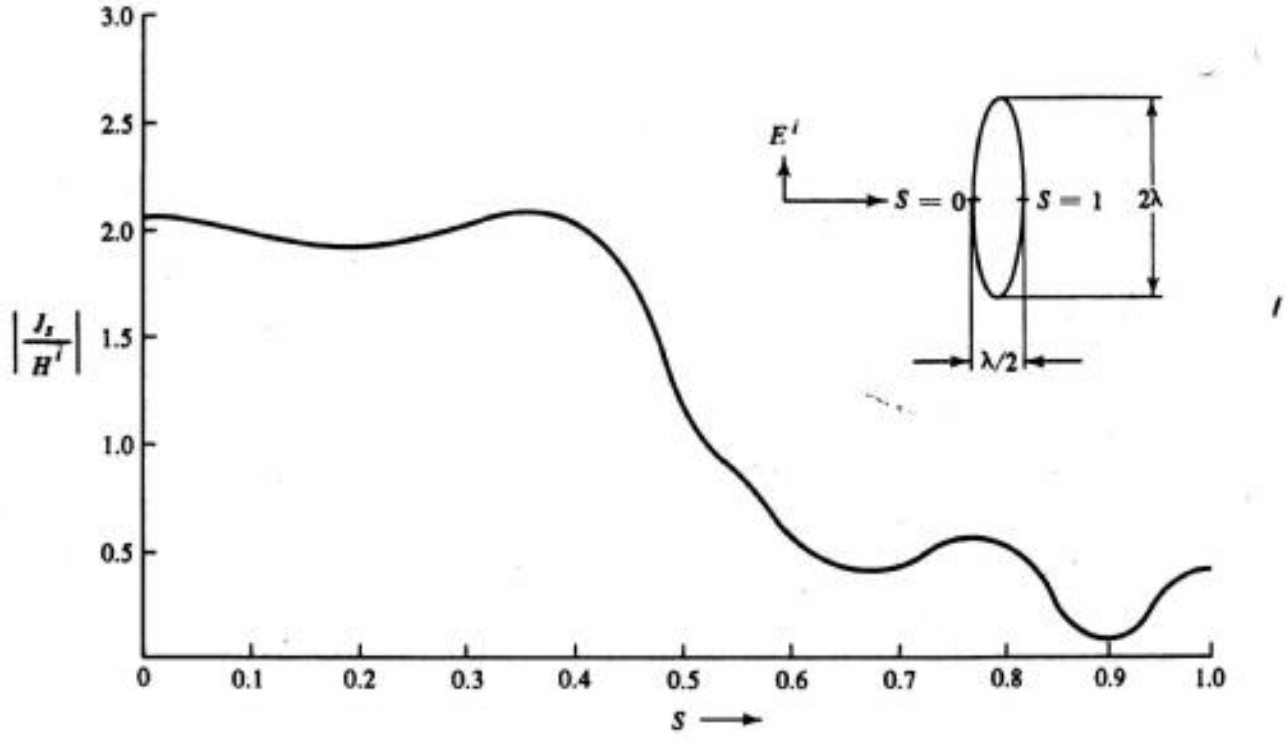

Figure 3-8. **Current density on a conducting elliptic cylinder excited by a plane wave, TE case (after Andreasen [3]).**

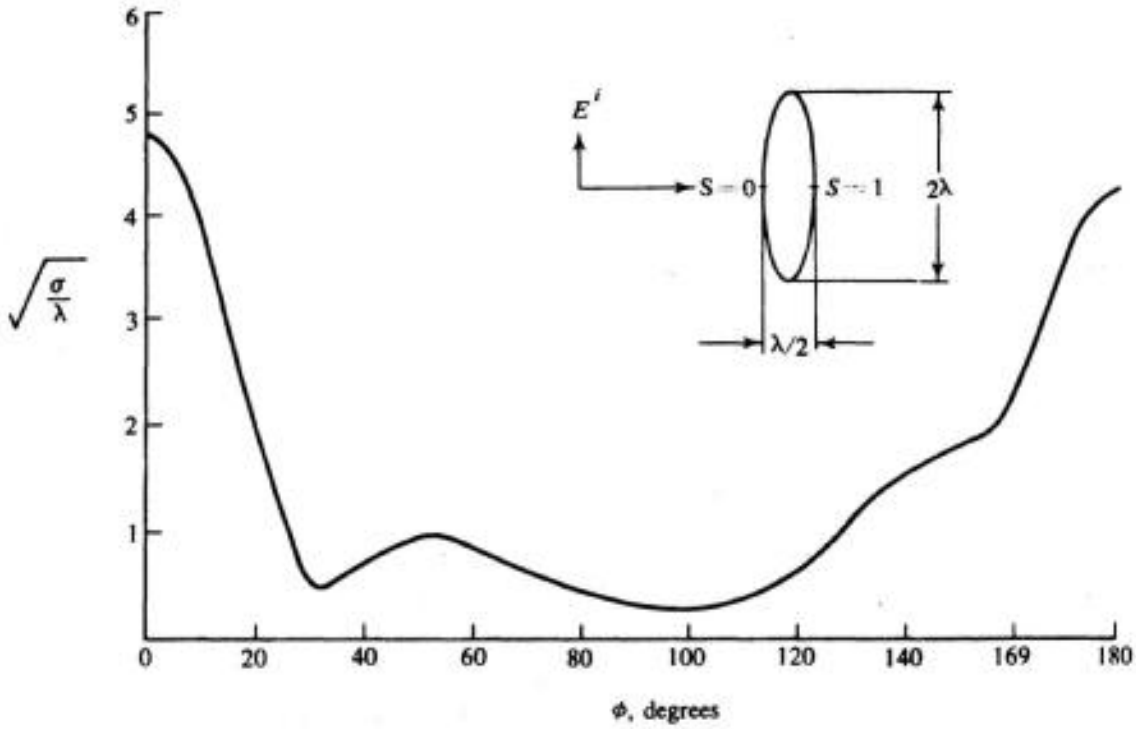

Figure 3-9. **Scattered field pattern for a conducting elliptic cylinder excited by a plane wave, TE case (after Andreasen [3]).**

approximations of the type illustrated by Fig. 3-4. Figure 3-9 shows the TE scattering pattern of the elliptic cylinder, which may be compared to the corresponding TM case of Fig. 3-3. Many other computations are available in the literature [2,3].

3-6. Alternative Formulation

The TM problem was treated by an *E*-field formulation in Section 3-2, and the TE problem was treated by an *H*-field formulation in Section 3-5. Actually, both cases can be treated either by an *E*-field method or an *H*-field method. To illustrate this, we reconsider the TE case by an *E*-field formulation.

Let Fig. 3-1 represent a conducting cylinder excited by an impressed TE field $\mathbf{E}^i$ transverse to z. The scattered field $\mathbf{E}^s$ is produced by transverse currents J on C according to the formulas of Section 3-4. For the present problem, these become

$$\mathbf{E}^s = -j\omega\mathbf{A} - \nabla\Phi \tag{3-52}$$

$$\mathbf{A}(\boldsymbol{\rho}) = \mu \oint_C J(\boldsymbol{\rho}')G(\boldsymbol{\rho}, \boldsymbol{\rho}')\, d\mathbf{l}' \tag{3-53}$$

$$\Phi(\boldsymbol{\rho}) = \frac{1}{\varepsilon} \oint_C \left(\frac{-1}{j\omega}\frac{dJ}{dl'}\right) G(\boldsymbol{\rho}, \boldsymbol{\rho}')\, dl' \tag{3-54}$$

where G is given by (3-31). The boundary condition is the tangential component of total $\mathbf{E}$ vanishes on the conductor; that is,

$$[E_l^i + E_l^s]_{\text{on } C} = 0 \tag{3-55}$$

Defining the operator

$$L(J) = -E_l^s|_{\text{on } C} = \left[j\omega A_l + \frac{\partial \Phi}{\partial l}\right]_{\text{on } C} \tag{3-56}$$

we can write (3-55) in operational notation as

$$L(J) = E_l^i|_{\text{on } C} \tag{3-57}$$

Note that the L of (3-56) contains derivatives, which require careful treatment.

If J is continuous and has a continuous derivative on C, we can solve (3-57) by the method of moments in a straightforward manner. However, this restriction on J is not convenient for cylinders of arbitrary shape. If J is expanded in terms of triangle functions, a point-matching solution works reasonably well unless the field is matched at the breakpoint of the triangles. If J is expanded in terms of pulse functions, dJ/dl gives impulse functions, and the point-matching solution becomes questionable. At any rate, it does not converge in the limit as the number of subsections become infinite. Perhaps the best procedure when using pulses is either to approximate the operator (Section 1-6), or to extend the operator (Section 1-7).

An approximate operator is obtained from (3-56) by replacing all derivatives by difference approximations. The procedure is identical to that given in Chapter 4 for three-dimensional wires, except that the Green's function is different. For a solution the approximate operator is used with pulse functions for expansion and point matching for testing. This procedure is presented in detail in Section 4-2, and we summarize only the results here. The transverse current J on C is represented as

$$J = \sum_n I_n P(l - l_n) \tag{3-58}$$

where $P(x)$ are the pulse functions of (1-49). The coefficients I_n are given by the matrix solution (4-21). The $[Z]$ matrix corresponds to the $[l]$ matrix in the general notation of Section 1-3. The elements Z_{mn} are given by (4-20) with $\Delta \mathrm{I}_n$ replaced by $\Delta \mathrm{C}_n$, and the ψ of (4-16) replaced by

$$\psi(n, m) = \frac{1}{4j\,\Delta C_n} \int_{\Delta C_n} H_0^{(2)}(k\rho_m)\, d\ell \tag{3-59}$$

where $\rho_m = \sqrt{(x - x_m)^2 + (y - y_m)^2}$. The excitation matrix is given by (4-14), with $\Delta \mathbf{l}_n$ replaced by $\Delta \mathbf{C}_n$. For a simple solution, we can use approximations similar to (3-12) and (3-14); that is,

$$\psi(n, m) \approx \begin{cases} \dfrac{1}{4j\,\Delta C_n} H_0^{(2)}(k\rho_{mn}) & m \neq n \\ \dfrac{1}{4j\,\Delta C_n}\left[1 - j\dfrac{2}{\pi}\log\left(\dfrac{\gamma k\,\Delta C_n}{4e}\right)\right] & m = n \end{cases} \tag{3-60}$$

where ρ_{mn} is the distance between the midpoints of ΔC_m and ΔC_n. For a higher-order solution, it is convenient to further subdivide C and use the methods of Section 3-3. For example, expansion functions of the type shown in Fig. 3-4 can be used, in which case the new Z_{mn} are given by (3-24) or (3-25) with the l_{ij} replaced by Z_{ij}.

Alternatively, we can extend the operator as follows. Define the inner product

$$\langle A, B \rangle = \oint_C A(\boldsymbol{\rho}) B(\boldsymbol{\rho})\, dl \tag{3-61}$$

for which L is self-adjoint, and consider a Galerkin solution. If J_m and J_n are two expansion functions for J, the elements of $[l]$ are given by

$$l_{mn} = \langle J_m, LJ_n \rangle = \oint_C J_m(\boldsymbol{\rho}) LJ_n(\boldsymbol{\rho})\, dl \tag{3-62}$$

Substituting from (3-56), we have

$$l_{mn} = \oint_C \left[j\omega J_m A_{ln} + J_m \frac{d\Phi_n}{dl} \right] dl \tag{3-63}$$

where the subscripts n on A and Φ denote that they are due to J_n. The first term in the brackets of (3-63) involves no derivatives, and gives no difficulty when pulse functions are used. The second term in the brackets may be integrated once by parts with respect to l. Boundary terms vanish if J_n is in the domain of L, and (3-63) reduces to

$$l_{mn} = \oint_C \left[j\omega J_m A_{ln} - \frac{dJ_m}{dl} \Phi_n \right] dl \tag{3-64}$$

An extended operator can now be defined by specifying that (3-64) apply even for J not in the original domain of L. This is permissible, because nothing is changed if J is in the original domain. Equation (3-64) gives convergent results

if J is expanded in triangles and reasonably good results if pulses are used. However, in applying (3-64) to pulse functions, it is better to replace dJ/dl by a difference approximation, in which case convergence is obtained in the limit. It is of interest to note that the latter procedure leads to precisely the same formulas as does the extended operator formulation given earlier, if the same approximations are used for $H_0^{(2)}$.

3-7. Dielectric Cylinders

Consider a dielectric cylinder of cross section S in an impressed field $\mathbf{E}^i$. The dielectric permittivity ε may be a function of x and y, but not of the axial coordinate z. The impressed field excites polarization currents $\mathbf{J}$ in the cylinder, which produce a scattered field $\mathbf{E}^s$. Let L represent the operation relating $-\mathbf{E}^s$ to $\mathbf{J}$; that is,

$$-\mathbf{E}^s = L(\mathbf{J}) \tag{3-65}$$

The total field is $\mathbf{E}^i + \mathbf{E}^s$, and the polarization current is related to the total field by

$$\mathbf{J} = j\omega(\varepsilon - \varepsilon_0)(\mathbf{E}^i + \mathbf{E}^s) \tag{3-66}$$

where ε_0 is the permittivity of free space. Combining (3-65) and (3-66), we have

$$L(\mathbf{J}) + \frac{1}{j\omega(\varepsilon - \varepsilon_0)}\mathbf{J} = \mathbf{E}^i \tag{3-67}$$

within S. In this equation $\mathbf{E}^i$ is known, and $\mathbf{J}$ is the unknown to be determined.

For the case of TM fields, the $\mathbf{E}$ and $\mathbf{J}$ have only z components, and L is given by (3-5); that is,

$$L(J) = \frac{-k\eta}{4}\iint_S J_z(\boldsymbol{\rho}')H_0^{(2)}(k\,|\boldsymbol{\rho} - \boldsymbol{\rho}'|)\,ds' \tag{3-68}$$

This is an integral operator, and (3-67) can be solved by the method of moments in a straightforward manner. The simplest procedure is to expand J_z in terms of pulse functions and use a point-matching procedure for testing. The details can be found in the literature [6]. An evaluation of the l_{mn} is found to be insensitive to the shape of the subareas Δs_n into which S is divided. Hence the l_{mn} can be conveniently evaluated by treating the Δs_n as if they were of circular cross section, which gives a particularly simple solution of excellent accuracy. Figure 3-10 shows the scattering cross section of a cylindrical shell computed by this method, and compares it to the exact eigenfunction solution. A total of 36 subareas of equal size were used for the matrix solution.

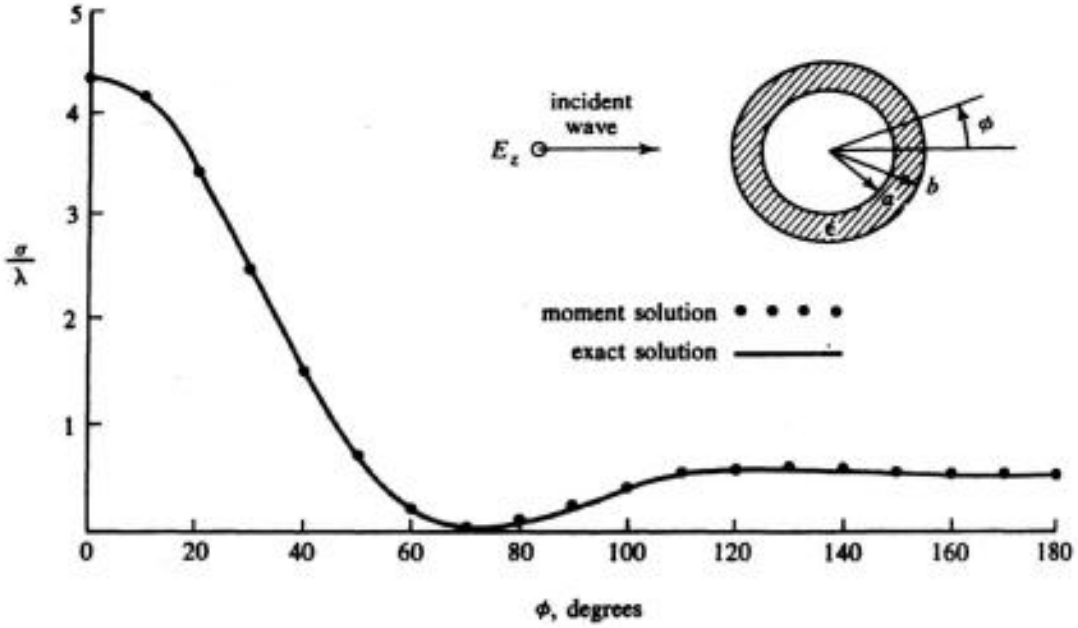

Figure 3-10. **Scattered power pattern for a circular dielectric tube, $a = 0.25\lambda$, $b = 0.30\lambda$, $\varepsilon_r = 4$, TM case (after Richmond [6]).**

In the TE case, L is the more complicated operator

$$L(\mathbf{J}) = j\omega\mathbf{A}(\mathbf{J}) + \nabla\Phi(\mathbf{J}) \tag{3-69}$$

where $\mathbf{A}$ and Φ are the potential integrals

$$4j\ \mathbf{A}(\mathbf{J}) = \mu \iint_S \mathbf{J}(\boldsymbol{\rho}')H_0^{(2)}(k\,|\boldsymbol{\rho} - \boldsymbol{\rho}'|)\,ds' \tag{3-70}$$

$$4j\ \Phi(\mathbf{J}) = \frac{1}{\varepsilon} \iint_S \left(-\frac{1}{j\omega}\nabla' \cdot \mathbf{J}\right) H_0^{(2)}(k\,|\boldsymbol{\rho} - \boldsymbol{\rho}'|)\,ds' \tag{3-71}$$

Because of the derivatives in (3-69) and (3-71), more care is necessary in applying the method of moments. Strictly speaking, pulse functions are not in the domain of L, and hence should not be used for expanding $\mathbf{J}$. However, if they are used in conjunction with a point-matching procedure, usable results can be obtained [7]. Figure 3-11 shows the scattering cross section of the cylindrical shell computed by this procedure using 38 subareas, and compares it to the eigenfunction solution. Note that, because of the crude treatment of the problem, the error is appreciable. Since $\sqrt{\sigma}$ is a continuous linear functional of J, we should expect even more error in J itself. Furthermore, we should not expect the solution to converge to the exact solution as the number of subareas is increased. More accurate computations can be obtained by using expansion functions in the domain of L. Alternatively, we can continue to use pulse functions with either

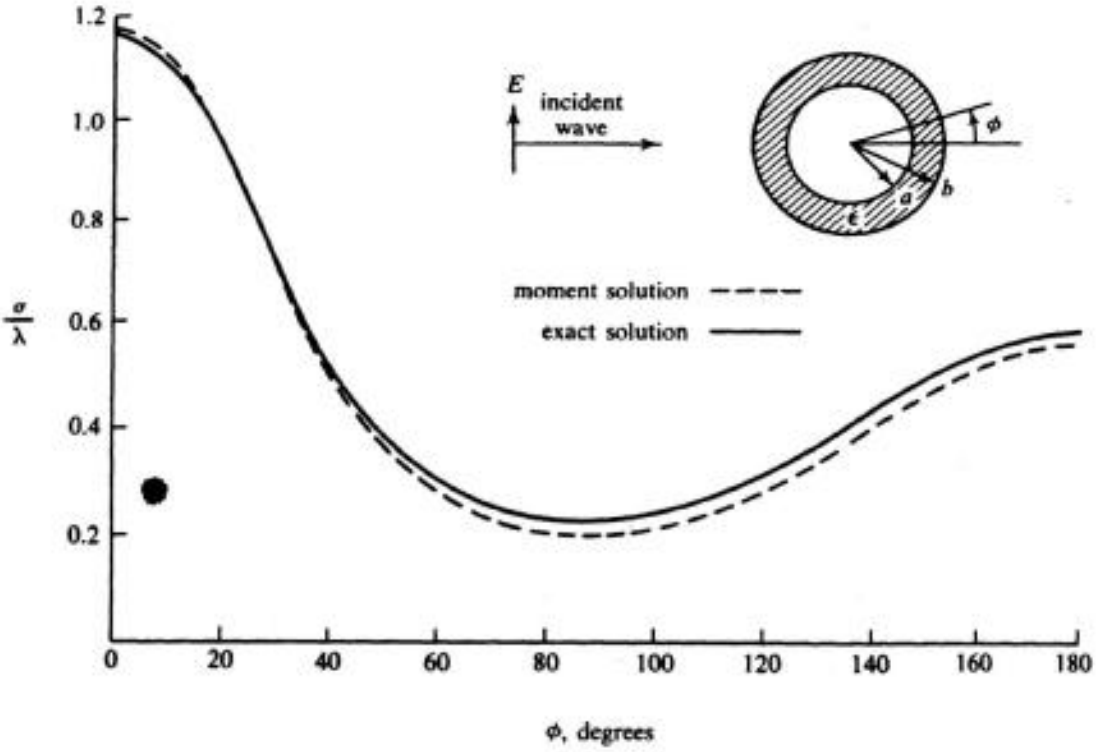

Figure 3-11. **Scattered power pattern for a circular dielectric tube, $a = 0.25\lambda$, $b = 0.30\lambda$, $\varepsilon_r = 4$, TE case (after Richmond [7]).**

an approximate L or an extended L, as discussed in Section 3-6. If properly done, TE solutions of accuracy comparable to that for TM solutions should be obtainable.

If the cylinder has a permeability μ different from μ_0 (that of free space), but $\varepsilon = \varepsilon_0$, the problem is dual to that just treated. The appropriate equation is dual to (3-67), that is, obtained from (3-67) by replacing ε by μ, $\mathbf{E}$ by $\mathbf{H}$, and $\mathbf{J}$ by $\mathbf{M}$ (magnetic current). Solution proceeds in the same manner as for the dielectric case. If the cylinder has both μ different from μ_0 and ε different from ε_0, the problem is more difficult. It involves a combination of (3-67) and its dual equation. We shall discuss this further in Section 5-7.

If the cylinder is homogeneous in both ε and μ, the problem can be formulated in terms of $\mathbf{E}$ and $\mathbf{H}$ on the contour C which bounds the cylinder [4]. This has the advantage of reducing the problem from two dimensions to one dimension; hence fewer subsections are needed for a solution. However, the procedure cannot be applied to inhomogeneous cylinders.

References

[1] R. F. Harrington, *Time-Harmonic Electromagnetic Fields*, McGraw-Hill Book Co., New York, 1961, pp. 223–230.

[2] K. Mei and J. Van Bladel, "Scattering by Perfectly Conducting Rectangular Cylinders," *IEEE Trans.*, Vol. **AP-11**, No. 2, March 1963, pp. 185–192. See also comments on this paper, Vol. **AP-12**, No. 2, March 1964, pp. 235–236.

[3] M. G. Andreasen, "Scattering From Parallel Metallic Cylinders with Arbitrary Cross Sections," *IEEE Trans.*, Vol. **AP-12**, No. 6, Nov. 1964, pp. 746–754.

[4] R. F. Harrington et al., *Matrix Methods for Solving Field Problems*, final report for Contract AF30(602)-3724 with Rome Air Development Center, Griffiss Air Force Base, Rome, N.Y., DDC No. AD 639744, August 1966.

[5] J. G. Van Bladel, "Some Remarks on Green's Dyadic for Infinite Space," *IRE Trans.*, Vol. **AP-9**, No. 6, Nov. 1961, pp. 563–566.

[6] J. H. Richmond, "Scattering by a Dielectric Cylinder of Arbitrary Cross Section Shape," *IEEE Trans.*, Vol. **AP-13**, No. 3, May 1965, pp. 334–341.

[7] J. H. Richmond, "TE Wave Scattering by a Dielectric Cylinder of Arbitrary Cross Section Shape," *IEEE Trans.*, Vol. **AP-14**, No. 4, July 1966, pp. 460–464.

CHAPTER

4

Wire Antennas and Scatterers

4-1. Formulation of the Problem

In this chapter we consider wire antennas and scatterers of arbitrary shape. These are perhaps the simplest three-dimensional problems because the current is constrained to flow in the axial direction of the wire. They are also important practical problems, particularly the wire antenna, which is in widespread use. The distinction between antennas and scatterers is primarily that of the location of the source. If the source is on the object it is considered an antenna; if the source is distant from the object it is viewed as a scatterer. Hence, by analyzing the object in an arbitrary impressed field, we are effectively considering both cases at once.

The solution is obtained by applying the method of moments to an appropriate superposition integral. The conventional retarded potential integral formulas are used for the analysis for simplicity, although other forms can be used [1]. The operator equation differs from classical integral equations in that derivatives appear as well as integrals. As discussed in Section 3-6, this type of equation can be handled by approximating the derivatives by finite differences.

A particularly descriptive exposition of the solution can be made in terms of network parameters. To effect a solution, the wire is considered as N short segments connected together. The end points of each segment define a pair of terminals in space. These N pairs of terminals can be thought of as forming an N-port network, and the wire object is obtained by short-circuiting all ports of the network. We can determine the impedance matrix for the N-port network by applying a current source to each port in turn, and calculating the open

circuit voltages at all ports. This procedure involves only current elements in empty space. The admittance matrix is the inverse of the impedance matrix. Once the admittance matrix is known, the port currents (current distribution on the wire) are found for any particular voltage excitation (applied field) by matrix multiplication. These matrices are special cases of the generalized network parameters discussed in Chapter 5.

The equation for the charge density σ and current $\mathbf{J}$ on a conducting body S in a known impressed field $\mathbf{E}^i$ is obtained as follows. The scattered field $\mathbf{E}^s$, produced by σ and $\mathbf{J}$, is expressed in terms of retarded potential integrals, and the boundary condition $\mathbf{n} \times (\mathbf{E}^i + \mathbf{E}^s) = 0$ on S is applied. This is summarized by

$$\mathbf{E}^s = -j\omega\mathbf{A} - \nabla\Phi \tag{4-1}$$

$$\mathbf{A} = \mu \iint_S \mathbf{J} \frac{e^{-jkR}}{4\pi R}\, ds \tag{4-2}$$

$$\Phi = \frac{1}{\varepsilon} \iint_S \sigma \frac{e^{-jkR}}{4\pi R}\, dS \tag{4-3}$$

$$\sigma = \frac{-1}{j\omega} \nabla \cdot \mathbf{J} \tag{4-4}$$

$$\mathbf{n} \times \mathbf{E}^s = -\mathbf{n} \times \mathbf{E}^i \qquad \text{on } S \tag{4-5}$$

Figure 4-1(a) represents an arbitrary thin-wire object, for which the following approximations are made: (1) The current is assumed to flow only in the

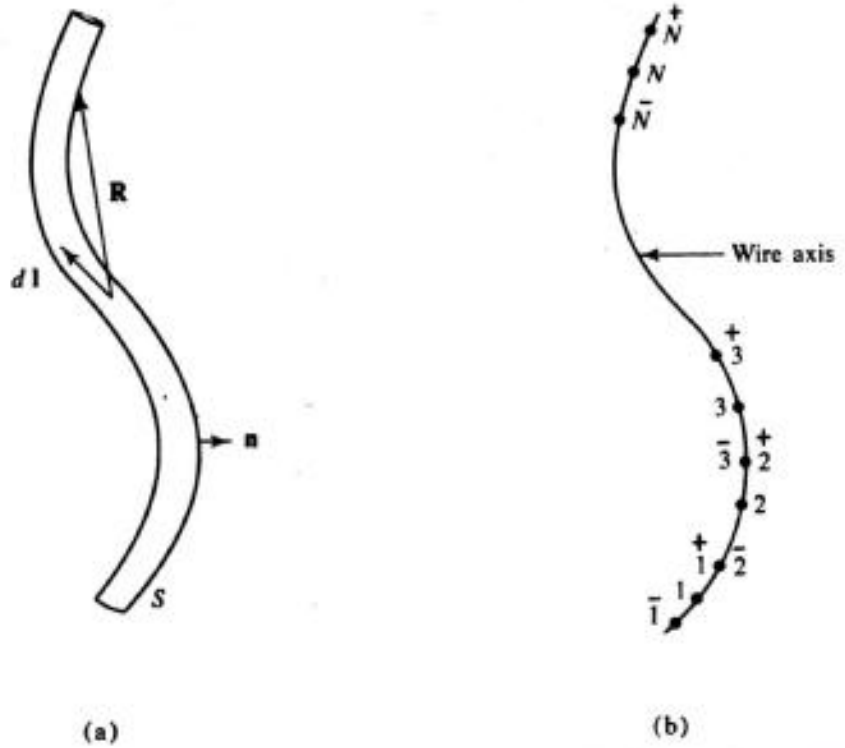

Figure 4-1. (*a*) Section of wire. (*b*) Wire axis divided into N segments.

direction of the wire axis, (2) the current and charge densities are approximated by filaments of current **I** and charge σ on the wire axis, and (3) the boundary condition (4-5) is applied only to the axial component of **E** at the wire surface. To this approximation, (4-1) through (4-5) become

$$-E_l^i = -j\omega A_l - \frac{\partial \Phi}{\partial l} \qquad \text{on } S \tag{4-6}$$

$$\mathbf{A} = \mu \int_{\text{axis}} \mathbf{I}(l) \frac{e^{-jkR}}{4\pi R}\, dl \tag{4-7}$$

$$\Phi = \frac{1}{\varepsilon} \int_{\text{axis}} \sigma(l) \frac{e^{-jkR}}{4\pi R}\, dl \tag{4-8}$$

$$\sigma = \frac{-1}{j\omega} \frac{dI}{dl} \tag{4-9}$$

where l is the length variable along the wire axis and R is measured from a source point on the axis to a field point on the wire surface.

4-2. Matrix Solution

A simple solution to the above equations is obtained as follows. Integrals are approximated by the sum of integrals over N small segments, obtained by treating I and q as constant over each segment. Derivatives are approximated by finite differences over the same intervals used for integration. Figure 4-1(b) illustrates the division of the wire axis into N segments, and defines the notation. The nth segment is identified by its starting point $\bar{n}$, its midpoint n, and its termination $\dot{n}$. An increment Δl_n denotes that between $\bar{n}$ and $\dot{n}$, $\Delta l_{\bar{n}}$ and $\Delta l_{\dot{n}}$ denote increments shifted one-half segment minus or plus along l. The desired approximations to (4-6) through (4-9) are then

$$-E_l^i(m) \approx -j\omega A_l(m) - \frac{\Phi\left(\bar{m}\right) - \Phi\left(\dot{m}\right)}{\Delta l_m} \tag{4-10}$$

$$\mathbf{A}(m) \approx \mu \sum_n \mathbf{I}(n) \int_{\Delta l_n} \frac{e^{-jkR}}{4\pi R}\, dl \tag{4-11}$$

$$\Phi\left(\dot{m}\right) \approx \frac{1}{\varepsilon} \sum_n \sigma\left(\dot{n}\right) \int_{\Delta l_n^+} \frac{e^{-jkR}}{4\pi R}\, dl \tag{4-12}$$

$$\sigma\left(\dot{n}\right) \approx \frac{-1}{j\omega} \frac{I(n+1) - I(n)}{\Delta l_n^+} \tag{4-13}$$

with equations similar to (4-12) and (4-13) for $\Phi\left(\bar{m}\right)$ and $\sigma\left(\bar{n}\right)$.

The σ's are given in terms of the I's by (4-13); hence (4-10) can be written in terms of the $I(n)$ only. We can view the N equations represented by (4-10) as the equations for an N-port network with terminal pairs $\left(\overset{+}{n}, \overset{-}{n}\right)$. The voltage applied to each port is approximately $\mathbf{E}^i \cdot \Delta\mathbf{l}_n$. Hence by defining matrices

$$[I] = \begin{bmatrix} I(1) \\ I(2) \\ \vdots \\ I(N) \end{bmatrix} \qquad [V] = \begin{bmatrix} \mathbf{E}^i(1) \cdot \Delta\mathbf{l}_1 \\ \mathbf{E}^i(2) \cdot \Delta\mathbf{l}_2 \\ \vdots \\ \mathbf{E}^i(N) \cdot \Delta\mathbf{l}_N \end{bmatrix} \tag{4-14}$$

we can rewrite (4-10) in matrix form as

$$[V] = [Z][I] \tag{4-15}$$

The elements of the matrix $[Z]$ can be obtained by substituting (4-11) to (4-13) in (4-10) and rearranging in the form of (4-15). Alternatively, we can apply (4-10) to (4-13) to two isolated elements and obtain the impedance elements directly. This latter procedure will be used because it is somewhat easier to follow.

Consider two representative elements of the wire scatterer, as shown in Fig. 4-2. The integrals in (4-11) and (4-12) are of the same form, and are denoted by

$$\psi(n, m) = \frac{1}{\Delta l_n} \int_{\Delta l_n} \frac{e^{-jkR_m}}{4\pi R_m}\, dl \tag{4-16}$$

where R_m is the distance from a point on Δl_n to the point m. Symbols + and − are used over m and n when appropriate. Evaluation of the ψ will be considered in Section 4-3. Let element n of Fig. 4-2 consist of a current filament $I(n)$, and two charge filaments of net charge

$$q\left(\overset{+}{n}\right) = \frac{1}{j\omega} I(n) \qquad q\left(\overset{-}{n}\right) = \frac{-1}{j\omega} I(n) \tag{4-17}$$

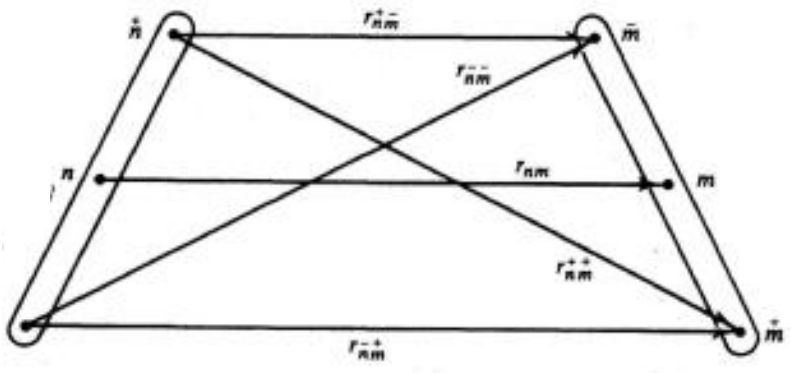

Figure 4-2. Two segments of a wire.

where $q = \sigma \Delta l$. The vector potential at m due to $I(n)$ is, by (4-11),

$$\mathbf{A} = \mu \mathbf{I}(n)\, \Delta l_n \psi(n, m) \tag{4-18}$$

The scalar potentials at $\overset{+}{m}$ and $\overset{-}{m}$ due to the charges (4-17) are, by (4-12),

$$\begin{aligned} \Phi\left(\overset{+}{m}\right) &= \frac{1}{j\omega\varepsilon}\left[I(n)\psi\left(\overset{+}{n}, \overset{+}{m}\right) - I(n)\psi\left(\overset{-}{n}, \overset{+}{m}\right)\right] \\ \Phi\left(\overset{-}{m}\right) &= \frac{1}{j\omega\varepsilon}\left[I(n)\psi\left(\overset{+}{n}, \overset{-}{m}\right) - I(n)\psi\left(\overset{-}{n}, \overset{-}{m}\right)\right] \end{aligned} \tag{4-19}$$

Substituting from (4-18) and (4-19) in (4-10), and forming $Z_{mn} = \mathbf{E}^i(m) \cdot \Delta \mathbf{l}_m / I(n)$, we obtain

$$Z_{mn} = j\omega\mu\, \Delta \mathbf{l}_n \cdot \Delta \mathbf{l}_m \psi(n, m) + \frac{1}{j\omega\varepsilon}\left[\psi\left(\overset{+}{n}, \overset{+}{m}\right) - \psi\left(\overset{-}{n}, \overset{+}{m}\right) - \psi\left(\overset{+}{n}, \overset{-}{m}\right) + \psi\left(\overset{-}{n}, \overset{-}{m}\right)\right] \tag{4-20}$$

This result applies for self-impedances ($m = n$) as well as for mutual impedances. When the two current elements are widely separated, a simpler formula based on the radiation field from a current element can be used.

The wire object is completely characterized by its impedance matrix, subject, of course, to the approximations involved. The object is defined by $2N$ points on the wire axis, plus the wire radius. The impedance elements are calculated by (4-20), and the voltage matrix is determined by the impressed field, according to (4-14). The current at N points on the scatterer is then given by the current matrix, obtained from the inversion of (4-15) as

$$[I] = [Y][V] \qquad [Y] = [Z^{-1}] \tag{4-21}$$

Once the current distribution is known, parameters of interest such as field patterns, input impedances, echo areas, etc., can be calculated by numerically evaluating the appropriate formulas.

According to the method of moments, the above solution is equivalent to using pulse functions for the expansion of both current and charge, and point matching for testing. To avoid differentiation, the procedure is applied to an approximate operator, obtained by replacing derivatives by finite differences. In terms of the general notation of Section 1-3, the $I(n)$ correspond to the α_n, the Z_{mn} to the l_{mn}, and the V_m to the g_m.

It should be noted that the end point of a wire is treated as the center of an interval with zero current. This is suggested in Fig. 4-1(b) by starting the intervals one-half subsection in from the wire ends. It is mathematically equivalent to the

boundary condition $I = 0$ at the ends of a wire. Note that the charge is not zero at the wire ends, which is consistent with representing charge as extending one-half interval beyond Δl.

4-3. Evaluation of Z_{mn}

The impedance elements (4-20) are known once $\psi(n, m)$ is evaluated. For this, we construct a local coordinate system with origin at n and the z axis along Δl_n, as shown in Fig. 4-3. Then

$$\psi(m, n) = \frac{1}{4\pi\,\Delta l_n} \int_{\bar{n}}^{+n} \frac{e^{-jkR_m}}{R_m}\, dz \tag{4-22}$$

where

$$R_m = \begin{cases} \sqrt{\rho_m + (z - z_m)^2} & m \neq n \\ \sqrt{a^2 + z^2} & m = n \end{cases} \tag{4-23}$$

and a is the wire radius. One approximation for ψ can be obtained by expanding the exponential in a Maclaurin series, obtaining

$$\psi = \frac{1}{4\pi\,\Delta l_n} \int_{\bar{n}}^{+n} \left(\frac{1}{R_m} - jk - \frac{k^2}{2} R_m + \cdots \right) dz \tag{4-24}$$

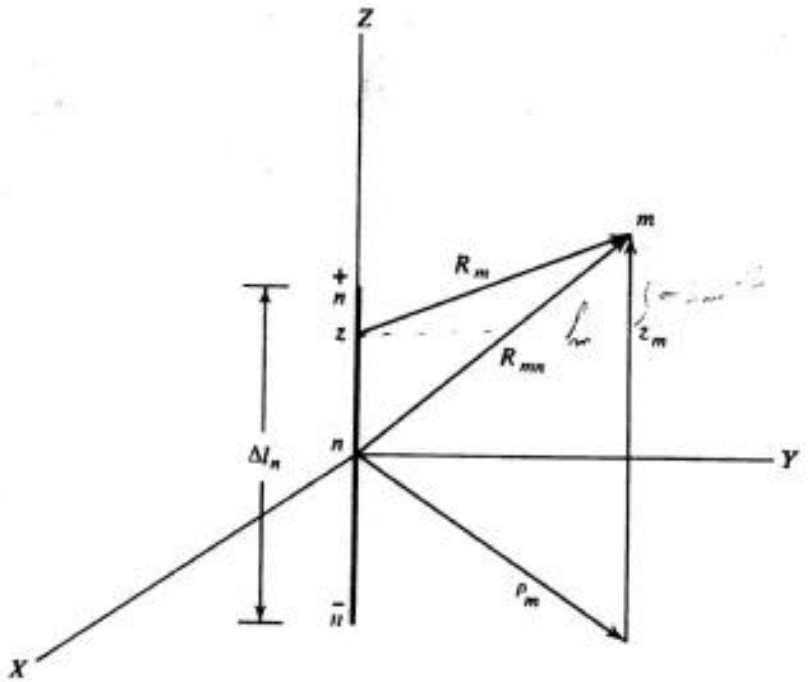

Figure 4-3. Geometry for evaluating $\psi(m, n)$.

The first term is identical to the electrostatic potential of a filament of charge. The second term is independent of R_m. For $m = n$, these two terms give reasonably good accuracy, and

$$\psi(n, n) \approx \frac{1}{2\pi\,\Delta l_n} \log\left(\frac{\Delta l_n}{a}\right) - \frac{jk}{4\pi} \tag{4-25}$$

For $m \neq n$, the crudest approximation is to consider R_m constant in the integration (4-22), and hence

$$\psi(m, n) \approx \frac{e^{-jkR_{mn}}}{4\pi R_{mn}} \tag{4-26}$$

where R_{mn} is the distance from n to m. The use of (4-25) and (4-26) is equivalent to the use of approximations (3-12) and (3-14) in the two-dimensional case. Since (4-26) is not exact in the limit $\Delta l \to 0$, there will be a residual error in the solution, as discussed in the example of Section 3-2.

Better solutions can be obtained either by a more accurate evaluation of (4-22) for the case $m \neq n$, or by the methods of Section 3-3. Formulas for more accurate evaluation of (4-22) are given in the literature [2]. However, the numerical procedures of Section 3-3 are just as good, and they also take the curvature of the wire into account. For example, each Δl of Fig. 4-1(b) can be subdivided into two subsections, in the manner of Fig. 3-4. Then, analogous to (3-24), we have

$$Z_{mn} = (\tfrac{1}{2}Z_{21} + Z_{22} + \tfrac{1}{2}Z_{23})_{mn} \tag{4-27}$$

Even further subdivision of the Δl may be used, especially for the elements Z_{nn}, $Z_{n,n-1}$, and $Z_{n,n+1}$, although (4-27) is accurate enough for most purposes. If desired, the Galerkin approximation equivalent to (3-25) may be used instead of (4-27). In this case the V_m should also be changed to the appropriate Galerkin approximation.

4-4. Wire Antennas

A wire excited by a lumped voltage source at one or more points along its length is a wire antenna. For the wire excited in the ith interval, the applied voltage matrix (4-14) is

$$[V^s] = \begin{bmatrix} 0 \\ \vdots \\ V_i \\ \vdots \\ 0 \end{bmatrix} \tag{4-28}$$

that is, all elements zero except the ith, which is equal to the source voltage. The current distribution is given by (4-21), which for the $[V]$ of (4-28) becomes

$$[I] = V_i \begin{bmatrix} Y_{1i} \\ Y_{2i} \\ \vdots \\ \vdots \\ Y_{Ni} \end{bmatrix} \tag{4-29}$$

Hence, the ith column of the admittance matrix is the current distribution for a unit voltage source applied to the ith interval. Inversion of the impedance matrix therefore simultaneously gives the current distributions for the antenna excited in any arbitrary interval along its length. The diagonal elements Y_{ii} of the admittance matrix are the input admittances of the wire object fed in the ith interval, and the Y_{ij} are the transfer admittances between a port in the ith interval and one in the jth interval.

The radiation pattern of a wire antenna is obtained by treating the antenna as an array of N current elements $I(n)\,\Delta\mathbf{l}_n$. By standard formulas, the far-zone vector potential is given by

$$\mathbf{A} = \frac{\mu e^{-jkr_0}}{4\pi r_0} \sum_n I(n)\,\Delta\mathbf{l}_n\, e^{jkr_n \cos \xi_n} \tag{4-30}$$

where $\mathbf{r}_0$ and $\mathbf{r}_n$ are the radius vectors to the distant field point and to the source points, respectively, and ξ_n are the angles between $\mathbf{r}_0$ and $\mathbf{r}_n$. The far-zone field components are [3]

$$E_\theta = -j\omega A_\theta \qquad E_\phi = -j\omega A_\phi \tag{4-31}$$

where θ and ϕ are the conventional spherical coordinate angles.

An alternative derivation of the radiation pattern can be obtained by reciprocity. Figure 4-4 represents a distant current element $I\mathbf{l}_r$ (r denotes "receiver"), adjusted to produce the unit plane wave

$$\mathbf{E}^r = \mathbf{u}_r e^{-j\mathbf{k}_r \cdot \mathbf{r}_n} \tag{4-32}$$

in the vicinity of the antenna. Here $\mathbf{u}_r$ is a unit vector specifying the polarization of the wave, $\mathbf{k}_r$ is a wavenumber vector pointing in the direction of travel of the wave, and $\mathbf{r}_n$ is the radius vector to a point n on the antenna. By reciprocity [3],

$$E_r = \frac{1}{Il_r} \int_{\text{antenna}} \mathbf{E}^r \cdot I\, d\mathbf{l} \tag{4-33}$$

where E_r is the $\mathbf{u}_r$ component of $\mathbf{E}$ from the antenna and I is the current on the antenna. The constant $1/Il_r$ is that needed to produce a plane wave of unit

amplitude at the origin, which is

$$\frac{1}{Il_r} = \frac{\omega\mu e^{-jkr_0}}{j4\pi r_0} \tag{4-34}$$

A numerical approximation to (4-33) is obtained by defining a voltage matrix

$$[V^r] = \begin{bmatrix} \mathbf{E}^r(1) \cdot \Delta\mathbf{l}_1 \\ \mathbf{E}^r(2) \cdot \Delta\mathbf{l}_2 \\ \vdots \\ \mathbf{E}^r(N) \cdot \Delta\mathbf{l}_N \end{bmatrix} \tag{4-35}$$

where $\mathbf{E}^r$ is given by (4-32), and approximating (4-33) as the matrix product

$$\begin{aligned} E_r &= \frac{\omega\mu e^{-jkr_0}}{j4\pi r_0} [\tilde{V}^r][I] \\ &= \frac{\omega\mu e^{-jkr_0}}{j4\pi r_0} [\tilde{V}^r][Y][V^s] \end{aligned} \tag{4-36}$$

where $[\tilde{V}]$ denotes the transpose of $[V]$. Note that $[V^r]$ is the same kind of matrix as (4-14); that is, it is the voltage matrix for plane-wave excitation of the wire. Equation (4-36) remains valid for an arbitrary excitation $[V^s]$; it is not restricted to the single source excitation (4-28).

The power-gain pattern for the $\mathbf{u}_r$ component of the radiation field is given by

$$g(\theta, \phi) = \frac{4\pi r_0^2}{\eta} \frac{|E_r(\theta, \phi)|^2}{P_{\text{in}}} \tag{4-37}$$

where $\eta = \sqrt{\mu/\varepsilon}$ is the intrinsic impedance of space and P_{in} is the power input to the antenna

$$P_{\text{in}} = \text{Re}\{[\tilde{V}^s][I^*]\} = \text{Re}\{[\tilde{V}^s][Y^*][V^{s*}]\} \tag{4-38}$$

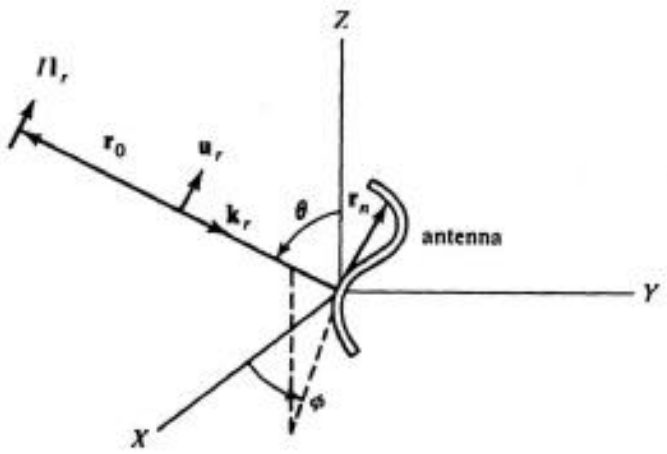

Figure 4-4. Wire antenna and distant dipole.

For the special case of a single source, equation (4-28), P_{in} becomes simply $\text{Re}\,(|V_i|^2 Y_{ii})$. Using (4-36) and (4-38) in (4-37), we have

$$g(\theta, \phi) = \frac{\eta k^2}{4\pi} \frac{|[\tilde{V}^r(\theta, \phi)][Y][V^s]|^2}{\text{Re}\,\{[\tilde{V}^s][Y^*][V^{s*}]\}} \tag{4-39}$$

where $[V^r(\theta, \phi)]$ is given by (4-35) for various angles of incidence θ and ϕ. Equation (4-39) gives the gain pattern for only a single polarization of the radiation field. If the total power-gain pattern is desired, the g's for two orthogonal polarizations may be added together.

Example. We here show some results for straight-wire antennas, of length l and diameter $2a$. Several different methods were tried, such as the use of (4-27), the use of triangle-expansion functions, and the use of triangles in Galerkin's method [2]. These three procedures all give about the same accuracy, and the actual computations were made by a triangle plus point-matching method. The computations here are for length/diameter ratios $l/2a = 74.2$, corresponding to $\Omega = 2 \log (l/2a) = 10$, and for $N = 32$ segments. An extensive table of other computations, for $l/2a$ ranging from 10 to 2000, and l/λ to 2.1, is available [4].

To indicate the accuracy obtainable, Fig. 4-5 shows the input admittance of the center-fed straight-wire antenna as a function of l/λ. It is compared to the second-order variational solution of Hu [5] and to the second iteration of Hallén's equation as computed by King and Middleton [6]. The input conductances are in close agreement, except for Hu's solution $l > 1.3\lambda$, in which case her trial functions are inadequate. The susceptances show poorer agreement, which is to be expected, since each solution treats the gap differently. In the matrix solution of this chapter, the gap is treated as if it were l/N in length. In Hu's solution, no trial function is used which can represent the singularity in charge at the source, and hence a low gap capacitance is obtained. The King-Middleton computations use an iterative procedure, and the susceptance depends on the number of iterations. Since they use a delta-function source, an exact solution must give infinite susceptance due to the infinite capacitance associated with zero gap.

As a further check on the accuracy of our computations, we computed a number of points using $N = 64$ segments. In going from $N = 32$ to $N = 64$, the change in input susceptance was usually less than 1 per cent, and always less than 3 per cent for the cases tried. The accuracy obtained using N segments and pulse expansion functions, that is, equation (4-20), was about the same as that obtained using $N/2$ segments and (4-27). Hence Fig. 4-5 is representative of a 64-segment solution using pulse expansion functions.

Figure 4-6 shows the input admittance to the antenna vs. l/λ for various source positions along the wire. Qualitatively, the antenna can be viewed as a set of resonators in parallel, and moving the feed point changes the coupling to these resonances. Figure 4-7 shows the current distribution on the antenna

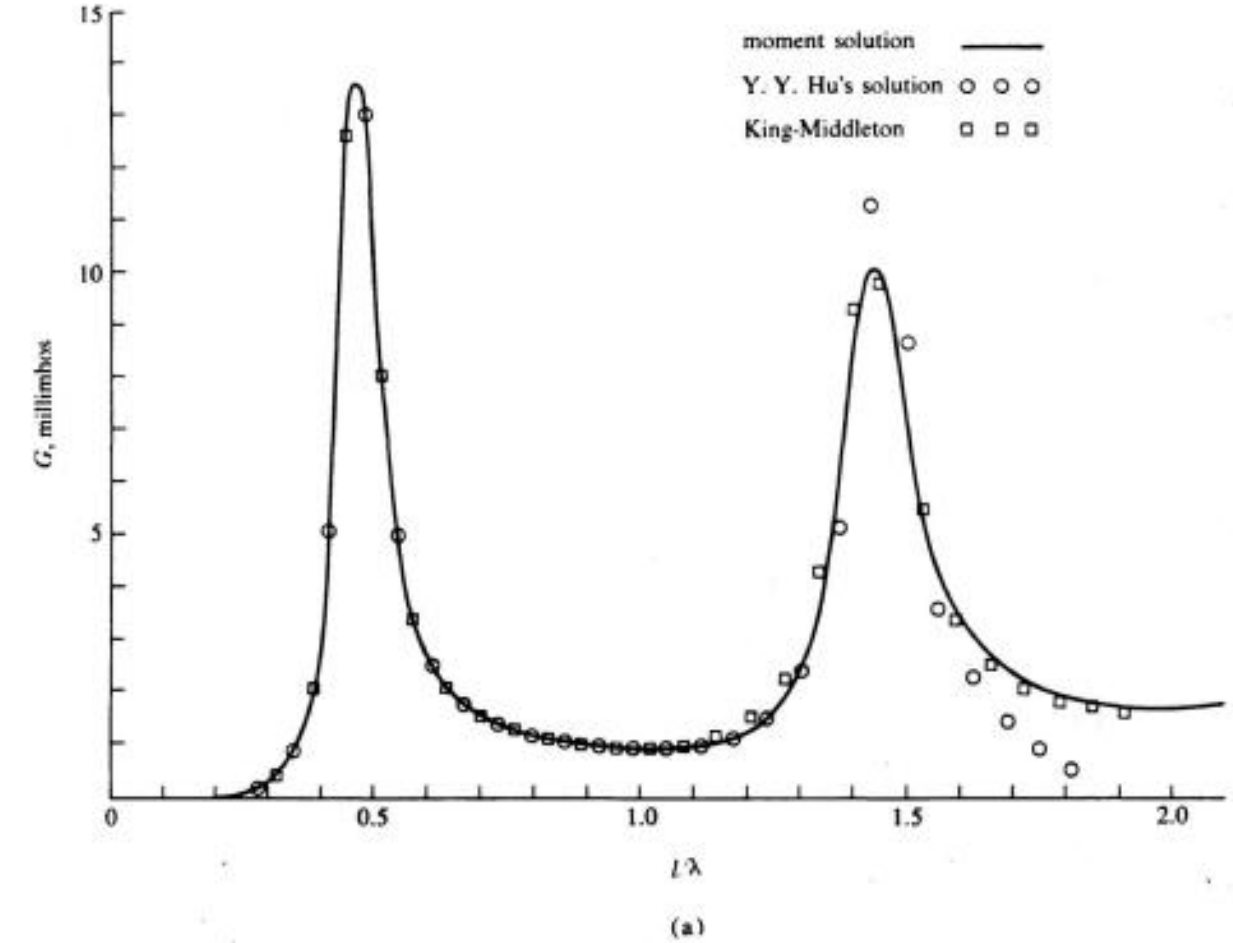

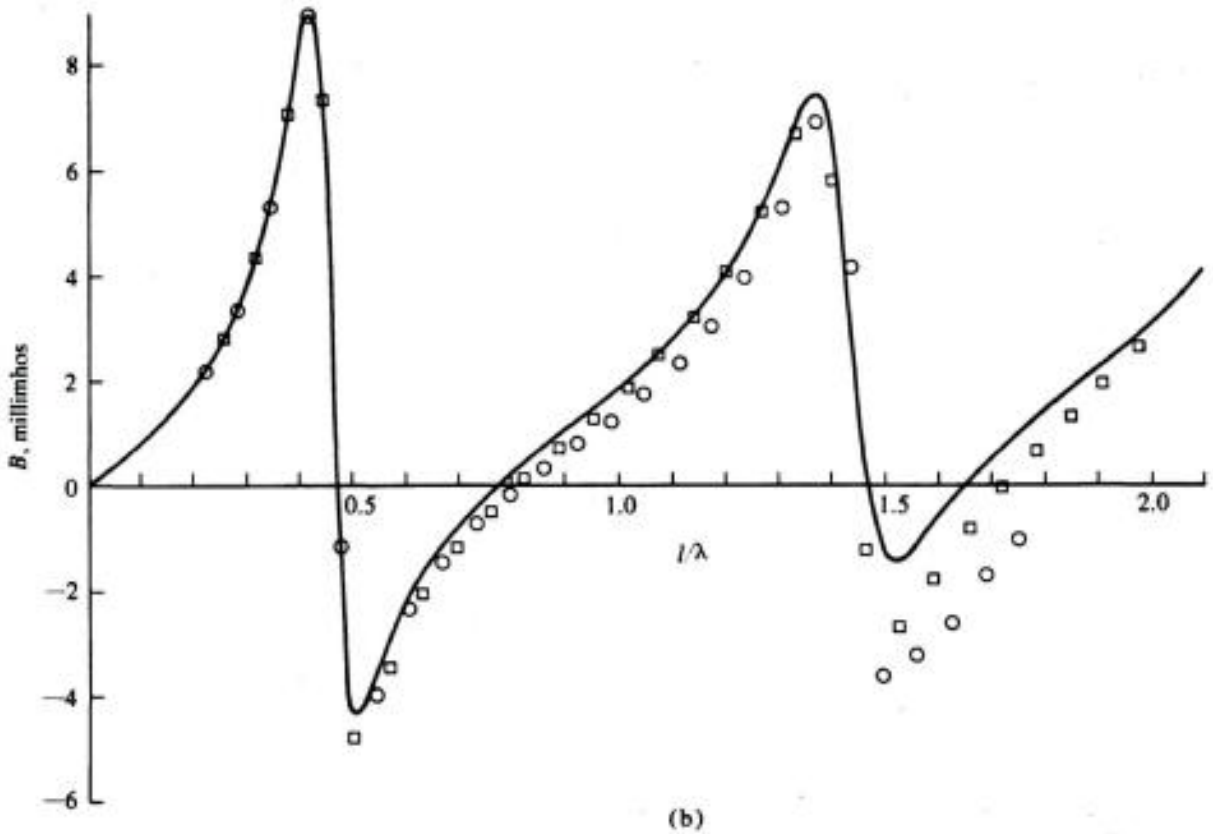

Figure 4-5. **Input admittance of a center-fed linear antenna, $l/2a = 74.2$. (*a*) Conductance, (*b*) susceptance.**

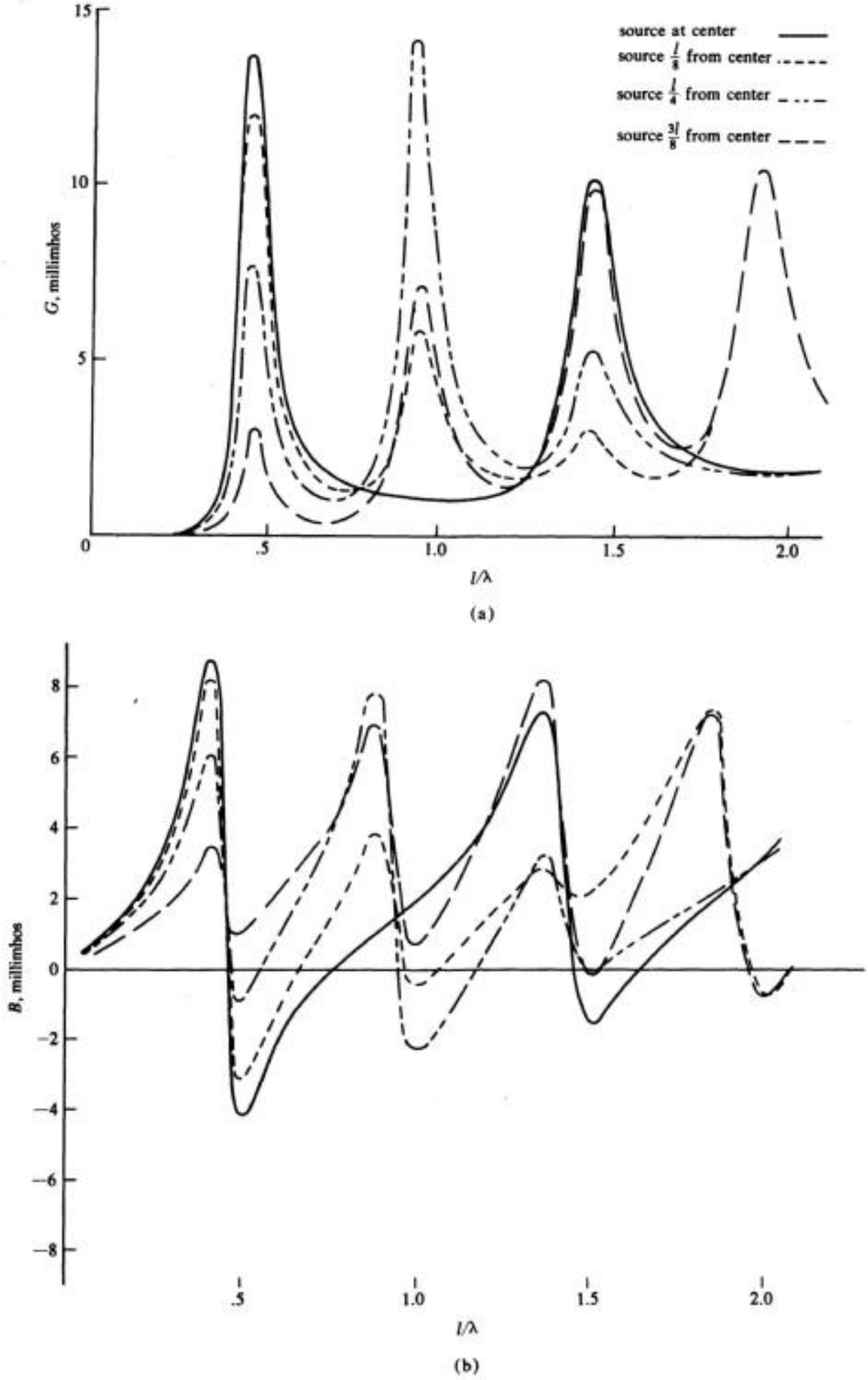

Figure 4-6. **Input admittance of a linear antenna, $l/2a = 74.2$, for various feed points. (*a*) Conductance, (*b*) susceptance.**

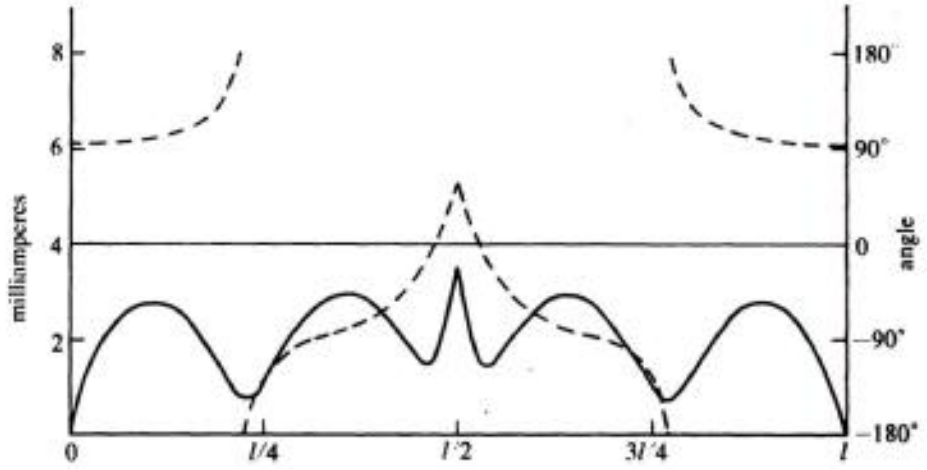

(a) Source at $z = l/2$

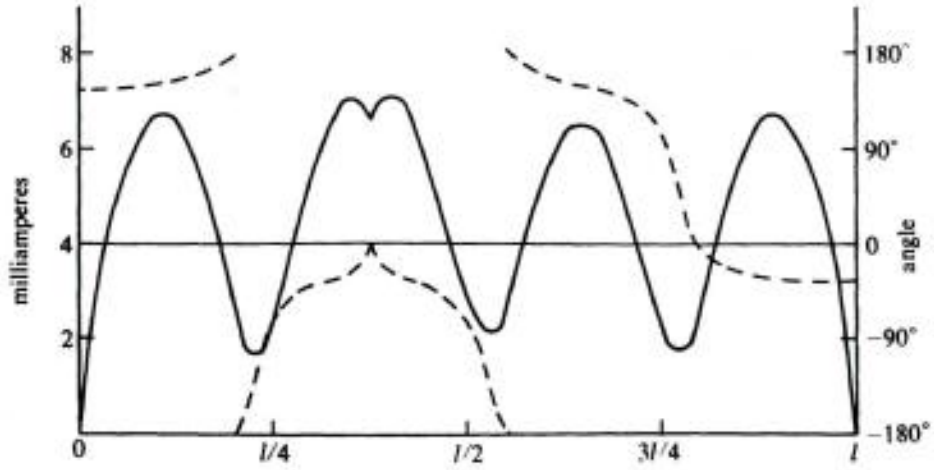

(b) Source at $z = 3l/8$

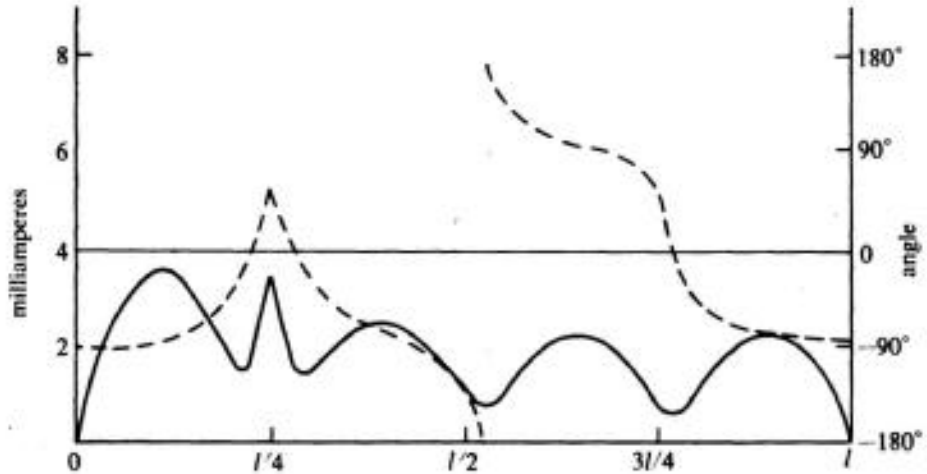

(c) Source at $z = l/4$

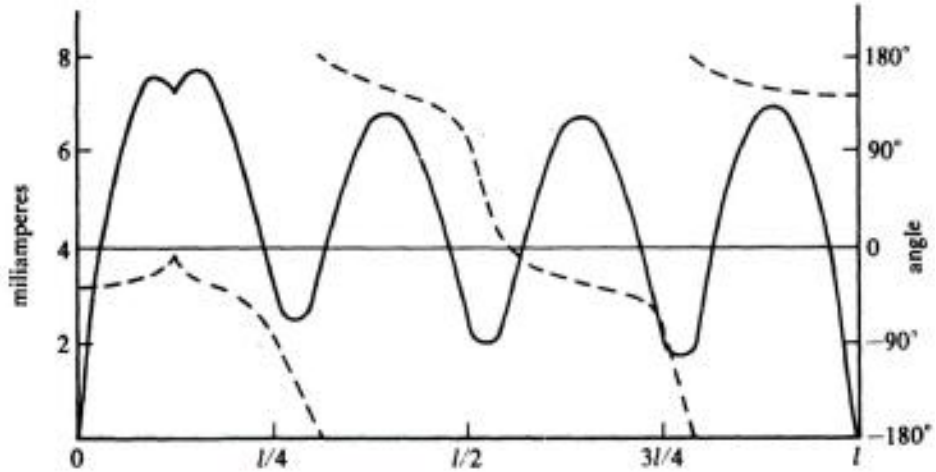

(d) Source at $z = l/8$

Figure 4-7. **Current, magnitude (solid) and phase (dashed), on a linear antenna, $l/2a = 74.2$, unit voltage source at various feed points.**

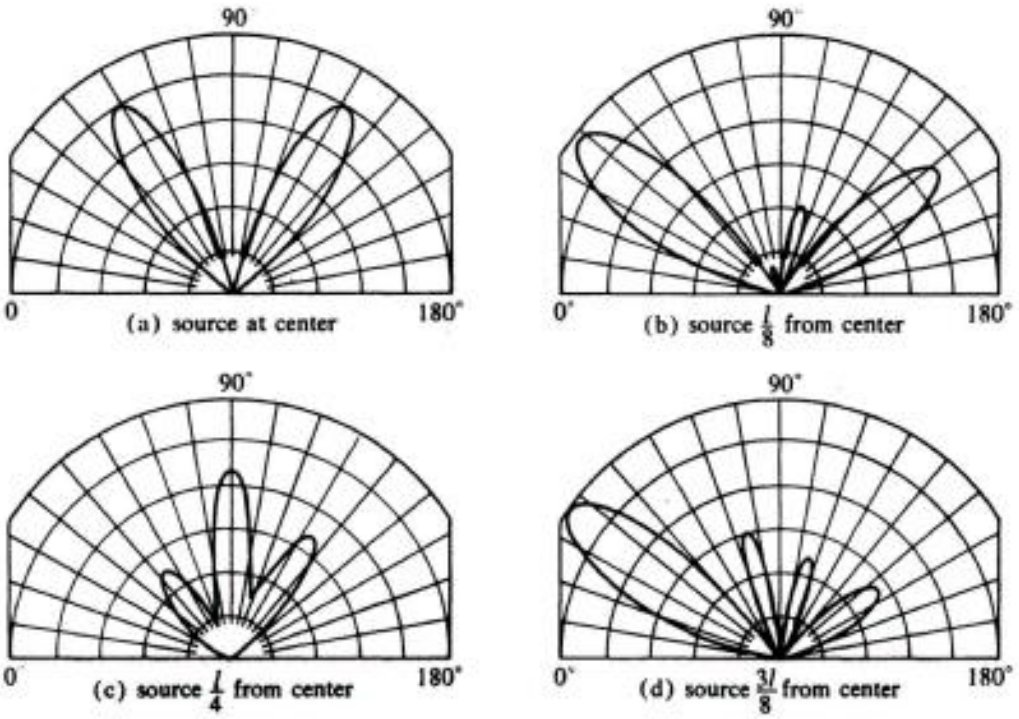

Figure 4-8. **Power-gain patterns for a linear antenna, $l/2a = 74.2$, for various feed points.**

for various feed positions, for the length $l = 2\lambda$. For the case $l = \lambda/2$, the current distribution is rather insensitive to feed position, a property well known to antenna engineers. Figure 4-8 shows the gain pattern of the antenna for the same cases for which the current is shown in Fig. 4-7. Each semicircular coordinate line represents a gain of one half that of an isotropic radiator. Figure 4-8(d) shows that the antenna behaves like a traveling-wave antenna as the source is moved to one end, an effect which becomes more pronounced as the antenna is made longer. For the case $l = \lambda/2$ the gain pattern is relatively insensitive to feed position, as expected.

4-5. Wire Scatterers

Consider now the field scattered by a wire object in a plane-wave incident field. Figure 4-9 represents a scatterer and two distant current elements, $I\mathbf{l}_t$ at the transmitting point $\mathbf{r}_t$, and $I\mathbf{l}_r$ at the receiving point $\mathbf{r}_r$. The $I\mathbf{l}_t$ is adjusted to produce a unit plane wave at the scatterer

$$\mathbf{E}^t = \mathbf{u}_t e^{-j\mathbf{k}_t \cdot \mathbf{r}_n} \tag{4-40}$$

where the notation is analogous to that of (4-32). The voltage excitation matrix (4-14) is then

$$[V^t] = \begin{bmatrix} \mathbf{E}^t(1) \cdot \Delta\mathbf{l}_1 \\ \mathbf{E}^t(2) \cdot \Delta\mathbf{l}_2 \\ \vdots \\ \mathbf{E}^t(N) \cdot \Delta\mathbf{l}_N \end{bmatrix} \tag{4-41}$$

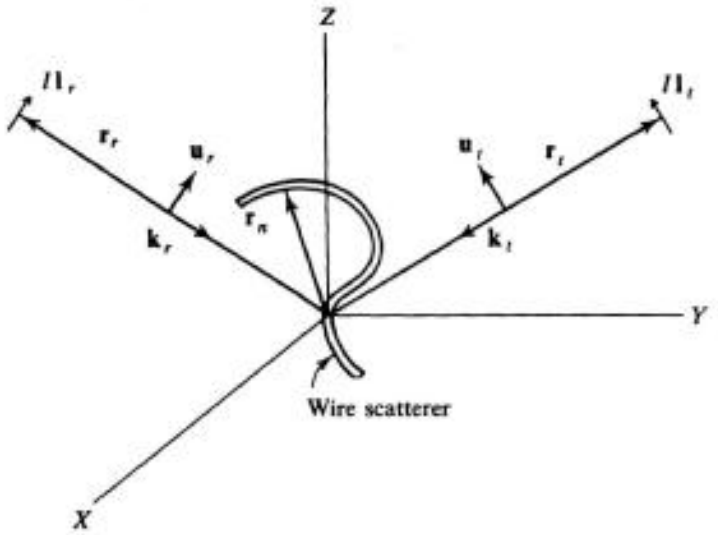

Figure 4-9. **Definitions for plane-wave scattering.**

and the current $[I]$ is given by (4-21) with $[V] = [V^t]$. The field produced by $[I]$ can then be found by numerical evaluation of the conventional formulas.

The distant scattered field can also be evaluated by reciprocity, the same as the antenna case. A dipole Π_r at the receiving point is adjusted to produce the unit plane wave (4-32) at the scatterer. The scattered field is then given by (4-36) with $[V^s]$ replaced by $[V^t]$; that is,

$$E_r = \frac{\omega\mu e^{-jkr_r}}{j4\pi r_r} [\tilde{V}^r][Y][V^t] \tag{4-42}$$

A parameter of interest is the bistatic scattering cross section σ, defined as that area for which the incident wave contains sufficient power to produce the field E_r by omnidirectional radiation. In equation form, this is

$$\begin{aligned} \sigma &= 4\pi r_r^2 |E_r|^2 \\ &= \frac{\eta^2 k^2}{4\pi} |[\tilde{V}^r][Y][V^t]|^2 \end{aligned} \tag{4-43}$$

For the monostatic cross section, set $[V^r] = [V^t]$ in (4-43). The cross section depends on the polarization of the incident wave and of the receiver. A better description of the scatterer can be made in terms of a scattering matrix [7].

Another parameter of interest is the total scattering cross section σ_t, defined as the ratio of the total scattered power to the power density of the incident wave. The total power radiated by $[I]$ is given by (4-38) for any excitation; therefore the scattered power is given by (4-38) with $[V^s]$ replaced by $[V^t]$. The incident power density is $1/\eta$; hence

$$\sigma_t = \eta \operatorname{Re}[\tilde{V}^t][Y^*][V^{t*}] \tag{4-44}$$

Note that σ_t is dependent on the polarization of the incident wave.

Example. We here consider the plane-wave scattering behavior of a straight piece of wire. The same $[Y]$ matrix is used as for the antenna example of Section 4-4; hence the length/diameter ratio is $l/2a = 74.2$ and the number of segments is $N = 32$. The computational procedure is a triangle plus point-matching one, and corresponds in accuracy to that obtainable from (4-27). The accuracy is also equivalent to that using (4-20) with $N = 64$ segments. Again an extensive table of other computations for $l/2a$ from 10 to 2000 is available [4].

Figure 4-10 shows the backscattering cross section for the wire, broadside incidence with E parallel to the wire. It is compared to Hu's second-order variational solution [5]. Again agreement is good in the range $L < 1.3\lambda$, where Hu's trial functions are adequate. Computations using (4-20), that is, pulse functions with $N = 32$ segments, give results almost as good as those shown in

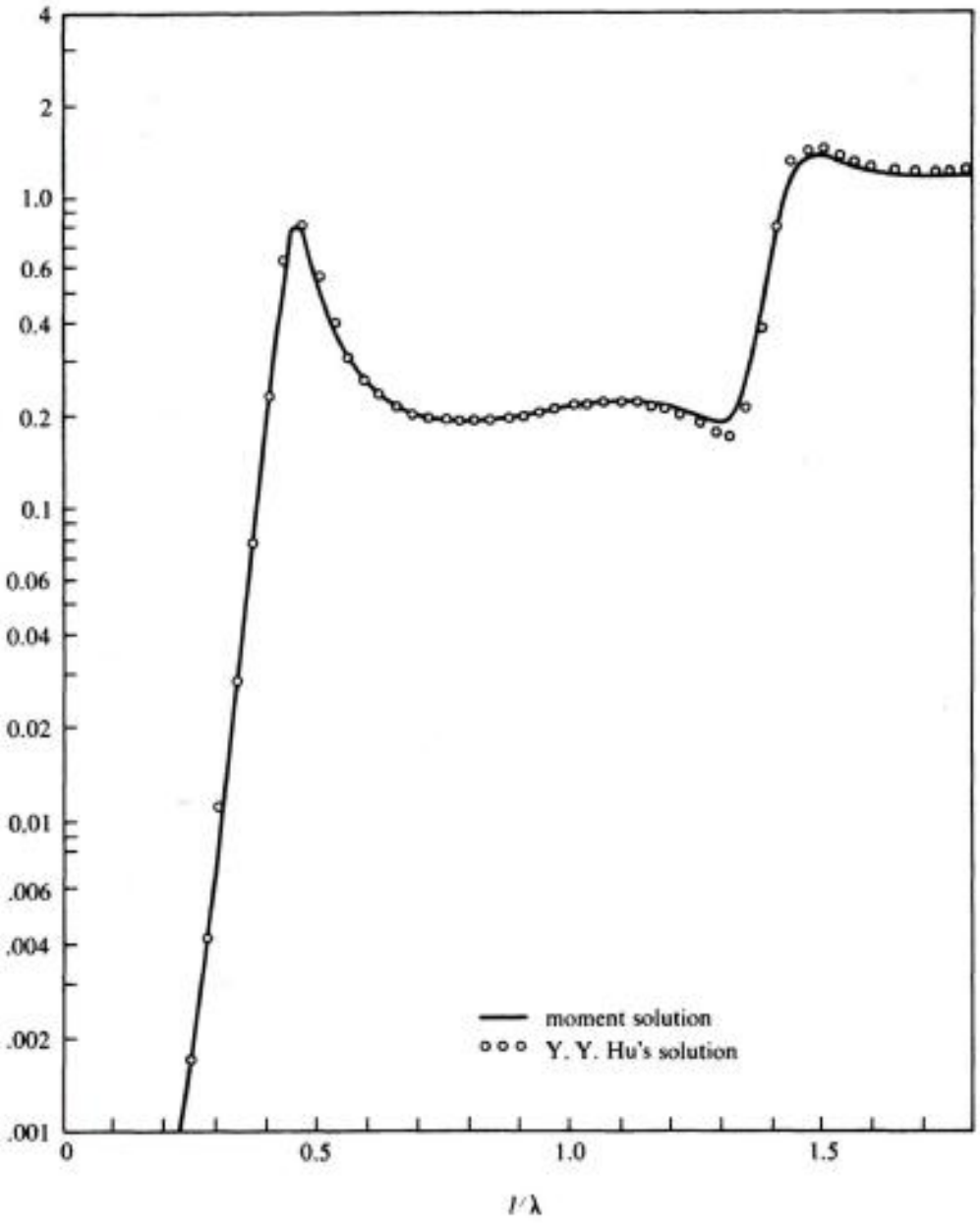

Figure 4-10. **Backscattering cross section for a straight wire, $l/2a = 74.2$, broadside incidence.**

(4-10). This is because $\sqrt{\sigma}$ is a continuous linear functional of I, as are all far-zone fields, and hence is insensitive to small errors in I. Furthermore, since the plane-wave excitation is a well-behaved impressed field, the convergence of the solution is much faster than for the antenna problem.

Figure 4-11 shows the current induced on a wire of length $l = 2\lambda$ as the angle of the incidence of the plane wave is changed. In each case the magnitude of the component of **E** parallel to the wire is 1 volt per wavelength, and the current is in milliamperes. Figure 4-12 shows the bistatic scattering cross sections for the same cases as the current is shown in Fig. 4-11. The angle of plane-wave incidence in each case is shown by an arrow. Each semicircular coordinate line

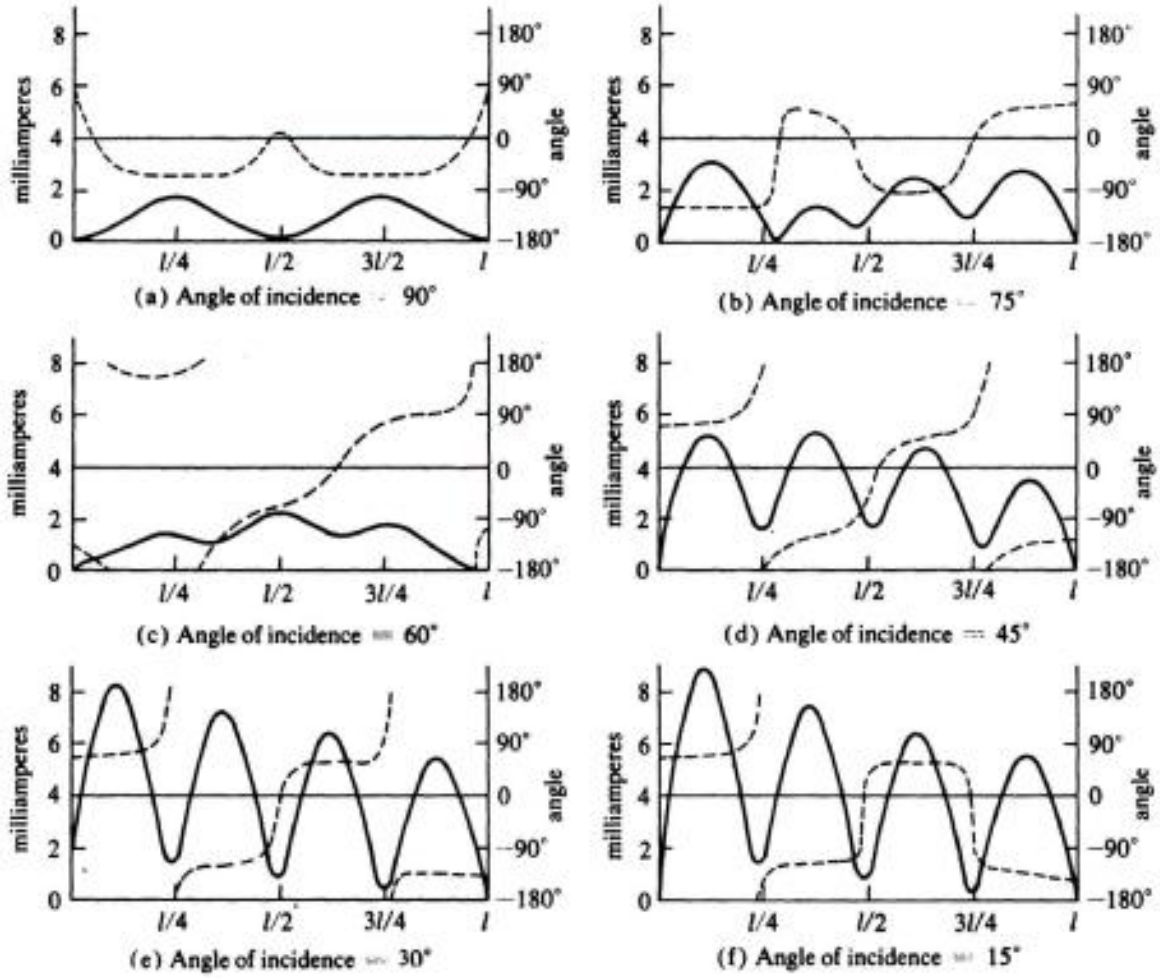

Figure 4-11. **Current, magnitude (solid) and phase (dashed), on a straight wire scatterer, $l/2a = 74.2, l = 2\lambda$, for various angles of incidence.**

represents a cross section of $0.5\lambda^2$. Note that there is a large lobe at an angle of scatter equal to the angle of incidence, but on the opposite side of the direction normal to the wire. This corresponds to specular reflection, and becomes more pronounced as the wire is made longer. For the special case $l = \lambda/2$, both the current on the wire and the scattering pattern are insensitive to the angle of incidence of the plane-wave excitation, as expected.

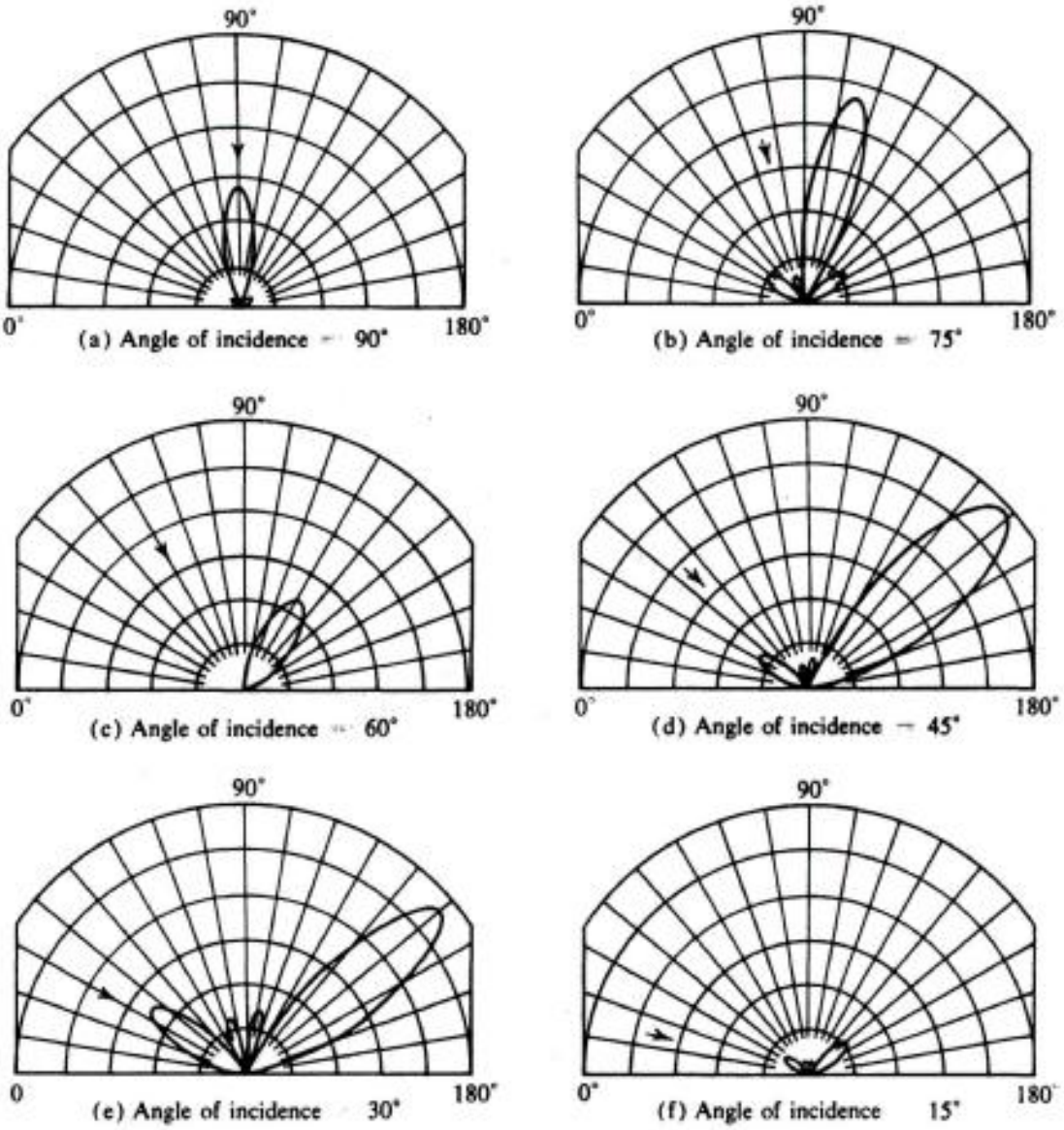

Figure 4-12. **Bistatic scattering cross-section patterns for a straight wire scatterer, $l/2a = 74.2$, $l = 2\lambda$, for various angles of incidence.**

4-6. Discussion

The solution of this chapter is a numerical approximation applied to the potential integral formulation of the problem. This equation can be transformed into other forms, the most common of which is Hallén's equation [1]. However, as long as a valid numerical procedure is used, there is no advantage to such transformations. For example, Hallén's equation is an integral equation obtained from (4-6) by a Green's function technique. A numerical solution of Hallén's equation can be related to our solution by a matrix Green's function technique. Hence, assuming equivalent approximations, the same accuracy is obtained from either (4-6) or Hallén's equation. We have verified this by making computations both ways, obtaining identical solutions.

A discussion of some of the problems associated with the convergence of the solution is in order. If the wire has no ends (for example, a loop), and if the

impressed field is well behaved (for example, an incident plane wave), solutions of high accuracy are obtained by the procedures of this chapter. If the wire has ends, the charge is singular (or almost so) at the ends. This singularity is poorly represented by a pulse-function basis, and hence is not accurately treated by the present solution. However, computations appear to justify our procedure, showing that this charge singularity has little effect on the current distribution, and almost no effect on far-zone quantities, such as radiation patterns and scattering cross sections. An accurate treatment of these end effects can be accomplished by including the appropriate functions in the basis, but the solution then depends on the shape of the wire ends (for example, hollow, rounded, etc.). Measurements on physical wire antennas have shown that the shape of wire ends has no significant effect on the input impedance [8].

There are also singularities at any source along the wire, particularly if the source is represented by an impulse function. An exact solution depends on the details of the source, which is undesirable for general procedures. A pulse basis cannot adequately account for singularities at the source, and they again are not accurately treated in our matrix solution. From an engineering standpoint, this is actually desirable, since to account for the type of source would destroy the generality of the solution. It has been found that the input conductance to a wire antenna is practically independent of the type of source, but the input susceptance depends on the source, both in the mathematical and physical problems.

The concept of viewing an object as an N-port network was here introduced as a consequence of the particular approximations made in the solution. Actually, the concept is quite general, being applicable to any body. We shall discuss this in terms of generalized network parameters in Chapter 5. The impedance or admittance form of solution is also convenient for the analysis of loaded antennas and scatterers, discussed in Chapter 6. The loads may be either lumped impedance elements, or continuous loads, as, for example, a dielectric coated conductor.

References

[1] K. K. Mei, "On the Integral Equations of Thin-Wire Antennas," *IEEE Trans.*, Vol. **AP-13**, No. 3, May 1965, pp. 374–378.

[2] R. F. Harrington et al., *Matrix Methods for Solving Field Problems*, Tech. Rept. No. RADC-TR-66-351, Vol. **I**, Rome Air Development Center, Griffiss Air Force Base, Rome, N.Y.; DDC No. AD 639744, Aug. 1966, Chaps. 3 and 4.

[3] R. F. Harrington, *Time-Harmonic Electromagnetic Fields*, McGraw-Hill Book Co., New York, 1961, Chap. 3.

[4] R. F. Harrington and J. Mautz, *Computations for Linear Wire Antennas and Scatterers*, Tech. Rept. No. RADC-TR-66-351, Vol. **II**, Rome Air Development Center, Griffiss Air Force Base, Rome, N.Y., DDC No. AD 639745, Aug. 1966.

[5] Y. Y. Hu, "Back-scattering Cross Sections of a Center-loaded Cylindrical Antenna," *IRE Trans.*, Vol. **AP-6**, Jan. 1958, pp. 140–148.

[6] R. W. P. King, *The Theory of Linear Antennas*, Harvard University Press, Cambridge, 1956, p. 172.

[7] R. F. Harrington, "Theory of Loaded Scatterers," *Proc. IEE* (*London*), Vol. **111**, No. 4, April 1964, pp. 617–623.

[8] G. H. Brown and O. M. Woodward, Jr., "Experimentally Determined Impedance Characteristics of Cylindrical Antennas," *Proc. IRE*, Vol. **33**, No. 4, Sect. VII, April 1945, pp. 257–262.

[9] R. F. Harrington, "Matrix Methods for Field Problems," *Proc. IEEE*, Vol. 55, No. 2, Feb. 1967, pp. 136–149.

CHAPTER

5

Generalized Network Parameters

5-1. Conducting Bodies

In Chapter 4 a solution in terms of an impedance matrix was obtained for wire objects, using somewhat qualitative reasoning. We here consider the general case, showing that the concept of "generalized impedance parameters" is rigorous and valid for any conducting body. The formulas of Chapter 4 are a special case of those of this section.

Figure 5-1 represents a material body in an impressed field $\mathbf{E}^i$ produced by external sources. For a perfect conductor, surface currents $\mathbf{J}$ are induced on S, which produce a scattered field $\mathbf{E}^s$. This scattered field can be found in terms of $\mathbf{J}$ by the potential integral method, equations (4-1) to (4-4). The boundary condition for the problem is (4-5); that is, tangential components of $(\mathbf{E}^i + \mathbf{E}^s)$ vanish on S. Defining the operator

$$\begin{aligned} L(\mathbf{J}) &= (-\mathbf{E}^s)_{\tan} \\ &= (j\omega\mathbf{A} + \nabla\Phi)_{\tan} \end{aligned} \tag{5-1}$$

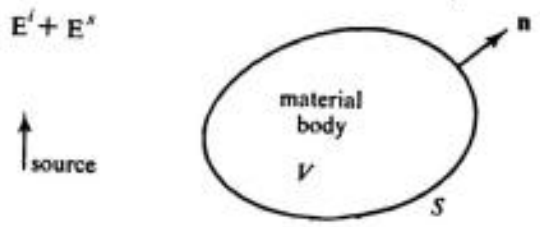

Figure 5-1. **Material body and external source.**

we can write the equation for $\mathbf{J}$ as

$$L(\mathbf{J}) = (\mathbf{E}^i)_{\tan} \tag{5-2}$$

where $(\ )_{\tan}$ means the tangential components of the bracketed quantity on S. A suitable inner product for the problem is

$$\langle \mathbf{J}, \mathbf{E} \rangle = \iint_S \mathbf{J} \cdot \mathbf{E}\, ds \tag{5-3}$$

which is a quantity called reaction [1]. Note that (5-3) involves only tangential components of $\mathbf{E}$, since $\mathbf{J}$ is tangential to S.

We now apply the method of moments to (5-2). Let $\mathbf{J}$ be expanded in a series of basis functions $\mathbf{J}_1, \mathbf{J}_2, \mathbf{J}_3, \ldots$, defined on S, as

$$\mathbf{J} = \sum_n I_n \mathbf{J}_n \tag{5-4}$$

where the I_n are complex coefficients. Substituting (5-4) in (5-2), and utilizing the linearity of L, we have

$$\sum_n I_n L(\mathbf{J}_n) = (\mathbf{E}^i)_{\tan} \tag{5-5}$$

Now define a set of testing functions $\mathbf{W}_1, \mathbf{W}_2, \mathbf{W}_3, \ldots$, which are tangential vectors on S; that is, they are current-type vectors. (In Galerkin's method, they would be equal to the $\mathbf{J}_n$.) The method of moments requires that (5-5) be valid for the inner product with each $\mathbf{W}_m$; that is,

$$\sum_n I_n \langle \mathbf{W}_m, L\mathbf{J}_n \rangle = \langle \mathbf{W}_m, \mathbf{E}^i \rangle \tag{5-6}$$

for all m. The subscript "tan" has been dropped from $\mathbf{E}^i$, since the inner products involve only tangential components. We define matrices

$$[I_n] = \begin{bmatrix} I_1 \\ I_2 \\ \vdots \\ \vdots \end{bmatrix} \qquad [V_m] = \begin{bmatrix} \langle \mathbf{W}_1, \mathbf{E}^i \rangle \\ \langle \mathbf{W}_2, \mathbf{E}^i \rangle \\ \vdots \\ \vdots \end{bmatrix} \tag{5-7}$$

$$[Z_{mn}] = \begin{bmatrix} \langle \mathbf{W}_1, L\mathbf{J}_1 \rangle & \langle \mathbf{W}_1, L\mathbf{J}_2 \rangle & \cdots \\ \langle \mathbf{W}_2, L\mathbf{J}_1 \rangle & \langle \mathbf{W}_2, L\mathbf{J}_2 \rangle & \cdots \\ \cdots & \cdots & \cdots \end{bmatrix} \tag{5-8}$$

and rewrite (5-6) in matrix form as

$$[Z_{mn}][I_n] = [V_m] \tag{5-9}$$

The elements of $[Z_{mn}]$ are called *generalized impedances*, those of $[I_n]$ *generalized currents*, and those of $[V_m]$ *generalized voltages*. The generalized impedances are the negative of reaction, as defined by Rumsey [1].

A solution for the expansion coefficients of $\mathbf{J}$ is given by the inversion of (5-9), or

$$[I_n] = [Y_{nm}][V_m] \tag{5-10}$$

where

$$[Y_{nm}] = [Z_{nm}^{-1}] \tag{5-11}$$

is the *generalized admittance* matrix. Defining the matrix of functions

$$[\mathbf{J}_n] = [\mathbf{J}_1 \quad \mathbf{J}_2 \quad \mathbf{J}_3 \quad \cdots] \tag{5-12}$$

we can write the solution (5-4) and (5-10) as

$$\mathbf{J} = [\mathbf{J}_n][I_n] = [\mathbf{J}_n][Y_{nm}][V_m] \tag{5-13}$$

This result is usually approximate but may be exact in some cases.

Note that the development of this section is exactly dual to that of Section 1-3; that is, it is merely the method of moments applied to a particular electromagnetic problem. The designation of the matrices as $[V]$, $[I]$, $[Z]$, and $[Y]$ is done, of course, to call attention to the analogy with multiport network theory [2]. The conducting body is characterized by its generalized impedance matrix $[Z]$, or its inverse, the generalized admittance matrix $[Y]$. These matrices depend on the geometry of the body and on the frequency, but not on the impressed field. The impressed electric field determines the voltage excitation $[V]$ of the generalized network according to (5-7). The resultant current $[I]$ then corresponds to the matrix of expansion coefficients for the current (5-4).

Example. The circular wire loop in an applied electromagnetic field will be used to illustrate these concepts. Although this problem can be treated quite well by the methods of Chapter 4, the alternative solution given here has the advantage of yielding a diagonal impedance matrix. Hence matrix inversion is trivial, and a larger series of expansion functions can be used. This simplification of solution is due to the circular symmetry of the problem.

Figure 5-2 shows the loop geometry and defines the coordinate system. We

start with the potential integral formulation of (4-6) to (4-9), and specialize it to the circular loop. The result is

$$E_\phi^i = j\omega A_\phi + \frac{1}{b}\frac{\partial \Phi}{\partial \phi} \tag{5-14}$$

$$A_\phi = \mu \int_0^{2\pi} I(\phi') \cos(\phi - \phi') \frac{e^{-jkR}}{4\pi R}\, b\, d\phi' \tag{5-15}$$

$$\Phi = \frac{-1}{j\omega\varepsilon} \int_0^{2\pi} \frac{1}{b}\frac{dI}{d\phi'}\frac{e^{-jkR}}{4\pi R}\, b\, d\phi' \tag{5-16}$$

where R is the distance from the wire axis to a point on the surface at $\rho = b$; that is,

$$R = \sqrt{b^2 + b^2 - 2b^2 \cos(\phi - \phi') + a^2}$$

$$= b\sqrt{4 \sin^2(\phi - \phi')/2 + (a/b)^2} \tag{5-17}$$

Here a is the wire radius and b the loop radius. If $b \gg a$, (5-17) is approximately true for all points on the wire surface. To write (5-14) to (5-16) in the form of (5-2), we define the operator

$$L(I) = \int_0^{2\pi} \left[j\omega\mu b I \cos(\phi - \phi') - \frac{1}{j\omega\varepsilon b}\frac{dI}{d\phi'}\frac{d}{d\phi} \right] \frac{e^{-jkR}}{4\pi R}\, d\phi' \tag{5-18}$$

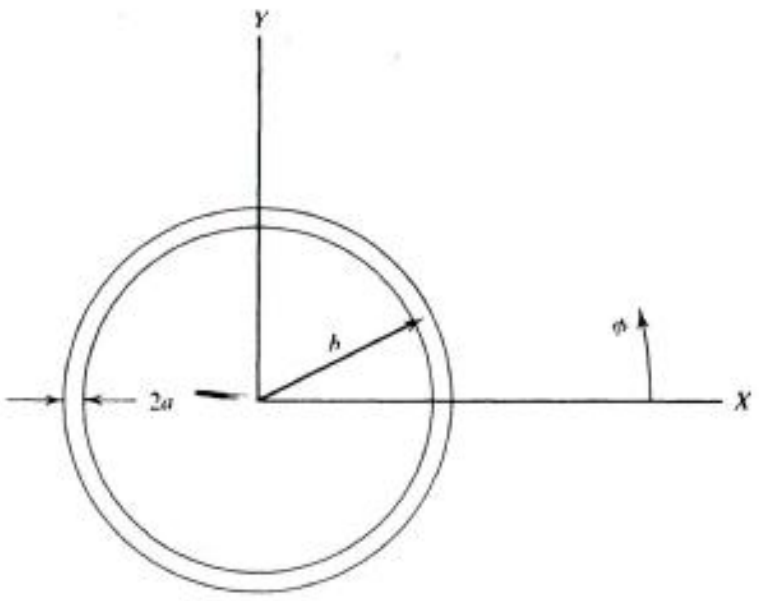

Figure 5-2. Circular wire loop and coordinate system.

Now the problem is stated by

$$L(I) = E_\phi^i \tag{5-19}$$

where E_ϕ^i is the impressed field evaluated at $\rho = b$, $z = 0$. This assumes that E_ϕ^i is a function only of ϕ; that is, it does not vary over the cross section of the wire.

For a generalized impedance solution, define the inner product

$$\langle I, E \rangle = \int_0^{2\pi} I(\phi)E(\phi)b\, d\phi \tag{5-20}$$

which is a specialization of (5-3). For expansion functions, choose $f_n = e^{jn\phi}$, so that (5-4) becomes

$$I(\phi) = \sum_n I_n e^{jn\phi} \tag{5-21}$$

where I_n are constants. For testing functions, choose

$$w_m = f_m^* = e^{-jm\phi} \tag{5-22}$$

which form a biorthogonal set with the f_n. Equations (5-21) and (5-22) are chosen so that a complex Fourier series solution is obtained. Note that both the f_n and w_n have derivatives of all orders, and hence the differentiation in (5-18) will cause no difficulty. The procedure of the method of moments now leads directly to (5-9), where the elements of $[V]$ are

$$V_m = \langle w_m, E_\phi^i \rangle = \int_0^{2\pi} e^{-jm\phi} E_\phi^i(\phi)b\, d\phi \tag{5-23}$$

and the elements of $[Z]$ are

$$Z_{mn} = \langle w_m, Lf_n \rangle = \int_0^{2\pi} e^{-jm\phi} L(e^{jn\phi})b\, d\phi \tag{5-24}$$

A solution for the coefficients I_n of the expansion (5-21) is then given by (5-10), where $[Y]$ is the inverse of $[Z]$.

We must now evaluate (5-24). For this, define the Fourier series

$$\frac{b}{R} e^{-jkR} = \sum_{n=-\infty}^{\infty} K_n e^{jn(\phi - \phi')} \tag{5-25}$$

where R is given by (5-17). The K_n are the usual Fourier coefficients

$$K_n = \frac{1}{2\pi}\int_0^{2\pi} \frac{e^{-jkb\sqrt{4\sin^2\phi/2+(a/b)^2}}}{\sqrt{4\sin^2\phi/2+(a/b)^2}} e^{-jn\phi}\,d\phi \tag{5-26}$$

Now substitute (5-25) in (5-18), and evaluate $Lf_n = Le^{jn\phi}$. The result is

$$Le^{jn\phi} = \frac{j}{2b}\left[\frac{\omega\mu b}{2}(K_{n-1}+K_{n+1}) - \frac{n^2}{\omega\varepsilon b}K_n\right]e^{jn\phi} \tag{5-27}$$

The fact that LI varies as $e^{jn\phi}$ when I varies as $e^{jn\phi}$ is to be expected from symmetry considerations, since $-LI$ is the E_ϕ field from I. Now, using (5-27) and (5-22) in (5-24), we have

$$Z_{mn} = 0 \qquad m \neq n \tag{5-28}$$

$$Z_{nn} = j\pi\eta kb\left[\frac{1}{2}K_{n-1} + \frac{1}{2}K_{n+1} - \left(\frac{n}{kb}\right)^2 K_n\right] \tag{5-29}$$

Hence $[Z]$ is diagonal, and its inverse $[Y]$ is also diagonal, with elements reciprocal to (5-29). The solution (5-21) therefore reduces to the simple form

$$I(\phi) = \sum_n \frac{V_n}{Z_{nn}} e^{jn\phi} \tag{5-30}$$

For exact solutions, n ranges from $-\infty$ to $+\infty$; for computation we take n from $-N$ to $+N$. Note that $Z_{nn} = Z_{-n-n}$, which follows from (5-29) and (5-26).

Functions proportional to the K_n of (5-26) were first evaluated by Oseen [3]. The simplest formulas for the K_n are those of Iizuka et al. [4].

$$K_0 = \frac{1}{\pi}\ln\frac{8b}{a} - \frac{1}{2}\int_0^{2kb}[\Omega_0(x) + jJ_0(x)]\,dx \tag{5-31}$$

$$K_{n+1} = K_n + \Omega_{2n+1}(kb) + jJ_{2n+1}(kb) \tag{5-32}$$

where J_n is the Bessel function of the first kind of order n and Ω_n is the Lommel-Weber function of order n. Formulas (5-31) and (5-32) assume $b \gg a$, and apparently give good results when $b \geq 10a$. To illustrate the behavior of the generalized impedances Z_{nn} of (5-29), Fig. 5-3 shows plots of the lower-order ones. Note that for small loops, all Z_{nn} are capacitive except Z_{00}, which is inductive. In fact, Z_{00} is the radiation impedance of a loop of uniform current.

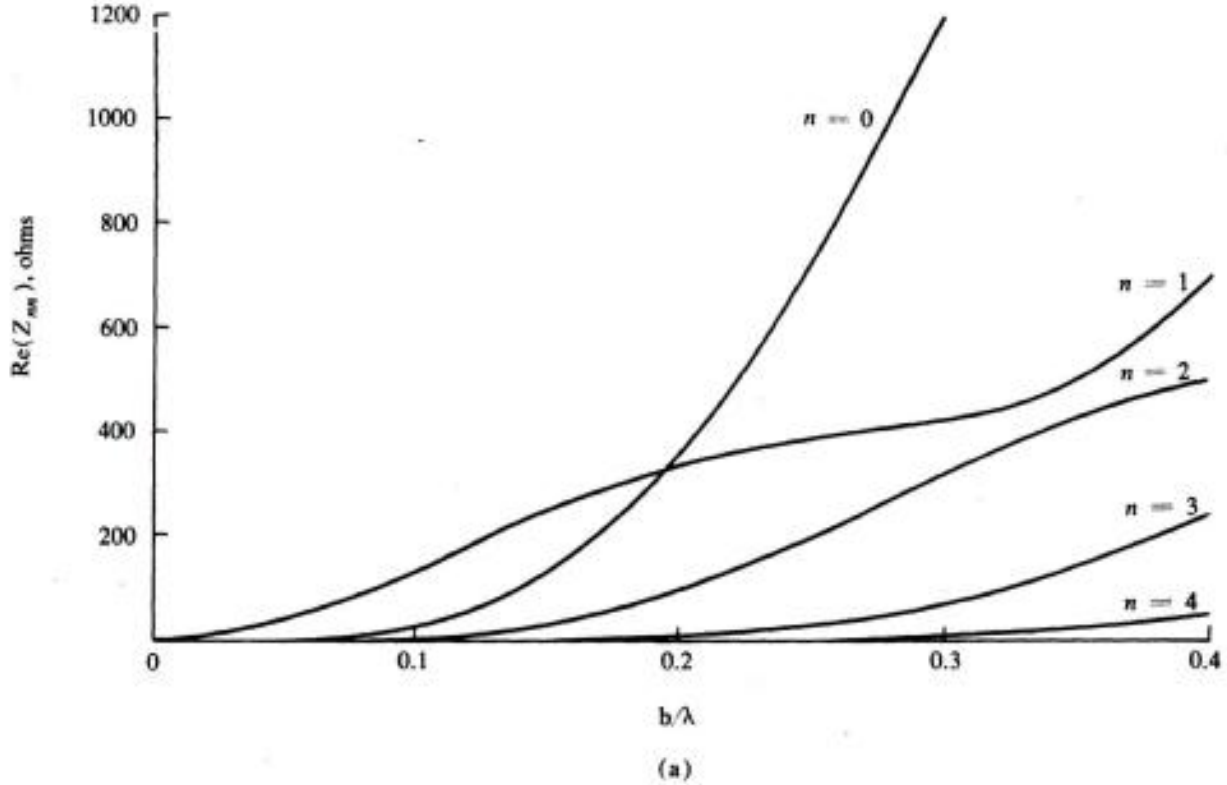

(a)

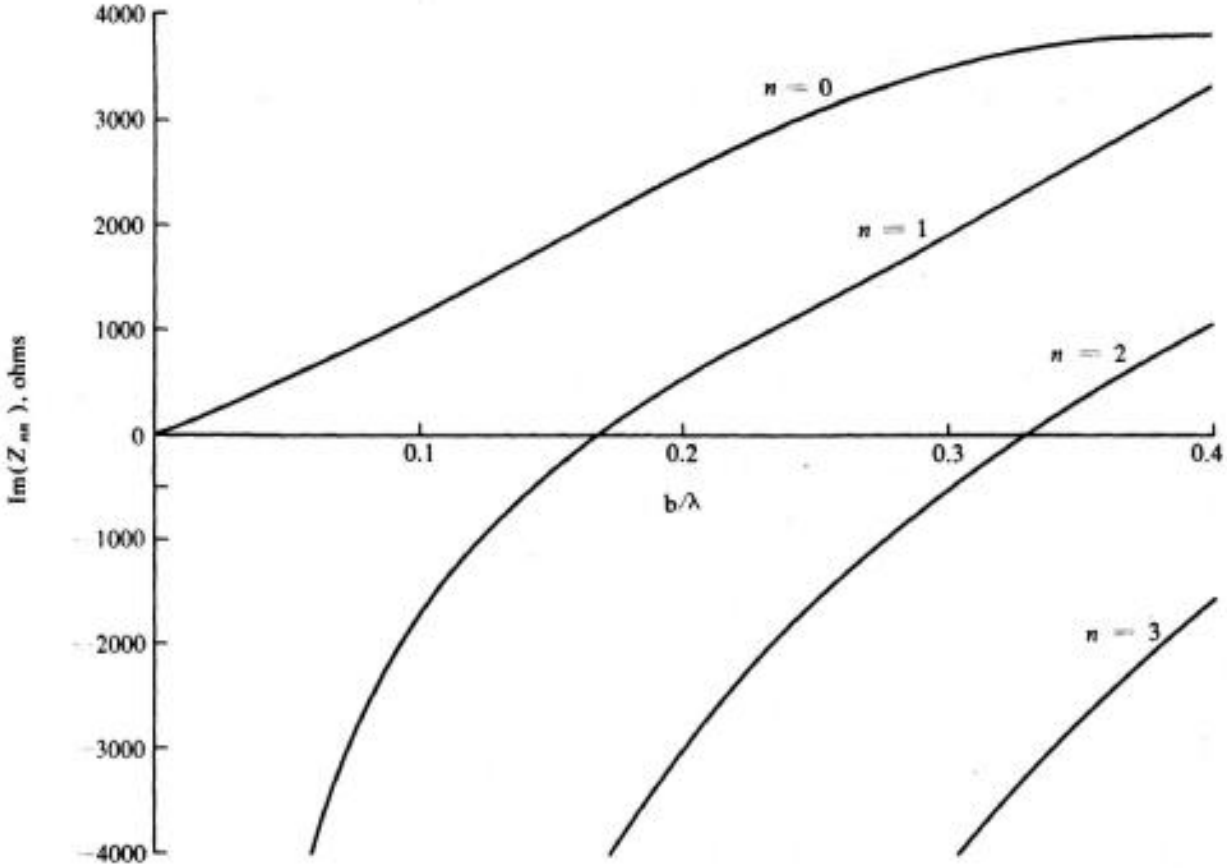

(b)

Figure 5-3. **Generalized impedances Z_{nn} for the circular wire loop. (*a*) Resistance, (*b*) reactance.**

5-2. Point-fed Antennas

We use the term *point-fed* to denote excitation by a current source applied to a pair of terminals separated a distance much smaller than a wavelength. This corresponds to the lumped source of circuit theory. Figure 5-4 shows a typical point-fed antenna problem, consisting of a conducting body excited by a current source I_s at its input port. The tangential component of the electric intensity is zero on the conductor, and its line integral across the gap is the source voltage V_s. The input admittance to the antenna is

$$Y_{ss} = \frac{I_s}{V_s} \tag{5-33}$$

When the method of moments is used, **J** is found by (5-13) and I_s is computed from **J** at the input terminals.

For an antenna with a single feed, the complex power input to the antenna is

$$P = V_s I_s^* = |V_s|^2 Y_{ss}^* \tag{5-34}$$

and the time-average power input is

$$P_{\text{in}} = \text{Re}(P) = \text{Re}(|V_s|^2 Y_{ss}) \tag{5-35}$$

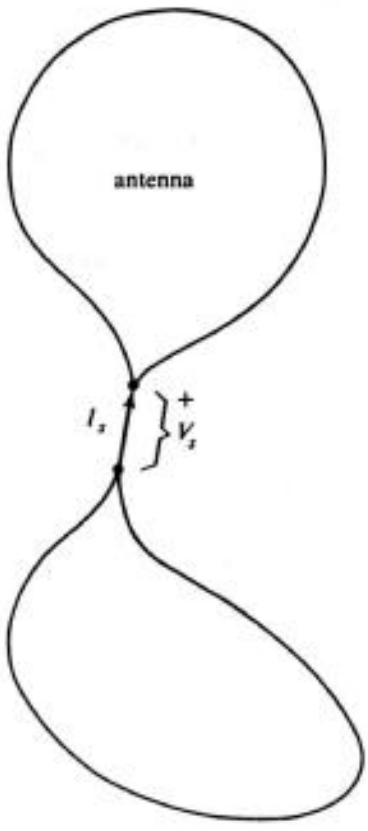

Figure 5-4. Point-fed antenna.

Sometimes it is desired to evaluate the power input for a more complicated excitation, for example, several lumped sources or an aperture excitation (Section 5-4). In general, we have

$$P = -\iint \mathbf{E}^s \cdot \mathbf{J}^* \, ds \tag{5-36}$$

where $\mathbf{E}^s$ is the field from $\mathbf{J}$. For a moment solution (5-13), this becomes

$$P = -\iint \mathbf{E}^s \cdot [\bar{\mathbf{J}}_n^*][Y_{nm}^*][V_m^*] \, ds \tag{5-37}$$

Now define the row matrix $[\hat{V}_n]$ to have elements

$$\hat{V}_n = \iint \mathbf{E}^i \cdot \mathbf{J}_n^* \, ds \tag{5-38}$$

and, since $\mathbf{E}_{\tan}^s = -\mathbf{E}_{\tan}^i$ on S, equation (5-37) can be written

$$P = [\hat{V}_n][Y_{nm}^*][V_m^*] \tag{5-39}$$

The time-average power is the real part of (5-39). In the special case $\mathbf{J}_n = \mathbf{W}_n =$ real (Galerkin's method with real expansion functions), equation (5-39) reduces to (4-38).

To evaluate the radiation field, consider a current element $I\mathbf{l}_r$ distant from the original antenna, as shown for a wire antenna in Fig. 4-4. For conducting antennas in general, analogous to (4-33) we have

$$E_r = \frac{1}{Il_r} \iint_{\text{antenna}} \mathbf{E}^r \cdot \mathbf{J} \, ds \tag{5-40}$$

where $\mathbf{E}^r$ is the field from $I\mathbf{l}_r$, and E_r is the component of $\mathbf{E}$ in the direction of $\mathbf{l}_r$ due to the current $\mathbf{J}$ on the antenna. For the matrix solution (5-13), equation (5-40) becomes

$$E_r = \frac{1}{Il_r} \iint \mathbf{E}^r \cdot [\bar{\mathbf{J}}_n][Y_{nm}][V_m] \, ds \tag{5-41}$$

Hence if we define a "receiver" voltage matrix $[V_n^r]$ with elements

$$V_n^r = \iint \mathbf{E}^r \cdot \mathbf{J}_n \, ds \tag{5-42}$$

equation (5-41) becomes

$$E_r = \frac{1}{Il_r} [\tilde{V}_n^r][Y_{nm}][V_m] \tag{5-43}$$

Finally, if Il_r is adjusted to produce the unit plane wave (4-32) in the vicinity of the antenna, then $1/Il_r$ is given by (4-34), and

$$E_r = \frac{\omega\mu e^{-jkr}}{j4\pi r} [\tilde{V}_n^r][Y_{nm}][V_m] \tag{5-44}$$

This is identical in form to (4-36), derived for the particular case of a subsectional solution of wire antennas. It should be noted that formula (5-44) is general, applying both to the near field and to the far field of the antenna.

Example. Consider the circular loop antenna, with feed at $\phi = 0$, as shown in Fig. 5-5. The solution of Section 5-1 applies directly, with an impressed field

$$E_\phi^i = \frac{V_s}{b}\delta(\phi) \tag{5-45}$$

where $\delta(\phi)$ is the Dirac delta function. The elements of the voltage excitation matrix are found from (5-23) and (5-45) to be all equal to V_s; that is,

$$[V_n] = \begin{bmatrix} \vdots \\ V_s \\ V_s \\ \vdots \end{bmatrix} \tag{5-46}$$

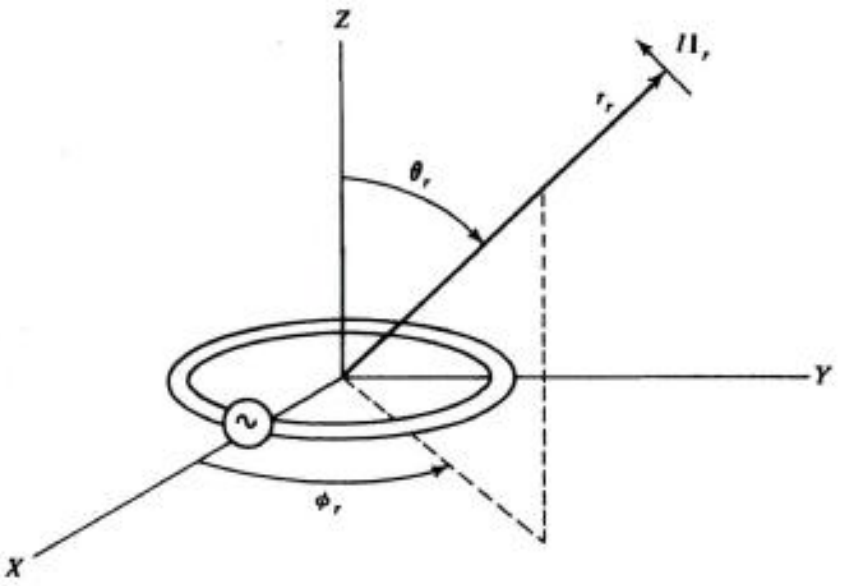

Figure 5-5. Circular loop antenna and distant dipole.

The current on the loop is then given by (5-30), which, since $Z_{nn} = Z_{-n-n}$, reduces to

$$I(\phi) = \frac{V_s}{Z_{00}} + 2V_s \sum_{n=1}^{\infty} \frac{\cos n\phi}{Z_{nn}} \tag{5-47}$$

The input admittance is given by (5-33), where $I_s = I(0)$; hence

$$Y_{ss} = \frac{I(0)}{V_s} = \frac{1}{Z_{00}} + 2\sum_{n=1}^{\infty} \frac{1}{Z_{nn}} \tag{5-48}$$

The loop input admittance is thus precisely the parallel combination of all generalized impedances. This result is due to the diagonal nature of $[Y]$.

The solution (5-47) and (5-48) was first obtained by Hallén [5], and first computed by Storer [6]. However, Storer's approximation of the infinite sum by an integral to obtain the susceptance is open to question, as shown by later computations [7]. We have computed the input admittance by (5-48) using terms up to $n = 20$, the results being shown in Fig. 5-6. The input conductance converges very rapidly, but the input susceptance does not. This is to be expected, since an exact analysis for the impressed field (5-45) must give infinite input capacitance because of the zero length gap.

For computation of the radiation pattern, we evaluate (5-42) for the currents $\mathbf{J}_n = \mathbf{u}_\phi e^{jn\phi}$. The coordinates θ_r and ϕ_r of the receiver are as defined in Fig. 5-5. The current element $I\mathbf{l}_r$ is perpendicular to $\mathbf{r}_r$, and may be pointed in either the ϕ or θ directions. To respond to the ϕ component of the radiation field, $I\mathbf{l}_r$ points in the ϕ direction, and, from (5-42) and (4-32), we can determine [8]

$$V_n^r = \pi b j^{n+1} e^{jn\phi_r}[J_{n+1}(kb \sin \theta_r) - J_{n-1}(kb \sin \theta_r)] \tag{5-49}$$

Use of this in (5-44) gives the E_ϕ of the radiation field. To respond to the θ component of the radiation field, $I\mathbf{l}_r$ points in the θ direction, and, from (5-42) and (4-32), we can calculate [8]

$$V_n^r = -\pi b j^n e^{jn\phi_r} \cos \theta_r[J_{n+1}(kb \sin \theta_r) + J_{n-1}(kb \sin \theta_r)] \tag{5-50}$$

Now (5-44) gives the E_θ component of the radiation field. Because of the diagonal nature of $[Y_{mn}]$, and the simple form (5-46) for $[V_n]$, equation (5-44) reduces to

$$E_i = \frac{\omega\mu e^{-jkr}}{j4\pi r} V_s \sum_n \frac{V_n^r}{Z_{nn}} \tag{5-51}$$

Here $i = \phi$ if (5-49) is used for V_n^r, and $i = \theta$ if (5-50) is used for V_n^r. Computation of the power gain pattern can be made by (4-39) for either the θ or ϕ component. The sum of these two patterns is the total gain pattern.

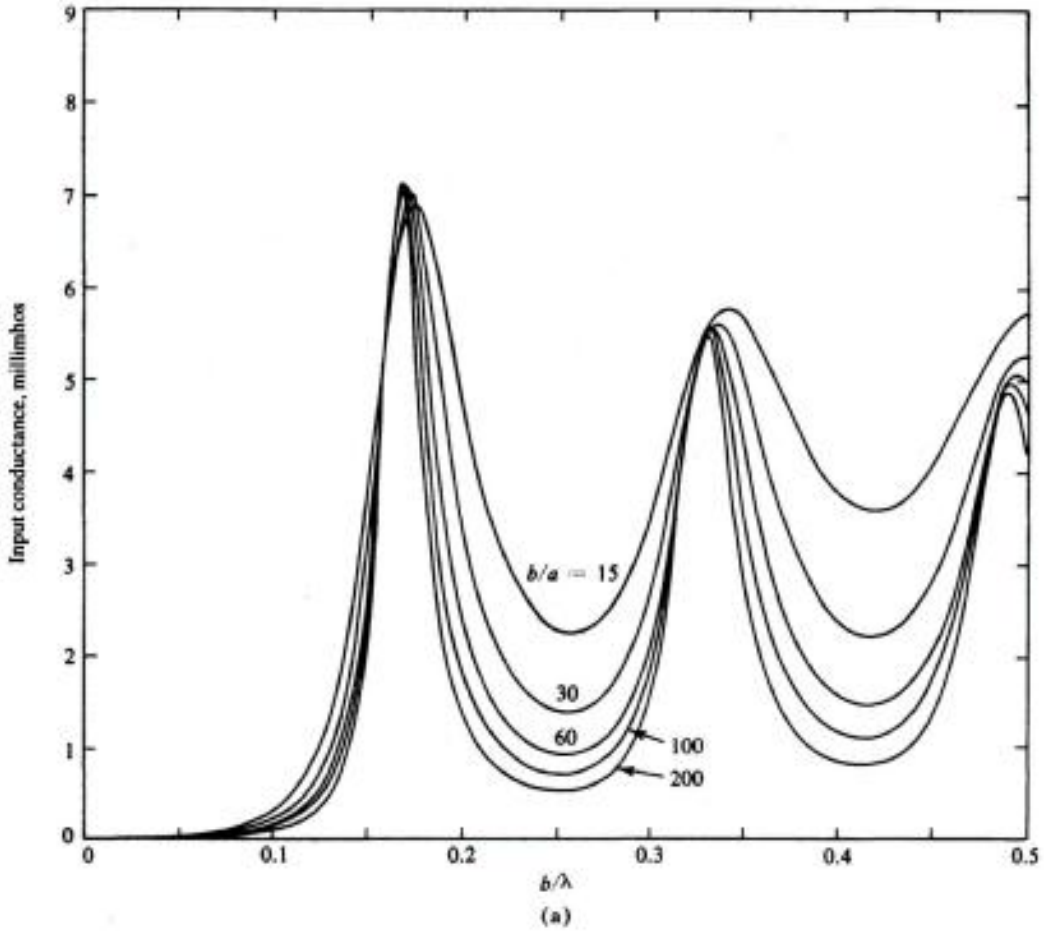

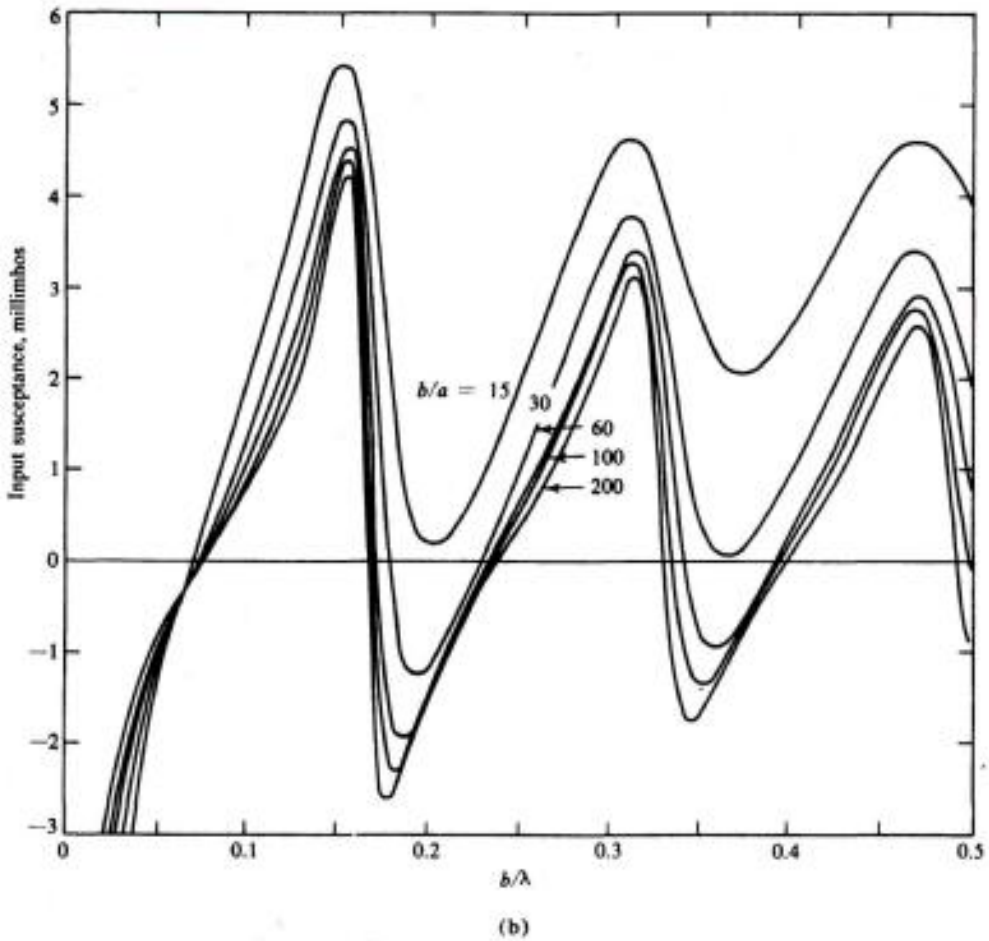

Figure 5-6. **Input admittance to the circular loop antenna. (*a*) Conductance, (*b*) susceptance.**

5-3. Conducting Scatterers

The general problem of scattering by conducting bodies is an extension of Section 4-5. Consider a conducting body and two current elements, as shown in Fig. 4-9 for the wire case. The current element Π_r represents the receiver, and the analysis is identical to that for the antenna problem, equations (5-40) to (5-44). The current element Π_t represents the transmitter, and it produces the impressed field $\mathbf{E}^i = \mathbf{E}^t$. The excitation matrix $[V_m] = [V_m^t]$ of (5-7) now has elements

$$V_m^t = \langle \mathbf{W}_m, \mathbf{E}^t \rangle = \oiint \mathbf{E}^t \cdot \mathbf{W}_m \, ds \tag{5-52}$$

Note that, for a Galerkin solution, this is of the same form as the measurement matrix (5-42). When Π_r is distant from the scatterer, (5-44) still applies. Finally, the scattering cross section is given by (4-43); that is,

$$\sigma = \frac{\eta^2 k^2}{4\pi} |[\bar{V}_n^r][Y_{nm}][V_m^t]|^2 \tag{5-53}$$

where the elements of $[V_n^r]$ are those of (5-42) with $\mathbf{E}^r$ given by (4-32), and the elements of $[V_m^t]$ are those of (5-52) with $\mathbf{E}^t$ given by (4-40).

Example. Consider plane-wave scattering by a circular wire loop. Let the loop lie in the xy plane, and define transmitter and receiver coordinates as in Fig. 4-9. The elements of $[V_n^r]$ are the same as those of the loop antenna, given by (5-49) for the ϕ-polarized case and (5-50) for the θ-polarized case. The elements of $[V_n^t]$ are the same as those of $[V_n^r]$ except that $-n$ replaces n because $f_n = e^{jn\phi}$ and $w_n = e^{-jn\phi}$. Hence, for Π_t pointing in the ϕ direction, analogous to (5-49) we have

$$V_n^t = \pi b j^{n+1} e^{-jn\phi_t} [J_{n+1}(kb \sin \theta_t) - J_{n-1}(kb \sin \theta_t)] \tag{5-54}$$

For Π_t pointing in the θ direction, analogous to (5-50) we have

$$V_n^t = \pi b j^n e^{-jn\phi_t} \cos \theta_t [J_{n+1}(kb \sin \theta_t) + J_{n-1}(kb \sin \theta_t)] \tag{5-55}$$

The scattering cross section is then given by (5-53), which, because of the diagonal nature of $[Y]$, reduces to

$$\sigma = \frac{\eta^2 k^2}{4\pi} \left| \sum_n \frac{V_n^r V_n^t}{Z_{nn}} \right|^2 \tag{5-56}$$

Computations for the case of backscattering were first made by Koumyoujian [9], who obtained the solution by the Rayleigh-Ritz variational procedure. Figure 5-7 shows the backscattering σ/λ^2 vs. b/λ for some representative values of b/a.

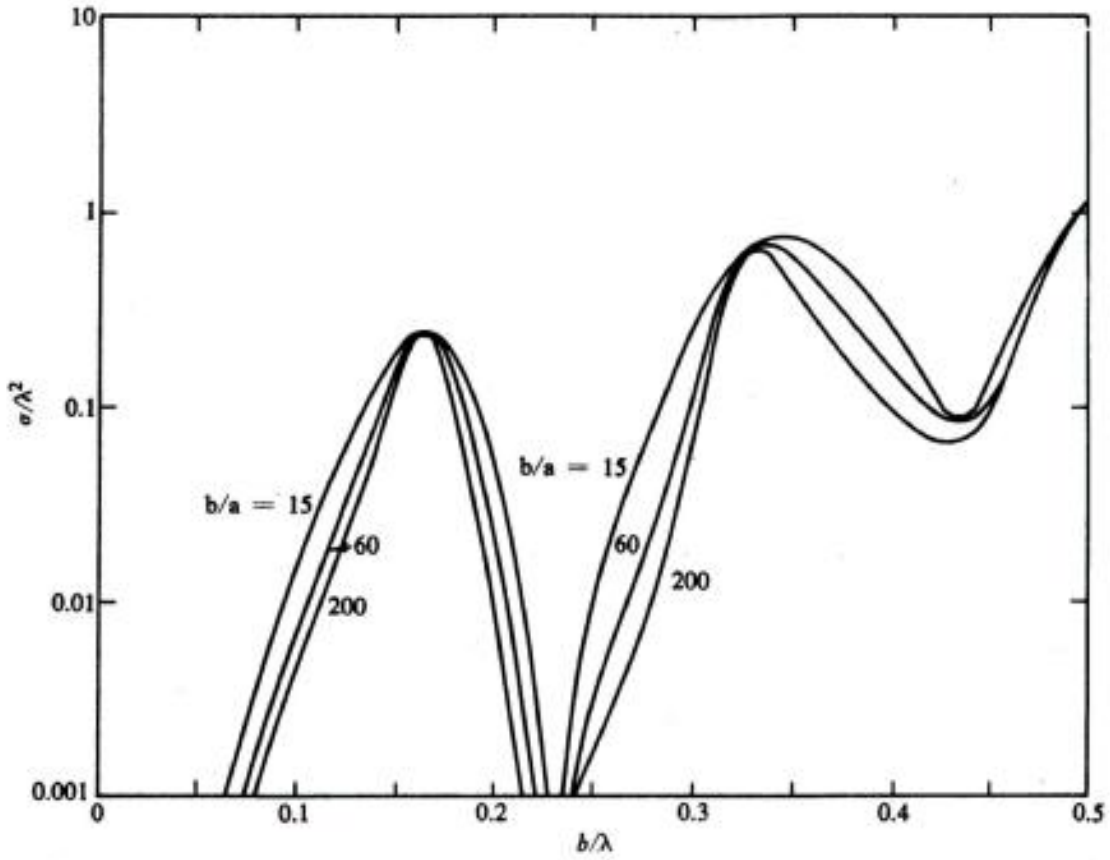

Figure 5-7. **Backscattering cross section for a circular loop scatterer, for various ratios b/a.**

Note that for any particular directions to the transmitter and receiver there are actually four possible cases, corresponding to $\phi - \phi$, $\theta - \theta$, $\phi - \theta$, and $\theta - \phi$ polarizations of the transmitter and receiver, respectively. A more complete description of the scattering properties of a body can be made in terms of the scattering matrix.

5-4. Aperture Antennas

An aperture antenna is a conducting body with one or more apertures in it, through which electromagnetic energy may pass. A knowledge of the tangential components of the **E** vector over a closed surface S is sufficient to uniquely specify the field external to S [10]. Over a conductor $\mathbf{E}_{tan} = 0$; hence a knowledge of $\mathbf{E}_{tan}$ over the apertures is sufficient to determine the external field. Figure 5-8 represents a conducting body with an aperture, shown dashed. Let S be a closed surface consisting of both the conductor and aperture and **J** be a distribution of surface current on S. Then the problem is represented by

$$L(\mathbf{J}) = -\mathbf{E}_{tan} \tag{5-57}$$

where L is the operator defined by (5-1), and $\mathbf{E}_{tan}$ is the known field on S. A solution of (5-57) determines **J**, which on the conductor is the current due to the

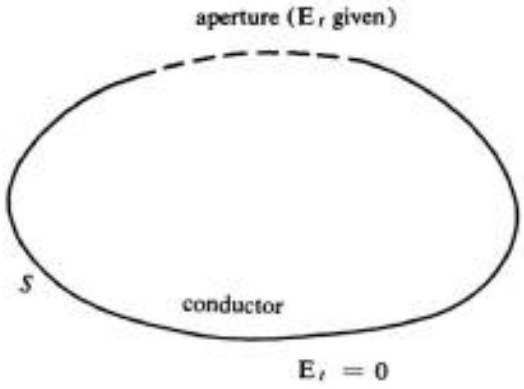

Figure 5-8. **Conducting body with an aperture antenna.**

aperture excitation, and over the aperture is an equivalent current [10]. In (5-57) the $\mathbf{E}_{tan}$ is that due to $\mathbf{J}$, and hence is $-\mathbf{E}^i_{tan}$ of (5-2).

To solve (5-57), we can use a moment solution as in (5-3) through (5-13). If the basis functions are sufficiently general, the generalized impedance matrix is the same one as the one used for point-fed antennas and for scatterers. In fact, a point-fed antenna can be viewed as an aperture antenna in which the gap at the feed is the aperture. Hence the analysis of aperture antennas is basically the same as that for point-fed antennas if the excitation matrix $[V_m]$ is kept general. For aperture antennas, its elements are given by

$$V_m = -\langle \mathbf{W}_m, \mathbf{E} \rangle = -\iint_{\text{aperture}} \mathbf{E} \cdot \mathbf{W}_m \, ds \tag{5-58}$$

Note that the integral need be taken only over the aperture, since $\mathbf{E}_{tan} = 0$ on the conductor. Once the solution (5-13) is obtained, parameters such as complex power is given by (5-39) and the radiation field by (5-44).

Example. Consider an aperture in the elliptical conducting cylinder analyzed in the example of Section 3-2. Let the aperture be $\lambda/2$ in width, and assume a field

$$E_z = \cos ks \tag{5-59}$$

in the aperture. Figure 5-9(a) shows the cylinder and aperture, centered on the x axis. The variable s is measured about the cylinder in the counterclockwise direction, starting on the positive x axis. The basis functions for J_z are the step functions (3-8), and point matching is used for testing. The impedance matrix is related to the $[I_{mn}]$ matrix according to (3-22). The measurement matrix continues to be given by (3-23), which is the two-dimensional analogue to (5-42). The excitation matrix, instead of (3-21), becomes

$$V_m = \begin{cases} \Delta C_m \cos ks_m & \text{in the aperture} \\ 0 & \text{on the conductor} \end{cases} \tag{5-60}$$

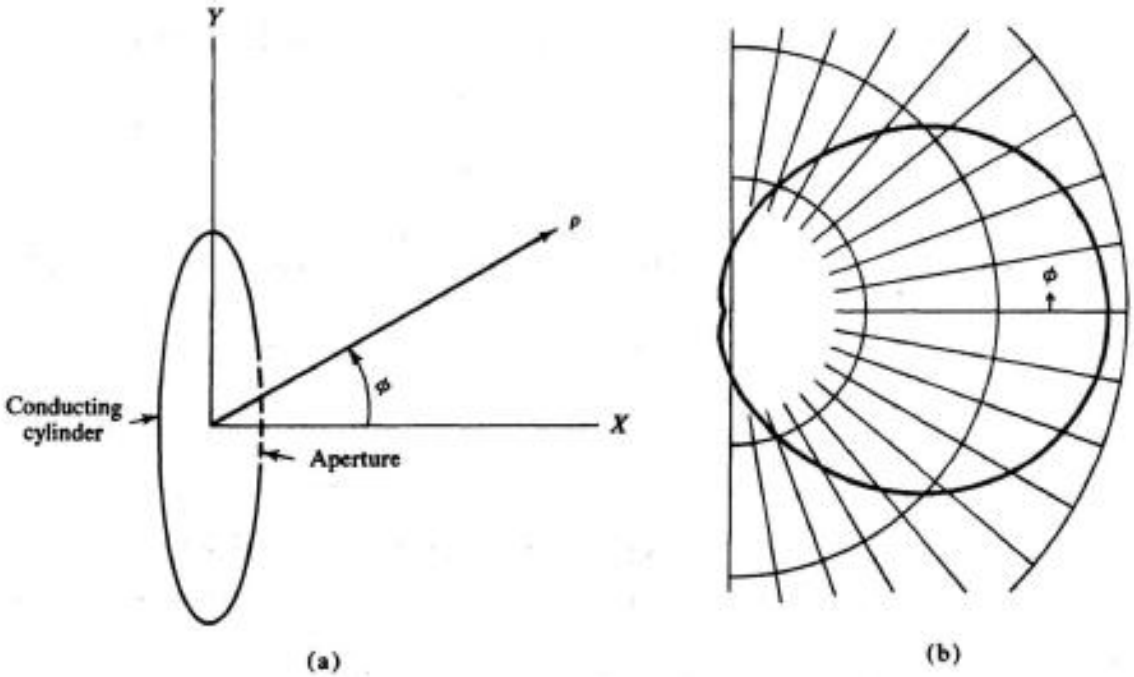

Figure 5-9. **(a) Conducting elliptic cylinder with $\lambda/2$ aperture, TM field. (b) Radiation field pattern.**

The radiation field is given by the two-dimensional analogue to (5-44), which is of the same matrix form, but with different radial dependence. To be explicit,

$$E_z = \frac{-j\omega\mu e^{-jk\rho}}{\sqrt{8\pi jk\rho}} [\tilde{V}_n'][Y_{nm}][V_m] \tag{5-61}$$

where ρ is the two-dimensional radius vector from the origin. The radiation pattern of $|E_z|$ as computed by the above formulas is shown in Fig. 5-9(b).

5-5. Dielectric Bodies

Let the material body of Fig. 5-1 be a dielectric with permittivity ε, which may be a function of position, or even a tensor. The incident field $\mathbf{E}^i$ induces a polarization current $\mathbf{J}$ in the dielectric, which produces a scattered field $\mathbf{E}^s$. Let L be the operator which relates $-\mathbf{E}^s$ to $\mathbf{J}$; that is,

$$L(\mathbf{J}) = -\mathbf{E}^s = j\omega\mathbf{A} + \nabla\Phi \tag{5-62}$$

where

$$\mathbf{A}(\mathbf{r}) = \mu_0 \iiint_{\text{body}} \mathbf{J}(\mathbf{r}') \frac{e^{-jkR}}{4\pi R} d\tau' \tag{5-63}$$

$$\Phi(\mathbf{r}) = \frac{1}{\varepsilon_0} \iiint_{\text{body}} q(\mathbf{r}') \frac{e^{-jkR}}{4\pi R} d\tau' \tag{5-64}$$

$$\nabla \cdot \mathbf{J} = -j\omega q \tag{5-65}$$

and $R = |\mathbf{r} - \mathbf{r}'|$. The total field at any point is $\mathbf{E}^i + \mathbf{E}^s$, and within the material body the polarization current is given by

$$\mathbf{J} = j\omega(\varepsilon - \varepsilon_0)(\mathbf{E}^i + \mathbf{E}^s) \tag{5-66}$$

where ε is the permeability of the body and ε_0 that of free space. Using (5-62), we can rewrite (5-66) as

$$L(\mathbf{J}) + \frac{\mathbf{J}}{j\omega\,\Delta\varepsilon} = \mathbf{E}^i \qquad \text{in } V \tag{5-67}$$

where $\Delta\varepsilon = \varepsilon - \varepsilon_0$ and V is the region occupied by the material body. This is the appropriate equation for $\mathbf{J}$. The left side of (5-67) could be redefined as a single operation on $\mathbf{J}$, but we shall not do so.

For a solution, define the inner product

$$\langle \mathbf{J}, \mathbf{E} \rangle = \iiint \mathbf{J} \cdot \mathbf{E}\, d\tau \tag{5-68}$$

which is again a reaction [1]. This differs from (5-3) only in that the integral is now a volume integral. Define basis functions $\mathbf{J}_1, \mathbf{J}_2, \mathbf{J}_3, \ldots$, over V, and expand $\mathbf{J}$ as

$$\mathbf{J} = \sum_n I_n \mathbf{J}_n \tag{5-69}$$

where the I_n are complex constants. Define testing functions $\mathbf{W}_1, \mathbf{W}_2, \mathbf{W}_3, \ldots$, over V, and apply the method of moments to (5-67). The resulting equations are

$$\sum_n I_n \left\langle \mathbf{W}_m, L\mathbf{J}_n + \frac{\mathbf{J}_n}{j\omega\,\Delta\varepsilon} \right\rangle = \langle \mathbf{W}_m, \mathbf{E}^i \rangle \tag{5-70}$$

for all m. To place this in matrix form, define $[I_n]$ and $[V_m]$ according to (5-7), $[Z_{mn}]$ according to (5-8), and the additional matrix

$$[Z_{mn}] = \begin{bmatrix} \left\langle \mathbf{W}_1, \dfrac{\mathbf{J}_1}{j\omega\,\Delta\varepsilon} \right\rangle & \left\langle \mathbf{W}_1, \dfrac{\mathbf{J}_2}{j\omega\,\Delta\varepsilon} \right\rangle & \cdots \\ \left\langle \mathbf{W}_2, \dfrac{\mathbf{J}_1}{j\omega\,\Delta\varepsilon} \right\rangle & \left\langle \mathbf{W}_2, \dfrac{\mathbf{J}_2}{j\omega\,\Delta\varepsilon} \right\rangle & \cdots \\ \cdots & \cdots & \end{bmatrix} \tag{5-71}$$

Now (5-70) can be written

$$[Z_{mn} + \hat{Z}_{mn}][I_n] = [V_m] \tag{5-72}$$

The solution for the expansion coefficients $[I_n]$ is again given by (5-10), where

$$[Y_{nm}] = [(Z + \hat{Z})^{-1}_{nm}] \tag{5-73}$$

The solution for the polarization current is represented by (5-13), which may be either approximate or exact, depending on the $\mathbf{J}_n$ and $\mathbf{W}_n$.

The matrix equation (5-72) was written in terms of two impedance matrices to call attention to an interesting analogy with N-port network theory, as represented by Fig. 5-10. The matrix $[Z]$ depends only on the geometry of the

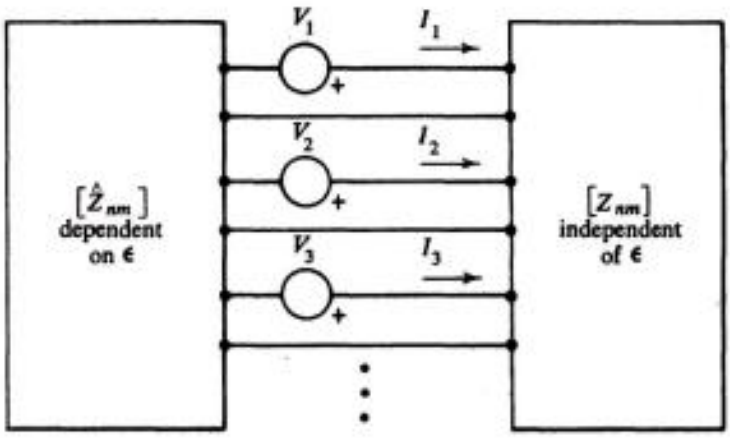

Figure 5-10. **Network analogue for a dielectric body in an impressed field.**

body and the wavelength, whereas the matrix $[\hat{Z}]$ depends also on ε. The impressed electric field determines the voltage excitation of these two networks connected in series, and the resultant terminal currents are the expansion coefficients $[I_n]$. Note that as $\varepsilon \to \infty$, the $[\hat{Z}]$ becomes a short-circuit on each port, and the network analogy becomes that of a conducting body. Hence we can think of $[\hat{Z}]$ as expressing the loading of space due to the permittivity of a body, with a conductor short-circuiting space. This latter picture is the one used in Chapter 4 for wire objects. Finally, if a subsectional method is used, the $[\hat{Z}]$ becomes a diagonal matrix, as discussed in Section 5-7. For examples of the application of these techniques to physical problems, refer to the analysis of dielectric cylinders discussed in Section 3-7.

5-6. Magnetic Bodies

If the body of Fig. 5-1 is magnetic, but not dielectric, the problem is dual to the dielectric case. The solution is obtained by replacing **E** by **H**, **J** by **M** (magnetic

current), μ by ε, and ε by μ in Eqs. (5-62) to (5-65). To be specific,

$$L(\mathbf{M}) = -\mathbf{H}^s = j\omega\mathbf{A}^m + \nabla\Phi^m \tag{5-74}$$

where

$$\mathbf{A}^m(\mathbf{r}) = \varepsilon_0 \iiint_{\text{body}} \mathbf{M}(\mathbf{r}') \frac{e^{-jkR}}{4\pi R}\, d\tau' \tag{5-75}$$

$$\Phi^m(\mathbf{r}) = \frac{1}{\mu_0} \iiint_{\text{body}} q^m(\mathbf{r}') \frac{e^{-jkR}}{4\pi R}\, d\tau' \tag{5-76}$$

$$\nabla \cdot \mathbf{M} = -j\omega q^m \tag{5-77}$$

Here the superscript m has been added to denote "magnetic quantity." Instead of (5-66), we have the magnetization current $\mathbf{M}$ given by

$$\mathbf{M} = j\omega(\mu - \mu_0)(\mathbf{H}^t + \mathbf{H}^s) \tag{5-78}$$

where μ is the permeability of the body and μ_0 that of free space. The operator equation is then dual to (5-67), or

$$L(\mathbf{M}) + \frac{\mathbf{M}}{j\omega\,\Delta\mu} = \mathbf{H}^i \qquad \text{in } V \tag{5-79}$$

where $\Delta\mu = \mu - \mu_0$ and V is the volume of the body.

To solve (5-79) for $\mathbf{M}$, define the inner product

$$\langle \mathbf{M}, \mathbf{H} \rangle = \iiint \mathbf{M} \cdot \mathbf{H}\, d\tau \tag{5-80}$$

which is dual to (5-68), and is the negative of reaction [1]. Define basis functions $\mathbf{M}_1, \mathbf{M}_2, \mathbf{M}_3, \ldots$, over V, and expand $\mathbf{M}$ as

$$\mathbf{M} = \sum_n V_n \mathbf{M}_n \tag{5-81}$$

where the V_n are complex constants. Define testing functions $\mathbf{W}_1, \mathbf{W}_2, \mathbf{W}_3, \ldots$, over V, and apply the method of moments to (5-79). The result is

$$\sum_n V_n \left\langle \mathbf{W}_m, L\mathbf{M}_n + \frac{\mathbf{M}_n}{j\omega\,\Delta\mu} \right\rangle = \langle \mathbf{W}_m, \mathbf{H}^i \rangle \tag{5-82}$$

for all m. This can again be placed in matrix form by defining

$$[V_n] = \begin{bmatrix} V_1 \\ V_2 \\ \vdots \end{bmatrix} \qquad [I_n] = \begin{bmatrix} \langle \mathbf{W}_1, \mathbf{H}^i \rangle \\ \langle \mathbf{W}_2, \mathbf{H}^i \rangle \\ \vdots \end{bmatrix} \tag{5-83}$$

$$[Y_{mn}] = \begin{bmatrix} \langle \mathbf{W}_1, L\mathbf{M}_1 \rangle & \langle \mathbf{W}_1, L\mathbf{M}_2 \rangle & \cdots \\ \langle \mathbf{W}_2, L\mathbf{M}_1 \rangle & \langle \mathbf{W}_2, L\mathbf{M}_2 \rangle & \cdots \\ \cdot & \cdot & \cdot \end{bmatrix} \tag{5-84}$$

$$[\hat{Y}_{mn}] = \begin{bmatrix} \left\langle \mathbf{W}_1, \dfrac{\mathbf{M}_1}{j\omega\,\Delta\mu} \right\rangle & \left\langle \mathbf{W}_1, \dfrac{\mathbf{M}_2}{j\omega\,\Delta\mu} \right\rangle & \cdots \\ \left\langle \mathbf{W}_2, \dfrac{\mathbf{M}_1}{j\omega\,\Delta\mu} \right\rangle & \left\langle \mathbf{W}_2, \dfrac{\mathbf{M}_2}{j\omega\,\Delta\mu} \right\rangle & \cdots \\ \cdot & \cdot & \cdot \end{bmatrix} \tag{5-85}$$

and rewriting (5-82) as

$$[Y_{mn} + \hat{Y}_{mn}][V_n] = [I_m] \tag{5-86}$$

The solution for the expansion coefficients is

$$[V_n] = [(Y + \hat{Y})^{-1}_{nm}][I_m] \tag{5-87}$$

and the solution for the magnetization current is

$$\mathbf{M} = [\tilde{\mathbf{M}}_n][(Y + \hat{Y})^{-1}_{nm}][I_m] \tag{5-88}$$

which is dual to (5-13).

Again we have a suggestive N-port network analogy to (5-86), represented by Fig. 5-11. Here the matrix $[Y]$ depends on the geometry and wavelength, and $[\hat{Y}]$ depends also on μ. The impressed magnetic field determines the current excitation of these two networks connected in parallel, and the resultant terminal voltages are the expansion coefficients $[V_n]$. We can interpret $[\hat{Y}]$ as representing the loading of space due to the permeability of the body, analogous to $[\hat{Z}]$ in the dielectric case. Again $[\hat{Y}]$ becomes a diagonal matrix if a subsectional method is used, as discussed in Section 5-7.

5-7. Bodies both Magnetic and Dielectric

If the body of Fig. 5-1 has both ε and μ different from their free-space values, a combination of the preceding two cases can be used. For this, in addition to

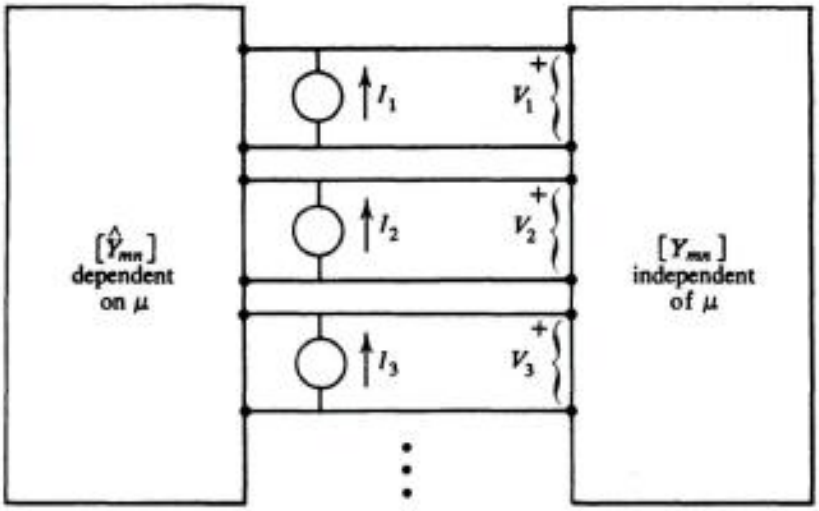

Figure 5-11. **Network analogue for a magnetic body in an impressed field.**

the relationship between electric current and its electric field, (5-62), and magnetic current and its magnetic field, (5-74), we need the relationship between electric current and its magnetic field:

$$\mathbf{H} = \frac{1}{\mu} \nabla \times \mathbf{A} = N(\mathbf{J}) \tag{5-89}$$

which defines the operator N, and the relationship between magnetic current and its electric field

$$\mathbf{E} = -\frac{1}{\varepsilon} \nabla \times \mathbf{A}^m = -N(\mathbf{M}) \tag{5-90}$$

where N is the same operator as in (5-89). The minus-sign difference in (5-89) and (5-90) reflects the minus-sign difference in the two curl equations of Maxwell. The appropriate operator equation is now a matrix combination of (5-67) and (5-79), with the appropriate interaction terms added. To be explicit,

$$\begin{bmatrix} L_e & N \\ N & -L_m \end{bmatrix} \begin{bmatrix} \mathbf{J} \\ -\mathbf{M} \end{bmatrix} + \begin{bmatrix} \mathbf{J}/j\omega\,\Delta\varepsilon \\ \mathbf{M}/j\omega\,\Delta\mu \end{bmatrix} = \begin{bmatrix} \mathbf{E}^i \\ \mathbf{H}^i \end{bmatrix} \tag{5-91}$$

where L_e is the L of (5-62) and L_m is the L of (5-74). The above is an equation for the matrix of vectors $\mathbf{J}$ and $-\mathbf{M}$. The minus signs are placed so that the matrix operators, identified below, will be self-adjoint.

Equation (5-91) is just a more complicated form of a standard operator equation. This is evident if we define

$$f = \begin{bmatrix} \mathbf{J} \\ -\mathbf{M} \end{bmatrix} \qquad g = \begin{bmatrix} \mathbf{E}^i \\ \mathbf{H}^i \end{bmatrix} \tag{5-92}$$

$$\mathscr{L} = \begin{bmatrix} L_e & N \\ N & -L_m \end{bmatrix} \qquad \mathscr{M} = \begin{bmatrix} \dfrac{1}{j\omega\,\Delta\varepsilon} & 0 \\ 0 & \dfrac{1}{j\omega\,\Delta\mu} \end{bmatrix} \tag{5-93}$$

and rewrite (5-90) as

$$\mathscr{L}(f) + \mathscr{M}(f) = g \tag{5-94}$$

Again $\mathscr{L}$ and $\mathscr{M}$ could be combined into a single operator, but we do not choose to do so. An appropriate inner product for the problem is

$$\langle f, g \rangle = \iiint \tilde{f} g \, d\tau = \iiint (\mathbf{J} \cdot \mathbf{E} - \mathbf{H} \cdot \mathbf{M}) \, d\tau \tag{5-95}$$

which is the general definition of reaction [1].

A solution by the method of moments is obtained as follows. Define "electric" expansion and testing functions as

$$f_n^e = \begin{bmatrix} \mathbf{J}_n \\ 0 \end{bmatrix} \qquad w_n^e = \begin{bmatrix} \mathbf{W}_n^e \\ 0 \end{bmatrix} \tag{5-96}$$

and "magnetic" expansion and testing functions as

$$f_n^m = \begin{bmatrix} 0 \\ -\mathbf{M}_n \end{bmatrix} \qquad w_n^m = \begin{bmatrix} 0 \\ -\mathbf{W}_n^m \end{bmatrix} \tag{5-97}$$

The expansion for f is then of the form

$$f = \sum_n (I_n f_n^e + V_n f_n^m) \tag{5-98}$$

Following the method of moments, we obtain the matrix equation

$$\begin{bmatrix} [Z_{mn}] & [B_{mn}] \\ [C_{mn}] & [Y_{mn}] \end{bmatrix} \begin{bmatrix} [I_n] \\ [V_n] \end{bmatrix} + \begin{bmatrix} [\hat{Z}_{mn}][I_n] \\ [\hat{Y}_{mn}][V_n] \end{bmatrix} = \begin{bmatrix} [V_m^i] \\ [I_m^i] \end{bmatrix} \tag{5-99}$$

Here the various matrices have the same definitions as in Sections 5-5 and 5-6, except that the superscript i has been added to the source terms (right side) to distinguish them from the response terms. The additional matrices $[B_{mn}]$ and $[C_{mn}]$ describe the interaction between electric and magnetic currents.

The network analogy of (5-99) is shown in Fig. 5-12. The network denoted $[L_{mn}]$ depends on geometry and wavelength, but not on ε or μ. The network

$[\hat{Z}_{mn}]$ is in series with the voltage sources, and depends on ε. The network $[\hat{Y}_{mn}]$ is in shunt with the current sources, and depends on μ. The voltage sources are determined by the impressed electric field according to the second of equations (5-7), and the current sources are determined by the impressed magnetic field by the second of (5-83).

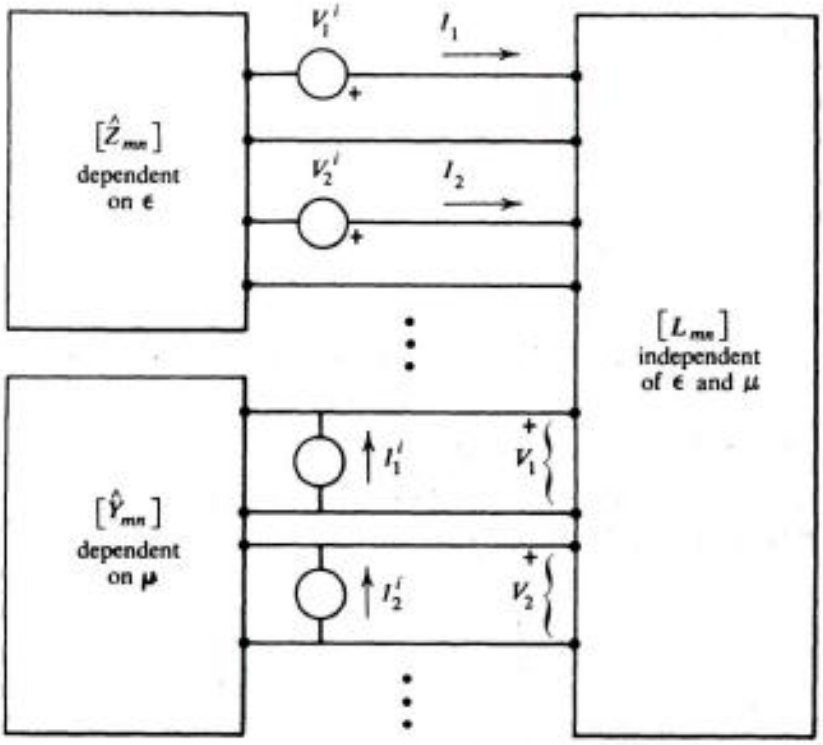

Figure 5-12. **Network analogue for a body with both dielectric and magnetic materials.**

When the method of subsections is used, we can interpret it as dividing the object into a number of pieces, and calculating the interactions according to the method of moments. This is basically the solution for wire objects given in Chapter 4. For conducting bodies, the interactions are a self-impedance for each subsection of current, and mutual impedances with every other element of current. In the case of dielectric (or magnetic) bodies, the interpretation is similar, except that the impedance (or admittance in the magnetic case) can be divided into two parts, one independent of ε (or μ) and the other dependent on ε (or μ). In the method of subsections, the careted networks (left side) of Figs. 5-10, 5-11, and 5-12 involve noninteracting elements, that is, become diagonal matrices. For example, the network representation of Fig. 5-12 becomes that of Fig. 5-13 when subsectional bases and testing are used. The effect of ε and μ is then expressible as simple lumped elements, basically a capacitance and inductance, respectively. Similar simplifications of Figs. 5-10 and 5-11 also result for the purely dielectric and purely magnetic problems.

Although we have in principle a solution to any problem, it is difficult to use it for large bodies because of the large orders of matrices involved. For example, if a cube 1 meter on a side were to be divided into subcubes 0.1 meter

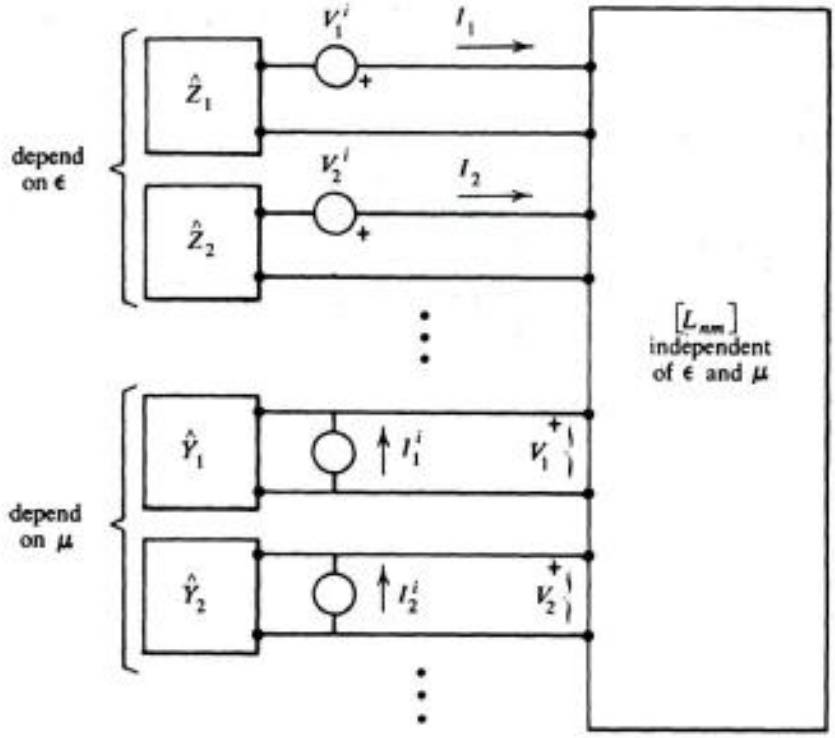

Figure 5-13. **Network analogue for a material body when a subsectional basis is used.**

on a side, there would be 1000 interacting elements. If each element had three electric current bases J_x, J_y, and J_z, and three magnetic current bases M_x, M_y, and M_z, the matrix operators would be of order 3000 by 3000. Storage and inversion would be impossible on even the largest computers. This emphasizes the need of ingenuity in the formulation of a problem to keep it manageable, and of experience to be able to use simplifying approximations.

References

[1] V. H. Rumsey, "The Reaction Concept in Electromagnetic Theory," *Phys. Rev.*, Ser. 2, Vol. **94**, June 15, 1954, pp. 1483–1491.

[2] R. F. Harrington, "Generalized Network Parameters in Field Theory," *Proceedings of the Symposium on Generalized Networks*, MRIS Series, Vol. **XVI**, Polytechnic Press, Brooklyn, 1966.

[3] C. W. Oseen, "Uber die Electromagnetische Spektrum einen Dunnen Ringes," *Arkiv. Mat. Astron. Fysik*, Vol. **9**, No. 28, 1913, pp. 1–34.

[4] K. Iizuka, R. King, and C. Harrison, Jr., "Self and Mutual Admittances of Two Identical Circular Loop Antennas," *IEEE Trans.*, Vol. **AP-14**, No. 4, July 1966, pp. 440–450.

[5] E. Hallén, "Theoretical Investigations into Transmitting and Receiving Qualities of Antennae," *Nova Acta Regial Soc. Sci. Upsaliensis*, Ser. IV, Vol. **2**, No. 4, Nov. 1938, pp. 1–44.

[6] J. E. Storer, "Impedance of Thin-wire Loop Antennas," *Trans. A.I.E.E.*, Part I, Vol. **75**, Nov. 1956, pp. 600–619.

[7] R. King, C. Harrison, Jr., and D. Tingley, "The Admittance of a Bare Circular Loop Antenna in a Dissipative Medium," *IEEE Trans.*, Vol. **AP-12**, No. 4, July 1964, pp. 434–438.

[8] R. F. Harrington and J. L. Ryerson, "Electromagnetic Scattering by Loaded Wire Loops," *Radio Science*, Vol. **1** (new series), No. 3, March 1966, pp. 347–352.

[9] R. G. Kouyoumjian, "Backscattering from a Circular Loop," *Appl. Sci. Res.*, Sect. B, Vol. **6**, 1956, pp. 165–179.

[10] R. F. Harrington, *Time-Harmonic Electromagnetic Fields*, McGraw-Hill Book Co., New York, 1961, Sects. 3-3 and 3-5.

CHAPTER

6

Multiport Systems

6-1. Network Representation

Many electromagnetic engineering problems involve excitation, measurement, tuning, etc., only at ports, that is, at terminal pairs close together compared to wavelength. This concept can be generalized to include ports which are individual modes of a waveguide [1,2]. In this chapter we consider ports as terminal pairs, although waveguide modal ports are included by implication.

Figure 6-1 represents material bodies for which a system of N ports is defined. To avoid confusion with the generalized network parameters of Chapter 5, we shall use lower-case letters to denote port parameters. Hence, let $[v]$ denote the matrix of port voltages and $[i]$ the matrix of port currents. The usual impedance matrix $[z]$ of network theory relates $[v]$ to $[i]$ according to

$$[v] = [z][i] \tag{6-1}$$

It has elements given by

$$z_{ab} = \left.\frac{v_a}{i_b}\right|_{\text{ports open-circuited}} \tag{6-2}$$

where i_b is a current source applied to port b and v_a is the voltage across the open circuit at port a. Alternatively, we can relate $[v]$ to $[i]$ by an admittance matrix $[y]$ according to

$$[i] = [y][v] \tag{6-3}$$

The elements of $[y]$ are given by

$$y_{ab} = \left.\frac{i_a}{v_b}\right|_{\text{ports short-circuited}} \tag{6-4}$$

where v_b is a voltage source applied to port b and i_a is the current in the short circuit at port a. If the inverses exist, it is evident from (6-1) and (6-3) that $[y] = [z^{-1}]$ and $[z] = [y^{-1}]$. Other matrix relationships, such as scattering matrices [3], may be used to relate port voltages and currents if desired.

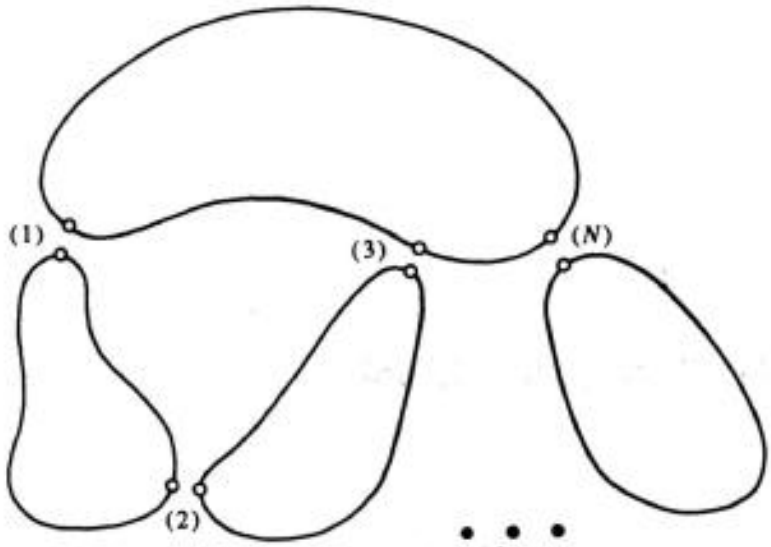

Figure 6-1. **Multiport system.**

The elements of $[z]$ are related to the electromagnetic fields $\mathbf{E}$ and $\mathbf{H}$ and currents $\mathbf{J}$ and $\mathbf{M}$, as follows. Let $\mathbf{E}^a$ and $\mathbf{H}^a$ be the fields when a current source i_a is applied to port a, all ports open-circuited. Let $\mathbf{J}^b$ and $\mathbf{M}^b$ be the currents resulting from a current source i_b applied to port b, all ports open-circuited. The impedance matrix element z_{ab} is then given by [4]

$$z_{ab} = \frac{-1}{i_a i_b} \iiint (\mathbf{E}^a \cdot \mathbf{J}^b - \mathbf{H}^a \cdot \mathbf{M}^b)\, d\tau \tag{6-5}$$

where the integration extends over all space. For nonmagnetic matter ($\mu = \mu_0$) there is no magnetization current $\mathbf{M}$, and (6-5) reduces to

$$z_{ab} = \frac{-1}{i_a i_b} \iiint \mathbf{E}^a \cdot \mathbf{J}^b\, d\tau \tag{6-6}$$

In the case of perfect conductors, the volume integral of (6-6) should be replaced by a surface integral over all conductors.

Now consider a solution in terms of the generalized network parameters of Chapter 5. For perfect conductors, the solution is represented by (5-13). Substituting this in (6-6), we have

$$z_{ab} = \frac{-1}{i_a i_b} [\tilde{V}^a][Y][V^b] \tag{6-7}$$

where $[Y]$ is the generalized admittance matrix, inverse to (5-8), and $[V^a]$ and $[V^b]$ are generalized voltage matrices with elements

$$V_n^a = \langle \mathbf{J}_n, \mathbf{E}^a \rangle \tag{6-8}$$

$$V_n^b = \langle \mathbf{W}_n, \mathbf{E}^b \rangle \tag{6-9}$$

Here $\mathbf{E}^a$ is the field resulting from i_a at port a and $\mathbf{E}^b$ is the field resulting from i_b at port b. If the medium is dielectric, the matrix $[Y]$ is given by (5-73) and the generalized voltages by (6-8) and (6-9). If the media is magnetic, but not dielectric ($\varepsilon = \varepsilon_0$), the concepts of Section 5-6 apply. In this case, $\mathbf{J}^b = 0$ in (6-5), and instead of (6-7) we obtain

$$z_{ab} = \frac{1}{i_a i_b} [\tilde{I}^a][Z][I^b] \tag{6-10}$$

Here $[I^a]$ and $[I^b]$ are generalized current matrices of the form (5-83), that is, dual to (6-8) and (6-9), and $[Z]$ is the impedance matrix appearing in (5-87). For the general case of matter both magnetic and dielectric, we can use a combination of (6-7) and (6-10), with interaction terms added, according to the concepts of Section 5-7.

The elements of $[y]$ can be related to the field quantities by equations dual to (6-5) to (6-10). For example, instead of (6-5), we have in general

$$y_{ab} = \frac{-1}{v_a v_b} \iiint (\mathbf{H}^a \cdot \mathbf{M}^b - \mathbf{E}^a \cdot \mathbf{J}^b)\, d\tau \tag{6-11}$$

Here $\mathbf{H}^a$, $\mathbf{E}^a$ is the field due to voltage source v_a applied to port a, all ports short-circuited, and $\mathbf{M}^b$, $\mathbf{J}^b$ is the current due to v_b applied to port b, all ports short-circuited. Note that the field quantities of (6-5) are not the same as those of (6-11), since in the former case all ports are open-circuited, and in the latter case they are short-circuited. In the case of nonmagnetic media, $\mathbf{M}^b = 0$ and (6-11) reduces to

$$y_{ab} = \frac{1}{v_a v_b} \iiint \mathbf{E}^a \cdot \mathbf{J}^b\, d\tau \tag{6-12}$$

If we use generalized network parameters, (6-12) becomes

$$y_{ab} = \frac{1}{v_a v_b} [\tilde{V}^a][Y][V^b] \tag{6-13}$$

which is dual to (6-10). In any particular problem, the choice between (6-7) and (6-13) is one of convenience. If the system is easier to analyze with all ports open-circuited, (6-7) is used, whereas if the system is easier to analyze with all ports short-circuited, (6-13) is used. Keep in mind that the $[Y]$'s of (6-7) and (6-13) are not the same, because the former is for open-circuited ports and the latter for short-circuited ports.

6-2. Loaded Antennas

A loaded antenna is a structure having two or more ports, fed at one port and loaded by admittance elements at the other ports. In this section we consider only singly loaded antennas; the multiply loaded case will be discussed in Section 6-4. Two examples of singly loaded antennas are the loaded dipole and loop of Fig. 6-2. These two-port structures have an admittance representation

$$\begin{bmatrix} i_1 \\ i_2 \end{bmatrix} = \begin{bmatrix} y_{11} & y_{12} \\ y_{21} & y_{22} \end{bmatrix} \begin{bmatrix} v_1 \\ v_2 \end{bmatrix} \tag{6-14}$$

We choose port 1 to be the input and port 2 the loaded port. The load admittance Y_L imposes the constraint

$$i_2 = -Y_L v_2 \tag{6-15}$$

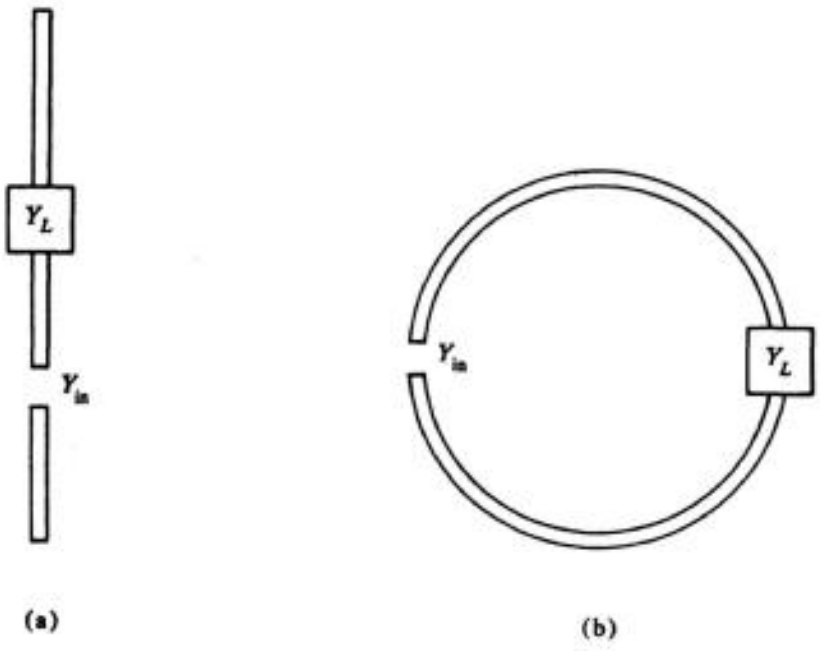

Figure 6-2. Wire antennas with lumped loads. (*a*) Loaded dipole, (*b*) loaded loop.

on port 2, where the minus sign arises from reference conditions. A direct solution of (6-14) and (6-15) for the input admittance $Y_{in} = i_1/v_1$ yields

$$Y_{in} = y_{11} - \frac{y_{12}y_{21}}{y_{22} + Y_L} \tag{6-16}$$

If all media are reciprocal, $y_{12} = y_{21}$. Alternatively, the impedance matrix $[z]$ could be used, obtaining

$$Z_{in} = z_{11} - \frac{z_{12}z_{21}}{z_{22} + Z_L} \tag{6-17}$$

which is dual to (6-16). Note that $Z_L = 1/Y_L$ and $Z_{in} = 1/Y_{in}$, but the z_{ij} are not the reciprocal of the y_{ij}. The various matrix elements of $[y]$ or $[z]$ can be calculated by the method of moments, as discussed in Section 6-1.

The simplest procedure for determining the current distribution on the antenna is to obtain v_2 from two-port network theory, and superimpose the currents due to v_1 and v_2. A direct solution of (6-14) and (6-15) yields

$$v_2 = \frac{-y_{21}}{y_{22} + Y_L} v_1 \tag{6-18}$$

as the voltage at port 2. For conducting bodies, the current on a single port antenna is given by (5-13). For the two-port case, by superposition, (5-13) becomes

$$\mathbf{J} = [\mathbf{J}_n][Y_{nm}][V_m^{(1)} + V_m^{(2)}] \tag{6-19}$$

where $[V_m^{(1)}]$ is the excitation matrix due to v_1 and $[V_m^{(2)}]$ is the excitation matrix due to v_2. The corresponding expression for v_2 in terms of $[z]$ is most simply obtained by substituting for the y_{ij} in (6-18) giving

$$v_2 = \frac{z_{12}}{z_{11} + Y_L \det|z|} v_1 \tag{6-20}$$

where $\det|z|$ denotes the determinant of $[z]$. Note that, because the excitation is a voltage excitation, it is more convenient to use (6-18) and $[y]$ than to use (6-20) and $[z]$.

Finally, the radiation pattern is also obtained by superposition. For a one-port antenna, the radiation field is given by (5-44). For a two-port antenna, it is given by

$$E_r = \frac{\omega\mu e^{-jkr}}{j4\pi r} [\tilde{V}_n'][Y_{nm}][V_m^{(1)} + V_m^{(2)}] \tag{6-21}$$

where $[V_m^{(1)}]$ is the excitation matrix due to v_1 and $[V_m^{(2)}]$ is that due to v_2, given by (6-18) or (6-20). Remember that the E_r of (6-21) is the component of **E** in the direction of the receiving dipole $I\mathbf{l}_r$, hence is an arbitrary component of the radiation field.

Example A. Consider the loaded dipole of Fig. 6-2(a), of length l, loaded at the center by Y_L, and fed $l/4$ from one end. For a particular example, let

$$Y_L = \frac{\cot(kl/4)}{j100} \tag{6-22}$$

which represents a short-circuited transmission line of length $l/4$ and characteristic impedance $Z_0 = 100$ ohms. The length/diameter ratio of the wire is taken as $l/2a = 74.2$, so the $[Y]$ matrix is the same as that used in the example of Section 4-4.

Figure 6-3 shows the input admittance for this case as a function of l/λ, computed according to (6-16). Here y_{11} and y_{22} are the input admittances for the wire when fed as an antenna at, respectively, the feed point and the position of Y_L. The $y_{12} = y_{21}$ are the transfer admittances from the feed point to the load point. For the analysis of Chapter 4 these are just single elements of $[Y]$, as discussed in Section 4-4. Figure 6-4 shows the current distribution on the wire

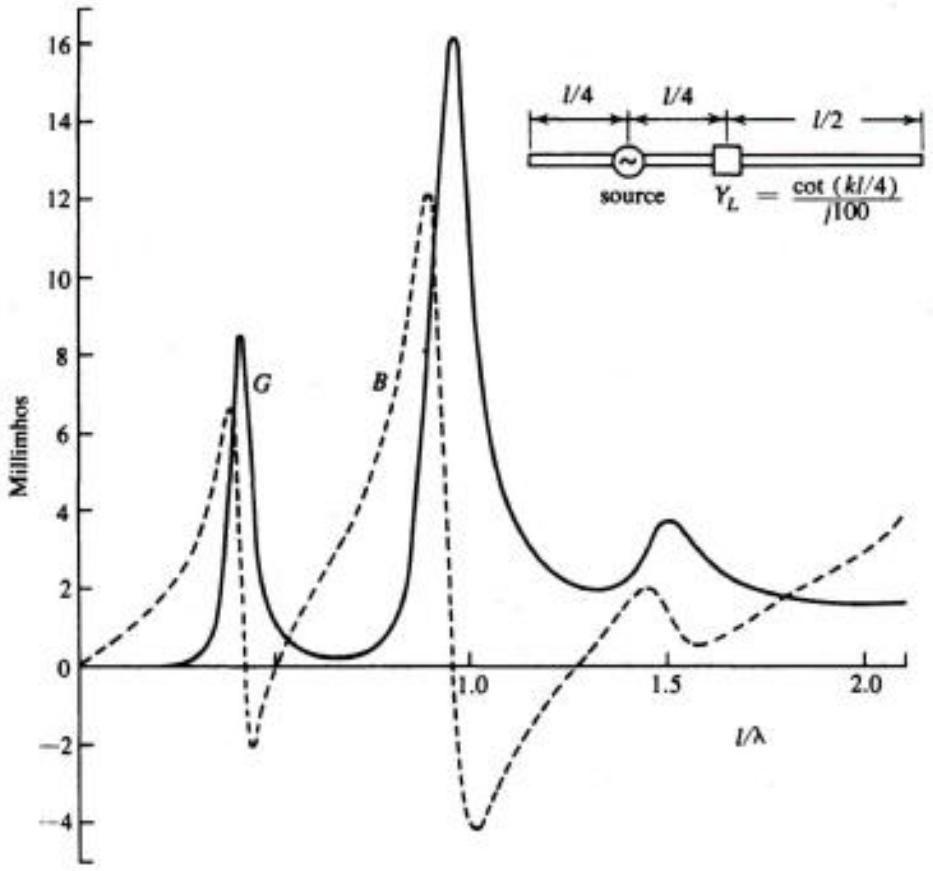

Figure 6-3. **Input admittance to a linear antenna, loaded by a short-circuited transmission-line stub, $l/2a = 74.2$.**

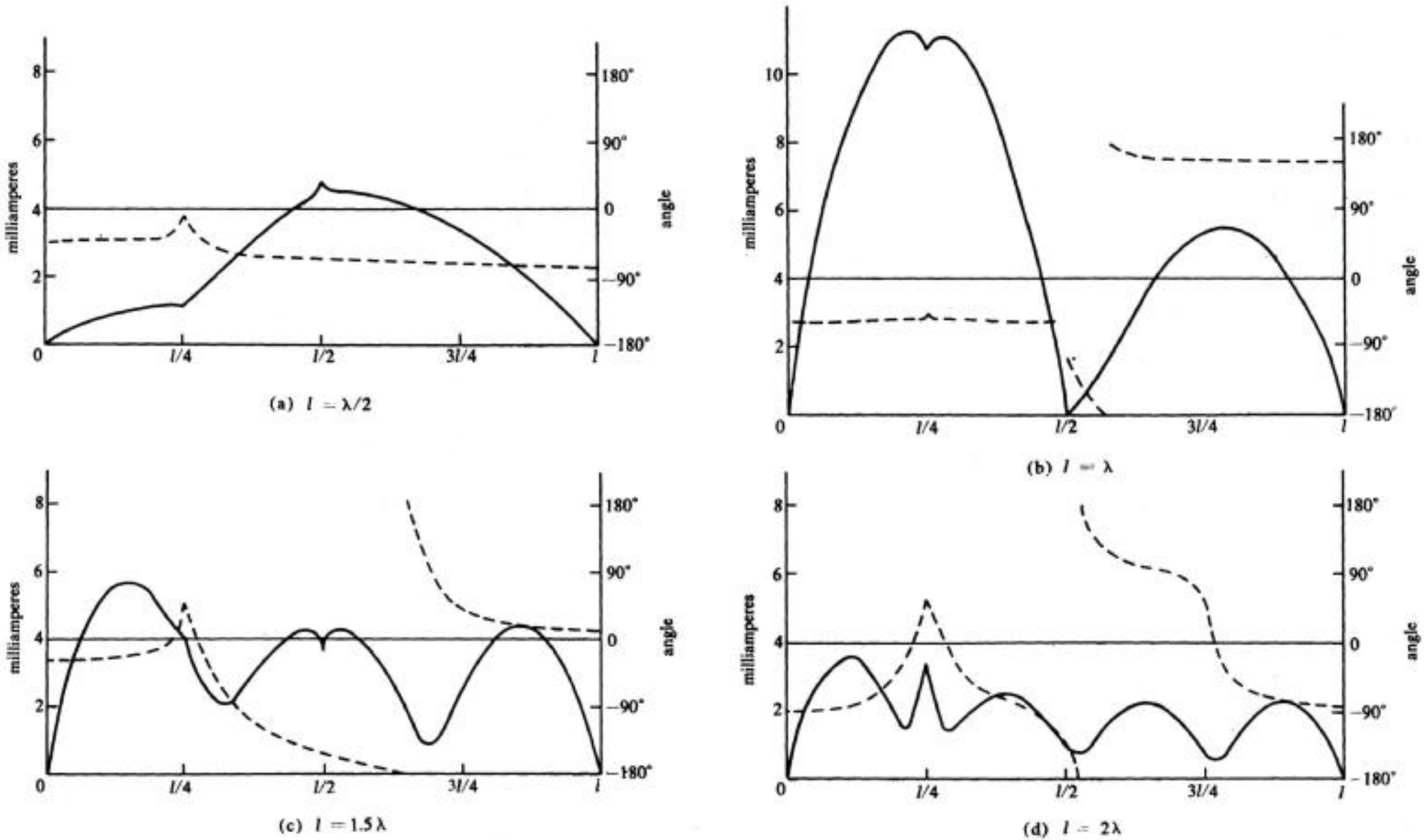

Figure 6-4. Current, magnitude (solid) and phase (dashed), on the loaded linear antenna of Fig. 6-3, unit voltage source.

for the special cases $l = \lambda/2$, λ, $3\lambda/2$, and 2λ, computed according to (4-21) with $[V]$ as in (6-19). Figure 6-5 shows the gain patterns for the antenna associated with the currents of Fig. 6-4. These are obtained from (4-39) with $[V^a]$ given by the right-hand matrix of (6-19).

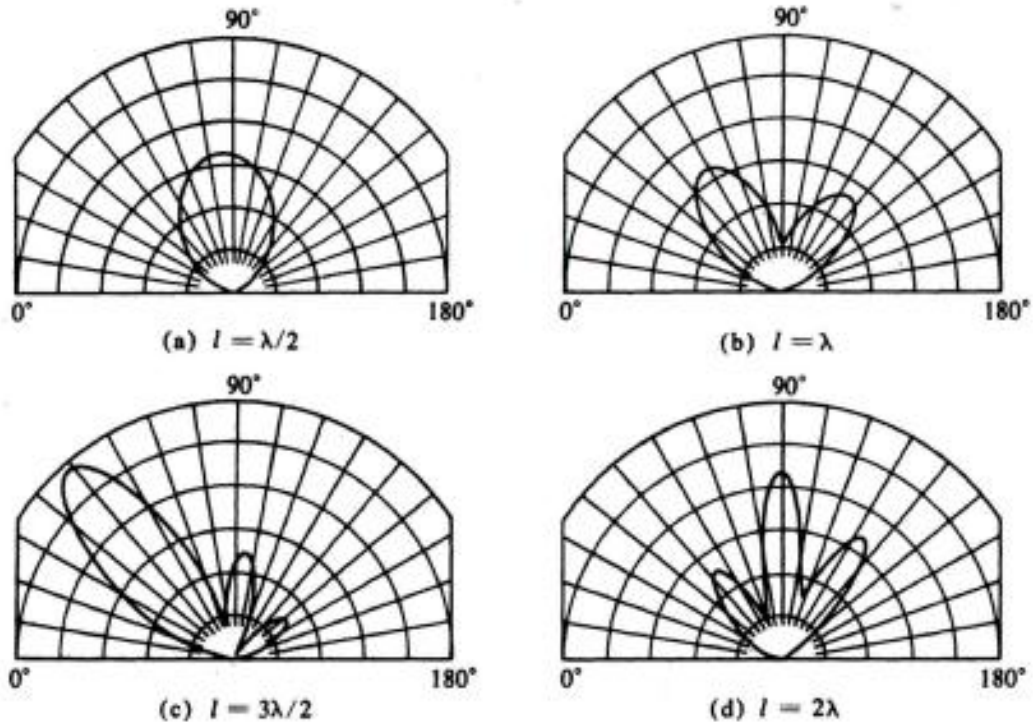

Figure 6-5. **Power-gain patterns for the loaded linear antenna of Fig. 6-3.**

Example B. The solution for a loaded loop antenna is obtained in a similar manner. A generalized admittance matrix $[Y]$ for the loop is the inverse of $[Z]$ with elements given by (5-28) and (5-29). The two-port elements y_{ij} of (6-14) are then given by (6-13), where $[V^b]$ is calculated from (5-23) with

$$E_\phi^i = \frac{v_b}{b}\,\delta(\phi - \phi_b) \tag{6-23}$$

This represents a voltage source v_b at $\phi = \phi_b$. The resultant elements of $[V^b]$ are

$$V_n^b = v_b\, e^{jn\phi_b} \tag{6-24}$$

Similarly, the elements of $[V^a]$ are obtained from (5-23) with $e^{jn\phi}$ replaced by $e^{-jn\phi}$, since $w_n = f_n^*$. Hence the elements of $[V^a]$ are

$$V_n^a = v_a\, e^{-jn\phi_a} \tag{6-25}$$

To conform to the notation of this section, let $a = 1$ and $b = 2$. Because of the

diagonal nature of [Y], equation (6-13) reduces to (5-48) for y_{11} and y_{22}, and to

$$y_{12} = y_{21} = \sum_{n=-\infty}^{\infty} \frac{e^{jn(\phi_2-\phi_1)}}{Z_{nn}}$$
$$= \frac{1}{Z_{00}} + 2\sum_{n=1}^{\infty} \frac{\cos n(\phi_2 - \phi_1)}{Z_{nn}} \tag{6-26}$$

where Z_{nn} are given by (5-29).

The current on the loop is given by (6-19), which reduces to (5-30) with

$$V_n = [V_n^{(1)} + V_n^{(2)}]$$
$$= v_1\left(e^{jn\phi_1} - \frac{y_{12}}{y_{22} + Y_L} e^{jn\phi_2}\right) \tag{6-27}$$

The radiation-field pattern is given by the equation analogous to (5-51), which is

$$E_t = \frac{\omega\mu e^{-jkr}}{j4\pi r} \sum_n \frac{V_n^r V_n}{Z_{nn}} \tag{6-28}$$

where V_n^r is given by (5-49) or (5-50) and V_n by (6-27). Some computations for the loaded loop antenna can be found in the literature [5]. The analysis used in this reference is equivalent to the above analysis but organized differently.

6-3. Loaded Scatterers

A loaded scatterer is one for which one or more ports are terminated by admittance elements [6]. Again we consider only the singly loaded case; the multiply loaded case will be discussed in Section 6-4. The analysis is basically the same as for the loaded antenna, except that the excitation is external to the structure rather than at a port.

Figure 6-6 represents a scatterer loaded at port s by Y_L, excited by a source impressed at port t on a transmitting antenna, and the scattered field measured at port r on a receiving antenna. This is a three-port system, for which the port currents and voltages are related by

$$\begin{bmatrix} i_r \\ i_t \\ i_s \end{bmatrix} = \begin{bmatrix} y_{rr} & y_{rt} & y_{rs} \\ y_{tr} & y_{tt} & y_{ts} \\ y_{sr} & y_{st} & y_{ss} \end{bmatrix} \begin{bmatrix} v_r \\ v_t \\ v_s \end{bmatrix} \tag{6-29}$$

When the scatterer is absent, we have a two-port system, for which

$$\begin{bmatrix} i_r^0 \\ i_t^0 \end{bmatrix} = \begin{bmatrix} y_{rr}^0 & y_{rt}^0 \\ y_{tr}^0 & y_{tt}^0 \end{bmatrix} \begin{bmatrix} v_r \\ v_t \end{bmatrix} \tag{6-30}$$

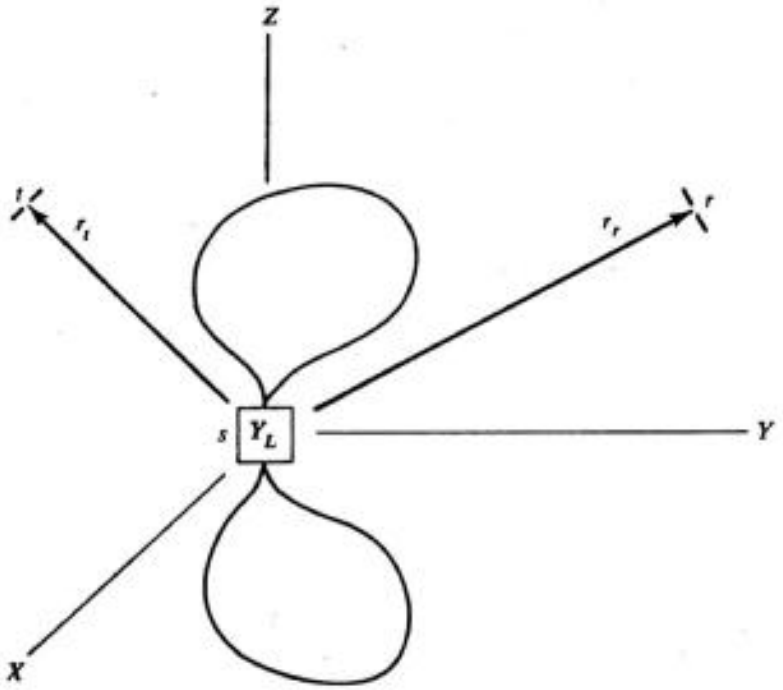

Figure 6-6. **Loaded scatterer and distant transmitting and receiving dipoles.**

where the superscript 0 denotes an absent scatterer. Subtracting (6-30) from (6-29), we have

$$\begin{bmatrix} \Delta i_r \\ \Delta i_t \\ i_s \end{bmatrix} = \begin{bmatrix} \Delta y_{rr} & \Delta y_{rt} & y_{rs} \\ \Delta y_{tr} & \Delta y_{tt} & y_{ts} \\ y_{sr} & y_{st} & y_{ss} \end{bmatrix} \begin{bmatrix} v_r \\ v_t \\ v_s \end{bmatrix} \tag{6-31}$$

where

$$\Delta i_j = i_j - i_j^0 \tag{6-32}$$

are the current changes at r and t due to the introduction of the scatterer, and

$$\Delta y_{ij} = y_{ij} - y_{ij}^0 \tag{6-33}$$

are the changes in admittance parameters due to the introduction of the scatterer. At port s on the scatterer a load admittance Y_L introduces the constraint

$$i_s = -Y_L v_s \tag{6-34}$$

where the minus sign results from reference conditions. For simplicity, take port r on the receiver to be short-circuited; that is,

$$v_r = 0 \tag{6-35}$$

Using (6-34) and (6-35) in (6-31), we then have

$$\begin{bmatrix} \Delta i_r \\ \Delta i_t \\ 0 \end{bmatrix} = \begin{bmatrix} \Delta y_{rr} & \Delta y_{rt} & y_{rs} \\ \Delta y_{tr} & \Delta y_{tt} & y_{ts} \\ y_{sr} & y_{st} & y_{ss} + Y_L \end{bmatrix} \begin{bmatrix} 0 \\ v_t \\ v_s \end{bmatrix} \tag{6-36}$$

This can be readily solved for Δi_r, giving

$$\Delta i_r = \left(\Delta y_{rt} - \frac{y_{rs} y_{st}}{y_{ss} + Y_L} \right) v_t \tag{6-37}$$

Note that (6-37) gives only the change in short-circuit current at the receiver, in contrast to the analysis of Section 6-2, which gives total current. The dual analysis in terms of impedance parameters is given in the literature [6].

Example A. Consider plane-wave scattering by a straight wire with a lumped load at its center. The details of the analysis are similar to those of Section 4-5, augmented by the addition of port s on the scatterer. The excitation of the scatterer is a plane wave incident from the transmitter, given by (4-40). The measurement matrix is calculated from a plane wave incident from the receiver, given by (4-32). Analogous to the development of (4-43), we obtain from (6-37) for the loaded scatterer a scattering cross section

$$\sigma = \frac{\eta^2 k^2}{4\pi} \left| \Delta y_{rt} - \frac{y_{rs} y_{st}}{y_{ss} + Y_L} \right|^2 \tag{6-38}$$

where

$$\Delta y_{rt} = [\tilde{V}^r][Y][V^t] \tag{6-39}$$

$$y_{rs} = [\tilde{V}^r][Y][V^s] \tag{6-40}$$

$$y_{st} = [\tilde{V}^s][Y][V^t] \tag{6-41}$$

$$y_{ss} = [\tilde{V}^s][Y][V^s] \tag{6-42}$$

Here $[Y]$ is the admittance matrix developed for wire objects in Chapter 4, $[V^t]$ is the excitation matrix (4-41), $[V^r]$ is the measurement matrix (4-35), and $[V^s]$ is the matrix (4-28) for excitation by a *unit* source at the position of the loading point. Because of the form of $[V^s]$, (6-40), (6-41), and (6-42) can be reduced to a simpler form. For example, y_{ss} is the input admittance of the wire when fed as an antenna at s, hence is just the appropriate diagonal element of $[Y]$.

Figure 6-7 shows the backscattering cross section for a center-loaded dipole for various loads Z_L for the case $l/2a = 74.2$. Shown for comparison are the

same results for a two-term variational analysis [7]. The present matrix solution gives somewhat better accuracy than the previous variational one because a better expansion for the current is used. The larger discrepancy between the two solutions for the case $Z_L = \infty$ (open circuit) is due to difference in gap capacitance, which is sensitive to the approximations used. The two curves can be brought into close agreement by an adjustment of this gap capacitance.

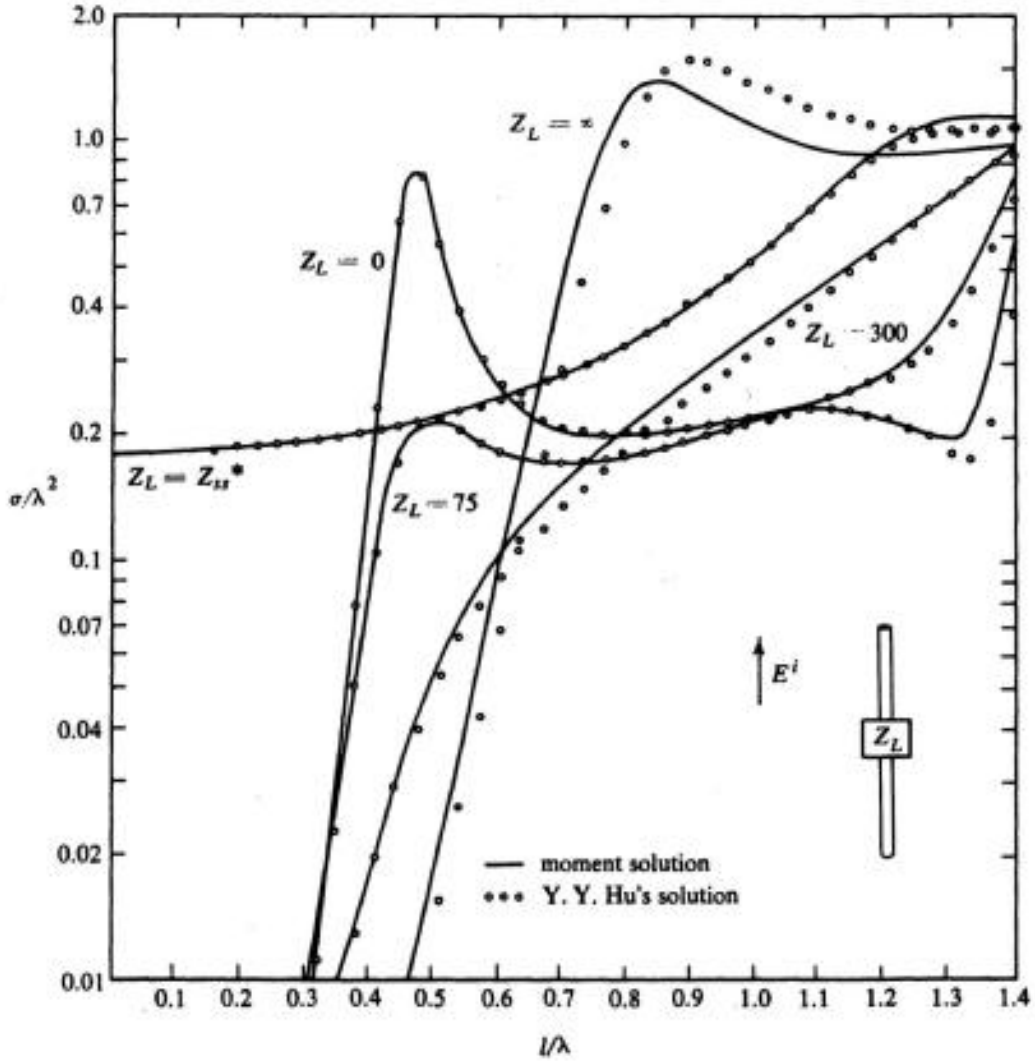

Figure 6-7. **Backscattering cross section for a center-loaded dipole, $l/2a = 74.2$, with various loads Z_L.**

Figure 6-8 shows the back-scattering cross section for a center-loaded dipole resonated at various l/λ by reactive loads. By definition, a resonant load is one which is a pure reactance equal to the negative of the input reactance at s when fed as an antenna [9]. In Fig. 6-8, curve (a) is for a dipole continuously tuned to resonance, and curves (b) and (c) are for a dipole resonated by an inductor at $l/\lambda = 0.25$ and 0.35, respectively. Curves (e) and (f) are for a dipole resonated by a capacitor at $l/\lambda = 0.55$ and 0.65, respectively. Curve (d) is for an open-circuited dipole. The curve for a short-circuited dipole is given in Fig. 4-10, and has a peak lying between (a) and (e) of Fig. 6-8.

Example B. Plane-wave scattering by a loaded circular loop can be treated using the generalized impedances of Chapter 5. The analysis is an extension of that for the unloaded circular loop (Section 5-3). The resultant formula for scattering cross section is again (6-38), with (6-39) to (6-42) applying with the

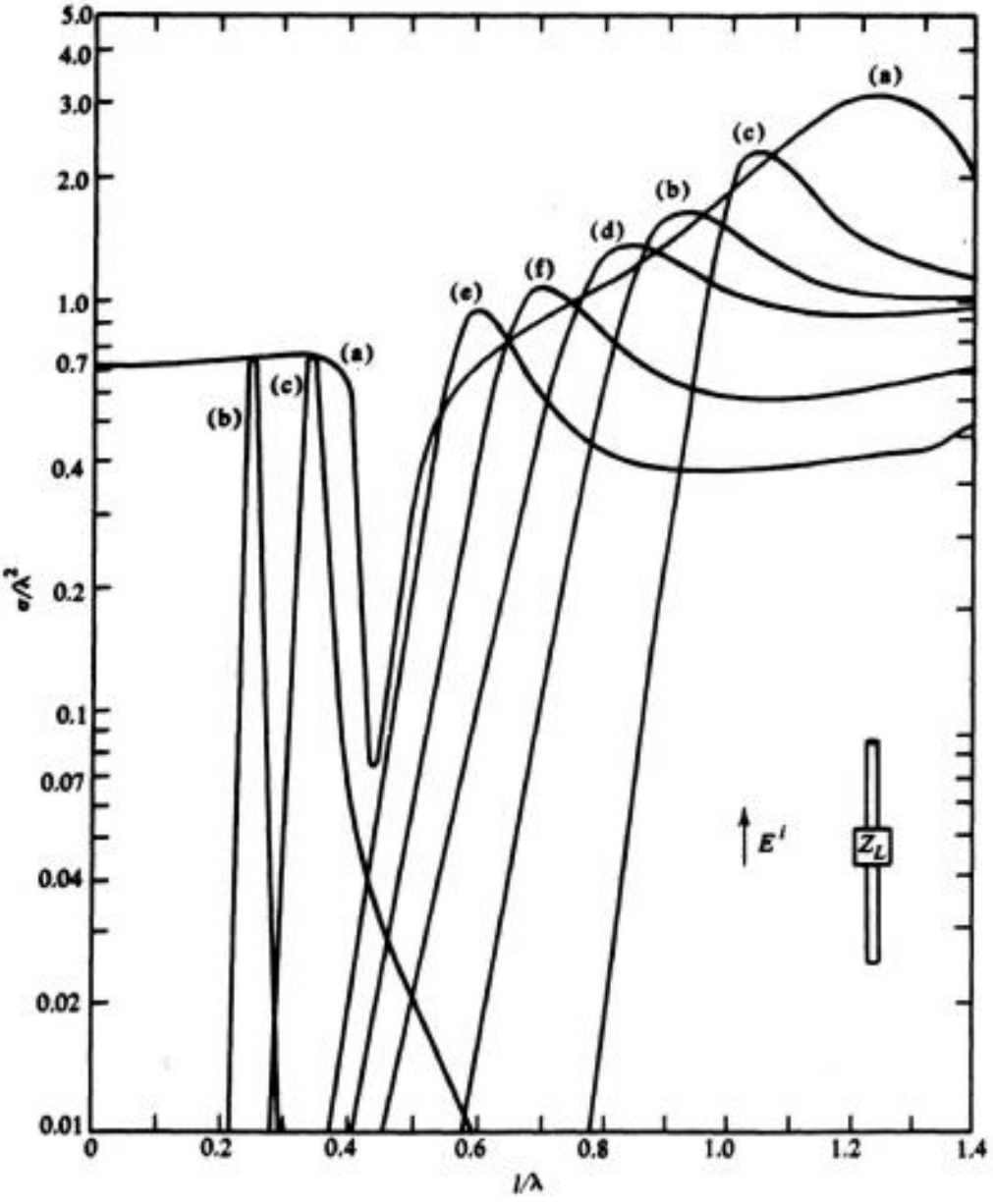

Figure 6-8. **Backscattering cross section for a resonated dipole, $l/2a = 74.2$. (*a*) Continuously resonated, (*b*) resonated by inductor at $l/\lambda = 0.25$, (*c*) resonated by inductor at $l/\lambda = 0.35$, (*d*) open-circuited dipole, (*e*) resonated by capacitor at $l/\lambda = 0.55$, (*f*) resonated by capacitor at $l/\lambda = 0.65$.**

following changes. The elements of $[V']$ are given by (5-49) for the ϕ-polarized case, or by (5-50) for the θ-polarized case. The elements of $[V']$ are given by (5-54) for the ϕ-polarized case, or by (5-55) for the θ-polarized case. The matrix $[V']$ is given by (5-46) with $V_s = 1$ if the load terminals s are at $\phi = 0$. More

generally, when the terminals s are at an arbitrary angle ϕ_s, the elements of $[V^s]$ are

$$V_n^s = e^{jn\phi_s} \tag{6-43}$$

The matrix $[\tilde{V}^s]$ in (6-41) and (6-42) must be replaced by the conjugate transpose (Hermitian) matrix, because f_n and w_n (expansion and testing functions) are conjugates of each other. The admittance matrix $[Y]$ is diagonal, with elements reciprocal to (5-29). Because of the diagonal nature of $[Y]$, equations (6-39) to (6-42) can be reduced to

$$\Delta y_{rt} = \sum_n \frac{V_n^r V_n^t}{Z_{nn}} \tag{6-44}$$

$$y_{rs} = \sum_n \frac{V_n^r e^{jn\phi_s}}{Z_{nn}} \tag{6-45}$$

$$y_{st} = \sum_n \frac{V_n^t e^{-jn\phi_s}}{Z_{nn}} \tag{6-46}$$

$$y_{ss} = \sum_n \frac{1}{Z_{nn}} \tag{6-47}$$

Note that (6-47) is just the input admittance to the loop antenna, given by (5-48).

Figure 6-9 shows the backscattering cross section for loaded circular loops resonated at various b/λ by reactive loads [8]. Curve (a) is for the complete (unloaded) loop. The dashed curve (b) is for a load continuously tuned to resonance; that is, $Y_L = -Y_{ss}$. Curves (c) and (d) are for a loop resonated by a capacitor at $b/\lambda = 0.03$ and 0.06, respectively. Curves (e), (f), and (g) are for a loop resonated by an inductor at $b/\lambda = 0.09$, 0.12, and 0.15, respectively. The curve for an open-circuited loop is not shown, but has a peak between curves (d) and (e).

6-4. Multiple Feeds and Loads

The generalization of the analysis of Section 6-2 to structures with multiple feeds and loads is straightforward if we replace most scalar quantities by matrix quantities [10]. Let Fig. 6-10 represent an electromagnetic field problem for which there are N ports excited by voltage sources $v_1, \ldots, v_N$, and M ports loaded by admittance elements $Y_1, \ldots, Y_M$. Let the N excited ports be denoted set 1, and the M loaded ports be denoted set 2. Then the matrix extension of (6-14) is

$$\begin{bmatrix} [I_1] \\ [I_2] \end{bmatrix} = \begin{bmatrix} [Y_{11}] & [Y_{12}] \\ [Y_{21}] & [Y_{22}] \end{bmatrix} \begin{bmatrix} [V_1] \\ [V_2] \end{bmatrix} \tag{6-48}$$

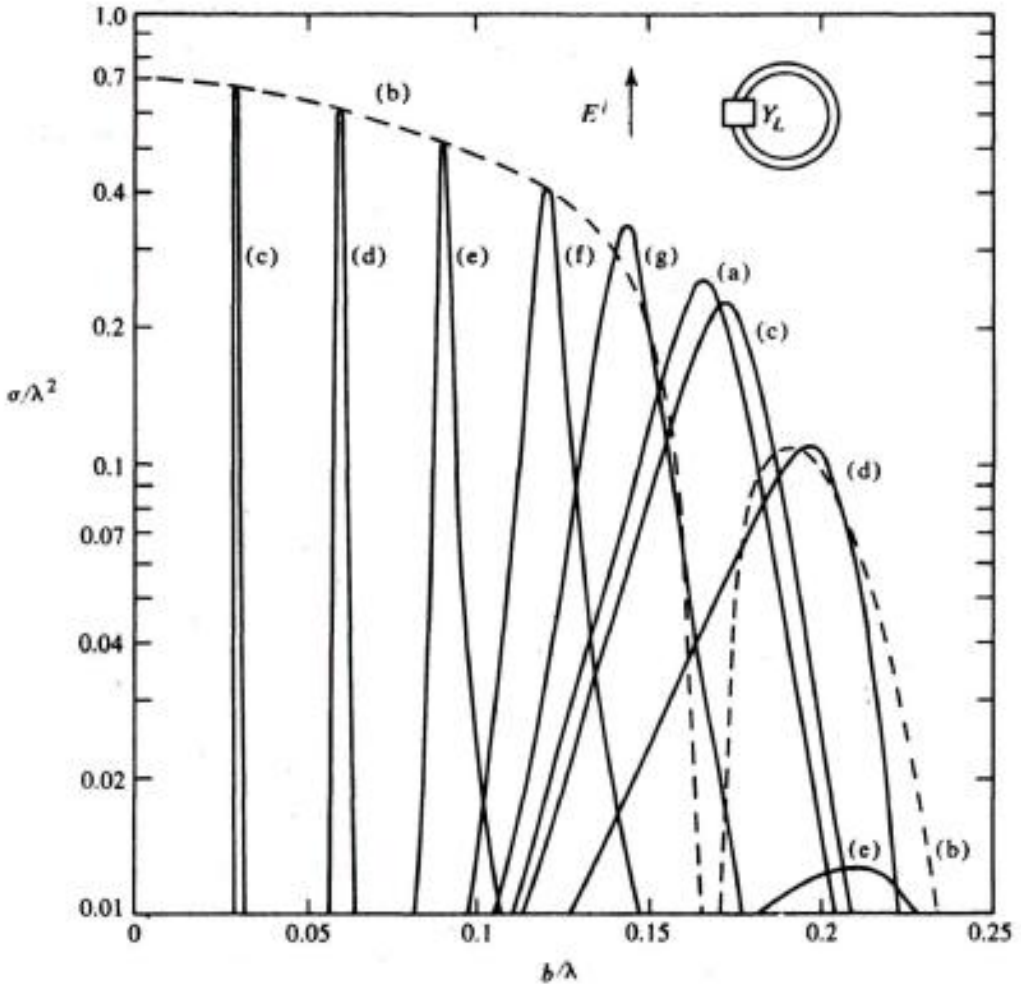

Figure 6-9. **Backscattering cross section for a resonated loop, $b/a = 100$. (*a*) Complete loop, (*b*) continuously resonated, (*c*) resonated by capacitor at $b/\lambda = 0.03$, (*d*) resonated by capacitor at $b/\lambda = 0.06$, (*e*) resonated by inductor at $b/\lambda = 0.09$, (*f*) resonated by inductor at $b/\lambda = 0.12$, (*g*) resonated by inductor at $b/\lambda = 0.15$.**

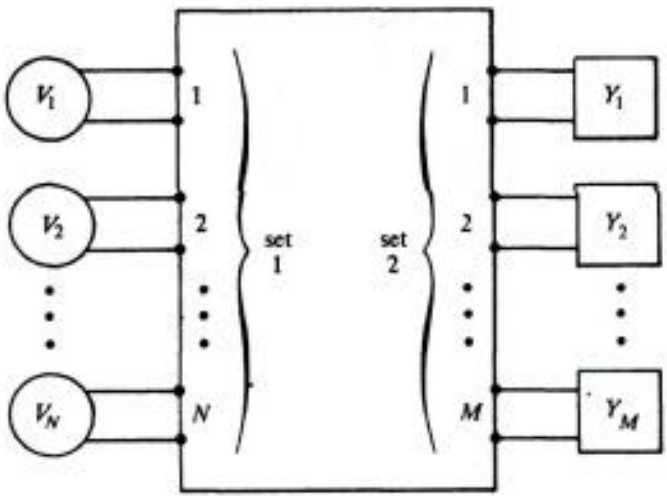

Figure 6-10. **Multiport system with N ports excited and M ports loaded.**

where the elements of $[I_1]$ are $i_1, \ldots, i_N$, and similarly for $[V_1]$, the elements of $[I_2]$ are $i_{N+1}, \ldots, i_{N+M}$, and similarly for $[V_2]$. The admittance matrix relating $[I]$ to $[V]$ is partitioned into the submatrices $[Y_{ij}]$ as shown in (6-48).

The load admittances $Y_1, \ldots, Y_M$ can be expressed in terms of a load matrix

$$[Y_L] = \begin{bmatrix} Y_1 & 0 & \cdots & 0 \\ 0 & Y_2 & \cdots & 0 \\ \cdot & \cdot & \cdot & \cdot \\ 0 & 0 & \cdots & Y_M \end{bmatrix} \tag{6-49}$$

and the constraint represented by loading the ports of set 2 becomes

$$[I_2] = -[Y_L][V_2] \tag{6-50}$$

analogous to (6-15). We can solve for the matrix of input admittances $[Y_{in}]$ seen at the ports of set 1, obtaining

$$[Y_{in}] = [Y_{11}] - [Y_{12}][Y_{22} + Y_L]^{-1}[Y_{21}] \tag{6-51}$$

analogous to (6-16). This result can be generalized to loads with coupling by replacing the diagonal matrix (6-49) by an arbitrary M by M network matrix.

The dual treatment in terms of impedance matrices leads to a matrix of input impedances

$$[Z_{in}] = [Z_{11}] - [Z_{12}][Z_{22} + Z_L]^{-1}[Z_{21}] \tag{6-52}$$

dual to (6-51) and analogous to (6-17). Other matrix representations, such as a scattering matrix, might be used to represent the system. The most convenient matrix to use depends on the particular problem.

Each element of the matrices $[Y_{ij}]$ or $[Z_{ij}]$ may be calculated by the methods of Section 6-1. For example, an element y_{ab} is defined by (6-4), and can be calculated by the method of moments according to (6-7). If the current distribution on a conducting body is desired, it is the superposition of the currents due to the voltage at each port, that is, an $N + M$ term expansion of the form (6-19). Similarly, the radiation field is the superposition of that due to the voltage at each port, which is an $N + M$ term superposition of the form (6-21).

Example A. A multiply fed and/or multiply loaded linear antenna can be treated by a simple extension of the analysis of Section 6-2, Example A. The admittance elements of (6-48) are identical to those of $[Y]$ of Chapter 4, because of the subsectional method of solution. Hence each element y_{ij} of (6-48) is the appropriate element of $[Y]$ inverse to $[Z]$ having elements (4-20). A continuously loaded linear antenna can be treated as one loaded in each interval along its

length. The effect of the finite conductivity of a metal can be determined by considering the antenna to be continuously loaded by an appropriate impedance.

Example B. A multiply fed and/or multiply loaded loop antenna requires the calculation of additional mutual admittance elements. The input admittance to the loop is independent of where it is fed; hence all y_{ii} elements of the admittance matrix are equal, and given by (5-48). For the mutual admittances, let various ports about the loop be defined by the angles ϕ_i. The elements y_{ij}, $i \neq j$, are then all given by (6-26) with angles arbitrary; that is,

$$y_{ij} = \frac{1}{Z_{00}} + 2\sum_{n=1}^{\infty} \frac{\cos n(\phi_i - \phi_j)}{Z_{nn}} \tag{6-53}$$

All elements of the admittance matrix of (6-48) can thus be calculated, and the analysis proceeds as outlined in the text.

6-5. Multiply Loaded Scatterers

The analysis of Section 6-3 can also be extended to multiply loaded scatterers by replacing scalars by matrices. Suppose the scatterer of Fig. 6-6 has N ports loaded by lumped admittances $Y_1, \ldots, Y_N$. The excitation is applied to port t on a transmitting antenna, and the measurement is made at port r on a receiving antenna. We now have an $N + 2$ port system, for which the generalization of (6-29) is

$$\begin{bmatrix} i_r \\ i_t \\ [I_s] \end{bmatrix} = \begin{bmatrix} y_{rr} & y_{rt} & [Y_{rs}] \\ y_{tr} & y_{tt} & [Y_{ts}] \\ [Y_{sr}] & [Y_{st}] & [Y_{ss}] \end{bmatrix} \begin{bmatrix} v_r \\ v_t \\ [V_s] \end{bmatrix} \tag{6-54}$$

Here $[Y_{ss}]$ is the admittance matrix for the ports on the scatterer. (If the transmitter and receiver are distant from the scatterer, $[Y_{ss}]$ is the admittance matrix for the system when viewed as an antenna.) The row and column matrices which express the receiver-scatterer and transmitter-scatterer admittances are

$$[Y_{rs}] = [y_{r1} \quad y_{r2} \quad \cdots \quad y_{rN}] \tag{6-55}$$

$$[Y_{ts}] = [y_{t1} \quad y_{t2} \quad \cdots \quad y_{tN}] \tag{6-56}$$

$$[Y_{sr}] = \begin{bmatrix} y_{1r} \\ y_{2r} \\ \vdots \\ y_{Nr} \end{bmatrix} \qquad [Y_{st}] = \begin{bmatrix} y_{1t} \\ y_{2t} \\ \vdots \\ y_{Nt} \end{bmatrix} \tag{6-57}$$

If all media are reciprocal, we have $[Y_{rs}] = [\tilde{Y}_{sr}]$ and $[Y_{ts}] = [\tilde{Y}_{st}]$.

When the scatterer is absent, equation (6-30) applies. The subtraction of (6-30) from (6-54) gives

$$\begin{bmatrix} \Delta i_r \\ \Delta i_t \\ [I_s] \end{bmatrix} = \begin{bmatrix} \Delta y_{rr} & \Delta y_{rt} & [Y_{rs}] \\ \Delta y_{tr} & \Delta y_{tt} & [Y_{ts}] \\ [Y_{sr}] & [Y_{st}] & [Y_{ss}] \end{bmatrix} \begin{bmatrix} v_r \\ v_t \\ [V_s] \end{bmatrix} \tag{6-58}$$

analogous to (6-31). The effect of the loading of the ports on the scatterer is expressed by the matrix equivalent of (6-34). This is

$$[I_s] = -[Y_L][V_s] \tag{6-59}$$

where $[Y_L]$ is given by (6-49) if the loads are distinct elements, and by an arbitrary admittance matrix if the loads are coupled. Finally, solving for the change in receiver current due to the introduction of the scatterer, we have

$$\Delta i_r = (\Delta y_{rt} - [Y_{rs}][Y_{ss} + Y_L]^{-1}[Y_{st}])v_t \tag{6-60}$$

which is analogous to (6-37). The various impedance elements can be found by the methods of Section 6-1.

Specialization of these results to scattering by multiloaded dipoles and loops involves the same procedures as used in the examples of Sections 6-2 to 6-4. Of particular interest is plane-wave scattering, in which case echo area is given by

$$\sigma = \frac{\eta^2 k^2}{4\pi} |\Delta y_{rt} - [Y_{rs}][Y_{ss} + Y_L]^{-1}[Y_{st}]|^2 \tag{6-61}$$

analogous to (6-38). The various matrix elements are all computed by formulas similar to (6-39) to (6-42). These must be modified slightly for the case $w_n \neq f_n$, as discussed in Example B of Section 6-3.

In all our examples of plane-wave scattering we have computed the radar cross section of the scatterer, which depends on the polarization properties of both the transmitter and the receiver. A general treatment of the scattering problem involves the use of a scattering matrix relating two orthogonal components of electric field at the receiver to two orthogonal components of incident field from the scatterer. This procedure requires two ports at the transmitter and two ports at the receiver; hence the elements y_{rr}, y_{rt}, y_{tr}, and y_{tt} of (6-54) must each be replaced by 2 by 2 matrices. The scattering properties of the loaded object can then be completely described by four elements of a scattering matrix. The details can be found in the literature [6].

References

[1] R. F. Harrington, *Time-Harmonic Electromagnetic Fields*, McGraw-Hill Book Co., New York, 1961, Chap. 8.

[2] S. Ramo, J. R. Whinnery, and T. Van Duzer, *Fields and Waves in Communication Electronics*, John Wiley & Sons, Inc., New York, 1965, Chap. 11.

[3] H. J. Carlin and A. B. Giordano, *Network Theory*, Prentice-Hall, Inc., Englewood Cliffs, N.J., 1964, Chap. 4.

[4] Reference [1], Sect. 3-8.

[5] K. Iizuka, "The Circular Loop Antenna Multiloaded with Positive and Negative Resistors," *IEEE Trans.*, Vol. **AP-13**, No. 1, Jan. 1965, pp. 7–20.

[6] R. F. Harrington, "Theory of Loaded Scatterers," *Proc. IEE* (*London*), Vol. **111**, No. 4, April 1964, pp. 617–623.

[7] Y. Y. Hu, "Back-Scattering Cross Sections of a Center-loaded Cylindrical Antenna," *IRE Trans.*, Vol. **AP-6**, No. 1, Jan. 1958, pp. 140–148.

[8] R. F. Harrington and J. L. Ryerson, "Electromagnetic Scattering by Loaded Wire Loops," *Radio Science*, Vol. **1** (new series), No. 3, March 1966, pp. 347–352; correction, Vol. **1**, No. 12, Dec. 1966.

[9] R. F. Harrington, "Small Resonant Scatterers and their Use for Field Measurements," *IRE Trans.*, Vol. **MTT-10**, No. 3, May 1962, pp. 167–174.

[10] L. Weinberg, "New Techniques for Modifying Monostatic and Multistatic Radar Cross Sections," *IEEE Trans.*, Vol. **AP-11**, No. 6, Nov. 1963, pp. 717–719.

CHAPTER

7

Eigenvalue Problems

7-1. Introduction

An eigenvalue equation is a homogeneous equation for which solutions (eigenfunctions) exist only for particular values (eigenvalues) of a parameter. The general linear eigenvalue equation is

$$L(f) = \lambda M(f) \tag{7-1}$$

where L and M are linear operators, the permissible λ's are *eigenvalues*, and the corresponding solutions f are *eigenfunctions*. The eigenvalue equation is important for two reasons: (1) The use of eigenfunctions as a basis in the method of moments leads to a diagonal matrix representation of the operator [1,2], and (2) characteristic parameters of physical problems often correspond to eigenvalues of an eigenvalue equation. Our use of eigenvalue equations will be primarily for the second purpose.

Again our general method of solution will be to reduce a functional eigenvalue equation to a matrix eigenvalue equation, which can then be solved by known computational algorithms. We consider the eigenvalue equation solved once it is reduced to a well-behaved matrix eigenvalue equation. The computer solution of eigenvalue equations is not as simple as that of deterministic equations. An iterative procedure is usually used, and Appendix C gives a widely used Jacobi method.

In complicated problems a straightforward application of the method of moments becomes difficult, and the various special techniques of Chapter 1

become useful. These techniques are not discussed again in this chapter, but will be used in some of the examples. On the other hand, the procedure of reducing a second-order differential equation to a set of first-order equations, which is equally applicable to the deterministic problems of Chapter 1, is discussed in detail here.

7-2. Method of Moments

Application of the method of moments to eigenvalue equations closely parallels its application to deterministic equations (Section 1-3). Given an eigenvalue equation (7-1), we choose a set of basis functions $f_1, f_2, f_3, \ldots$, in the domain of L and M, and let

$$f = \sum_n \alpha_n f_n \tag{7-2}$$

where the α_n are constants. Substituting (7-2) in (7-1), and using the linearity of L and M, we have

$$\sum \alpha_n L(f_n) = \lambda \sum \alpha_n M(f_n) \tag{7-3}$$

It is assumed that a suitable inner product $\langle f, g \rangle$ has been defined according to (1-2) to (1-4). We then choose a set of testing functions $w_1, w_2, w_3, \ldots$, in the range of L and M, and take the inner product of (7-3) with each w_m. This results in

$$\sum_n \alpha_n \langle w_m, Lf_n \rangle = \lambda \sum_n \alpha_n \langle w_m, Mf_n \rangle \tag{7-4}$$

$m = 1, 2, 3, \ldots$, which can be written as the matrix eigenvalue equation

$$[l_{mn}][\alpha_n] = \lambda [m_{mn}][\alpha_n] \tag{7-5}$$

Here

$$[m_{mn}] = \begin{bmatrix} \langle w_1, Mf_1 \rangle & \langle w_1, Mf_2 \rangle & \cdots \\ \langle w_2, Mf_1 \rangle & \langle w_2, Lf_2 \rangle & \cdots \\ \cdots & \cdots & \cdots \end{bmatrix} \tag{7-6}$$

$[l_{mn}]$ is the corresponding matrix of the $\langle w_m, Lf_n \rangle$, given by (1-25), and $[\alpha_n]$ is the column matrix of the α_n, given by (1-26).

Equation (7-5) can have solutions only if

$$\det |l_{mn} - \lambda m_{mn}| = 0 \tag{7-7}$$

where $\det |a_{mn}|$ denotes the determinant of the matrix $[a_{mn}]$. The determinant (7-7) is a polynomial in λ, with roots $\lambda_1, \lambda_2, \lambda_3, \ldots$. These λ_i are eigenvalues of

the matrix equation (7-5) and they approximate the eigenvalues of the functional equation (7-1). The corresponding matrices $[\alpha_n]_1$, $[\alpha_n]_2$, $[\alpha_n]_3$, . . . are eigenvectors of (7-5), and are coefficients of functions

$$f_i^a = [\tilde{f}_n][\alpha_n]_i \tag{7-8}$$

which approximate the eigenfunctions of (7-1). In (7-8), the $[f_n]$ is a matrix of the basis functions and $\sim$ denotes transpose. Just as in the deterministic case, the success of the method of moments depends on our ingenuity in choosing appropriate f_n and w_n. The particular choice $w_n = f_n$ is Galerkin's method.

Often the canonical form of the eigenvalue equation is given as $L(f) = \lambda f$ instead of (7-1), that is, M = identity operator. In many cases of practical interest M is a positive definite operator. The quantity $\langle f, Mg \rangle$ then satisfies postulates (1-2) to (1-4) for an inner product, and can be used as a new weighted inner product. In this case the inverse operator M^{-1} exists, and (7-1) can be written

$$M^{-1}L(f) = \lambda f \tag{7-9}$$

Hence an analysis of (7-9) with the weighted inner product $\langle f, Mg \rangle$ is identical to an analysis of (7-1) with the unweighted inner product $\langle f, g \rangle$. Finally, the algorithm of Appendix C for solving matrix eigenvalue equations is for the case $[l_{mn}][\alpha_n] = \lambda[\alpha_n]$, and hence (7-5) must be multiplied by $[m^{-1}]$ before applying this algorithm.

Example. To illustrate these concepts, let us consider the same operator $L = -d^2/dx^2$ used for the examples of Chapter 1. In particular, consider the eigenvalue problem

$$-\frac{d^2f}{dx^2} = \lambda f \tag{7-10}$$

$$f(0) = f(1) = 0 \tag{7-11}$$

As is well known, the eigenvalues for this problem are

$$\lambda_i = (i\pi)^2 \qquad i = 1, 2, 3, \ldots \tag{7-12}$$

and the eigenfunctions are

$$f_i = \sqrt{2}\sin(i\pi x) \tag{7-13}$$

These have been normalized with respect to the inner product

$$\langle f, g \rangle = \int_0^1 f(x)g(x)\,dx \tag{7-14}$$

We wish to reconsider the problem by the method of moments.

For a power-series solution, choose expansion functions

$$f_n = x - x^{n+1} \tag{7-15}$$

which satisfy the boundary conditions (7-11), that is, are in the domain of L. For testing functions choose

$$w_n = f_n = x - x^{n+1} \tag{7-16}$$

so that the method of moments reduces to that of Galerkin. An evaluation of the matrix elements $l_{mn} = \langle w_m, Lf_n \rangle$ for the inner product (7-14) in this case gives

$$l_{mn} = \frac{mn}{m+n+1} \tag{7-17}$$

The operator M is the identity operator and the matrix elements $m_{mn} = \langle w_m, f_n \rangle$ are found as

$$m_{mn} = \frac{mn(m+n+6)}{3(m+3)(n+3)(m+n+3)} \tag{7-18}$$

Note that even though M is the identity operator $[m_{mn}]$ is not the identity matrix.

To illustrate convergence, let us consider approximate solutions as the number of basis functions N is increased. For $N = 1$, $l_{11} = 1/3$, $m_{11} = 1/30$, and (7-5) reduces to

$$\frac{1}{3}\alpha_1 = \lambda \frac{1}{30}\alpha_1 \tag{7-19}$$

Hence our first approximation to λ_1 is $\lambda_1^{(1)} = 10$, compared to the true value π^2. Here the superscript (1) denotes the $N = 1$ approximation. To compare the approximate eigenfunction $f_1^{(1)} = \alpha_1(x - x^2)$ to (7-13), we normalized $f_1^{(1)}$ according to

$$1 = \langle f_1^{(1)}, f_1^{(1)} \rangle = \alpha_1^2 (\tfrac{1}{30}) \tag{7-20}$$

whence $\alpha_1 = \sqrt{30}$ and

$$f_1^{(1)} = \sqrt{30}(x - x^2) \tag{7-21}$$

A comparison with the exact $f_1 = \sqrt{2} \sin \pi x$ is shown in Fig. 7-1(a).

For $N = 2$, that is, for a two-term expansion (7-2), equation (7-5) becomes

$$\begin{bmatrix} 1/3 & 1/2 \\ 1/2 & 4/5 \end{bmatrix} \begin{bmatrix} \alpha_1 \\ \alpha_2 \end{bmatrix} = \lambda \begin{bmatrix} 1/30 & 1/20 \\ 1/20 & 8/105 \end{bmatrix} \begin{bmatrix} \alpha_1 \\ \alpha_2 \end{bmatrix} \tag{7-22}$$

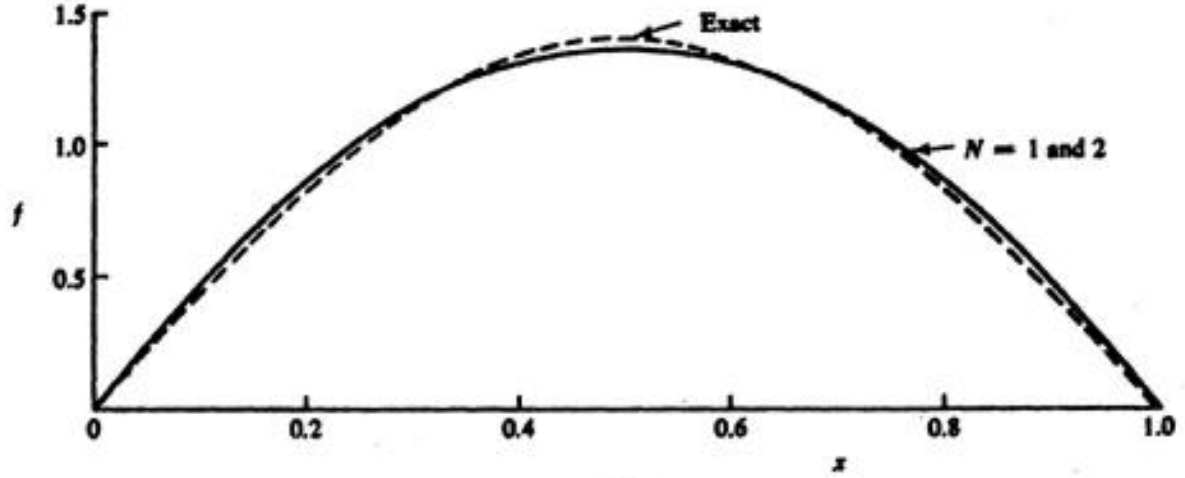

(a)

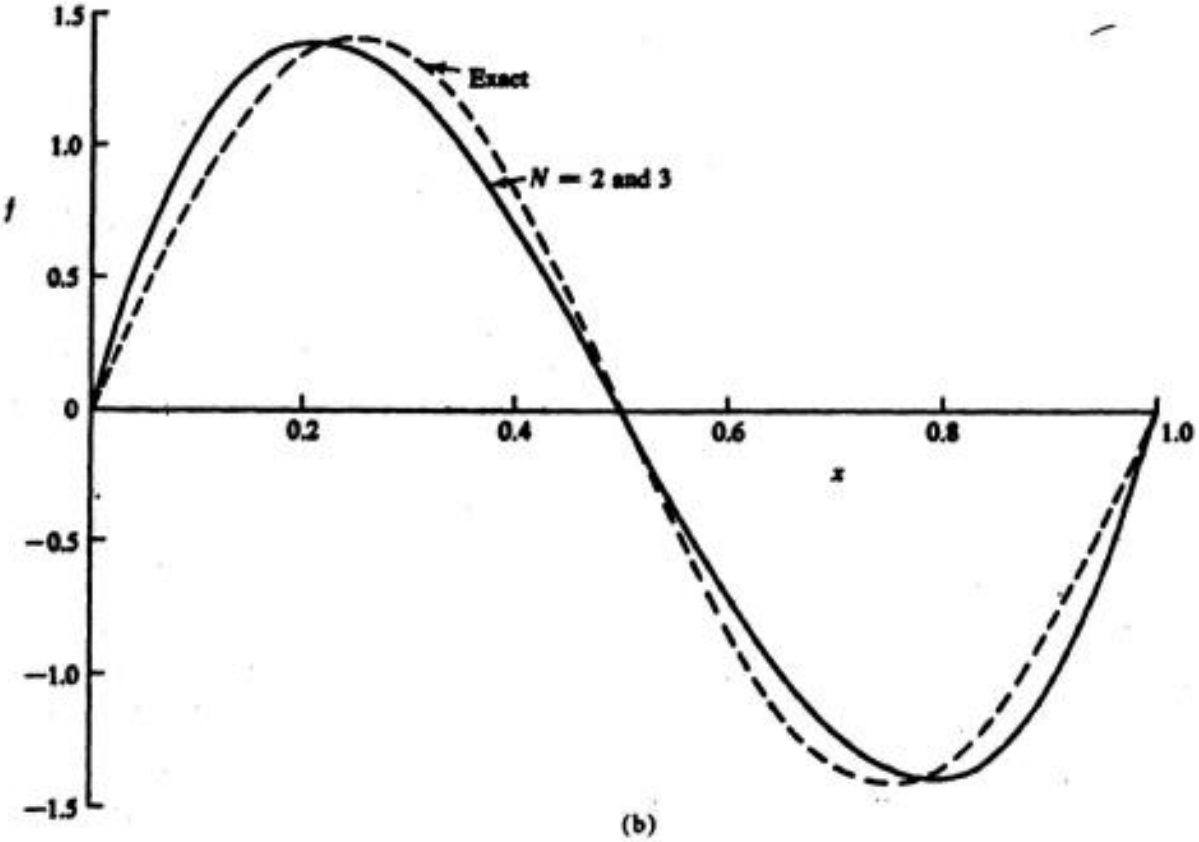

(b)

Figure 7-1. (*a*) First eigenfunction, approximate and exact. (*b*) Second eigenfunction, approximate and exact.

The eigenvalues are found from the determinant (7-7), which is

$$\frac{(10-\lambda)(84-8\lambda)}{(30)(105)} - \frac{(10-\lambda)^2}{400} = 0 \tag{7-23}$$

This is a quadratic equation in λ, which has solutions

$$\begin{aligned} \lambda_1^{(2)} &= 10 \\ \lambda_2^{(2)} &= 42 \end{aligned} \tag{7-24}$$

If $\lambda_1^{(2)}$ is substituted for λ in (7-22), α_2 can be determined in terms of α_1, and α_1 determined from the normalization

$$1 = \langle f_1^{(2)}, f_1^{(2)} \rangle = [\tilde{\alpha}_m][m_{mn}][\alpha_n] \tag{7-25}$$

The second eigenvector $f_n^{(2)}$ can be similarly determined. The results are

$$\begin{aligned} f_1^{(2)} &= \sqrt{30}(x - x^2) = f_1^{(1)} \\ f_2^{(2)} &= 3\sqrt{210}(x - x^2) - 2\sqrt{210}(x - x^3) \end{aligned} \tag{7-26}$$

Figure 7-1(a) shows $f_1^{(2)} = f_1^{(1)}$ compared to the exact solution, and Fig. 7-1(b) shows $f_2^{(2)}$ compared to the exact solution.

For higher N, solutions are best carried out on a computer using the procedure of Appendix C. Table 7-1 lists the eigenvalues as N is increased. Note that the eigenvalues $\lambda_i^{(N)}$ are always larger than the exact eigenvalues λ_i. This must be so if the operator is self-adjoint and positive definite, as is the present operator.

TABLE 7-1. Approximate Eigenvalues for an N-term Galerkin Solution with $f_n = (x - x^{n+1})$, Second-order Operator

N	$\lambda_1^{(N)}$	$\lambda_2^{(N)}$	$\lambda_3^{(N)}$	$\lambda_4^{(N)}$
1	10.0000			
2	10.0000	42.000		
3	9.8697	42.000	102.133	
4	9.8697	39.497	102.133	200.583
Exact	9.8696	39.478	88.826	157.914

7-3. Nonuniform Transmission Lines

We wish to discuss a number of methods for treating eigenvalue problems representable by second-order differential equations. So that the reader can more easily appreciate the physical significance of the mathematical manipulations, the equations will here be related to those for a nonuniform transmission line. The equations for this problem are quite general in form.

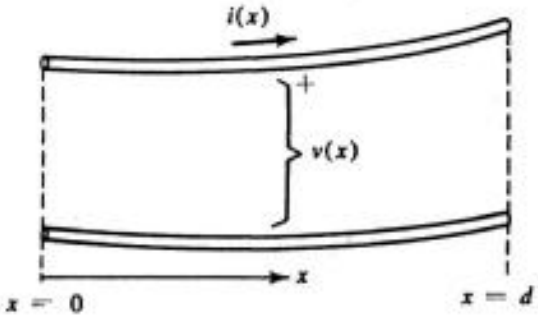

Figure 7-2. Section of a transmission line.

Figure 7-2 represents a section of loss-free transmission line, in general nonuniform. Let x denote position along the line, $l(x)$ the series inductance per unit length, and $c(x)$ the shunt capacitance per unit length. We restrict consideration to the time-harmonic case, in which case

$$v(x, t) = \mathrm{Re}[V(x)e^{j\omega t}] \tag{7-27}$$

$$i(x, t) = \mathrm{Re}[I(x)e^{j\omega t}] \tag{7-28}$$

where $v(x, t)$ and $i(x, t)$ are the line voltage and current, $V(x)$ and $I(x)$ are the complex phasors, and Re denotes *real part of*. Then, by an application of Kirchhoff's voltage and current laws to a differential length of line, we can derive the time-harmonic *transmission-line equations* [3]

$$\frac{dV}{dx} = -j\omega l(x)I \tag{7-29}$$

$$\frac{dI}{dx} = -j\omega c(x)V \tag{7-30}$$

To completely specify the eigenvalue problem, boundary conditions at the ends of the line can be specified. For our examples, let the line be open-circuited at the ends $x = 0$ and $x = d$, in which case the boundary condition is

$$I(0) = I(d) = 0 \tag{7-31}$$

Our problem now is to determine the natural resonances ω_i of the line.

Equations (7-29) and (7-30) can be written in standard operator form by defining the following matrices:

$$f = \begin{bmatrix} V(x) \\ I(x) \end{bmatrix} \tag{7-32}$$

$$L = \begin{bmatrix} 0 & -\dfrac{d}{dx} \\ \dfrac{d}{dx} & 0 \end{bmatrix} \tag{7-33}$$

$$M = \begin{bmatrix} c(x) & 0 \\ 0 & -l(x) \end{bmatrix} \tag{7-34}$$

Then, assuming the usual rules for matrix multiplication, the equation

$$Lf = j\omega Mf \tag{7-35}$$

is equivalent to (7-29) and (7-30). Here $j\omega$ corresponds to the eigenvalue λ. To complete the formulation, boundary conditions such as (7-31) must be specified.

If $c(x)$ is differentiable, the transmission-line equations can be combined into a second-order differential equation as follows. Take the derivative of (7-30) and obtain

$$\frac{d^2I}{dx^2} = -j\omega\left(\frac{dc}{dx}V + c\frac{dV}{dx}\right) \tag{7-36}$$

Substituting for V from (7-30) and for dV/dx from (7-29), we have

$$-\frac{d^2I}{dx^2} + \frac{1}{c}\frac{dc}{dx}\frac{dI}{dx} = \omega^2 lcI \tag{7-37}$$

By an analogous procedure, if $l(x)$ is differentiable the second-order equation for V is found to be

$$-\frac{d^2V}{dx^2} + \frac{1}{l}\frac{dl}{dx}\frac{dV}{dx} = \omega^2 lcV \tag{7-38}$$

Equations (7-37) and (7-38) are called *telegrapher's equations.*

To express (7-37) in standard form, define operators

$$L = -\frac{d^2}{dx^2} + \frac{1}{c}\frac{dc}{dx}\frac{d}{dx} \tag{7-39}$$

$$M = l(x)c(x) \tag{7-40}$$

and write

$$LI = \omega^2 MI \tag{7-41}$$

This again is an eigenvalue equation with eigenvalues ω^2 and eigenfunctions I. Again boundary conditions must be specified to restrict the domain of L, and we continue to take (7-31) for our examples. Equation (7-38) can similarly be written in standard form by defining suitable operators L and M.

7-4. Second-order Differential Operator

If the second-order differential representation (7-39) to (7-41) is considered, and the unweighted inner product

$$\langle I_1, I_2 \rangle = \int_0^a I_1(x) I_2(x)\, dx \tag{7-42}$$

defined, we can show that the operator L is not self-adjoint unless c is a constant. This causes very little trouble, because the adjoint operator can readily be determined as

$$L^a I = -\frac{d^2 I}{dx^2} - \frac{d}{dx}\left(I\frac{1}{c}\frac{dc}{dx}\right) \tag{7-43}$$

However, the theory is complicated somewhat by the necessity of considering an adjoint eigenvalue equation. For second-order operators, it is always possible to define a weighted inner product for which L is formally self-adjoint, circumventing this complication.

The general second-order differential eigenvalue problem, known as the Sturm-Liouville problem, has been studied extensively [2]. Any second-order eigenvalue problem can be written in the form

$$-\frac{1}{w}\frac{d}{dx}\left(p\frac{df}{dx}\right) - qf = \lambda r f \tag{7-44}$$

It is then easy to show that the operator represented by the left side of (7-44) is self-adjoint with respect to the weighted inner product

$$\langle f_1, f_2 \rangle = \int_0^d w(x) f_1(x) f_2(x)\, dx \tag{7-45}$$

The particular operator (7-39) can be written in the form of the left side of (7-44) as

$$LI = -e^{\log c} \frac{d}{dx}\left[e^{-\log c} \frac{dI}{dx}\right] \tag{7-46}$$

A comparison of (7-46) with (7-44) shows that $w = e^{-\log c}$ and therefore the weighted inner product

$$\langle I_1, I_2 \rangle = \int_0^d e^{-\log c(x)} I_1(x) I_2(x)\, dx \tag{7-47}$$

makes the operator (7-39) self-adjoint.

Example. For comparison with other solutions, let us consider the second-order equation using a Galerkin solution with pulse functions for expansion and testing. For simplicity, let l and c be constants, in which case (7-37) reduces to

$$-\frac{d^2 I}{dx^2} = \lambda I \tag{7-48}$$

where

$$\lambda = \omega^2 lc \tag{7-49}$$

Also, let $d = 1$, in which case the boundary conditions (7-31) reduce to

$$I(0) = I(1) = 0 \tag{7-50}$$

and the inner product (7-42) becomes

$$\langle I_1, I_2 \rangle = \int_0^1 I_1(x) I_2(x)\, dx \tag{7-51}$$

Note that the problem is now precisely the same as the example of Section 7-2.

For a Galerkin solution using triangle functions, let

$$f_n = w_n = T(x - x_n) \tag{7-52}$$

where $T(x)$ is the triangle function discussed in Section 1-5 and defined by (1-50).

Following the method of moments, the matrix equation (7-5) results, with

$$l_{mn} = \begin{cases} 2(N+1) & m = n \\ -(N+1) & |m-n| = 1 \\ 0 & |m-n| > 1 \end{cases} \tag{7-53}$$

as shown in Section 1-5, and

$$m_{mn} = \begin{cases} \dfrac{2}{3(N+1)} & m = n \\ \dfrac{1}{6(N+1)} & |m-n| = 1 \\ 0 & |m-n| > 1 \end{cases} \tag{7-54}$$

Now the matrix eigenvalue problem is

$$[l_{mn}][\alpha_n] = \lambda[m_{mn}][\alpha_n] \tag{7-55}$$

which can be solved by hand for small orders N, or by computer for the larger orders. Table 7-2 shows the approximate eigenvalues for an N-term expansion of triangle functions. A comparison of these results with Table 7-1 shows that the power-series solution of Table 7-1 converges slightly faster than the piecewise linear solution of Table 7-2. This is to be expected, because the power functions are better behaved than the triangle functions.

TABLE 7-2. Approximate Eigenvalues for an N-term Galerkin Solution with $f_n = T(x - x_n)$, Second-order Operator

N	$\lambda_1^{(N)}$	$\lambda_2^{(N)}$	$\lambda_3^{(N)}$	$\lambda_4^{(N)}$
1	12.000			
2	10.800	54.000		
3	10.386	48.000	128.868	
4	10.198	44.903	116.118	227.838
Exact	9.870	39.478	88.826	157.914

7-5. First-order Differential Operator

A second-order differential equation can be expressed as a pair of first-order differential equations. For example, the transmission-line problem of Section 7-3 can be either in terms of the second-order equations (7-37) or the first-order

equations (7-29) and (7-30). We wish to show that, for similar approximations, solutions to the first-order equations converge faster than those to the second-order equations.

The transmission-line problem is sufficiently general for our purposes. The first-order formulation is given by (7-32) to (7-35), or

$$\begin{bmatrix} 0 & -d/dx \\ d/dx & 0 \end{bmatrix}\begin{bmatrix} V \\ I \end{bmatrix} = j\omega\begin{bmatrix} c(x) & 0 \\ 0 & -l(x) \end{bmatrix}\begin{bmatrix} V \\ I \end{bmatrix} \tag{7-56}$$

For illustrative purposes, the line length is normalized so that $d = 1$, and the boundary conditions are

$$I(0) = I(1) = 0 \tag{7-57}$$

A suitable inner product for the problem is

$$\begin{aligned} \langle f_1, f_2 \rangle &= \int_0^1 \tilde{f}_1 f_2 \, dx \\ &= \int_0^1 [V_1(x)V_2(x) + I_1(x)I_2(x)] \, dx \end{aligned} \tag{7-58}$$

where f is the matrix (7-32). This inner product satisfies postulates (1-2) to (1-4), as required.

The matrix operators in (7-56) are self-adjoint with respect to (7-58), as we shall now show. For M, defined by (7-34), note that $\tilde{M} = M$, and

$$\begin{aligned} \langle f_1, Mf_2 \rangle &= \int_0^1 \tilde{f}_1 M f_2 \, dx = \int_0^1 \tilde{f}_2 \tilde{M} f_1 \, dx \\ &= \langle f_2, Mf_1 \rangle \end{aligned} \tag{7-59}$$

For L defined by (7-33), let L^a denote its adjoint operator and f^a functions in the domain of L^a. Then

$$\begin{aligned} \langle f^a, Lf \rangle &= \int_0^1 [V^a \quad I^a] \begin{bmatrix} -\dfrac{dI}{dx} \\ \dfrac{dV}{dx} \end{bmatrix} dx \\ &= \int_0^1 \left(-V^a \frac{dI}{dx} + I^a \frac{dV}{dx} \right) dx \end{aligned} \tag{7-60}$$

An integration by parts gives

$$\langle f^a, Lf \rangle = \int_0^1 \left(I \frac{dV^a}{dx} - V \frac{dI^a}{dx} \right) dx + [-V^a I + I^a V]_0^1 \tag{7-61}$$

From the form of (7-61), it is evident that if

$$L^a = L = \begin{bmatrix} 0 & -\dfrac{d}{dx} \\ \dfrac{d}{dx} & 0 \end{bmatrix} \tag{7-62}$$

then

$$\langle f^a, Lf \rangle = \langle f, Lf^a \rangle + [I^a V - V^a I]_0^1 \tag{7-63}$$

The last terms vanish if I^a satisfies the same boundary conditions (7-57) as I. Hence L is self-adjoint, since $L^a = L$ and the domain of L^a is that of L.

Example A. The crudest moment solution of (7-56) is to take the pulse functions (1-49) for both expansion and testing. This solution is identical to that obtained by analyzing the lumped-element equivalent network of the transmission line. Let us first discuss this equivalent network, and later show that it is the same as a Galerkin solution using pulse functions.

Figure 7-3(a) represents the physical transmission line and Fig. 7-3(b) the approximate equivalent network, derived as follows. Let the physical line be divided into N intervals $\Delta x = x_n - x_{n-1}$ and $N + 1$ shifted intervals $\Delta x' = x'_n - x'_{n-1}$. Define equivalent lumped inductors as

$$L_n = \int_{x_{n-1}}^{x_n} l(x)\, dx \tag{7-64}$$

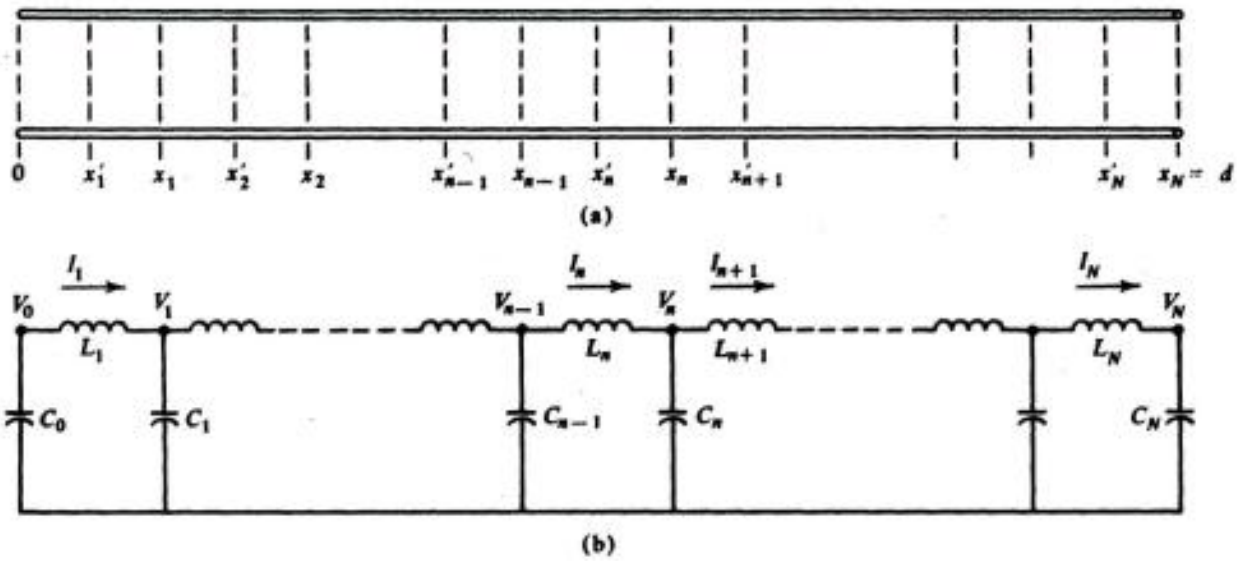

Figure 7-3. **Approximate equivalent circuit of a transmission line. (*a*) Physical line, (*b*) ladder equivalent.**

and equivalent lumped capacitors as

$$C_n = \int_{x'_n}^{x'_{n+1}} c(x)\,dx \tag{7-65}$$

Note that the two end capacitors C_0 and C_N are integrated over half-intervals. Let V_n denote the line voltages at x_n, and I_n the line currents at x'_n. Then, by the laws of circuit theory applied to each element of Fig. 7-3(b), we have

$$I_{n+1} - I_n = -j\omega C_n V_n \tag{7-66}$$

$$V_{n+1} - V_n = -j\omega L_n I_n \tag{7-67}$$

$n = 0, 1, 2, \ldots, N$. The currents at each end are obviously

$$I_0 = I_{N+1} = 0 \tag{7-68}$$

which correspond to the boundary conditions (7-57). Equations (7-66) and (7-67) are a set of first-order *difference equations*, which can be placed into matrix form as

$$\left[\begin{array}{c|c} 0 & \Delta_I \\ \hline -\Delta_V & 0 \end{array}\right]\begin{bmatrix} V \\ \hline I \end{bmatrix} = j\omega\left[\begin{array}{c|c} C & 0 \\ \hline 0 & -L \end{array}\right]\begin{bmatrix} V \\ \hline I \end{bmatrix} \tag{7-69}$$

Here the submatrices are

$$\Delta_I = \begin{bmatrix} 1 & 0 & 0 & \cdot & \cdots \\ -1 & 1 & 0 & \cdot & \cdots \\ 0 & -1 & 1 & \cdot & \cdots \\ \cdot & \cdot & \cdot & \cdot & \cdots \\ \cdot & \cdot & \cdot & \cdot & -1 \end{bmatrix} \qquad \Delta_V = \begin{bmatrix} -1 & 1 & 0 & 0 & \cdot & \cdots \\ 0 & -1 & 1 & 0 & \cdot & \cdots \\ 0 & 0 & -1 & 1 & \cdot & \cdots \\ \cdot & \cdot & \cdot & \cdot & \cdot & \cdots \\ \cdot & \cdot & \cdot & \cdot & -1 & 1 \end{bmatrix} \tag{7-70}$$

$$C = \begin{bmatrix} C_0 & 0 & 0 & \cdot & \cdots \\ 0 & C_1 & 0 & \cdot & \cdots \\ 0 & 0 & C_3 & \cdot & \cdots \\ \cdot & \cdot & \cdot & \cdot & \cdots \\ \cdot & \cdot & \cdot & 0 & C_N \end{bmatrix} \qquad L = \begin{bmatrix} L_1 & 0 & 0 & \cdot & \cdots \\ 0 & L_2 & 0 & \cdot & \cdots \\ 0 & 0 & L_3 & \cdot & \cdots \\ \cdot & \cdot & \cdot & \cdot & \cdots \\ \cdot & \cdot & \cdot & 0 & L_N \end{bmatrix} \tag{7-71}$$

$$V = \begin{bmatrix} V_0 \\ V_1 \\ \vdots \\ V_N \end{bmatrix} \qquad I = \begin{bmatrix} I_1 \\ I_2 \\ \vdots \\ I_N \end{bmatrix} \tag{7-72}$$

Note the similarity of (7-69) to the corresponding differential equation (7-56). The Δ matrices of (7-70) are finite-difference approximations to the derivative, called *first differences*.

We wish now to obtain (7-69) as a special case of the method of moments. Let the x_n of Fig. 7-3(a) divide the transmission line into N equal segments, and let the x_n' be shifted one-half interval toward the origin, that is,

$$\begin{aligned} x_n &= \frac{n}{N} \\ x_n' &= \frac{n - \frac{1}{2}}{N} \end{aligned} \tag{7-73}$$

With respect to the inner product (7-58), it is evident that (7-64) and (7-65) are obtained if both w_n and f_n are constant in the interval Δx_n, and zero elsewhere. For this we define the pulse function

$$P(x) = \begin{cases} 1 & |x| < 1/2N \\ 0 & |x| > 1/2N \end{cases} \tag{7-74}$$

and express w_n and f_n as a set of "voltage-type" functions

$$f_n^V = w_n^V = \begin{bmatrix} P(x - x_n) \\ 0 \end{bmatrix} \tag{7-75}$$

$n = 0, 1, 2, \ldots, N$, plus a set of "current-type" functions

$$f_n^I = w_n^I = \begin{bmatrix} 0 \\ P(x - x_n') \end{bmatrix} \tag{7-76}$$

$n = 1, 2, 3, \ldots, N$. In other words, we are approximating V by pulses centered on the x_n and I by pulses centered on the x_n'. Now the matrix (7-6) can be written in terms of submatrices as

$$[m_{mn}] = \left[\begin{array}{c:c} \langle w_m^V, Mf_n^V \rangle & \langle w_m^V, Mf_n^I \rangle \\ \hdashline \langle w_m^I, Mf_n^V \rangle & \langle w_m^I, Mf_n^I \rangle \end{array}\right] \tag{7-77}$$

where M is given by (7-34). An evaluation of (7-77) gives

$$[m_{mn}] = \left[\begin{array}{c:c} C & 0 \\ \hdashline 0 & -L \end{array}\right] \tag{7-78}$$

where the matrices C and L are given by (7-71). To evaluate the $[l_{mn}]$ matrix, we need the derivative of the $P(x)$, which does not exist as an ordinary function. In terms of symbolic functions, it is

$$\frac{dP}{dx} = \delta\left(x + \frac{1}{2N}\right) - \delta\left(x - \frac{1}{2N}\right) \tag{7-79}$$

where $\delta(x)$ is the Dirac delta function. Evaluation of the left-hand matrix of (7-56) then gives

$$[l_{mn}] = \left[\begin{array}{c|c} 0 & \Delta_I \\ \hline -\Delta_V & 0 \end{array}\right] \tag{7-80}$$

which is the left-hand matrix of (7-69). Hence, we have obtained (7-69), as anticipated.

The matrix equation (7-69) can be reduced to a form more convenient for computation. First, note that if $\omega = 0$, a solution is

$$[V_0] = \begin{bmatrix} 1 \\ 1 \\ \vdots \\ 1 \end{bmatrix} \qquad [I_0] = \begin{bmatrix} 0 \\ 0 \\ \vdots \\ 0 \end{bmatrix} \tag{7-81}$$

Hence $\omega_0 = 0$ is an eigenvalue, and the corresponding eigenfunction f_0 corresponds to a charged line. The other eigenvalues of (7-69) come in pairs $+\omega_i$ and $-\omega_i$, shown as follows. We can rewrite (7-69) as the pair of equations

$$\Delta_I I = -j\omega C V \tag{7-82}$$

$$\Delta_V V = -j\omega L I \tag{7-83}$$

These are finite-difference approximations to the transmission-line equations, (7-29) and (7-30). From (7-71) it is evident that L^{-1} and C^{-1} exist as diagonal matrices. Premultiplying (7-82) by C^{-1} and then by Δ_V, we have

$$\Delta_V C^{-1} \Delta_I I = -j\omega \Delta_V V \tag{7-84}$$

A substitution from (7-83) and premultiplication by L^{-1} gives

$$-L^{-1} \Delta_V C^{-1} \Delta_I I = \omega^2 I \tag{7-85}$$

which is an eigenvalue equation with eigenvalues ω^2. Note that (7-85) is a difference-equation approximation to the telegrapher's equation, (7-37). It can also be

shown that (7-83) constitutes the Kirchhoff loop equations for the equivalent circuit of Fig. 7-3(b). A difference equation in V, similar to (7-85) and corresponding to (7-38), could also be written. It would have the eigenvalue $\omega_0^2 = 0$ as well as the $\omega_i^2 > 0$, whereas (7-85) does not have the eigenvalue $\omega_0^2 = 0$.

To illustrate the rate of convergence of the above approximate solution, consider the uniform line (l and c are constants). The exact solution is known, having eigenvalues

$$\lambda_i = \omega_i^2 lc = i^2\pi^2 \tag{7-86}$$

$i = 1, 2, \ldots$, and eigenfunctions

$$f_i = \begin{bmatrix} j\sqrt{l/c}\cos i\pi x \\ \sin i\pi x \end{bmatrix} \tag{7-87}$$

The approximate eigenvalues, calculated from (7-85) for the lowest-order solutions ($N = 1, 2, 3, 4$), are summarized in Table 7-3. Figure 7-4 shows the equivalent circuit for each order, and the first eigenfunction ($i = 1$), compared to the exact eigenfunction, shown dashed.

TABLE 7-3. Approximate Eigenvalues for a Galerkin Solution of the First-order Equations, Using N Current Pulses and $N+1$ Voltage Pulses

N	$\lambda_1^{(N)}$	$\lambda_2^{(N)}$	$\lambda_3^{(N)}$	$\lambda_4^{(N)}$
1	4.000			
2	7.000	16.000		
3	9.000	27.000	36.000	
4	9.373	29.614	54.627	64.000
Exact	9.870	39.478	88.826	157.914

A comparison of Table 7-3 with Tables 7-1 and 7-2 shows that the convergence of the present solution is slower than the previous ones. However, for a transmission line with arbitrary $l(x)$ and $c(x)$, the first-order formulation is easier to program on a computer for a general program. We also note that the eigenvalues of Table 7-3 are all less than the exact eigenvalues, whereas those of Tables 7-1 and 7-2 are greater than the exact eigenvalues. We have found this to be the case for all Galerkin solutions to the first-order equations. Apparently, such solutions provide a lower bound to the eigenvalues, whereas Galerkin solutions to the second-order equations provide upper bounds.

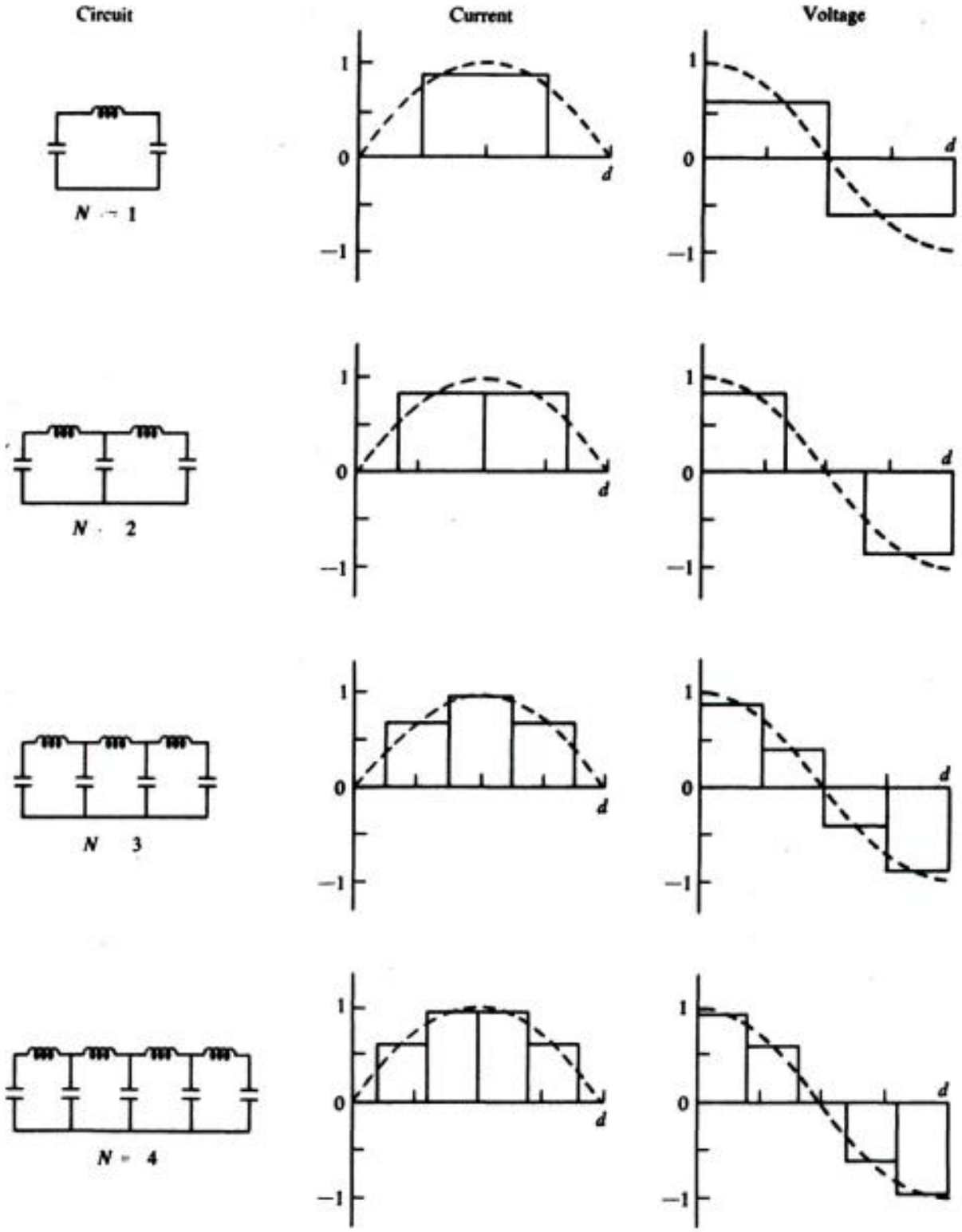

Figure 7-4. **Equivalent circuits and eigenfunctions for the lower-order modes of the open-circuited transmission line.**

Example B. We now reconsider the Galerkin solution of the first-order equations using triangle functions

$$T(x) = \begin{cases} 1 - N|x| & |x| < 1/N \\ 0 & |x| > 1/N \end{cases} \tag{7-88}$$

for expansion and testing. These give a piecewise linear approximation to the voltage and current. For a solution, we choose voltage-type functions

$$f_n^V = w_n^V = \begin{bmatrix} T(x - x_n) \\ 0 \end{bmatrix} \tag{7-89}$$

$n = 0, 1, 2, \ldots, N$, plus a set of current-type functions

$$f_n^I = w_n^I = \begin{bmatrix} 0 \\ T(x - x_n) \end{bmatrix} \tag{7-90}$$

$n = 1, 2, \ldots, N - 1$. Note that there are two more f_n^V than f_n^I, which corresponds to the boundary condition $I(0) = I(1) = 0$. Note also that the T's of (7-89) and (7-90) are centered on the same x_n's, in contrast to the shifted pulses of (7-75) and (7-76).

The $[m]$ matrix can again be divided into submatrices of the form (7-77), which reduces to (7-78) with

$$C = \begin{bmatrix} \alpha_{11} & \alpha_{12} & 0 & 0 & \cdots \\ \alpha_{21} & \alpha_{22} & \alpha_{23} & 0 & \cdots \\ 0 & \alpha_{32} & \alpha_{33} & \alpha_{34} & \cdots \\ \cdot & \cdot & \cdot & \cdot & \cdots \end{bmatrix} \tag{7-91}$$

$$L = \begin{bmatrix} \beta_{11} & \beta_{12} & 0 & 0 & \cdots \\ \beta_{21} & \beta_{22} & \beta_{23} & 0 & \cdots \\ 0 & \beta_{32} & \beta_{33} & \beta_{34} & \cdots \\ \cdot & \cdot & \cdot & \cdot & \cdots \end{bmatrix} \tag{7-92}$$

where

$$\alpha_{mn} = \int_0^1 c(x)T(x - x_m)T(x - x_n)\,dx \tag{7-93}$$

$$\beta_{mn} = \int_0^1 l(x)T(x - x_m)T(x - x_n)\,dx \tag{7-94}$$

Similarly, the [I] matrix reduces to the form (7-80), where

$$\Delta_I = \tfrac{1}{2}\begin{bmatrix} -1 & 0 & 0 & 0 & \cdot & \cdots \\ 0 & -1 & 0 & 0 & \cdot & \cdots \\ 1 & 0 & -1 & 0 & \cdot & \cdots \\ 0 & 1 & 0 & -1 & \cdot & \cdots \\ \cdot & \cdot & \cdot & \cdot & \cdot & \cdots \\ \cdot & \cdot & \cdot & 0 & 0 & 1 \end{bmatrix} \tag{7-95}$$

$$\Delta_V = \tfrac{1}{2}\begin{bmatrix} 1 & 0 & -1 & 0 & \cdot & \cdots \\ 0 & 1 & 0 & -1 & \cdot & \cdots \\ 0 & 0 & 1 & 0 & \cdot & \cdots \\ 0 & 0 & 0 & 1 & \cdot & \cdots \\ \cdot & \cdot & \cdot & \cdot & \cdot & \cdots \\ \cdot & \cdot & \cdot & 1 & 0 & -1 \end{bmatrix} \tag{7-96}$$

These are first differences with respect to points separated by two intervals, instead of one interval as for (7-70).

Again we illustrate convergence by applying this approximation to the uniform transmission line. In this case the C and L matrices reduce to

$$C = \frac{c}{6N}\begin{bmatrix} 2 & 1 & 0 & 0 & \cdot & \cdots \\ 1 & 4 & 1 & 0 & \cdot & \cdots \\ 0 & 1 & 4 & 1 & \cdot & \cdots \\ \cdot & \cdot & \cdot & \cdot & \cdot & \cdots \\ \cdot & \cdot & \cdot & 0 & 1 & 2 \end{bmatrix} \tag{7-97}$$

$$L = \frac{l}{6N}\begin{bmatrix} 4 & 1 & 0 & 0 & \cdot & \cdots \\ 1 & 4 & 1 & 0 & \cdot & \cdots \\ 0 & 1 & 4 & 1 & \cdot & \cdots \\ \cdot & \cdot & \cdot & \cdot & \cdot & \cdots \\ \cdot & \cdot & \cdot & 0 & 1 & 4 \end{bmatrix} \tag{7-98}$$

where N is the number of intervals along the line. These tridiagonal matrices are easy to invert by special techniques [4]. The matrix eigenvalue equation (7-85), with matrices (7-95) to (7-98), can now be solved for the approximate eigenvalues. The results are summarized by Table 7-4 for the line divided into two, three, four, and five intervals.

A comparison of Table 7-4 with Table 7-3 shows that the piecewise linear solution (triangle functions) converges significantly faster than the step approximation (pulse functions). This is because the piecewise linear approximation can more closely approximate the solution than the step approximation for a given

TABLE 7-4. Approximate Eigenvalues for a Galerkin Solution of the First-order Equations Using N Current Triangles and $N + 2$ Voltage Triangles

N	$\lambda_1^{(N)}$	$\lambda_2^{(N)}$	$\lambda_3^{(N)}$	$\lambda_4^{(N)}$
2	9.000			
3	9.720	27.000		
4	9.824	36.000	43.073	
5	9.851	38.171	71.173	54.804
Exact	9.870	39.478	88.826	157.914

number of functions. A comparison of Table 7-4 with Table 7-2 shows that the piecewise linear solution of the first-order equation converges significantly faster than that for the second-order equation. This is because in the first-order solution we are testing both the function and its derivative, whereas in the second-order solution we are testing only the function itself. Finally, the eigenvalues of Table 7-4 converge a little slower than those of Table 7-1, indicating that the better behaved the expansion functions are, the faster the convergence. However, we usually pay for faster convergence by having more difficult integrations to perform or more matrix elements to evaluate.

More rapidly converging solutions to the first-order equations could be obtained by using a power-series solution. For example, the expansion functions can be defined as

$$f_n^V = w_n^V = \begin{bmatrix} x^n \\ 0 \end{bmatrix} \tag{7-99}$$

$n = 0, 1, 2, \ldots, N$, and

$$f_n^I = w_n^I = \begin{bmatrix} 0 \\ (x - d)x^n \end{bmatrix} \tag{7-100}$$

$n = 1, 2, \ldots, N - 1$. Note that the f_n^I satisfy the boundary conditions $I(0) = I(1) = 0$, as they must unless the operator is extended. When (7-99) and (7-100) are used, all elements of the matrices, C, L, Δ_I, and Δ_V are nonzero, even for the uniform line. An even better choice of expansion functions is

$$f_n^V = w_n^V = \begin{bmatrix} \cos n\pi x \\ 0 \end{bmatrix} \tag{7-101}$$

$n = 0, 1, 2, \ldots, N$, and

$$f_n^I = w_n^I = \begin{bmatrix} 0 \\ \sin n\pi x \end{bmatrix} \tag{7-102}$$

$n = 1, 2, \ldots, N$. Now for the *uniform line* ($l = c =$ constant), the exact solution is obtained for each order N. This dramatically illustrates how the ease of solution and rate of convergence depend on the choice of expansion and weighting functions.

7-6. Extended Operators

It is sometimes convenient to use expansion functions that do not satisfy the boundary conditions of the problem, that is, are not in the domain of the operator. As discussed in Section 1-7, an extended operator can be defined such that it is the same as the original operator in its domain, and has an extended meaning when applied to functions outside the original domain. Example B of Section 1-7 gives the extended operator for the second-order operator $L = -d^2/dx^2$ and the boundary conditions $f(0) = f(1) = 0$. Explicitly, this extended operator L^e is

$$\langle w, L^e f \rangle = \int_0^1 wLf\, dx - \left[f \frac{dw}{dx} \right]_0^1 \tag{7-103}$$

If the boundary conditions are changed to $f'(0) = f'(1) = 0$, the extended operator L^e is

$$\langle w, L^e f \rangle = \int_0^1 wLf\, dx + \left[w \frac{df}{dx} \right]_0^1 \tag{7-104}$$

The choice is dictated by the condition that the last term (boundary terms) of (7-103) or (7-104) must vanish when f is in the domain of L.

The first-order operator

$$L = \begin{bmatrix} 0 & -\dfrac{d}{dx} \\ \dfrac{d}{dx} & 0 \end{bmatrix} \tag{7-105}$$

can be similarly extended to apply to functions

$$f = \begin{bmatrix} V \\ I \end{bmatrix} \tag{7-106}$$

not in the domain of L. For example, if the boundary conditions are $I(0) = I(1)$, and the inner product is (7-58), then the extended operator L^e is defined by

$$\langle w, L^e f \rangle = \langle w, Lf \rangle + [W_V I]_0^1 \tag{7-107}$$

where, in general, the testing function is

$$w = \begin{bmatrix} W_V \\ W_I \end{bmatrix} \tag{7-108}$$

It is easy to show that L^e of (7-107) is self-adjoint, and that $L^e = L$ if $I(0) = I(1) = 0$. Similarly, if the boundary conditions on L were $V(0) = V(1) = 0$, the extended operator would be

$$\langle w, L^e f \rangle = \langle w, Lf \rangle - [W_I V]_0^1 \tag{7-109}$$

instead of (7-107). Again the choice of (7-107) or (7-109) is dictated by the condition that the last term must vanish when f is the domain of L.

Example. To illustrate the use of an extended operator for an eigenvalue problem, consider the second-order operator $L = -d^2/dx^2$ and the boundary condition $f(0) = f(1) = 0$, that is, the problem stated by (7-10) and (7-11). The extended operator in this case is (7-103). For expansion and testing functions, take

$$f_n = w_n = x^n \tag{7-110}$$

$n = 1, 2, \ldots, N$. Note that these satisfy the boundary condition at $x = 0$, but not at $x = 1$. Following the method of moments, we use the inner product (7-14) and determine the matrix elements as

$$l_{mn} = \langle w_m, L^e f_n \rangle = \frac{-n(n-1)}{n+m-1} - m \tag{7-111}$$

$$m_{mn} = \langle w_m, f_n \rangle = \frac{1}{m+n+1} \tag{7-112}$$

The eigenvalues and eigenfunctions can now be found by the algorithm of Appendix C. Table 7-5 tabulates the eigenvalues as N is increased. Figure 7-5 shows the first and second approximate eigenfunctions, normalized according to

$$1 = \langle f_i^{(N)}, f_i^{(N)} \rangle = [\tilde{\alpha}_m][m_{mn}][\alpha_n] \tag{7-113}$$

and compared to the exact eigenfunctions.

An interesting phenomenon is the appearance of an extraneous eigenvalue, as shown in Table 7-5. (There are two extraneous ones if both boundary conditions are violated.) Note also that this extraneous eigenvalue is negative, whereas all eigenvalues of the original operator are positive. Even though the

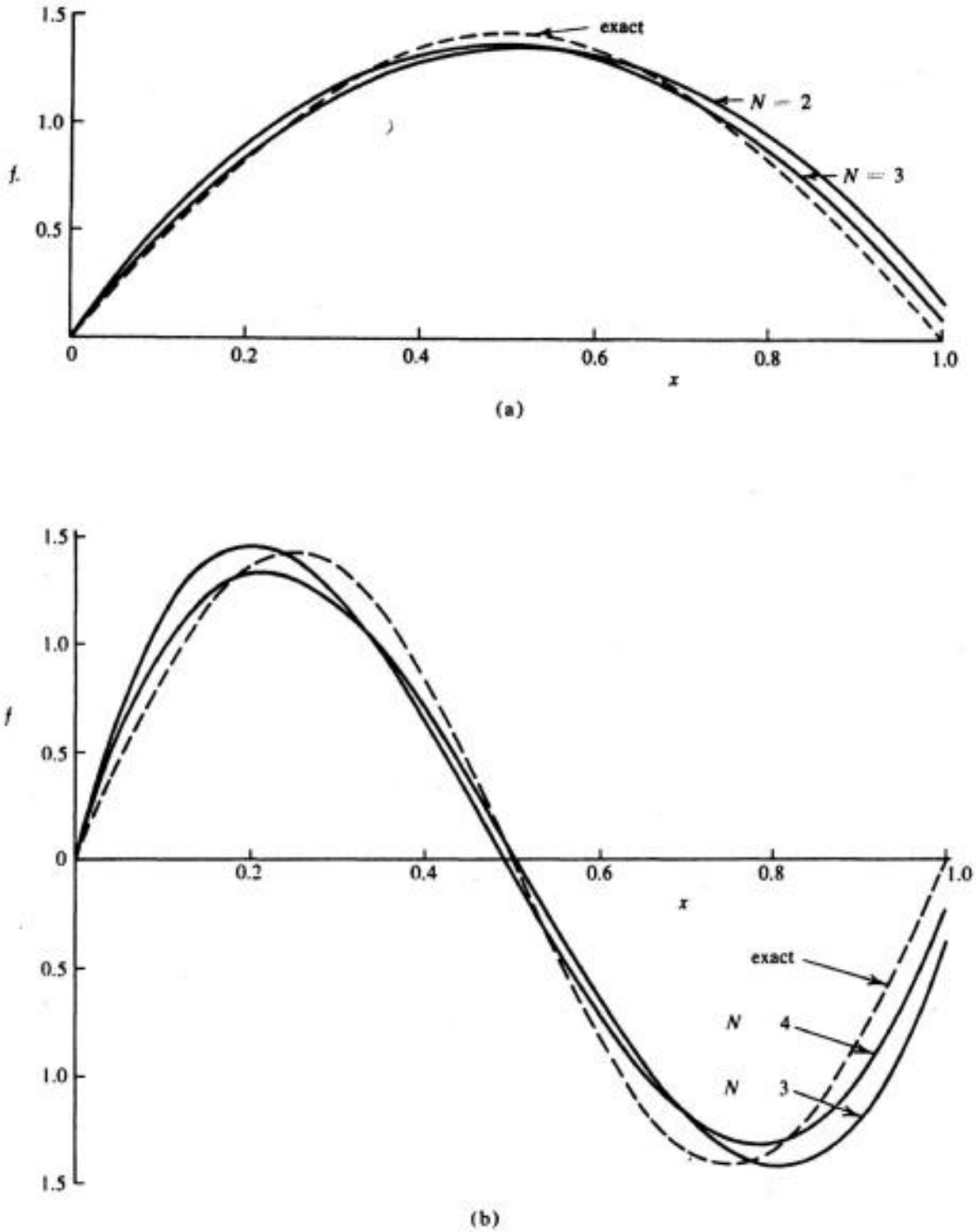

Figure 7-5. **Convergence of the first and second eigenfunctions, using the extended operator and a power expansion.**

TABLE 7-5. Approximate Eigenvalues Calculated Using the Extended Operator and N Terms of a Power Series

N	Extraneous eigenvalue	$\lambda_1^{(N)}$	$\lambda_2^{(N)}$	$\lambda_3^{(N)}$
1	−3.00			
2	−31	10.161		
3	−128.75	10.086	43.664	
4	−353.41	9.871	43.028	108.383
5	−780.69	9.870	39.490	106.131
Exact	—	9.870	39.478	88.826

original operator is positive definite, the extended operator (7-103) is not positive definite. It is usually easy to recognize extraneous eigenvalues introduced by extending an operator, because they do not converge to a limit and the corresponding eigenfunctions tend to be irregular and do not satisfy the boundary conditions.

References

[1] B. Friedman, *Principles and Techniques of Applied Mathematics*, John Wiley & Sons, Inc., New York, 1956.

[2] J. W. Dettman, *Mathematical Methods in Physics and Engineering*, McGraw-Hill Book Co., New York, 1962.

[3] S. Ramo, J. R. Whinnery, and T. Van Duzer, *Fields and Waves in Communication Electronics*, John Wiley & Sons, Inc., New York, 1965, Chap. 1.

[4] P. Henrici, *Discrete Variable Methods in Ordinary Differential Equations*, John Wiley & Sons, Inc., New York, 1962, pp. 350–355.

CHAPTER

8

Cylindrical Waveguides

8-1. Second-order Differential Equation

In this chapter we consider the problem of electromagnetic waves in a hollow conducting cylinder of arbitrary cross section. The medium within the cylinder is assumed to be homogeneous and isotropic, such as free space. Waveguides containing inhomogeneous and/or anisotropic media can be treated by methods similar to those used for resonant cavities in Chapter 9.

The usual second-order differential equation formulation for the problem will first be summarized. Let Fig. 8-1 represent the cross section of a waveguide with conducting boundary C. The transverse coordinates are denoted x and y, and the axial coordinate z. The electromagnetic field is then related to a scalar wave function ψ which satisfies the Helmholz equation

$$\frac{\partial^2 \psi}{\partial x^2} + \frac{\partial^2 \psi}{\partial y^2} + k^2 \psi = 0 \tag{8-1}$$

For TM (transverse magnetic) modes, ψ is subject to the Dirichlet boundary conditions

$$\psi = 0 \qquad \text{on } C \tag{8-2}$$

and, for TE (transverse electric) modes, ψ is subject to the Neumann boundary conditions

$$\frac{\partial \psi}{\partial n} = 0 \qquad \text{on } C \tag{8-3}$$

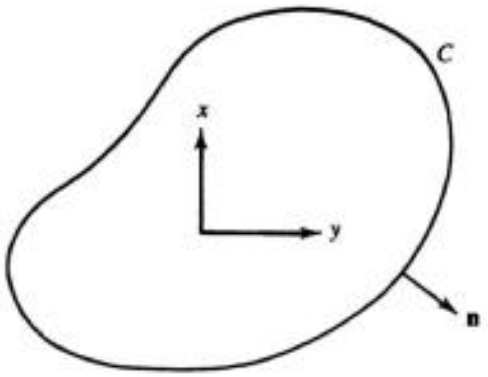

Figure 8-1. **Cross section of a cylindrical waveguide.**

Here n is the direction normal to C and k is the cutoff wavenumber, related to the cutoff wavelength λ_{co} of the waveguide by

$$k = \frac{2\pi}{\lambda_{co}} \tag{8-4}$$

The relationship of ψ to the electromagnetic field, and of k to various waveguide parameters, can be found in many texts, for example, reference [1].

To place (8-1) into the standard form $L\psi = \lambda\psi$, define the operator

$$L = -\nabla^2 = -\frac{\partial^2}{\partial x^2} - \frac{\partial^2}{\partial y^2} \tag{8-5}$$

and the eigenvalue $\lambda = k^2$. Sections 8-2 and 8-3 consider approximate solutions to this eigenvalue problem.

8-2. Second-order Difference Operator

The simplest numerical solution of (8-1) is obtained by approximating the differential operator (8-5) by a difference operator. The second-order difference approximation to $\partial^2\psi/\partial x^2$ is given by (1-55), with a corresponding formula holding for $\partial^2\psi/\partial y^2$. If we take equal increments $\Delta x = \Delta y = h$, the finite-difference approximation to (8-5) becomes

$$L\psi \approx L^d\psi = \frac{1}{h^2}[\psi(x+h, y) + \psi(x-h, y) + \psi(x, y+h) + \psi(x, y-h) - 4\psi(x, y)] \tag{8-6}$$

To obtain a set of algebraic equations, the equation

$$L^d\psi = \lambda\psi \tag{8-7}$$

can be satisfied at discrete points in the guide cross section. As discussed later, this is equivalent to using pulse functions as a basis and point matching for testing.

To obtain the classical method of nets, define a grid of lines spaced a distance h apart, as shown in Fig. 8-2. This defines a mesh of points to which (8-7) is applied. For example, at point 0 of Fig. 8-2, equation (8-7) becomes

$$\frac{1}{h^2}(\psi_a + \psi_b + \psi_c + \psi_d - 4\psi_0) = \lambda\psi_0 \tag{8-8}$$

For the boundary conditions $\psi = 0$ on C all points on the boundary are zero; hence $\psi_c = 0$ in (8-8). If the boundary does not coincide with grid lines, such as on the top and right sides of Fig. 8-2, special techniques are required. One way is to define extra points on the boundary and modify L^d to account for unequal intervals [2]. Another way is to use the method of moments as shown below.

For the boundary conditions $\partial\psi/\partial n = 0$ on C, the usual approach is as follows. For a point 0′ on the boundary (Fig. 8-2), we set $\psi_{d'} = \psi_{b'}$, and the modified (8-8) for the point becomes

$$\frac{1}{h^2}(\psi_{a'} + 2\psi_{b'} + \psi_{c'} - 4\psi_{0'}) = \lambda\psi_{0'} \tag{8-9}$$

If the points are not on the boundary the modification is more difficult. Again the method of moments provides a more direct way to treat boundary conditions, as we now discuss.

For a moment solution, expand ψ as

$$\psi = \sum \alpha_n f_n \tag{8-10}$$

where the basis functions are pulse functions

$$f_n = P(x - x_n)P(y - y_n) \tag{8-11}$$

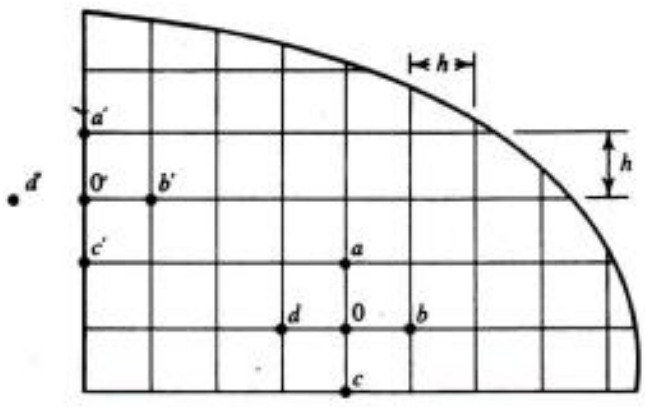

Figure 8-2. Mesh points in a waveguide cross section.

In other words, if Δs_n is a square of sides h centered on x_n and y_n, then $f_n = 1$ on Δs_n and zero elsewhere. For testing, let $w_n = f_n$. As an inner product, take

$$\langle f, g \rangle = \iint_R f(x, y)g(x, y)\, dx\, dy \tag{8-12}$$

where R is the waveguide cross section within C. Now a routine application of Galerkin's method yields

$$[l_{mn}][\alpha_n] = \lambda[m_{mn}][\alpha_n] \tag{8-13}$$

where $[l_{mn}]$ is a second difference matrix and $[m_{mn}]$ is a diagonal matrix. To be explicit, define the distance function

$$d(m, n) = \sqrt{(x_m - x_n)^2 + (y_m - y_n)^2} \tag{8-14}$$

Then, for the boundary condition $\psi = 0$ on C, the elements of $[l_{mn}]$ are

$$l_{mn} = \begin{cases} 2 & d(m, n) = 0 \\ -1 & d(m, n) = h \\ 0 & d(m, n) > h \end{cases} \tag{8-15}$$

and those of $[m_{mn}]$ are

$$m_{mn} = \begin{cases} h^2 & m = n \\ 0 & m \neq n \end{cases} \tag{8-16}$$

For the boundary condition $\partial\psi/\partial n = 0$ on C, the interior pulses give elements the same as (8-15) and (8-16), whereas pulses on the boundary give modified elements

$$\begin{aligned} l_{mn}(\text{modified}) &= (A_m/h^2)l_{mn} \\ m_{nn}(\text{modified}) &= A_n \end{aligned} \tag{8-17}$$

where A_m is the area of f_m within C. When the boundary coincides with mesh points, the moment solution is identical to that obtained from (8-8).

The rate of convergence of the solution can be increased by using higher-order difference operators [2, 3], but this increases the complexity of the matrices. Another possibility is that of constraining every other element of the matrices, in a manner similar to that suggested in Section 3-3. This has the effect of giving approximately the same accuracy for the lower-order eigenvalues, but the matrix is only one fourth the size of the original matrix.

Solutions of high accuracy can be obtained by using many mesh points [4]. However, the matrices are then of high order, and iterative solutions become more practicable than direct matrix methods. The procedure usually used is to make an initial guess at ψ and λ, and then apply (8-8) to each mesh point. This

is a *successive approximation method*, also called a *relaxation method*. After several passes over the mesh, the resultant approximate ψ is substituted into the Rayleigh quotient

$$\lambda = \frac{\sum_n \psi_n L^d \psi_n}{\sum_n \psi_n^2} \tag{8-18}$$

to determine a new approximation to the eigenvalue λ. Because of the stationary nature of (8-18), if ψ_n is correct to an order x per cent, λ will be correct to an order x^2 per cent. The new λ is then used in (8-8), additional passes made over the mesh, resulting in a still better approximation to ψ, and so on. A good description of the procedure is given in reference [4]. There is an extensive body of literature on difference equations and relaxation methods, as referenced in [3] and [4].

Example A. A number of examples obtained by using a mesh approximation to the boundary have been given by Davies and Muilwyk [4]. By using very large numbers of mesh points, the effect of the approximate boundary becomes small. The relaxation method of obtaining the eigenvalues and eigenfunctions is used because of the large number of points. Boundary conditions are imposed by taking $\psi = 0$ on the boundary points for the TM case and by using (8-9) for the TE case. Table 8-1 summarizes the results for a waveguide with circular cross

TABLE 8-1. Difference Equation Results for a Circular Waveguide of Diameter d, Using the Best-fit Inside Mesh [4]

(a) Fundamental TE mode (true $kd = 3.6820$)

d/h	Approx. kd	Per cent errror	Extrapolated
8	3.4389	6.6	
16	3.5269	4.2	
32	3.5978	2.3	3.9122
64	3.6329	1.3	3.6681

(b) Fundamental TM mode (true $kd = 4.8100$)

d/h	Approx. kd	Per cent error	Extrapolated
8	5.6665	17.7	
16	5.2471	9.1	
32	4.9996	3.9	4.6739
64	4.8994	1.9	4.8339
128	4.8533	0.9	4.8150
256	4.8327	0.5	4.8160

section of diameter d. The convergence is relatively slow, but by using an extrapolation procedure [5] accurate results are obtained. For example, in the TE case, the extrapolated error in kd is 0.38 per cent for $d/h = 64$. In the TM case the extrapolated error is 0.12 per cent for $d/h = 256$.

Example B. We here consider some problems that arise with boundary points. Consider the Neumann case $\partial\psi/\partial n = 0$ on C (TE modes). Figure 8-3(a) represents three possible mesh point patterns in the vicinity of a boundary B. Figure 8-3(b) shows the corresponding pulse approximation to be used in the moment solution. For case I, the moment solution gives the result usually obtained by difference equations. For case II, the difference equation approach is to set $\phi_d = \phi_0$, and obtain

$$\frac{1}{h^2}(\psi_a + \psi_b + \psi_c - 3\psi_0) = \lambda\psi_0 \tag{8-19}$$

instead of (8-9). The moment approach again gives the same result. For case III, a difference equation approach taken by Tang and Lo [3] is to set $\phi_d = \phi_0$, and again obtain (8-19). However, as evident from Fig. 8-3(b) (case III), the corresponding pulse basis is incomplete, and poor convergence is obtained. Table 8-2 illustrates convergence of $kb = \sqrt{\lambda}$ for the dominant TE_{10} mode of the

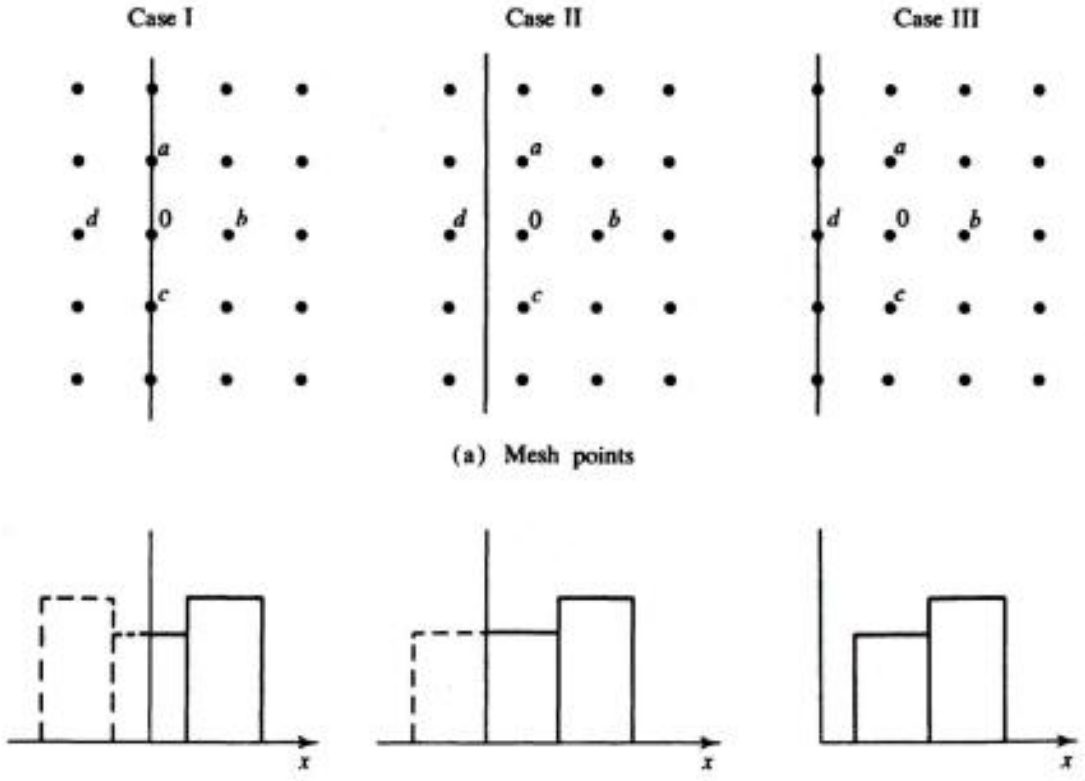

(a) Mesh points

(b) Pulse bases

Figure 8-3. **Possible mesh patterns and corresponding pulse bases.**

TABLE 8-2. Convergence of kb Using Difference Equations with Boundary Treated as in Fig. 8-4 (Rectangular Waveguide, $b = 2a$, dominant TE_{10} mode)

No. of field points	Cases I and II	Case III
2	2.82	4.24
3	3.00	4.00
4	3.06	3.82
5	3.08	3.70
6	3.10	3.62
7	3.12	3.56
Exact kb	3.14	3.14

rectangular waveguide, using the three cases of Fig. 8-3. The poor convergence of case III is clearly evident. Unfortunately Tang and Lo [3] use case III for computations, and hence their TE results converge slowly. However, if the boundary pulses are extended an extra half-interval to the boundary, meshes of type III can be used with good results.

8-3. Moment Solutions

We now consider moment solutions using the differential operator. Pulse functions cannot be used for expansion because they are not in the domain of L. However, triangle functions can be used to obtain approximate solutions for waveguides of arbitrary cross section. For now we assume that all expansion functions satisfy the boundary condition at C. If they do not, the extended operator, discussed in Section 8-4, can be used.

Again let the waveguide cross section be covered by a mesh, as shown in Fig. 8-2. The mesh intersections define a net of points a distance h apart. Let the expansion and testing functions be

$$f_n = w_n = T(x - x_n)T(y - y_n) \tag{8-20}$$

where x_n, y_n are the mesh points and

$$T(x) = \begin{cases} 1 - \dfrac{|x|}{h} & |x| < h \\ 0 & |x| > h \end{cases} \tag{8-21}$$

are the triangle functions discussed in Section 1-5. To evaluate the matrix elements, use (8-20), the operator (8-5), and the inner product (8-12). When the

expansion functions lie wholly within the guide cross section, the elements of $[l_{mn}]$ are

$$l_{mn} = \begin{cases} 8/3 & d(m, n) = 0 \\ -1/3 & d(m, n) = h \text{ or } h\sqrt{2} \\ 0 & d(m, n) > h\sqrt{2} \end{cases} \tag{8-22}$$

where $d(m, n)$ is the distance function defined by (8-14). Similarly, the elements of $[m_{mn}]$ are

$$m_{mn} = \begin{cases} \frac{4}{9}h^2 & d(m, n) = 0 \\ \frac{1}{9}h^2 & d(m, n) = h \\ \frac{1}{36}h^2 & d(m, n) = h\sqrt{2} \\ 0 & d(m, n) > h\sqrt{2} \end{cases} \tag{8-23}$$

A convenient way of illustrating these results is by matrix patterns, as shown by Fig. 8-4(b). For comparison, the matrix patterns for the usual difference equation approach are shown in Fig. 8-4(a).

In the case $\psi = 0$ on C (TM modes), mesh points on the boundary are taken as having no expansion functions at them. All other points have expansion functions lying wholly within C, and all matrix elements are given by (8-22) and (8-23). For the case $\partial\psi/\partial n = 0$ on C (TE modes), interior points have expansion

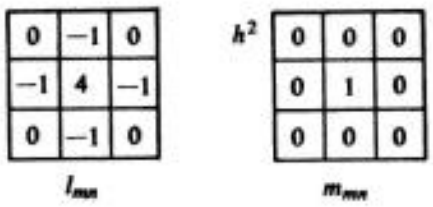

(a)

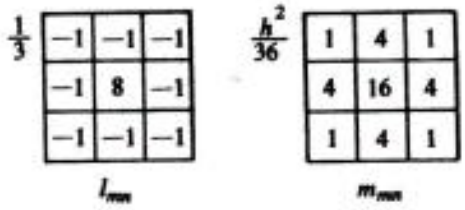

(b)

Figure 8-4. **Matrix patterns for the solutions of Sections 8-2 and 8-3. (*a*) Difference equation, pulse functions, (*b*) differential equation, triangle functions.**

functions which are zero at the boundary. To satisfy the boundary condition, we either add additional expansion functions at the boundary points, or modify the expansion functions adjacent to the boundary points so that they are not zero on C. The first method requires additional expansion functions, and hence increases the size of the matrices. The second method keeps the size of the matrices the same for both TE and TM modes, which is an advantage from a computational standpoint.

Example. To compare convergence of the various methods, consider the rectangular waveguide of Fig. 8-5(a). Let the sides be $b = 2a$, and cover the cross section by a mesh which has equal increments h in the x and y directions, as shown. (A modification for unequal increments is simple.) For TM modes ($\psi = 0$ on C), we use the pyramid expansion functions of (8-20). Since all mesh points are interior points, equations (8-22) and (8-23) apply, and the solution is obtained in a straightforward manner. Table 8-3 shows convergence of the lowest-order TM_{11} mode and of the higher-order TM_{21} and TM_{31} modes, and compares them to the corresponding difference equation solutions. It is interesting to note that whereas the difference equation converges from below the correct solution, the moment solution converges from above. Because the operator is positive definite, a Galerkin solution ($f_n = w_n$) using the exact operator must converge from above. Neither solution converges particularly fast, and both give about the same accuracy.

For TE modes ($\partial\psi/\partial n = 0$ on C), the solution can be obtained either by adding additional expansion functions at the boundary points or by modifying the pulses at the boundary as shown in Fig. 8-5(b). For comparison we shall call the first method case I and the second case II. In case I, the l_{mn} and m_{mn} matrix elements for boundary points must be modified from (8-22) and (8-23). In case II, the matrix elements for points adjacent to the boundary points must be modified. Table 8-4 shows convergence of kb for the TE_{10} and TE_{11} modes, and compares it with the corresponding difference-equation solution. Again all Galerkin solutions must converge to the eigenvalues from above, because the

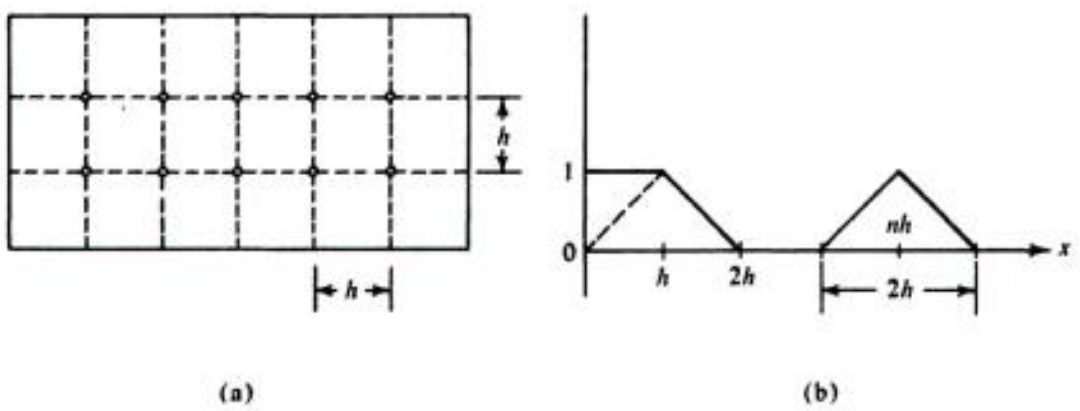

Figure 8-5. **Modification of expansion functions for TE modes. (*a*) Mesh points, (*b*) expansion functions.**

operator is positive definite. In interpreting Table 8-4, keep in mind that case I and the difference equation involve larger matrices than case II because of the additional boundary points.

TABLE 8-3. Convergence of kb Obtained by a Moment Solution and by a Difference Solution (Rectangular Waveguide, $b = 2a$, TM Modes)

Mesh points	TM_{11}		TM_{21}		TM_{31}	
	Triangles	Diff. eq.	Triangles	Diff. eq.	Triangles	Diff. eq.
1×3	7.641	6.432	9.798	8.000	13.220	9.307
2×5	7.305	6.756	9.301	8.485	12.297	10.392
3×7	7.179	6.873	9.116	8.659	11.876	10.794
4×9	7.124	6.927	9.033	8.740	11.678	10.984
Exact	7.025		8.886		11.327	

TABLE 8-4. Convergence of kb for Moment and Difference Solutions: Case I, Additional Triangles on Boundary; Case II, Modified Pulses (Rectangular waveguide, $b = 2a$, TE Modes)

Interior mesh points	TE_{10}			TE_{21}		
	Case I	Case II	Diff. eq.	Case I	Case II	Diff. eq.
1×3	3.223	3.464	3.061	9.798	—	8.000
2×5	3.178	3.247	3.106	9.295	10.579	8.485
3×7	3.162	3.191	3.121	9.115	9.614	8.659
4×9	3.155	3.170	3.129	9.033	9.284	8.740
Exact	3.142			8.886		

A considerable simplification of the computations for the rectangular waveguide is possible. The expansion for the unknown in all cases (including pulses with the difference operator) can be written

$$\begin{aligned} f = \sum \alpha_n f_n &= [\sum \beta_i X_i(x)][\sum \gamma_j Y_j(y)] \\ &= X(x)Y(y) \end{aligned} \tag{8-24}$$

Hence f is a product solution such as obtained in the usual method of separation of variables. The equations therefore separate into two one-dimensional equations

$$\begin{aligned} -\frac{d^2X}{dx^2} &= \lambda_x X \\ -\frac{d^2Y}{dy^2} &= \lambda_y Y \end{aligned} \tag{8-25}$$

and each can be solved separately, either exactly or approximately. The two-dimensional problem has eigenvalues

$$(kb)^2 = \lambda = \lambda_x + \lambda_y \tag{8-26}$$

and eigenfunctions (8-24). Tables 8-3 and 8-4 were constructed using this simplification. However, the procedure is not applicable to guides of cross section other than rectangular.

8-4. Extended Operators

When the waveguide walls do not coincide with the mesh boundary, as in Fig. 8-2, we can either modify the expansion functions at the boundary or extend the operator. In this section the latter approach is considered.

To summarize the problem, we have $L\psi = \lambda\psi$, where $\lambda = k^2$ and

$$L = -\nabla^2 = -\frac{\partial^2}{\partial x^2} - \frac{\partial^2}{\partial y^2} \tag{8-27}$$

This operator is formally self-adjoint with respect to the inner product

$$\langle f, g \rangle = \iint_R f(x, y) g(x, y)\, dx\, dy \tag{8-28}$$

where R is the cross section of the waveguide. When the Dirichlet ($\psi = 0$ on C) or the Neumann ($\partial\psi/\partial n = 0$ on C) boundary conditions are met, L is self-adjoint and positive definite.

If the expansion and testing functions do not satisfy the boundary conditions, we can extend the operator for a moment solution. By Gauss' theorem, it is easy to show that in general

$$\langle g, Lf \rangle = \langle Lg, f \rangle + \oint_C \left(f \frac{dg}{dn} - g \frac{df}{dn} \right) dl \tag{8-29}$$

where C is the waveguide boundary and n is the outward normal. We wish to define an extended operator L^e so that $L^e f = Lf$ when f satisfies the boundary conditions and

$$\langle g, L^e f \rangle = \langle L^e g, f \rangle \tag{8-30}$$

when f does not satisfy the boundary conditions. For TM modes ($\psi = 0$ on C) these conditions can be met if L^e is defined by

$$\langle g, L^e_{\text{TM}} f \rangle = \langle g, Lf \rangle - \oint_C f \frac{dg}{dn}\, dl \tag{8-31}$$

That (8-30) is now satisfied is evident from (8-29). For TE modes ($\partial\psi/\partial n = 0$ on C), the extended operator L^e can be defined as

$$\langle g, L^e_{\text{TE}} f\rangle = \langle g, Lf\rangle + \oint_C g \frac{df}{dn}\, dl \tag{8-32}$$

Again it is evident from (8-29) that (8-30) is satisfied.

Once we have the appropriate extended operator, the moment solution proceeds in the usual manner. We shall not give examples here because of the detail involved. In general, solutions converge in a manner similar to the one-dimensional problems treated in Section 7-6.

8-5. First-order Differential Equations

Any second-order differential equation can be represented as a set of first-order differential equations. The equations

$$\begin{aligned} -\frac{\partial\psi}{\partial x} &= ku \\ -\frac{\partial\psi}{\partial y} &= kv \\ \frac{\partial u}{\partial x} + \frac{\partial v}{\partial y} &= k\psi \end{aligned} \tag{8-33}$$

are easily shown, by substitution, to be equivalent to (8-1). To place (8-33) in standard form, define

$$L = \begin{bmatrix} 0 & \dfrac{\partial}{\partial x} & \dfrac{\partial}{\partial y} \\ -\dfrac{\partial}{\partial x} & 0 & 0 \\ -\dfrac{\partial}{\partial y} & 0 & 0 \end{bmatrix} \tag{8-34}$$

and

$$f = \begin{bmatrix} \psi \\ u \\ v \end{bmatrix} \tag{8-35}$$

Now the eigenvalue problem is represented by

$$Lf = kf \tag{8-36}$$

where k is the eigenvalue.

An appropriate inner product for the new function space is

$$\langle f_1, f_2 \rangle = \iint_R \bar{f}_1 f_2 \, dx \, dy$$

$$= \iint_R (\psi_1 \psi_2 + u_1 u_2 + v_1 v_2) \, dx \, dy \tag{8-37}$$

which satisfies postulates (1-2) to (1-4). The formal adjoint of L is found as follows:

$$\langle f_1, Lf_2 \rangle = \iint_R [\psi_1 \quad u_1 \quad v_1] \begin{bmatrix} 0 & \frac{\partial}{\partial x} & \frac{\partial}{\partial y} \\ -\frac{\partial}{\partial x} & 0 & 0 \\ -\frac{\partial}{\partial y} & 0 & 0 \end{bmatrix} \begin{bmatrix} \psi_2 \\ u_2 \\ v_2 \end{bmatrix} ds$$

$$= \iint_R \left[\psi_1 \left(\frac{\partial u_2}{\partial x} + \frac{\partial v_2}{\partial y} \right) - u_1 \frac{\partial \psi_2}{\partial x} - v_1 \frac{\partial \psi_2}{\partial y} \right] ds \tag{8-38}$$

Making use of the rule for differentiating a product, we can rearrange this to

$$\langle f_1, Lf_2 \rangle = \iint_R \left[\psi_2 \left(\frac{\partial u_1}{\partial x} + \frac{\partial v_1}{\partial y} \right) - u_2 \frac{\partial \psi_1}{\partial x} - v_2 \frac{\partial \psi_1}{\partial y} \right] ds$$

$$+ \iint_R \left[\frac{\partial}{\partial x} (\psi_1 u_2 - u_1 \psi_2) + \frac{\partial}{\partial y} (\psi_1 v_2 - v_1 \psi_2) \right] ds \tag{8-39}$$

The first integral is $\langle Lf_1, f_2 \rangle$. The second integral can be reduced to a boundary integral by the Gaussian integral theorem [6]. The result is

$$\langle f_1, Lf_2 \rangle = \langle Lf_1, f_2 \rangle + \oint_C [n_x(\psi_1 u_2 - u_1 \psi_2) + n_y(\psi_1 v_2 - v_1 \psi_2)] \, dl \tag{8-40}$$

where n_x and n_y are the x and y components of $\mathbf{n}$, respectively. Hence L is formally self-adjoint. For TM modes, $\psi = 0$ on C, the boundary terms of (8-40) vanish, and L is self-adjoint. For TE modes, $\partial\psi/\partial n = 0$ on C, which is equivalent to

$$n_x u + n_y v = 0 \qquad \text{on } C \tag{8-41}$$

Again the boundary terms of (8-40) vanish and L is self-adjoint.

8-6. Moment Solutions

Solution of the first-order equations by the method of moments proceeds in a manner analogous to that for the one-dimensional case (Section 7-5). It is assumed for now that all expansion functions satisfy the appropriate boundary conditions. For convenience, we define three types of expansion and testing functions,

$$f_n^{\psi} = w_n^{\psi} = \begin{bmatrix} \psi_n(x, y) \\ 0 \\ 0 \end{bmatrix} \tag{8-42}$$

$$f_n^{u} = w_n^{u} = \begin{bmatrix} 0 \\ u_n(x, y) \\ 0 \end{bmatrix} \tag{8-43}$$

$$f_n^{v} = w_n^{v} = \begin{bmatrix} 0 \\ 0 \\ v_n(x, y) \end{bmatrix} \tag{8-44}$$

Now the unknown f is expanded as

$$f = \sum \alpha_n f_n^{\psi} + \sum \beta_n f_n^{u} + \sum \gamma_n f_n^{v} \tag{8-45}$$

where α_n, β_n, and γ_n are constants. It is not necessary that there be the same number of n in each summation. An application of the method of moments to (8-36) gives the partitioned matrix equation

$$\left[\begin{array}{c|c|c} 0 & l_{mn}^{\psi u} & l_{mn}^{\psi v} \\ \hline l_{mn}^{u\psi} & 0 & 0 \\ \hline l_{mn}^{v\psi} & 0 & 0 \end{array}\right] \left[\begin{array}{c} \alpha_n \\ \hline \beta_n \\ \hline \gamma_n \end{array}\right] = k \left[\begin{array}{c|c|c} m_{mn}^{\psi\psi} & 0 & 0 \\ \hline 0 & m_{mn}^{uu} & 0 \\ \hline 0 & 0 & m_{mn}^{vv} \end{array}\right] \left[\begin{array}{c} \alpha_n \\ \hline \beta_n \\ \hline \gamma_n \end{array}\right] \tag{8-46}$$

where the elements of the submatrices are

$$l_{mn}^{\psi u} = l_{nm}^{u\psi} = \iint_R \psi_m \frac{\partial u_n}{\partial x}\, dx\, dy \tag{8-47}$$

$$l_{mn}^{\psi v} = \psi_{nm}^{v\psi} = \iint_R \psi_m \frac{\partial v_n}{\partial y}\, dx\, dy \tag{8-48}$$

$$m_{mn}^{gg} = \iint_R g_m g_n\, dx\, dy \tag{8-49}$$

with $g = \psi$, u, or v. The matrix (8-46) represents a set of three matrix equations.

The problem can be reduced to a single matrix equation as follows. From the last row of (8-46) we obtain

$$[\gamma_m] = \frac{1}{k}[m^{vv}]^{-1}[l^{v\psi}][\alpha_n] \tag{8-50}$$

Similarly, from the second row of (8-46) we obtain

$$[\beta_m] = \frac{1}{k}[m^{uu}]^{-1}[l^{u\psi}][\alpha_n] \tag{8-51}$$

These two results can now be substituted in the first row of (8-46) to give the eigenvalue equation

$$[L_{mn}][\alpha_n] = k^2[\alpha_n] \tag{8-52}$$

where

$$[L_{mn}] = [m^{\psi\psi}]^{-1}\{[l^{\psi u}][m^{uu}]^{-1}[l^{u\psi}] + [l^{\psi v}][m^{vv}]^{-1}[l^{v\psi}]\} \tag{8-53}$$

We can now solve (8-52) in the usual manner for eigenvalues k^2 and eigenvectors $[\alpha_n]$. The corresponding $[\gamma_n]$ and $[\beta_n]$ are then determined by (8-50) and (8-51). The approximate eigenvalues k of the original equation (8-36) are now $\pm\sqrt{k^2}$, and the corresponding approximate eigenfunctions are given by (8-45).

Example. Again consider the rectangular waveguide, Fig. 8-5(a). Pulse functions can be used for expansion, but the convergence is slow. (See Table 7-3 in the one-dimensional case.) Triangle functions for expansion and testing give much faster convergence, as illustrated by Table 7-4. Hence we choose

$$\psi_n = u_n = v_n = T(x - x_n)T(y - y_n) \tag{8-54}$$

where the T are triangle functions of width $2h$ and centered on a mesh point x_n, y_n. Evaluation of the matrix elements (8-47) to (8-49) is simple, and details are not given here. For TM modes, $\psi = 0$ on C, and hence ψ_n centered on interior points only are used. However, u and v do not have boundary restrictions, and either additional boundary functions must be used or the functions adjacent to the boundary must be modified as in Fig. 8-5(b). For TE modes, ψ is not subjected to boundary conditions, but u and v require boundary conditions according to (8-41). To illustrate convergence, Table 8-5 gives the results for the TM_{21} mode of a rectangular waveguide of sides $b = 2a$. A comparison of this result

with the TM_{21} mode of Table 8-3 shows that the convergence is significantly faster when first-order equations are used. Basically, this is because we are expanding and testing both ψ and its derivatives, instead of only ψ itself, and the operator involves only first derivatives.

TABLE 8-5. Convergence of kb for First-order Equations, Triangle Expansion Functions (Rectangular Waveguide, $b = 2a$, TM_{21} mode)

Mesh points	TM_{21} mode
1×3	8.483
2×5	8.818
3×7	8.866
4×9	8.878
Exact	8.886

8-7. Extended Operators

If the expansion functions for a moment solution do not satisfy the boundary conditions, the operator must be extended. We have already derived the general relationship between $\langle f_1, Lf_2 \rangle$ and $\langle Lf_1, f_2 \rangle$ in Section 8-5, given by (8-40). To extend the operator, boundary terms must be added so that L^e is self-adjoint and $L^e = L$ when f is in the domain of L. For TM modes, $\psi = 0$ on C, and the appropriate extended operator is defined by

$$\langle f_1, L^e_{TM} f_2 \rangle = \langle f_1, Lf_2 \rangle + \oint_C \psi_2 (n_x u_1 + n_y v_1)\, dl \tag{8-55}$$

That L^e_{TM} is self-adjoint follows from (8-40). For TE modes, $n_x u + n_y v = 0$ on C, and the extended operator is defined by

$$\langle f_1, L^e_{TE} f_2 \rangle = \langle f_1, Lf_2 \rangle - \oint_C \psi_1 (n_x u_2 + n_y v_2)\, dl \tag{8-56}$$

Again it is evident from (8-40) that L^e_{TE} is self-adjoint.

Once the extended operator is known, a moment solution proceeds as in Section 8-6. The only change is the use of the extended operator in place of the original operator. For TM modes, this involves no change in the formulas for

matrix elements, (8-47) to (8-49). However, for TE modes, we find (8-47) and (8-48) must be replaced by

$$I^{\psi u}_{mn} = I^{u\psi}_{nm} = -\iint_R \frac{\partial \psi_m}{\partial x} u_n \, dx \, dy \tag{8-57}$$

$$I^{\psi v}_{mn} = I^{v\psi}_{nm} = -\iint_R \frac{\partial \psi_m}{\partial y} v_n \, dx \, dy \tag{8-58}$$

while (8-49) is unchanged. Note that (8-47) and (8-57) are equal if the original boundary conditions are met but differ if they are not met, and similarly for (8-48) and (8-58). It is interesting to note that we need never evaluate the contour integrals of (8-55) and (8-56).

8-8. Use of Generalized Impedances

The modes of a waveguide can be determined using the generalized impedance concept discussed in Chapter 5. We here consider only waveguides containing homogeneous isotropic matter. The procedure can be extended to waveguides containing arbitrary media by adding additional impedance terms as described in Section 5-3. Similar methods also apply to resonant cavities.

The waveguide cross section is again defined by Fig. 8-1. Let the field internal to the waveguide be expressed in terms of the current $\mathbf{J}$ on the waveguide walls as

$$\mathbf{E}(\boldsymbol{\rho}) = \oint_C \mathbf{J}(\boldsymbol{\rho}')\Gamma(\boldsymbol{\rho}, \boldsymbol{\rho}', k) \, dl' \tag{8-59}$$

where Γ is the free-space tensor Green's function. The wavenumber k is shown explicitly in the argument of Γ because it is the eigenvalue to be determined. Specializing (8-59) to C, and setting $\mathbf{n} \times \mathbf{E} = 0$ on C, we obtain the appropriate eigenvalue equation

$$0 = \mathbf{n} \times \oint_C \mathbf{J}(\boldsymbol{\rho}')\Gamma(\boldsymbol{\rho}, \boldsymbol{\rho}', k) \, dl' \qquad \boldsymbol{\rho} \text{ on } C \tag{8-60}$$

The cutoff wavenumbers of the guide are those k for which (8-60) is satisfied.

To reduce the problem to a matrix equation, we apply the procedure of Section 5-1. The only difference between (5-2) and (8-60) is that $\mathbf{E}^i = 0$; that is, there is no incident field. Hence the appropriate matrix equation is (5-9) with the right side zero; that is,

$$[Z_{mn}][I_n] = 0 \tag{8-61}$$

Here Z_{mn} and I_n are the generalized network parameters of Section 5-1. For TM modes in a cylindrical waveguide, the Z_{mn} are given by (3-22), and for TE modes, by (4-20) with ψ given by (3-59).

The Z_{mn} are in general complex, and so also are the eigenvalues k obtained from (8-61). This is because (8-61) is an approximate representation of the problem, and any approximation to the correct $\mathbf{J}$ must radiate some field. In other words, the field external to C is not identically zero. We can modify the procedure to avoid this complication as follows. The field from $\mathbf{J}$ need not satisfy the radiation condition because the true field vanishes external to C. The imaginary part of Γ has the appropriate singularity at a source point, and the equation

$$0 = \mathbf{n} \times \oint_C \mathbf{J}(\boldsymbol{\rho}') \operatorname{Im}[\Gamma(\boldsymbol{\rho}, \boldsymbol{\rho}', k)]\, dl' \qquad \boldsymbol{\rho} \text{ on } C \tag{8-62}$$

is equally valid for the problem. The matrix approximation to (8-62) now becomes

$$[X_{mn}][I_n] = 0 \tag{8-63}$$

instead of (8-61). The elements I_n are real, and X_{mn} is $\operatorname{Im}(Z_{mn})$. Hence we need consider only the reactive parts of the generalized impedances.

The eigenvalue equations (8-62) and (8-63) are nonlinear in k; that is, the eigenvalue k does not appear as a simple proportionality factor. For the matrix equation (8-63), the eigenvalues k are determined by

$$\det |X_{mn}(k)| = 0 \tag{8-64}$$

This can be solved by successive approximation. Perhaps the simplest method is that of Newton, summarized as follows. Let $\det |X|$ be expanded in a Taylor series about some approximate k_a as

$$\det |X| = \det |X(k_a)| + \frac{d}{dk_a} [\det |X(k_a)|]\, \Delta k + \cdots \tag{8-65}$$

where $\Delta k = k - k_a$ is the change in k. Hence the correction to k is

$$\Delta k = -\frac{\det |X(k_a)|}{\dfrac{d}{dk_a} [\det |X|]} \tag{8-66}$$

Because the derivative of a determinant is a complicated expression, a difference approximation is used in the denominator of (8-66). Convergence to the eigen-

values of (8-64) is normally rapid. Once the k is found, the eigenvector $[I]$ can be found from (8-63) by matrix inversion, after eliminating one of the constituent equations.

If the waveguide cross section is symmetrical about an axis in the xy plane, the problem can be reduced to two cases, one for modes with even symmetry and one for odd symmetry. The complete reactance matrix is then of the form

$$[X] = \begin{bmatrix} [A] & [B] \\ [B^R] & [A^R] \end{bmatrix} \tag{8-67}$$

where $[A^R]$ and $[B^R]$ are reversed matrices, obtained from $[A]$ and $[B]$ by reversing the order of both rows and columns. Now k for the even modes is found from

$$\det |A + B| = 0 \tag{8-68}$$

and for the odd modes from

$$\det |A - B| = 0 \tag{8-69}$$

The determinant of $[X]$ is the product of the determinants (8-68) and (8-69).

Example. Consider the TM modes of a cylindrical waveguide. The appropriate specialization of (8-60) is (3-5) with $E_z = 0$. The modified equation (8-62) is the imaginary part of this, or

$$0 = \oint_C J_z(\boldsymbol{\rho}') N_0(k|\boldsymbol{\rho} - \boldsymbol{\rho}'|)\, dl' \qquad \boldsymbol{\rho} \text{ on } C \tag{8-70}$$

where N_0 is the Neumann function. The elements of the reactance matrix of (8-63) can be approximated by the imaginary part of (3-22), which, with an appropriate change of multipliers, is

$$X_{mn} = \begin{cases} (\Delta C_n)^2 \dfrac{2}{\pi} \log\left(\dfrac{\alpha}{k\,\Delta C_n}\right) & m = n \\ \Delta C_m\, \Delta C_n\, N_0(k|\boldsymbol{\rho}_m - \boldsymbol{\rho}_n|) & m \neq n \end{cases} \tag{8-71}$$

where $\alpha = 6.11\ldots$. These formulas have been applied to rectangular waveguides with sides $b/a = 9/4$. Equation (8-71) was used for 52 points on C, and every other point constrained according to (3-24), giving a 26 by 26 matrix. Use of symmetry conditions according to (8-68) and (8-69) further reduced the problem to two 13 by 13 matrices.

Figure 8-6 shows a plot of $\det |A + B|$ for the TM even modes. There are appropriate zeros corresponding to the TM_{11} and TM_{12} modes, but there are

also some extraneous zeros. These are due to the approximations made in the matrix equation. They correspond to solutions of (8-68), but not of (8-70). These extraneous roots will change as the expansion functions are changed, whereas the correct roots are fixed. When the eigenvectors are computed using

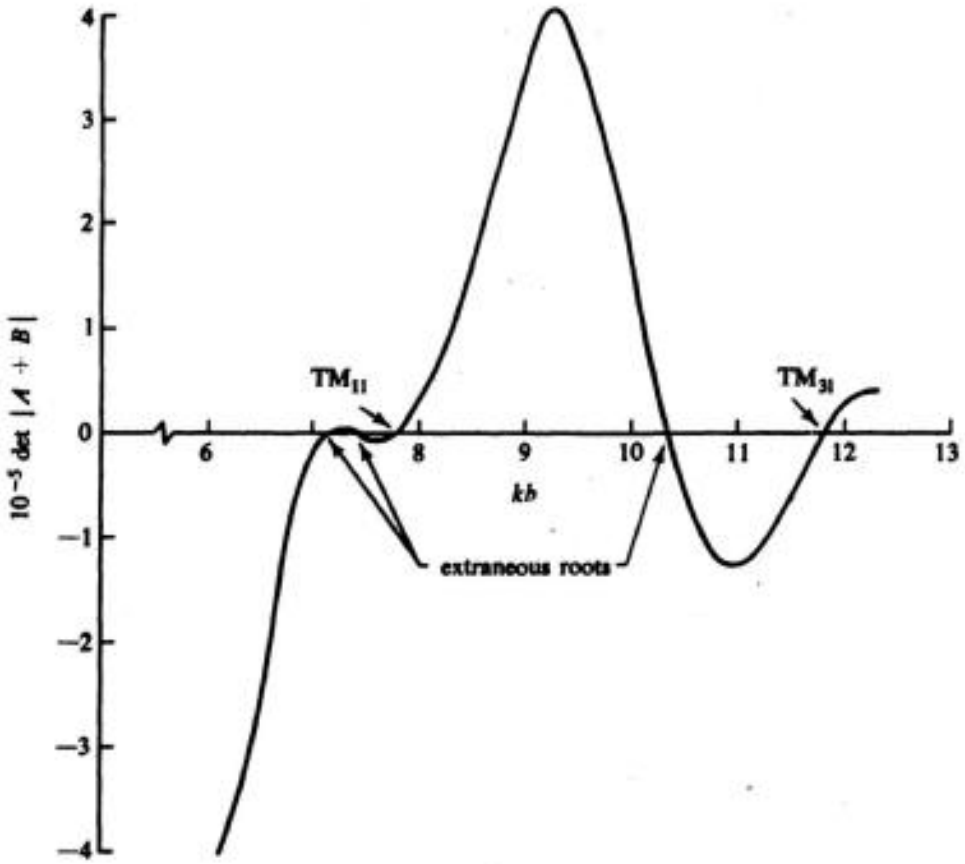

Figure 8-6. Plot of $\det|A + B|$, showing eigenvalues and extraneous zeros.

(8-63), the correct roots yield good approximations to the current on the waveguide walls. The extraneous roots tend to give eigenvectors which do not represent continuous distributions of currents on the walls, and can be recognized as extraneous by this characteristic. Table 8-6 summarizes the approximate eigenvalues obtained from the correct roots and compares them with the exact eigenvalues.

TABLE 8-6. Approximate Eigenvalues Obtained by the Generalized Impedance Method (Rectangular Waveguide, $b/a = 9/4$, TM Modes)

Mode	TM_{11}	TM_{21}	TM_{31}
kb approx.	7.76	9.49	11.81
kb exact	7.74	9.46	11.78

CHAPTER

9

Cavity Resonators

9-1. Statement of the Problem

The general problem of a resonant cavity of arbitrary shape, filled with an arbitrary inhomogeneous and/or anisotropic medium, is considered in this chapter. We explicitly discuss the solution in terms of the modes of the empty cavity, but other sets of expansion functions can be used if desired. A medium anisotropic with respect to electromagnetic fields is one characterized by a tensor permeability and/or a tensor permittivity. The conductivity is here considered a part of the permittivity, and hence it too may be a tensor. Important special cases of anisotropic media are ferrites in a d-c magnetic field (tensor permeability) and plasmas in a d-c magnetic field (tensor permittivity). The name *gyrotropic media* is often given to such ferrites and plasmas. The general solution is specialized to the case of a rectangular cavity uniformly filled with gyrotropic plasma, and representative numerical results are given in Section 9-4.

The solution is obtained by the method of moments, as discussed in Chapter 7. The modes are expressed as an expansion in terms of a set of functions complete over the cavity space. The result is a matrix eigenvalue equation of infinite dimension, the eigenvalues of which are the resonant frequencies and the eigenvectors of which are the coefficients of the modal expansion. For numerical results the matrix equations are truncated and the resultant finite equations solved by digital computation. In those cases for which the exact solution can be expressed as a finite sum of the expansion functions, the matrix solution reduces to the exact solution.

Once Maxwell's equations are written in standard operator notation, the solution can be obtained in a straightforward manner. For time-harmonic fields, $\exp(j\omega t)$ time dependence, Maxwell's equations are

$$\begin{aligned} \nabla \times \mathbf{E} &= -j\omega\mu_0[\mu]\mathbf{H} \\ \nabla \times \mathbf{H} &= j\omega\varepsilon_0[\varepsilon]\mathbf{E} \end{aligned} \tag{9-1}$$

where $[\mu]$ is the relative permeability tensor, $[\varepsilon]$ the relative permittivity tensor, μ_0 the free-space permeability, and ε_0 the free-space permittivity. Energy dissipation may be included in the $[\mu]$ and $[\varepsilon]$ when present.

To express (9-1) in operator form, define a field matrix

$$\phi = \begin{bmatrix} \mathbf{E} \\ \mathbf{H} \end{bmatrix} \tag{9-2}$$

and the operators

$$L = \begin{bmatrix} 0 & -\nabla \times \\ \nabla \times & 0 \end{bmatrix} \qquad M = \begin{bmatrix} \varepsilon_0[\varepsilon] & 0 \\ 0 & -\mu_0[\mu] \end{bmatrix} \tag{9-3}$$

Then Maxwell's equations are

$$L\phi = j\omega M\phi \tag{9-4}$$

To fully specify the eigenvalue problem, boundary conditions on ϕ must be given. For cavities bounded by perfect electric conductors

$$\mathbf{n} \times \mathbf{E} = 0 \qquad \text{on } S \tag{9-5}$$

where S is the cavity boundary and $\mathbf{n}$ the unit outward normal. Other boundary conditions may be chosen if desired. Equations (9-4) and (9-5) define an eigenvalue problem with eigenvalues $j\omega$ and eigenfunctions ϕ.

A suitable inner product for the problem is

$$\langle \phi_1, \phi_2 \rangle = \iiint_\tau (\mathbf{E}_1 \cdot \mathbf{E}_2 + \mathbf{H}_1 \cdot \mathbf{H}_2)\, d\tau \tag{9-6}$$

where τ is the region bounded by S. It is easy to show, by means of the divergence theorem, that L is self-adjoint; that is,

$$\langle \phi_1, L\phi_2 \rangle = \langle L\phi_1, \phi_2 \rangle \tag{9-7}$$

for the domain defined by (9-5). The adjoint of M denoted by M^a and defined by

$$\langle \phi_1, M\phi_2 \rangle = \langle M^a\phi_1, \phi_2 \rangle \tag{9-8}$$

is readily determined as

$$M^a = \begin{bmatrix} \varepsilon_0[\tilde{\varepsilon}] & 0 \\ 0 & -\mu_0[\tilde{\mu}] \end{bmatrix} \tag{9-9}$$

where $[\tilde{\varepsilon}]$ and $[\tilde{\mu}]$ are the transposes of $[\varepsilon]$ and $[\mu]$. Hence the adjoint equation to (9-4) is

$$L\phi^a = j\omega M^a\phi^a \tag{9-10}$$

where the boundary conditions on ϕ^a are the same as on ϕ, given by (9-5). The eigenvalues of (9-10) are, of course, the same as those of (9-4).

Note that solutions to the adjoint equation are the modes and resonant frequencies for the same cavity filled with matter characterized by permeability and permittivity tensors which are the transposes of those in the original problem. Hence transposing the constitutive tensors leaves the resonances (eigenvalues) unchanged, but the modes (eigenfunctions) are different.

9-2. Moment Solution

Following the method of moments, we express solutions of the original problem and the adjoint problem as

$$\phi = \sum_i \alpha_i f_i \tag{9-11}$$

$$\phi^a = \sum_i \beta_i g_i \tag{9-12}$$

where f_i and g_i are functions in the domain of L, and α_i and β_i are constants. We then substitute (9-11) into (9-4) and take the inner product with each g_i. The result is

$$\left\langle g_i, L\sum_j \alpha_j f_j \right\rangle = \left\langle g_i, j\omega M\sum_j \alpha_j f_j \right\rangle \tag{9-13}$$

for all i. Since L and M are linear, (9-13) reduces to

$$\sum_j \alpha_j \langle g_i, Lf_j \rangle = j\omega \sum_j \alpha_i \langle g_i, Mf_j \rangle \tag{9-14}$$

for all i. Hence we have a set of equations, or a matrix equation, to solve. For simplified notation, define

$$l_{ij} = \langle g_i, Lf_j \rangle \tag{9-15}$$

$$m_{ij} = \langle g_i, Mf_j \rangle \tag{9-16}$$

Let $[l]$ and $[m]$ denote the matrices with elements l_{ij} and m_{ij}, respectively, and $[\alpha]$ the column matrix of the α_i. Then (9-14) can be written

$$[l][\alpha] = j\omega[m][\alpha] \tag{9-17}$$

This is a matrix eigenvalue equation with eigenvalues $j\omega$ and eigenvectors $[\alpha]$. The eigenvalues are solutions to

$$\det |l_{ij} - j\omega m_{ij}| = 0 \tag{9-18}$$

The eigenvectors $[\alpha]$ corresponding to the eigenvalues $j\omega$ define approximate eigenfunctions to the original problem by (9-11). If complete sets of f_i and g_i are used, exact solutions to the original problem are obtained, at least in principle.

The eigenfunctions of the adjoint equations are not needed, but may be found by a dual procedure. Instead of (9-14), we have

$$\sum_j \beta_j \langle f_i, Lg_j \rangle = j\omega \sum_j \beta_j \langle f_i, M^a g_j \rangle \tag{9-19}$$

Since L is self-adjoint, and M^a related to M by (9-8), equation (9-19) can be written in terms of the transposes of the matrices $[l]$ and $[m]$ as

$$[\tilde{l}][\beta] = j\omega[\tilde{m}][\beta] \tag{9-20}$$

Hence the equation for $[\beta]$ is the transpose of the equation for $[\alpha]$, (9-17). The eigenvalues are still solutions to (9-18), because transposing the matrices does not change the determinant.

The solution for a one-term representation gives

$$j\omega = \frac{\langle \phi^a, L\phi \rangle}{\langle \phi^a, M\phi \rangle} \tag{9-21}$$

which is the usual stationary expression for the eigenvalues. If we start from (9-21), use expansions (9-11) and (9-12), and apply the Rayleigh-Ritz constraints

$$\frac{\partial \omega}{\partial \alpha_i} = \frac{\partial \omega}{\partial \beta_i} = 0 \qquad \text{for all } i \tag{9-22}$$

then (9-17) and (9-20) are obtained. Hence the two methods are equivalent. In terms of the field vectors, (9-21) can be written

$$j\omega = \frac{\iiint (\mathbf{H}^a \cdot \nabla \times \mathbf{E} + \mathbf{E}^a \cdot \nabla \times \mathbf{H})\, d\tau}{\iiint (\varepsilon_0 \mathbf{E}^a \cdot [\varepsilon]\mathbf{E} - \mu_0 \mathbf{H}^a \cdot [\mu]\mathbf{H})\, d\tau} \tag{9-23}$$

This reduces to Berk's result when specialized to loss-free ferrite media [1].

A complete set of functions, corresponding to the modes of empty cavities having the same boundary S, are chosen for the expansions (9-11) and (9-12). The normalized electric mode functions are defined by

$$\nabla \times \nabla \times \mathbf{E}_i^0 = (\omega_i^0)^2 \varepsilon_0 \mu_0 \mathbf{E}_i^0 \tag{9-24}$$

$$\mathbf{n} \times \mathbf{E}_i^0 = 0 \quad \text{on } S \tag{9-25}$$

$$\iiint_\tau \varepsilon_0 \mathbf{E}_i^0 \cdot \mathbf{E}_i^0\, d\tau = 1 \tag{9-26}$$

where the superscript 0 denotes "empty cavity" and subscript i is the mode index. The eigenvalue $\omega_i^0 = 0$ is of infinite degeneracy and an infinite set of irrotational electric mode functions $\mathbf{F}_i^0$ are defined by

$$\nabla \times \mathbf{F}_i^0 = 0 \tag{9-27}$$

where (9-25) and (9-26) apply also to the $\mathbf{F}_i^0$. Methods of constructing orthonormal sets of $\mathbf{F}_i^0$ are discussed by Slater [2]. Similarly, a set of normalized magnetic mode functions are defined by

$$\nabla \times \nabla \times \mathbf{H}_i^0 = (\omega_i^0)^2 \varepsilon_0 \mu_0 \mathbf{H}_i^0 \tag{9-28}$$

$$\mathbf{n} \times \nabla \times \mathbf{H}_i^0 = 0 \quad \text{on } S \tag{9-29}$$

$$-\iiint_\tau \mu_0 \mathbf{H}_i^0 \cdot \mathbf{H}_i^0\, d\tau = 1 \tag{9-30}$$

The boundary conditions (9-29) are not necessary, but this choice ensures that the ω_i^0 of (9-28) are equal to those of (9-24). Again, $\omega_i^0 = 0$ is of infinite degeneracy, and a set of irrotational magnetic mode functions $\mathbf{G}_i^0$ are defined by

$$\nabla \times \mathbf{G}_i^0 = 0 \tag{9-31}$$

$$\mathbf{n} \cdot \mathbf{G}_i^0 = 0 \quad \text{on } S \tag{9-32}$$

and normalized according to (9-30). An orthonormal set of $\mathbf{G}_i^0$ is constructed in a manner analogous to that for the $\mathbf{F}_i^0$.

A complete set of f_i and g_i can now be chosen as

$$f_i^E = g_i^E = \begin{bmatrix} \mathbf{E}_i^0 \\ 0 \end{bmatrix} \qquad f_i^F = g_i^F = \begin{bmatrix} \mathbf{F}_i^0 \\ 0 \end{bmatrix} \tag{9-33}$$

$$f_i^H = g_i^H = \begin{bmatrix} 0 \\ \mathbf{H}_i^0 \end{bmatrix} \qquad f_i^G = g_i^G = \begin{bmatrix} 0 \\ \mathbf{G}_i^0 \end{bmatrix} \tag{9.34}$$

Note that this is an orthonormal set with respect to the empty cavity operator

$$M_0 = \begin{bmatrix} \varepsilon_0 & 0 \\ 0 & -\mu_0 \end{bmatrix} \tag{9-35}$$

as weight function; that is,

$$\begin{aligned} \langle f_i^A, M_0 f_j^B \rangle &= 0 \qquad \text{if } A \neq B \\ \langle f_i^A, M_0 f_j^B \rangle &= \delta_{ij} \qquad \text{if } A = B \end{aligned} \tag{9-36}$$

where A and B are arbitrary permutations of E, F, H, G, and δ_{ij} is the Kronecker delta. As further shorthand, define

$$\begin{aligned} m_{ij}^{AB} &= \langle f_i^A, M f_j^B \rangle \\ l_{ij}^{AB} &= \langle f_i^A, L f_j^B \rangle \end{aligned} \tag{9-37}$$

For M defined by (9-3), we find

$$\begin{aligned} m_{ij}^{EH} = m_{ij}^{FH} = m_{ij}^{EG} = m_{ij}^{FG} = 0 \\ m_{ij}^{HE} = m_{ij}^{HF} = m_{ij}^{GE} = m_{ij}^{GF} = 0 \end{aligned} \tag{9-38}$$

with all other m_{ij} not identically zero. For L defined by (9-3), we find all $l_{ij} = 0$ except the diagonal elements, and

$$[l_{ij}^{EH}] = [l_{ij}^{HE}] = \begin{bmatrix} j\omega_1^0 & 0 & 0 & \cdots \\ 0 & j\omega_2^0 & 0 & \cdots \\ 0 & 0 & j\omega_3^0 & \cdots \\ \cdot & \cdot & \cdot & \cdots \end{bmatrix} \tag{9-39}$$

This is a diagonal matrix with elements equal to j times the empty cavity resonant frequencies.

In terms of the expansion functions (9-33) and (9-34), the matrix equation (9-17) is now

$$\begin{bmatrix} 0 & 0 & l_{ij}^{EH} & 0 \\ 0 & 0 & 0 & 0 \\ l_{ij}^{HE} & 0 & 0 & 0 \\ 0 & 0 & 0 & 0 \end{bmatrix} \begin{bmatrix} \alpha_j^E \\ \alpha_j^F \\ \alpha_j^H \\ \alpha_j^G \end{bmatrix} = j\omega \begin{bmatrix} m_{ij}^{EE} & m_{ij}^{EF} & 0 & 0 \\ m_{ij}^{FE} & m_{ij}^{FF} & 0 & 0 \\ 0 & 0 & m_{ij}^{HH} & m_{ij}^{HG} \\ 0 & 0 & m_{ij}^{GH} & m_{ij}^{GG} \end{bmatrix} \begin{bmatrix} \alpha_j^E \\ \alpha_j^F \\ \alpha_j^H \\ \alpha_j^G \end{bmatrix} \tag{9-40}$$

where each element is a submatrix and the elements of $[\alpha_j^A]$ are the coefficients of f_j^A. From the second row of (9-40), we find

$$[\alpha^F] = -[m^{FF}]^{-1}[m^{FE}][\alpha^E] \tag{9-41}$$

Similarly, from the last row of (9-40), we find

$$[\alpha^G] = -[m^{GG}]^{-1}[m^{GH}][\alpha^H] \tag{9-42}$$

Hence the coefficients of the irrotational functions F_i^0 and G_i^0 are determined once those for the solenoidal functions E_i^0 and H_i^0 are known. Substitution from (9-41) and (9-42) in (9-40) gives

$$[l^{EH}][\alpha^H] = j\omega[m^E][\alpha^E] \tag{9-43}$$

$$[l^{HE}][\alpha^E] = j\omega[m^H][\alpha^H] \tag{9-44}$$

where

$$[m^E] = [m^{EE}] - [m^{EF}][m^{FF}]^{-1}[m^{FE}] \tag{9-45}$$

$$[m^H] = [m^{HH}] - [m^{HG}][m^{GG}]^{-1}[m^{GH}] \tag{9-46}$$

Finally, we can eliminate either $[\alpha^H]$ or $[\alpha^E]$ from (9-43) and (9-44) and obtain

$$\frac{1}{\omega^2}[\alpha^E] = -[l^{EH}]^{-1}[m^H][l^{EH}]^{-1}[m^E][\alpha^E] \tag{9-47}$$

$$\frac{1}{\omega^2}[\alpha^H] = -[l^{EH}]^{-1}[m^E][l^{EH}]^{-1}[m^H][\alpha^H] \tag{9-48}$$

Equations (9-47) and (9-48) are eigenvalue equations with eigenvalues $1/\omega^2$ and eigenvectors $[\alpha^E]$ and $[\alpha^H]$, respectively. Only one of (9-47) or (9-48) need be solved, because if the $[\alpha^E]$ are known the $[\alpha^H]$ may be found from (9-43) or (9-44), or vice versa. Finally, the $[\alpha^F]$ are given by (9-41) and the $[\alpha^G]$ by (9-42).

9-3. Plasma-filled Rectangular Cavity

The general solution is here specialized to the case of a rectangular cavity uniformly filled with gyrotropic plasma. This case was chosen because it approximates some experiments performed on plasmas [3]. The geometry for the problem is defined in Fig. 9-1. The cavity is uniformly filled with an ideal plasma, and

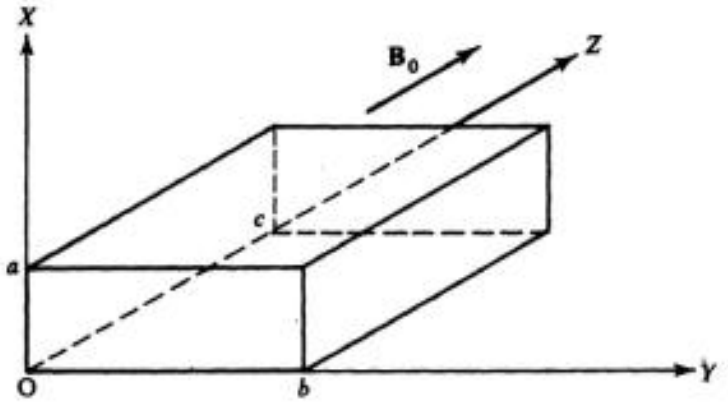

Figure 9-1. Plasma-filled rectangular cavity.

a uniform d-c magnetic field B_0 exists in the z-direction. The relative permittivity tensor, in Cartesian coordinates, is then given by [4]

$$[\varepsilon] = \begin{bmatrix} \varepsilon_1 & -j\varepsilon_2 & 0 \\ j\varepsilon_2 & \varepsilon_1 & 0 \\ 0 & 0 & \varepsilon_3 \end{bmatrix} \tag{9-49}$$

where

$$\varepsilon_1 = 1 - \frac{(\omega_p/\omega)^2[1 - (j\nu_c/\omega)]}{[1 - (j\nu_c/\omega)]^2 - (\omega_b/\omega)^2}$$

$$\varepsilon_2 = \frac{(\omega_p/\omega)^2(\omega_b/\omega)}{[1 - (j\nu_c/\omega)]^2 - (\omega_b/\omega)^2} \tag{9-50}$$

$$\varepsilon_3 = 1 - \frac{(\omega_p/\omega)^2}{[1 - (j\nu_c/\omega)]}$$

Here $\omega_p = q_e\sqrt{n_e/m_e\varepsilon_0}$ is the plasma frequency, $\omega_b = q_e(B_0/m_e)$ the cyclotron frequency, n_e the electron density, q_e the charge of the electron, m_e the mass of the electron, and ν_c the electron collision frequency for momentum transfer. The relative permeability of the medium is $\mu = 1$.

The general solution simplifies for the case $[\varepsilon]$ = tensor and $\mu = 1$. The **H** mode vectors now form an orthonormal set with respect to weight function M, and

$$m_{ij}^{HG} = m_{ij}^{GH} = 0$$
$$m_{ij}^{HH} = m_{ij}^{GG} = m_{ij}^{H} = \delta_{ij} \tag{9-51}$$

Hence the eigenvalue equation (9-47) becomes

$$\frac{1}{\omega^2}[\alpha^E] = [\Omega][m^E][\alpha^E] \tag{9-52}$$

where

$$[\Omega] = \begin{bmatrix} \left(\frac{1}{\omega_1^0}\right)^2 & 0 & 0 & \cdots \\ 0 & \left(\frac{1}{\omega_2^0}\right)^2 & 0 & \cdots \\ 0 & 0 & \left(\frac{1}{\omega_3^0}\right)^2 & \cdots \\ \cdot & \cdot & \cdot & \cdots \end{bmatrix} \tag{9-53}$$

The magnetic field coefficients are found from (9-44) as

$$\alpha_i^H = -j\frac{\omega^0}{\omega}\alpha_i^E \tag{9-54}$$

From (9-42) we see that $\alpha_i^G = 0$; that is, the magnetic field is solenoidal. The coefficients of the irrotational part of the electric field are still given by (9-41). For the dual case of a gyrotropic ferrite medium, ε is a scalar and $[\mu]$ a tensor, and an analogous simplification of the general equations can be made.

Equation (9-52) involves only the electric field matrix $[m^E]$. The normalized electric mode vectors $\mathbf{E}_i^0$ for an empty rectangular cavity and the corresponding electric irrotational mode vectors $\mathbf{F}_i^0$ are readily constructed by the method of separation of variables. The evaluation of the matrix elements m_{ij}^{EE}, m_{ij}^{EF}, m_{ij}^{FE}, and m_{ij}^{FF} is straightforward, but involves considerable detail. The results are tabulated in the Appendix of reference [5].

When the plasma is lossy ($\nu_c \neq 0$) the elements of $[\varepsilon]$, as given by (9-49) and (9-50), are complex, and so are the eigenvalues $1/\omega^2$ of (9-52). It is convenient to give the results in terms of the change in resonance $\Delta\omega$ caused by the introduction of a plasma into an empty cavity. Then the change in resonant frequency

$\Delta\omega$ and the change in quality factor Q are related to the complex ω according to [6].

$$\frac{\Delta\omega}{\omega^0} = \mathrm{Re}\left(\frac{\omega - \omega^0}{\omega^0}\right) \tag{9-55}$$

$$\Delta\left(\frac{1}{Q}\right) = \mathrm{Im}\left(2\frac{\omega - \omega^0}{\omega^0}\right) \tag{9-56}$$

where ω^0 is the empty cavity resonant frequency. If the Q is large, say $Q > 10$, it is equal to the usual quality factor defined on an energy basis, and is also the reciprocal of the fractional frequency bandwidth between half-power points on the resonance curve.

Most studies of plasmas in cavities have used a perturbation analysis [4]. The usual first-order perturbation formulas can be obtained from the general solution by taking a one-or-more-term expansion for (9-11). For the plasma case, take $f = [\mathbf{E}^0, 0]$, where $\mathbf{E}^0$ is the empty cavity mode to be perturbed, as the only term in (9-11). Equation (9-52) then reduces to

$$\frac{\alpha}{\omega^2} = \frac{\alpha}{(\omega^0)^2}\iiint \varepsilon_0 \mathbf{E}^0 \cdot [\varepsilon]\mathbf{E}^0 \, d\tau \tag{9-57}$$

Let $[\Delta\varepsilon] = [\varepsilon] - [I]$, where $[I]$ is the identity matrix. Then, since $\mathbf{E}^0$ is normalized according to (9-26), (9-57) becomes

$$\frac{1}{\omega^2} = \frac{1}{(\omega^0)^2}\left(1 + \iiint \varepsilon_0 \mathbf{E}^0 \cdot [\Delta\varepsilon]\mathbf{E}^0 \, d\tau\right) \tag{9-58}$$

which can be rearranged to

$$\frac{(\omega - \omega^0)(\omega + \omega^0)}{\omega^2} = -\iiint \varepsilon_0 \mathbf{E}^0 \cdot [\Delta\varepsilon]\mathbf{E}^0 \, d\tau \tag{9-59}$$

If we now approximate ω by ω^0 in all but the difference term, the usual perturbation formula

$$\frac{\omega - \omega^0}{\omega^0} \approx -\frac{1}{2}\iiint \varepsilon_0 \mathbf{E}^0 \cdot [\Delta\varepsilon]\mathbf{E}^0 \, d\tau \tag{9-60}$$

is obtained. If the original empty-cavity mode is degenerate, then the expansion (9-11) should contain all modes of the degeneracy. If $[\mu]$ is perturbed as well as $[\varepsilon]$, then the empty-cavity magnetic field should be included in the expansion (9-11). Note that the perturbation formulas derived in this way are also variational formulas, since the method of moments yields stationary results.

9-4. Numerical Results

For calculations the infinite-dimensional matrices were approximated by finite-dimensional matrices, and the algorithm of Appendix C was used. The modes in the plasma-filled cavity (Fig. 9-1) cannot be classified as TE or TM to z. However, as the plasma density is reduced to zero the modes reduce to those of the empty cavity, which can be classified as TE or TM to z. Hence the terminology *quasi TE* or *quasi TM* is used to denote the modes, corresponding to their empty-cavity designation. Numerical calculations have been made for the TE_{011}, TE_{101}, TM_{110}, TE_{111}, and TM_{111} quasi modes of the rectangular cavity for sides in the ratio $b/a = 2.25$ and $c/a = 3$. The results are presented in terms of the fractional frequency shift and change in reciprocal Q, as defined by (9-55) and (9-56). Similar results for first-order perturbation theory, equation (9-60), are also given in a few cases for comparison.

The following considerations were used to select the modes to include in the matrix solution:

1. In a plasma-filled waveguide, modes propagating parallel to a uniform magnetic field possess reflection symmetry only in the axial direction. This suggests that the z-coordinate dependence of the fields in the cavity of Fig. 9-1 should be the same as for the empty cavity. Since this particular example is concerned only with modes either independent of z or having one-half cycle sinusoidal variation with z, only the $(m, n, 0)$ and $(m, n, 1)$ modes were used for most calculations. To check this postulate, the $(m, n, 2)$ modes were included in a few cases, with no change in the result.

2. In the low-plasma-density case, that is, when $\omega_p^2 < |\omega^2 - \omega_b^2|$, one would expect the largest term of the field expansion to be the corresponding empty-cavity mode. It has been shown [7] by a perturbation analysis that the coefficients of the expansion decrease rapidly as the empty-cavity resonant frequencies become larger than that of the mode of interest. Hence, modes included in the matrix solution were those having empty-cavity resonant frequencies less than the mode of interest, plus a few having slightly greater resonant frequencies. However, for large plasma densities, that is, $\omega_p^2 > |\omega^2 - \omega_b^2|$, it was necessary to include many more modes of higher resonant frequencies to obtain accurate results.

3. The number of empty-cavity modes used in the matrix solution was limited to 36 by the size of computer available, which was an IBM 7074. To determine the rate of convergence of the solution the problem was first solved for 6 modes, then 17, then 33, and then 36, chosen as shown in Table 9-1.

Some representative results are given as follows. Figure 9-2 shows the percentage frequency shift and the change in reciprocal Q vs. cyclotron frequency ω_b (proportional to B_0) for the dominant quasi TE_{011} mode, plasma frequency ω_p and collision frequency ν_c kept constant. Because of the relatively small values of ω_p and ν_c, the perturbational solution, shown dashed, is a good

TABLE 9-1

Modes (m, n, p) used	Solution			
	I	II	III	IV
x-variation m	0, 1	0, 1, 2	0, 1, 2, 3	0, 1, 2
y-variation n	0, 1	0, 1, 2	0, 1, 2, 3	0, 1, 2
z-variation p	0, 1	0, 1	0, 1	0, 1, 2
No. of solenoidal modes	5	13	25	28
No. of irrotational modes	1	4	8	8
Total no. of modes used	6	17	33	36

approximation to the matrix solution. Figure 9-3 shows the same situation for the quasi TM_{111} mode. Figure 9-4 shows the percentage frequency shift vs. plasma frequency ω_p for the TE_{011} mode for several values of ω_b and ν_c. Note how the perturbation solution, curves (b), becomes poorer as ω_p increases, that is, as the plasma becomes more dense. Figure 9-5 shows the $\Delta(1/Q)$ values for the same cases. Figures 9-6 and 9-7 show $\Delta\omega/\omega_0$ and $\Delta(1/Q)$ vs. ω_b for the TE_{011} mode for several ν_c and fixed ω_p. Figures 9-8 and 9-9 show $\Delta\omega/\omega_0$ and $\Delta(1/Q)$ vs. ω_p for the TE_{011} mode for several ν_c and fixed ω_b. Additional examples may be found in the original dissertation [7].

9-5. Discussion

The solution is general in that it applies to arbitrary cavity shapes and arbitrary linear media. Use of the empty-cavity modes for the field expansion assumes that they are known, although other field expansions may be used. The matrix solution reduces to the exact solution whenever it can be expressed as a finite number of empty-cavity modes. The number of terms required in the field expansion for good accuracy increases as ε and μ deviate more from the uniform scalar case. In principle the solution can be carried to any degree of accuracy, although in practice we are limited by the size of computer available.

In the theory it is assumed that ε and μ are not functions of ω, yet in practice they often are. For example, in plasmas the elements of $[\varepsilon]$ depend on ω as shown by (9-51). Since ω is different for each mode, the matrix solution gives the modes as they would exist if ε did not vary with ω. This is equivalent to assuming that the physical constants ω_p, ω_b, and ν_c differ from each mode such that the ratios ω_p/ω, ω_b/ω, and ν_c/ω are constant. Hence the modes obtained from any one solution of (9-53) do not exist simultaneously in a given plasma. However, by solving the problem for a range of ratios ω_p/ω, ω_b/ω, and ν_c/ω, we can determine the modes for given ω_p, ω_b, and ν_c by interpolation. Alternatively, we can use a successive approximation (contraction mapping) approach to obtain the solutions for a given plasma.

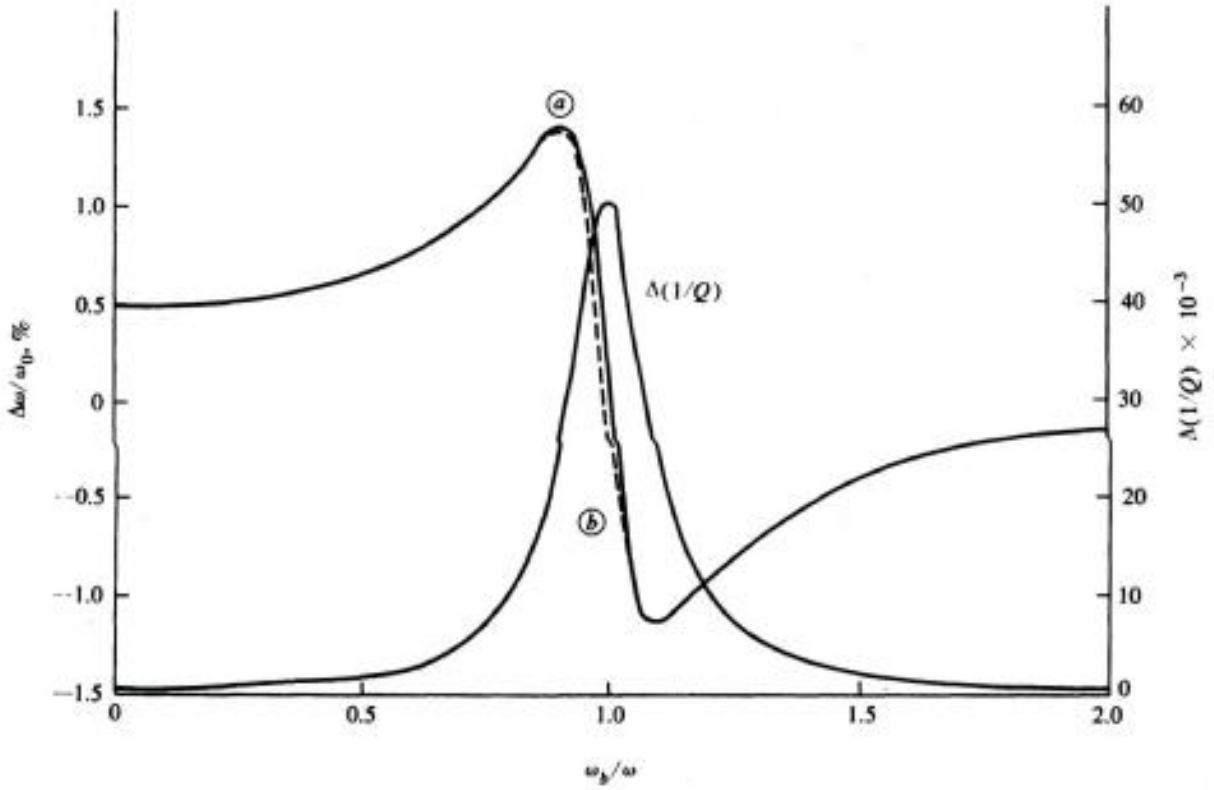

Figure 9-2. **Per cent frequency shift and change in $1/Q$ vs. cyclotron frequency for the quasi TE_{011} mode, $\omega_p/\omega = \nu_c/\omega = 0.1$. (*a*) Moment solution, (*b*) perturbation solution.**

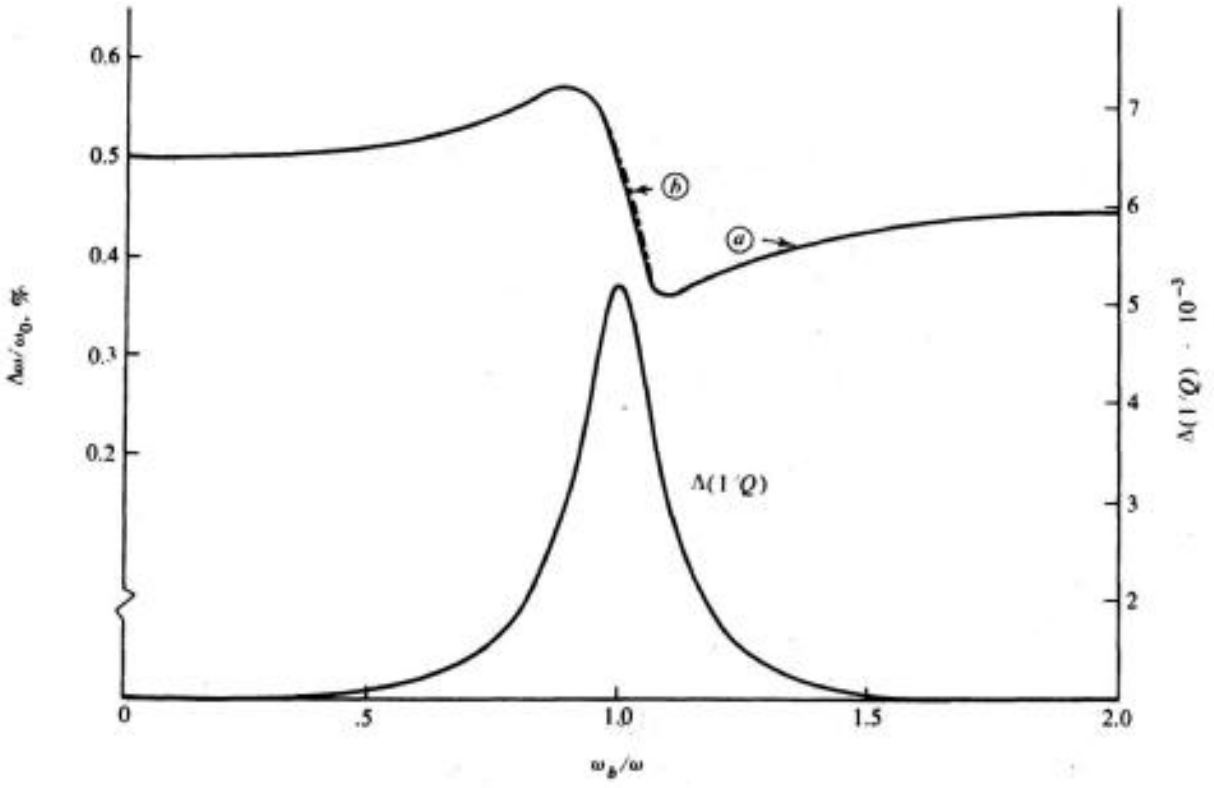

Figure 9-3. **Per cent frequency shift and change in $1/Q$ vs. cyclotron frequency for the quasi TM_{111} mode, $\omega_p/\omega = \nu_c/\omega = 0.1$. (*a*) Moment solution, (*b*) perturbation solution.**

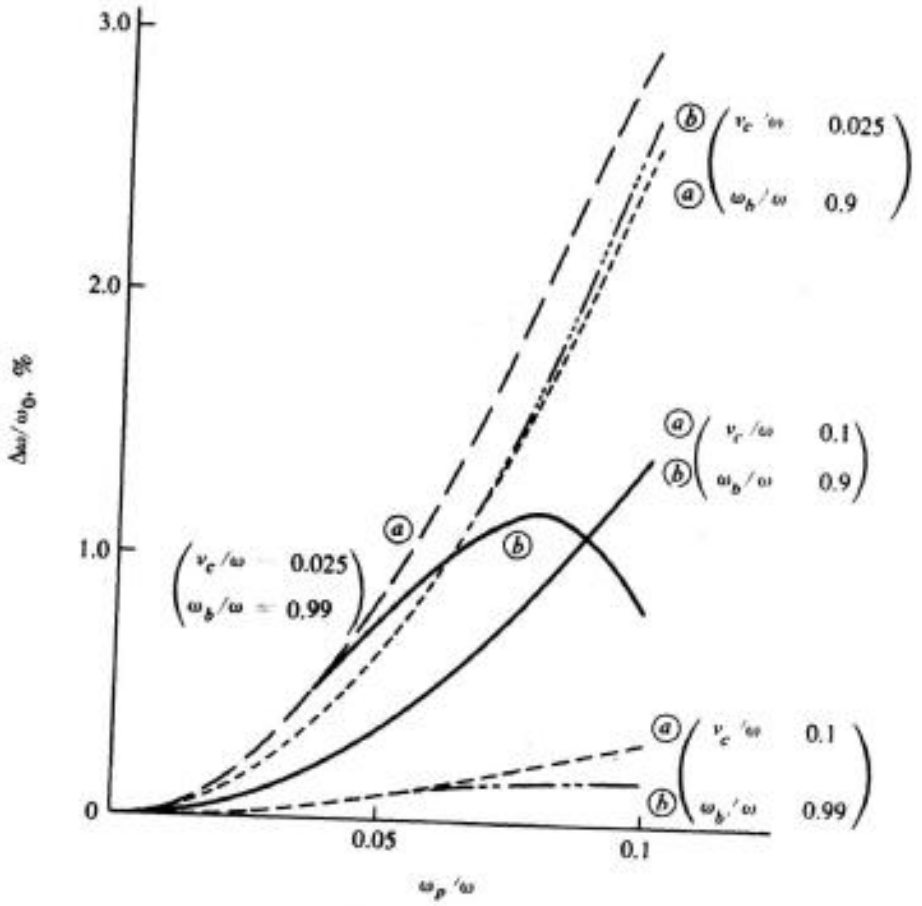

Figure 9-4. **Per cent frequency shift vs. plasma frequency for the quasi TE_{011} mode, ν_c and ω_b kept constant. (*a*) Moment solution, (*b*) perturbation solution.**

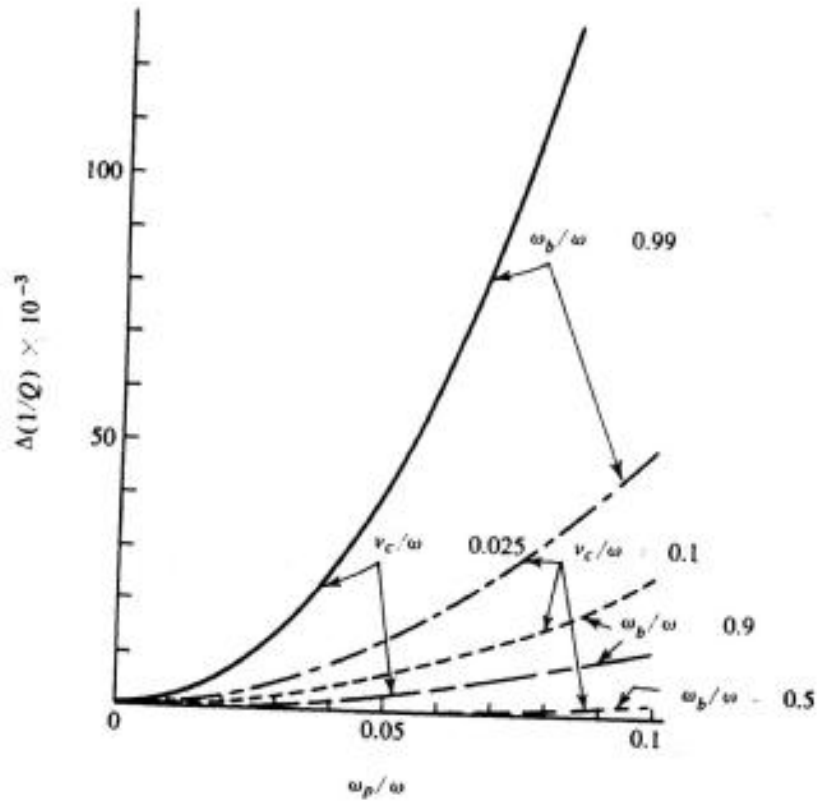

Figure 9-5. **Change in $1/Q$ vs. plasma frequency for the quasi TE_{011} mode, ν_c and ω_b kept constant.**

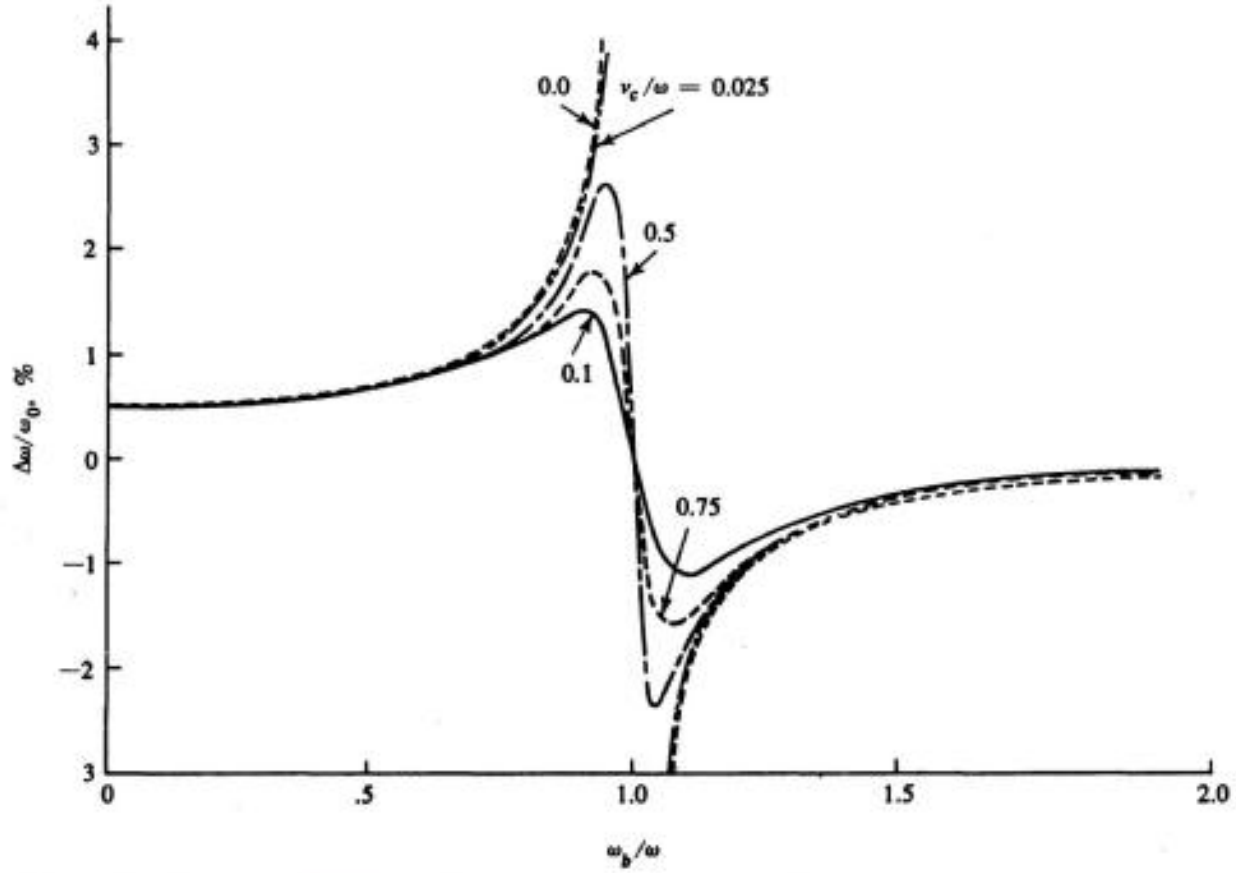

Figure 9-6. **Per cent frequency shift vs. cyclotron frequency for the quasi TE_{011} mode, $\omega_p/\omega = 0.1$, ν_c kept constant.**

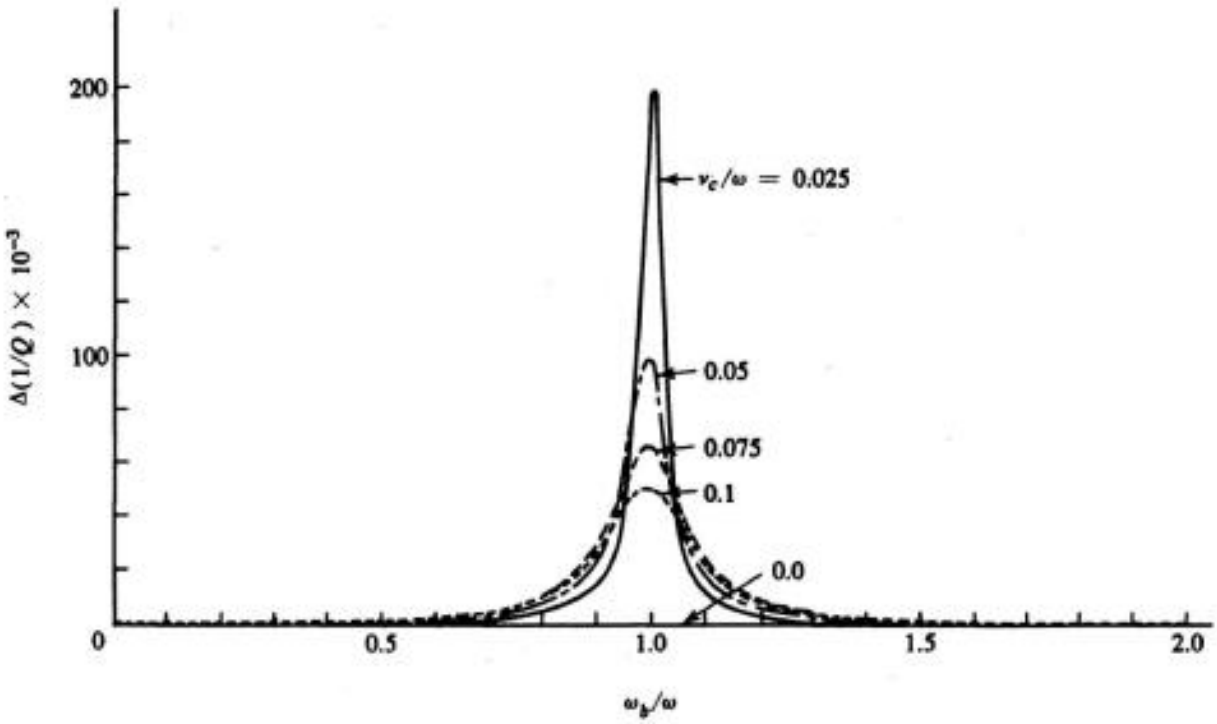

Figure 9-7. **Change in $1/Q$ vs. cyclotron frequency for the quasi TE_{011} mode, $\omega_p/\omega = 0.1$, ν_c kept constant.**

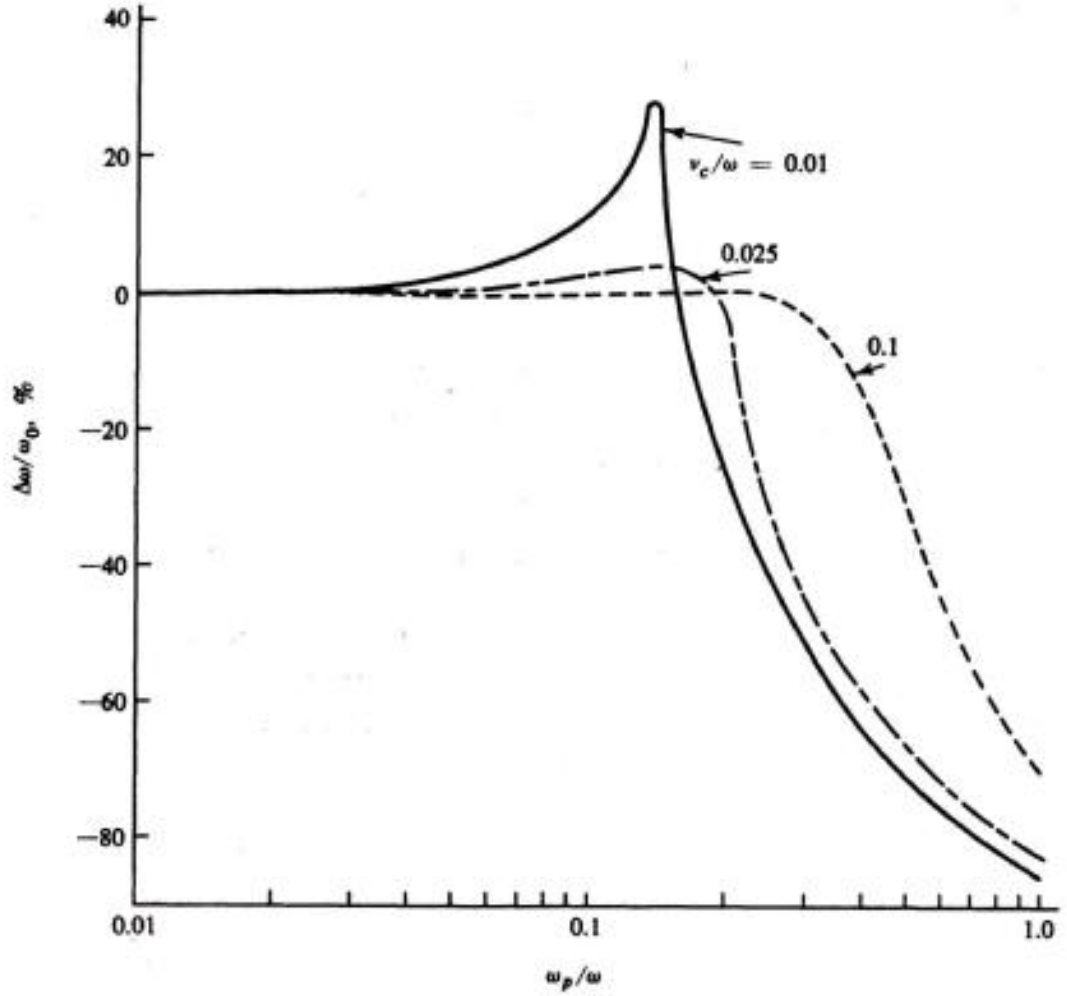

Figure 9-8. **Per cent frequency shift vs. plasma frequency for the quasi TE_{011} mode, $\omega_b/\omega = 0.99$, ν_c kept constant.**

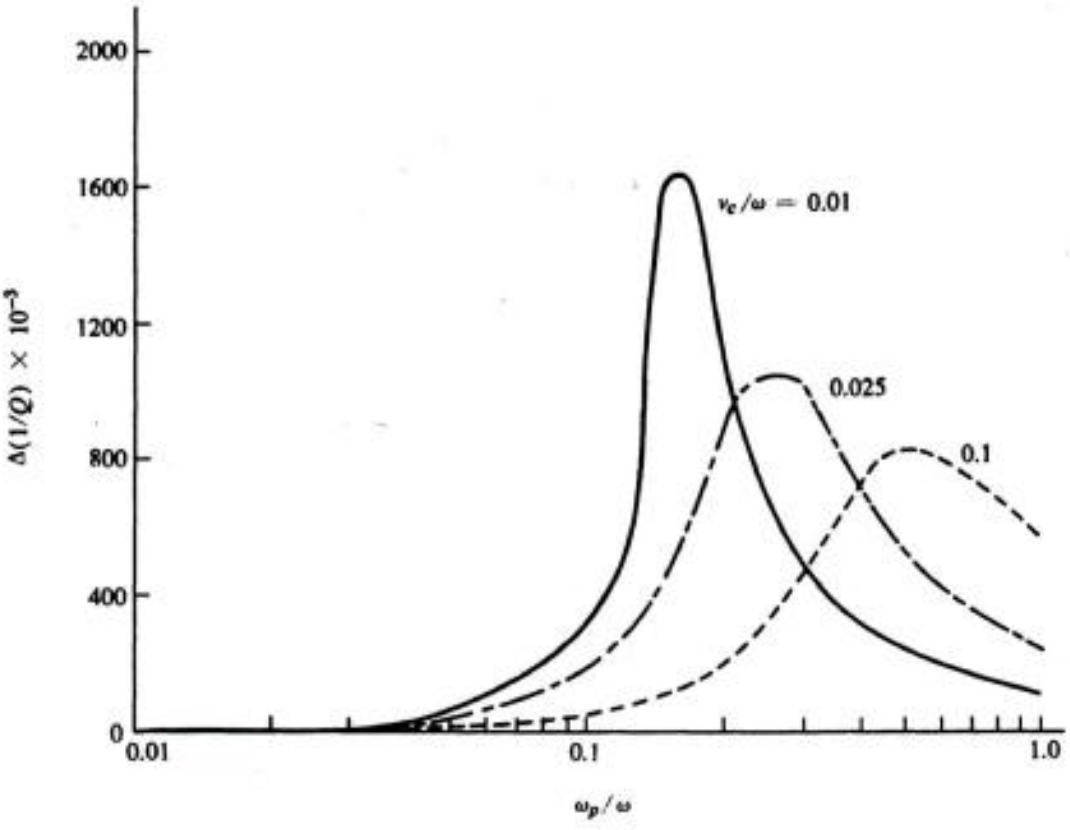

Figure 9-9. **Change in $1/Q$ vs. plasma frequency for the quasi TE_{011} mode, $\omega_b/\omega = 0.99$, ν_c kept constant.**

The following are some conclusions drawn from the calculations for gyrotropic plasmas in a rectangular cavity:

1. Many more empty cavity modes are needed to approximate the fields in dense plasmas than in tenuous plasmas.
2. The perturbation solution gives good results for tenuous plasmas, except in the vicinity of $\omega_b = \omega$.
3. The gyrotropic plasma removes the degeneracy in the TE_{111} and TM_{111} modes and probably removes all other degeneracies.
4. The TM_{mn0} modes are independent of the static magnetic field, i.e., of ω_b. In this case the matrix solution reduces to an exact solution.
5. The $\Delta\omega/\omega_0$ and $\Delta(1/Q)$ are approximately equal for all TM modes considered.
6. The $\Delta(1/Q)$ of all modes (except TM_{mn0} modes) increases as $\omega_b \to \omega$.
7. The magnitude of $\Delta\omega/\omega_0$ of all modes (except TM_{mn0} modes) reaches peaks just above and below $\omega = \omega_b$. For TE modes the shift is positive when $\omega > \omega_b$ and negative when $\omega < \omega_b$. The shift for TM modes is always positive.

References

[1] A. D. Berk, "Variational Principles for Electromagnetic Radiators and Waveguides," *IRE Trans.*, Vol. **AP-4**, No. 2, April 1956, pp. 104–110.

[2] J. C. Slater, *Microwave Electronics*, D. Van Nostrand Co., New York, 1950, Chap. 4.

[3] R. R. Gupta and R. F. Harrington, Research reports on *Interaction of Plasmas with High Intensity R-F Fields*, Contract No. AF 49(683)-1374 between Air Force Office of Scientific Research and Syracuse University.

[4] S. Buschbaum, L. Mower, and S. C. Brown, "Interaction between Cold Plasmas and Guided Electromagnetic Waves," *Phys. Fluids*, Vol. **3**, No. 5, Sept. 1960.

[5] R. R. Gupta and R. F. Harrington, "Cavity Resonators Containing Anisotropic Media," *Appl. Sci. Res.*, Vol. **16**, 1966, pp. 46–64.

[6] R. F. Harrington, *Time-Harmonic Electromagnetic Fields*, McGraw-Hill Book Co., New York, 1961, Chap. 7.

[7] R. R. Gupta, *A Study of Cavities and Waveguides Containing Anisotropic Media*, Ph.D. dissertation, Syracuse University, Syracuse, N.Y., July 1965.

CHAPTER

10

Optimization

10-1. Hermitian Forms

A matrix $[A]$ is said to be *Hermitian* if its elements satisfy $A_{mn} = A^*_{nm}$. Let $[A]$ be an N by N Hermitian matrix and $[\alpha]$ an N-element column matrix. Then

$$H = [\tilde{\alpha}^*][A][\alpha] \tag{10-1}$$

is called a *Hermitian quadratic form*. It is easy to show that $H = H^*$, and hence H is real for all α. Furthermore, it can be shown that all eigenvalues of a Hermitian matrix are real [1,2].

In the case of functions, the quadratic functional

$$H = \langle f^*, Lf \rangle \tag{10-2}$$

is also called a *Hermitian form* if H is real for all f in the domain of L. The corresponding L is called a *Hermitian operator*. Again all eigenvalues of a Hermitian operator are real. Suppose we approximate the function f by an N-term expansion

$$f \approx \sum_n \alpha_n f_n \tag{10-3}$$

and substitute in (10-2). Then

$$H \approx [\tilde{\alpha}^*_m][l_{mn}][\alpha_n] \tag{10-4}$$

where

$$l_{mn} = \langle f_m^*, Lf_n \rangle \tag{10-5}$$

If L is a Hermitian operator, it follows that $[l_{mn}]$ is a Hermitian matrix. Hence any functional Hermitian form can be approximated by a matrix Hermitian form.

Example A. The power dissipated in a linear N-port network is a Hermitian form involving the port currents or voltages. To show this, let $[Z]$ represent the impedance matrix of an N port, $[I]$ the column matrix of the port currents, and $[V]$ the column matrix of the port voltages. Then the power dissipated in the network is

$$\begin{aligned} P &= \text{Re}\,[\bar{I}^*][V] = \text{Re}\,[\bar{I}^*][Z][I] \\ &= [\bar{I}^*][\tfrac{1}{2}(Z + \bar{Z}^*)][I] \end{aligned} \tag{10-6}$$

If the network is reciprocal, then

$$[\text{Re}\,Z] = [\tfrac{1}{2}(Z + \bar{Z}^*)] \tag{10-7}$$

is a matrix with elements $\text{Re}\,Z_{mn}$. In the nonreciprocal case, (10-7) defines the matrix [Re Z]. Now (10-6) can be written

$$P = [\bar{I}^*][\text{Re}\,Z][I] \tag{10-8}$$

which is a Hermitian form. If the network is passive, P of (10-8) is never negative, and [Re Z] is a positive semidefinite matrix. It is positive definite if the network is lossy.

In terms of the port voltages, the power dissipated in an N-port network is

$$P = [\bar{V}^*][\text{Re}\,Y][V] \tag{10-9}$$

where $[Y]$ is the admittance matrix of the network and

$$[\text{Re}\,Y] = [\tfrac{1}{2}(Y + \bar{Y}^*)] \tag{10-10}$$

The derivation of (10-9) is analogous to that for (10-8). Again [Re Y] is a positive semidefinite matrix in general, and positive definite if the network is lossy.

Example B. The power radiated by sources of the scalar wave equation can be expressed as a Hermitian form. To illustrate this, let ψ be a scalar field and ρ its source. The field satisfies the Helmholtz equation

$$\nabla^2\psi + k^2\psi = \frac{4\pi}{jk}\rho \tag{10-11}$$

where $k = 2\pi/\lambda$ is the wavenumber. If the boundary condition is the radiation condition at infinity, the well-known integral of (10-11) is

$$\psi = L\rho = \iiint \rho \frac{e^{-jkR}}{-jkR}\, d\tau \tag{10-12}$$

where R is the distance from a source point to the field point. The power radiated by the sources is known to be

$$P = \text{Re} \iiint \rho^* \psi \, d\tau = \text{Re}\, \langle \rho^*, \psi \rangle \tag{10-13}$$

where the last equality defines the inner product. In terms of the operator (10-12), the power radiated can be written

$$P = \text{Re}\langle \rho^*, L\rho \rangle = \tfrac{1}{2}(\langle \rho^*, L\rho \rangle + \langle \rho, L^*\rho^* \rangle) \tag{10-14}$$

Now L and L^* are self-adjoint, so the last term can be written $\langle \rho^*, L^*\rho \rangle$. Hence

$$P = \langle \rho^*, (\text{Re}\, L)\rho \rangle \tag{10-15}$$

where (Re L) is the operator

$$(\text{Re}\, L)\rho = \tfrac{1}{2}(L + L^*)\rho = \iiint \rho \frac{\sin kR}{kR}\, d\tau \tag{10-16}$$

Equation (10-15) is a Hermitian form, and, since the power radiated must be positive, (Re L) is a positive definite operator.

10-2. Optimization Procedure

Systems can often be characterized by performance indices which are ratios of quadratic forms. Examples are gain of an antenna, signal-to-noise ratio, quality factor, efficiency, and so on. Let ρ be such a performance index,

$$\rho = \frac{[\tilde{\alpha}^*][A][\alpha]}{[\tilde{\alpha}^*][B][\alpha]} \tag{10-17}$$

where $[A]$ and $[B]$ are square Hermitian matrices and $[\alpha]$ is an unknown column matrix. We desire to find the maximum value of ρ and the matrix $[\alpha]$ which corresponds to it.

The maximization of (10-17) can be accomplished in the usual manner by treating each element α_i of $[\alpha]$ as a variable, and setting

$$\frac{\partial \rho}{\partial \alpha_i} = 0 \qquad \text{and} \qquad \frac{\partial \rho}{\partial \alpha_i^*} = 0 \tag{10-18}$$

for all i. The reason for both conditions (10-18) is that the α_i are in general complex, and ρ must be maximized with respect to two parameters for each α_i. To show that (10-18) accomplishes this, let $\alpha_i' = \mathrm{Re}(\alpha_i)$ and $\alpha_i'' = \mathrm{Im}(\alpha_i)$, so that

$$\begin{aligned} \alpha_i &= \alpha_i' + j\alpha_i'' \\ \alpha_i^* &= \alpha_i' - j\alpha_i'' \end{aligned} \tag{10-19}$$

We can show that (10-18) is equivalent to

$$\frac{\partial \rho}{\partial \alpha_i'} = 0 \qquad \text{and} \qquad \frac{\partial \rho}{\partial \alpha_i''} = 0 \tag{10-20}$$

as follows. By the chain rule of differentiation

$$\begin{aligned} \frac{\partial \rho}{\partial \alpha_i'} &= \frac{\partial \rho}{\partial \alpha_i}\frac{\partial \alpha_i}{\partial \alpha_i'} + \frac{\partial \rho}{\partial \alpha_i^*}\frac{\partial \alpha_i^*}{\partial \alpha_i'} \\ \frac{\partial \rho}{\partial \alpha_i''} &= \frac{\partial \rho}{\partial \alpha_i}\frac{\partial \alpha_i}{\partial \alpha_i''} + \frac{\partial \rho}{\partial \alpha_i^*}\frac{\partial \alpha_i^*}{\partial \alpha_i''} \end{aligned} \tag{10-21}$$

The second partial derivatives of each term are readily evaluated from (10-19), and (10-21) reduces to

$$\begin{aligned} \frac{\partial \rho}{\partial \alpha_i'} &= \frac{\partial \rho}{\partial \alpha_i} + \frac{\partial \rho}{\partial \alpha_i^*} = 0 \\ \frac{\partial \rho}{\partial \alpha_i''} &= j\left(\frac{\partial \rho}{\partial \alpha_i} - \frac{\partial \rho}{\partial \alpha_i^*}\right) = 0 \end{aligned} \tag{10-22}$$

It is now evident that (10-22) can be satisfied only if (10-18) are satisfied.

To apply (10-18), let (10-17) be written in the alternative form

$$\rho = \frac{N}{D} = \frac{\sum_{j,k} \alpha_j^* A_{jk} \alpha_k}{\sum_{j,k} \alpha_j^* B_{jk} \alpha_k} \tag{10-23}$$

Application of the conditions (10-18) results in

$$\frac{\partial \rho}{\partial \alpha_i} = \frac{1}{D^2}\left[D \sum_j \alpha_j^* A_{ji} - N \sum_j \alpha_j^* B_{ji}\right] = 0 \tag{10-24}$$

$$\frac{\partial \rho}{\partial \alpha_i^*} = \frac{1}{D^2}\left[D \sum_k A_{ik}\alpha_k - N \sum_k B_{ik}\alpha_k\right] = 0 \tag{10-25}$$

for all i. Now, assuming $D \neq 0$ (else ρ has no maximum), equation (10-25) can be written

$$[A][\alpha] = \rho[B][\alpha] \tag{10-26}$$

where we have replaced N/D by ρ. Equation (10-24) also reduces to (10-26) because both $[A]$ and $[B]$ are Hermitian. Note that (10-26) is an eigenvalue equation with eigenvalue ρ. Hence the maximum value of ρ is the largest eigenvalue of (10-26). This result is a well-known theorem in the theory of matrices [3].

Example. Let Fig. 10-1 represent N generators with internal impedances Z_1, Z_2, . . . , Z_N, connected to an N-port load network. It is desired to adjust the generator currents I_1, I_2, . . . , I_N to maximize the ratio of the power dissipated in the load to that dissipated in the generators. Letting this ratio be denoted by ρ, using (10-8) we have

$$\rho = \frac{P_{\text{load}}}{P_{\text{gen}}} = \frac{[\tilde{I}^*][\text{Re } Z_{\text{load}}][I]}{[\tilde{I}^*][\text{Re } Z_{\text{gen}}][I]} \tag{10-27}$$

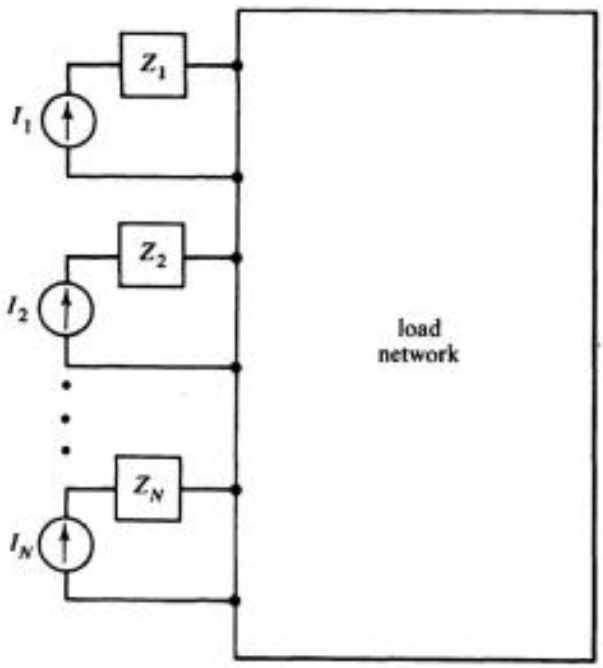

Figure 10-1. *N* **generators feeding an** *N***-port network.**

Here $[I]$ is the matrix of terminal currents, Z_{load} is the impedance matrix of the load network, and Z_{gen} is that of the source. For the special case shown in Fig. 10-1, $[Z_{gen}]$ is the diagonal matrix

$$[Z_{gen}] = \begin{bmatrix} Z_1 & 0 & \cdots & \cdot & \cdot \\ 0 & Z_2 & \cdots & \cdot & \cdot \\ \cdot & \cdot & \cdots & \cdot & \cdot \\ \cdot & \cdot & \cdots & 0 & Z_N \end{bmatrix}$$

although the theory applies to arbitrary $[Z_{gen}]$. According to the theory of this section, the maximum of ρ is given by the largest eigenvalue of the equation

$$[\text{Re } Z_{load}][I] = \rho[\text{Re } Z_{gen}][I] \tag{10-28}$$

and the excitation $[I]$ for maximum ρ is given by the corresponding eigenvector. This eigenvalue and eigenvector can be determined by the general algorithm of Appendix C, or by special techniques for finding the maximum eigenvalue of a matrix [3].

10-3. Antenna Gain

Consider an arbitrary antenna array with N input ports plus a distant "test" antenna, as represented by Fig. 10-2. We assume only one input port to the test antenna, in which case it receives or transmits only one polarization. The array plus the test antenna form an $N + 1$ port network whose terminal characteristics can be described by an $N + 1$ by $N + 1$ matrix. Choosing the open-circuit impedance matrix, we have

$$\begin{bmatrix} V_t \\ [V_a] \end{bmatrix} = \begin{bmatrix} Z_{tt} & [Z_{ta}] \\ [Z_{at}] & [Z_{aa}] \end{bmatrix} \begin{bmatrix} I_t \\ [I_a] \end{bmatrix} \tag{10-29}$$

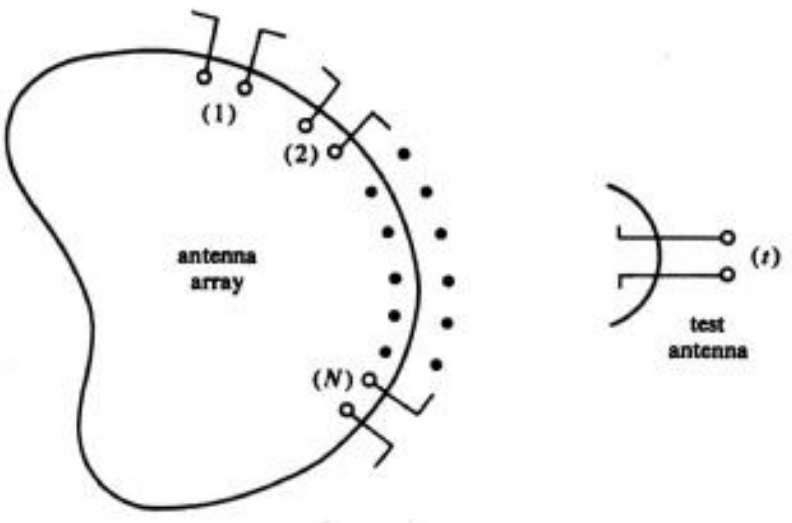

Figure 10-2. Antenna array and distant test antenna.

where V_t and I_t are the terminal voltage and current at the test antenna, $[V_a]$ and $[I_a]$ are the voltage and current matrices at the array terminals

$$[V_a] = \begin{bmatrix} V_1 \\ V_2 \\ \vdots \\ V_N \end{bmatrix} \qquad [I_a] = \begin{bmatrix} I_1 \\ I_2 \\ \vdots \\ I_N \end{bmatrix} \tag{10-30}$$

Z_{tt} is the input impedance to the test antenna, $[Z_{aa}]$ is the impedance matrix of the antenna array

$$[Z_{aa}] = \begin{bmatrix} Z_{11} & Z_{12} & \cdots & Z_{1N} \\ Z_{21} & Z_{22} & \cdots & Z_{2N} \\ \cdot & \cdot & \cdots & \cdot \\ \cdot & \cdot & \cdots & \cdot \\ Z_{N1} & Z_{N2} & \cdots & Z_{NN} \end{bmatrix} \tag{10-31}$$

and $[Z_{ta}]$ and $[Z_{at}]$ are matrices of mutual impedances between the test antenna and the array ports,

$$\begin{aligned} [Z_{ta}] &= [Z_{t1} \quad Z_{t2} \quad \cdots \quad Z_{tN}] \\ [\tilde{Z}_{at}] &= [Z_{1t} \quad Z_{2t} \quad \cdots \quad Z_{Nt}] \end{aligned} \tag{10-32}$$

If the antennas and surrounding media are reciprocal, $[Z_{aa}] = [\tilde{Z}_{aa}]$ and $[Z_{ta}] = [\tilde{Z}_{at}]$.

Alternatively, we can choose the short-circuit admittance matrix to describe the $N + 1$ port antenna system of Fig. 10-2. In this case, instead of (10-29) we have

$$\begin{bmatrix} I_t \\ [I_a] \end{bmatrix} = \begin{bmatrix} Y_{tt} & [Y_{ta}] \\ [Y_{at}] & [Y_{aa}] \end{bmatrix} \begin{bmatrix} V_t \\ [V_a] \end{bmatrix} \tag{10-33}$$

All the parameters of (10-33) have interpretations dual to those in the impedance case, described previously.

Now let the array be excited by a set of current sources $I_1, I_2, \ldots, I_N$, and the test antenna open-circuited, as represented by Fig. 10-3. The power input is given by

$$P_{in} = \tfrac{1}{2}[\tilde{I}_a^*][Z_{aa} + \tilde{Z}_{aa}^*][I_a] \tag{10-34}$$

as shown in Section 10-1. The test antenna is assumed to be distant from the array and hence in the plane-wave far field of the array. Under polarization-matched conditions, the square of the magnitude of the test antenna terminal

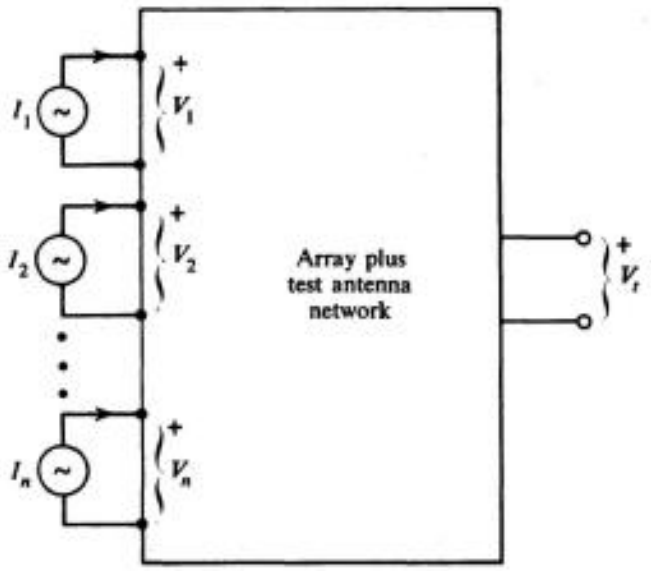

***Figure 10-3.* Excitation for array transmitting.**

voltage is proportional to the radiation intensity of the incident field. From (10-29), with $I_t = 0$, we have

$$|V_t|^2 = |[Z_{ta}][I_a]|^2 = [\tilde{I}_a^*][\tilde{Z}_{ta}^*][Z_{ta}][I_a] \tag{10-35}$$

Hence the radiation intensity in the direction of the test antenna is

$$\begin{aligned} \text{Radiation intensity} &= \frac{1}{8\pi} K_1 |V_t|^2 \\ &= \frac{1}{8\pi} K_1 [\tilde{I}_a^*][\tilde{Z}_{ta}^*][Z_{ta}][I_a] \end{aligned} \tag{10-36}$$

where K_1 is a constant related to the receiving aperture of the test antenna.

The power gain of an antenna is defined by

$$G = \frac{4\pi \times \text{radiation intensity}}{\text{power input to the antenna}} \tag{10-37}$$

which is the ratio of the radiation intensity of the given antenna to that of an omnidirectional antenna, both having the same power input. Substituting from (10-34) and (10-36) in (10-37), we have

$$G = K_1 \frac{[\tilde{I}_a^*][\tilde{Z}_{ta}^*][Z_{ta}][I_a]}{[\tilde{I}_a^*][Z_{aa} + \tilde{Z}_{aa}^*][I_a]} \tag{10-38}$$

This is the ratio of Hermitian forms, as discussed in Section 10-2. The dual problem is to excite the array by a set of voltage sources $V_1, V_2, \ldots, V_N$, and

short-circuit the test antenna. Then formulas dual to (10-34) and (10-36) apply, and the power gain is given by

$$G = K_2 \frac{[\tilde{V}_a^*][\tilde{Y}_{ta}^*][Y_{ta}][V_a]}{[\tilde{V}_a^*][Y_{aa} + \tilde{Y}_{aa}^*][V_a]} \tag{10-39}$$

The choice between (10-38) and (10-39) is one of convenience. We are used to specifying dipole antenna inputs in terms of currents, but voltages are often more convenient for aperture antennas.

The procedure for optimizing (10-38) is that of Section 10-2. The result is the eigenvalue equation [4]

$$[\tilde{Z}_{ta}^*][Z_{ta}][I_a] = \frac{G}{K_1}[Z_{aa} + \tilde{Z}_{aa}^*][I_a] \tag{10-40}$$

where G/K_1 is the eigenvalue. From the properties of impedance matrices it follows that $[Z_{aa} + \tilde{Z}_{aa}^*]$ is positive definite, and $[\tilde{Z}_{ta}^*][Z_{ta}]$ is positive semidefinite. Hence all eigenvalues are zero or positive. Furthermore, since $[\tilde{Z}_{ta}^*][Z_{ta}]$ is a one-term dyad, all eigenvalues are zero except one. The problem therefore reduces to one of finding the only nonzero eigenvalue of (10-40) and the corresponding eigenvector $[I_a]$. This result is a generalization of that obtained by Cheng and Tseng [5].

The eigenvalues and eigenvectors can be found by standard techniques but, for our problem, the following special technique applies. Let $[\hat{I}_N]$ denote the eigenfunction associated with the only nonzero eigenvalue of (10-40), and let $[\hat{I}_1], [\hat{I}_2], \ldots, [\hat{I}_{N-1}]$ denote any set of linearly independent vectors associated with the eigenvalue $G/K_1 = 0$. Define the weighted scalar product

$$\langle I_i, I_j \rangle = [\tilde{I}_i^*][Z_{aa} + \tilde{Z}_{aa}^*][I_j] \tag{10-41}$$

From the theory of eigenvalue equations, eigenvectors associated with different eigenvalues are orthogonal to each other, and hence

$$\langle \hat{I}_N, \hat{I}_i \rangle = [\tilde{\hat{I}}_N^*][Z_{aa} + \tilde{Z}_{aa}^*][\hat{I}_i] = 0 \tag{10-42}$$

for all $i = 1, 2, \ldots, N-1$. Now, it is particularly easy to find $N-1$ independent solutions to (10-40) with $G/K_1 = 0$ because of the special form of $[\tilde{Z}_{ta}^*][Z_{ta}]$. For example, the set

$$[\hat{I}_1] = \begin{bmatrix} 1/Z_{t1} \\ -1/Z_{t2} \\ 0 \\ \vdots \\ 0 \end{bmatrix} \quad [\hat{I}_2] = \begin{bmatrix} 1/Z_{t1} \\ 0 \\ -1/Z_{t3} \\ \vdots \\ 0 \end{bmatrix} \quad \cdots \quad [\hat{I}_{N-1}] = \begin{bmatrix} 1/Z_{t1} \\ 0 \\ 0 \\ \vdots \\ -1/Z_{tN} \end{bmatrix} \tag{10-43}$$

where Z_{ti} is the ith element of $[Z_{ta}]$, satisfies $[Z_{ta}][I_a] = 0$, and hence are solutions to (10-40) with the right side zero. Now, since $[\hat{I}_N]$ must be orthogonal to all $[\hat{I}_j]$ according to (10-42), we can construct the $[\hat{I}_N]$ by the Schmidt orthogonalization process [1,2]. A physical interpretation of this result is as follows. The $[\hat{I}_i]$ of (10-43) are the array excitations which produce no field at the test antenna. The excitation $[\hat{I}_N]$, which produces maximum gain, is orthogonal to all those which produce zero gain.

Alternatively, we can substitute for G/K_1 from (10-38) in (10-40), cancel the common term $[Z_{ta}][I_a]$, and obtain

$$[Z_{ta}^*] = \frac{[I_a^*][\tilde{Z}_{ta}^*]}{[I_a^*][Z_{aa} + \tilde{Z}_{aa}^*][I_a]} [Z_{aa} + \tilde{Z}_{aa}^*][I_a] \tag{10-44}$$

The quotient term on the right side is just a complex number, which we shall denote by $1/C$. The required current distribution is obtained by inversion of (10-44), which is

$$[I_a] = C[Z_{aa} + \tilde{Z}_{aa}^*]^{-1}[\tilde{Z}_{ta}^*] \tag{10-45}$$

We can now substitute this result in (10-38) for the maximum gain, which reduces to

$$G_{max} = K_1[Z_{ta}][Z_{aa} + \tilde{Z}_{aa}^*]^{-1}[\tilde{Z}_{ta}^*] \tag{10-46}$$

The formulas of Bloch et al. [6] and of Tai [7] are specializations of (10-45) to impressed sources in empty space.

The results for voltage excitation of an array are dual to those given above. Hence, optimization of (10-39) gives

$$[\tilde{Y}_{ta}^*][Y_{ta}][V_a] = \frac{G}{K_2} [Y_{aa} + \tilde{Y}_{aa}^*][V_a] \tag{10-47}$$

as the eigenvalue equation from which the excitation $[V_a]$ for maximum gain can be found. The maximum gain must, of course, be the same for both current excitation and voltage excitation, but the eigenvectors $[\hat{I}_N]$ and $[\hat{V}_N]$ will be different. An explicit expression for the voltage excitation for maximum gain is

$$[V_a] = C[Y_{aa} + \tilde{Y}_{aa}^*]^{-1}[\tilde{Y}_{ta}^*] \tag{10-48}$$

which is dual to (10-45). Finally, we can substitute this result in the gain formula (10-39) and obtain

$$G_{max} = K_2[Y_{ta}][Y_{aa} + \tilde{Y}_{aa}^*]^{-1}[\tilde{Y}_{ta}^*] \tag{10-49}$$

for the maximum gain in terms of short-circuit parameters.

Example. Consider an array of N point sources of a scalar field ψ, which satisfies the Helmholtz equation (10-11). Let $I_1, I_2, \ldots, I_n$ denote the complex excitation of the sources and $\mathbf{r}_1, \mathbf{r}_2, \ldots, \mathbf{r}_N$ the position vectors of the sources. Figure 10-4 illustrates the geometry of the array. The field from the array is given by the superposition integral (10-12), where ρ consists of a sum of impulsive sources. The result is the summation

$$\psi = \sum_{n=1}^{N} I_n \frac{e^{-jk|\mathbf{r}_0 - \mathbf{r}_n|}}{-jk|\mathbf{r}_0 - \mathbf{r}_n|} \tag{10-50}$$

where $\mathbf{r}_0$ is the position vector to the field point. When r_0 is much greater than all r_n, (10-50) reduces to the far-field expression

$$\psi = \frac{e^{-jkr_0}}{-jkr_0} \sum_{n=1}^{N} I_n e^{jkr_n \cos \xi_n} \tag{10-51}$$

where ξ_n is the angle between $\mathbf{r}_0$ and $\mathbf{r}_n$, as shown in Fig. 10-4.

The power supplied by the sources is given by (10-15), which, for the case of point sources, becomes

$$P = \sum_{m=1}^{N} \sum_{m=1}^{N} I_m I_n \frac{\sin k|\mathbf{r}_m - \mathbf{r}_n|}{k|\mathbf{r}_m - \mathbf{r}_n|} \tag{10-52}$$

The radiation intensity is defined as the distant power density per unit solid angle. For the present problem, this is

$$\text{Rad. int.} = \frac{1}{4\pi} |kr_0 \psi|^2 \tag{10-53}$$

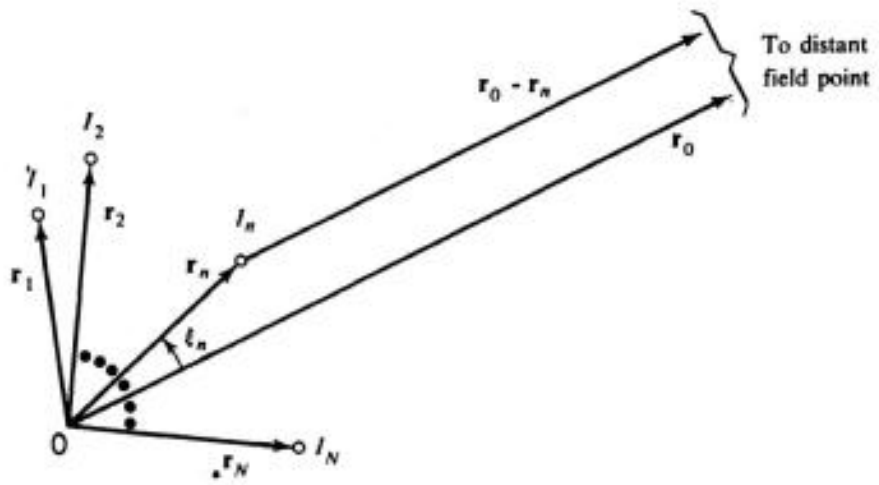

Figure 10-4. Array of N point sources.

which, using (10-51), becomes

$$\text{Rad. int.} = \frac{1}{4\pi}\left|\sum_{n=1}^{N} I_n e^{jkr_n \cos \xi_n}\right|^2$$

$$= \frac{1}{4\pi}\sum_{m=1}^{N}\sum_{m=1}^{N} I_m^* I_n e^{jk(r_n \cos \xi_n - r_m \cos \xi_m)} \tag{10-54}$$

Now, substituting from (10-52) and (10-54) in the gain formula (10-37), we have

$$G = \frac{[\tilde{I}^*][A][I]}{[\tilde{I}^*][B][I]} \tag{10-55}$$

Here $[I]$ is the column matrix of the I_n, $[A]$ is a square matrix with elements

$$A_{mn} = e^{jk(r_n \cos \xi_n - r_m \cos \xi_m)} \tag{10-56}$$

and $[B]$ is a square matrix with elements

$$B_{mn} = \frac{\sin k|\mathbf{r}_m - \mathbf{r}_n|}{k|\mathbf{r}_m - \mathbf{r}_n|} \tag{10-57}$$

In terms of the general theory, the elements (10-56) are those of $[\tilde{Z}_{ta}^*][Z_{ta}]$ in (10-38), and the elements (10-57) are the real parts of the impedance matrix (10-31).

As discussed in the text, the maximum gain is the largest eigenvalue G of the equation

$$[A][I] = G[B][I] \tag{10-58}$$

Because of the special form of $[A]$, this eigenvalue is also the only nonzero one. The corresponding eigenvector is given by (10-45), which for (10-58) becomes

$$[I_m] = [B_{mn}^{-1}][e^{-jkz_n \cos \xi_n}] \tag{10-59}$$

The right-hand matrix corresponds to $[Z_{ta}]$ in the general theory. Finally, we can substitute (10-59) in (10-55), and obtain an explicit expression for maximum gain,

$$G_{\max} = [e^{jkz_m \cos \xi_m}][B_{mn}^{-1}][e^{-jkz_n \cos \xi_n}] \tag{10-60}$$

Here the first matrix is a row matrix, and the last one is a column matrix. Equation (10-60) corresponds to (10-46) in the general case.

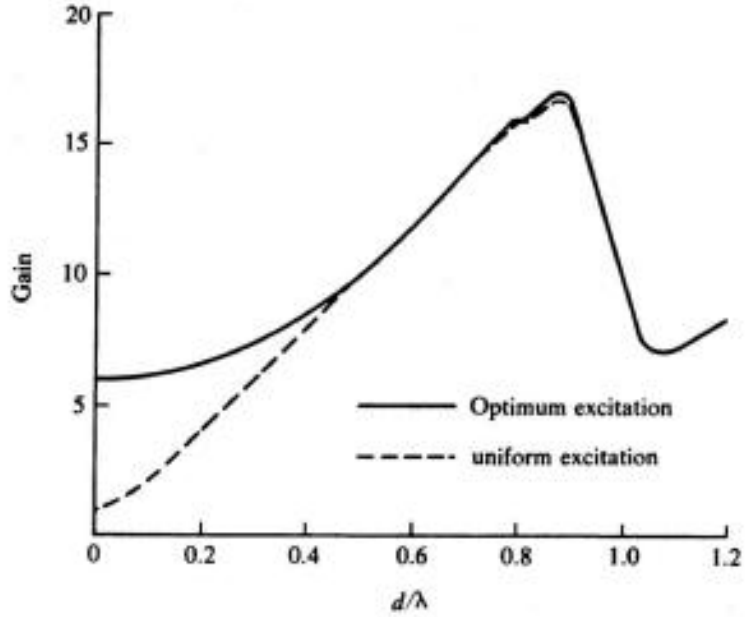

Figure 10-5. **Maximum broadside gain for a 10-element linear array, compared to uniform excitation (after Tai [7]).**

Computations have been made for linear arrays with broadside maxima [7], with endfire maxima [5,8], and for circular arrays [8]. For the linear array with uniform element separation d, Fig. 10-5 shows the variation in maximum broadside gain as d/λ changes. The gain for the same array with uniform excitation and phase is shown dashed. Figure 10-6 shows the variation in maximum endfire gain for the same array, with the case of uniform amplitude and progressive

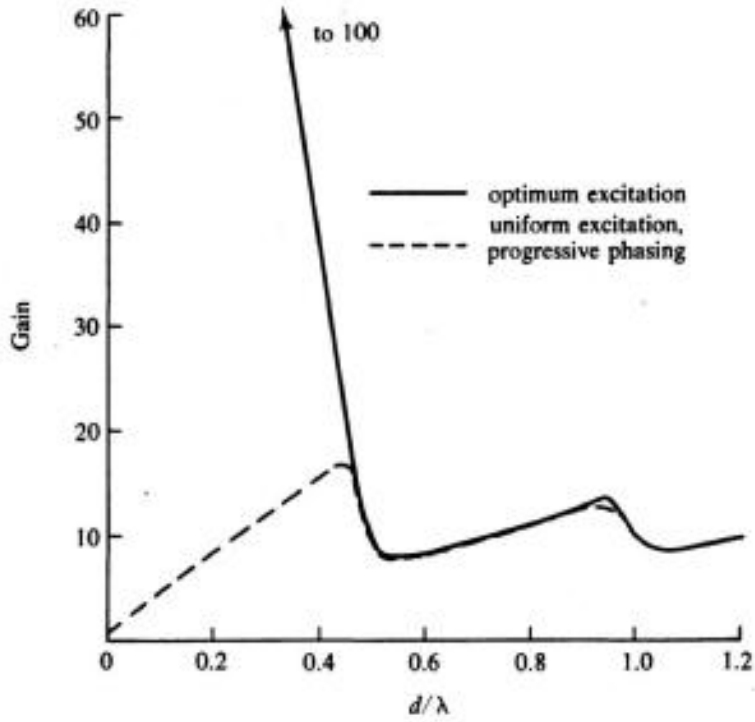

Figure 10-6. **Maximum endfire gain for a 10-element linear array, compared to uniform excitation with progressive phasing (after Lo et al. [8]).**

phasing shown dashed. It can be shown that, as $d/\lambda \to 0$, the maximum gain for an N element uniformly spaced linear array in the broadside case is [7]

$$G_{max} \approx \begin{cases} \dfrac{2N}{\pi} & N \text{ even} \\ \dfrac{2N+1}{\pi} & N \text{ odd} \end{cases} \tag{10-61}$$

while for the endfire case it is [8]

$$G_{max} = N^2 \tag{10-62}$$

However, as d becomes smaller than $\lambda/2$ we encounter a situation known as *supergain*. In Figs. 10-5 and 10-6 the supergain region is that for $d < \lambda/2$, where the dashed curves differ markedly from the maximum gain curves. The supergain condition will be discussed in Sections 10-5 and 10-6. For now, let it suffice to say that it is extremely difficult to make use of supergain antennas in practice.

10-4. Absorption Area

Now consider the array of Fig. 10-2 to be receiving, and the distant test antenna to be transmitting. The optimization problem in this case is that of loading the array to extract maximum power from an incident plane wave. The parameter of interest is the absorption area

$$A = \frac{\text{power delivered to matched load}}{\text{power density of incident wave}} \tag{10-63}$$

If the antenna or surrounding space contain nonreciprocal media, such as ferrites or plasmas in a d-c magnetic field, the G and A are independent quantities. When all media are reciprocal and linear, and the same distribution network is used for transmitting and receiving, we have the reciprocity relationship

$$G = \frac{4\pi}{\lambda^2} A \tag{10-64}$$

This relationship applies to lossy antennas as well as to loss-free antennas.

For the analysis, consider the test antenna to be excited by a current source I_t, and the array to be loaded by a network, as represented by Fig. 10-7. Using $[V_a]$ as given by (10-29), we find the complex power to the load as

$$\begin{aligned} P &= -[\bar{I}_a^*][V_a] \\ &= -[\bar{I}_a^*][Z_{at}]I_t - [\bar{I}_a^*][Z_{aa}][I_a] \end{aligned} \tag{10-65}$$

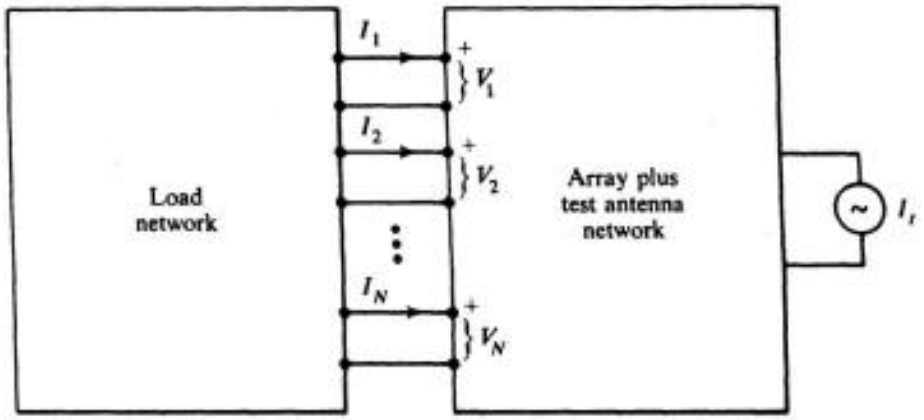

Figure 10-7. **Array receiving and distant test antenna excited.**

The minus signs arise because the current reference directions are toward the array. The power delivered to the load is the real part of (10-65), which reduces to

$$P_{\text{load}} = -\frac{I_t}{2}\{[\bar{I}_a^*][Z_{at}] + [\bar{Z}_{at}^*][I_a] + [\bar{I}_a^*][Z_{aa} + \bar{Z}_{aa}^*][I_a]\} \tag{10-66}$$

The power density of the wave incident on the array is proportional to $|I_t|^2$. Hence

$$\text{Incident power density} = \frac{-1}{2K_3}|I_t|^2 \tag{10-67}$$

where K_3 is a constant of the test antenna. It is convenient to define a relative current matrix

$$[I_a] = \frac{1}{I_t}[I_a] \tag{10-68}$$

Now, using (10-66) to (10-68) in (10-63), we have

$$A = K_3\{[\bar{i}_a^*][Z_{at}] + [\bar{Z}_{at}^*][i_a] + [\bar{i}_a^*][Z_{aa} + \bar{Z}_{aa}^*][i_a]\} \tag{10-69}$$

This expresses the absorption area of the antenna array as a function of its terminal currents.

The dual problem is to express A as a function of its terminal voltages. For this, we excite the test antenna by a voltage source V_t, and formulas dual to (10-65) to (10-69) apply. Hence, in terms of the relative voltages

$$[v_a] = \frac{1}{V_t}[V_a] \tag{10-70}$$

the absorption area of the loaded antenna is

$$A = K_4\{[\tilde{v}_a^*][Y_{at}] + [\tilde{Y}_{at}^*][v_a] + [\tilde{v}_a^*][Y_{aa} + \tilde{Y}_{aa}^*][v_a]\} \tag{10-71}$$

where K_4 is a constant of the test antenna.

To optimize the absorption area, we take (10-69) and set

$$\frac{\partial A}{\partial i_j} = \frac{\partial A}{\partial i_j^*} = 0 \tag{10-72}$$

for all $j = 1, 2, \ldots, N$. The resultant equation is

$$[I_a] = -\ [Z_{aa} + \tilde{Z}_{aa}^*]^{-1}[Z_{at}]I_t \tag{10-73}$$

where we have substituted for $[i_a]$ from (10-68). Equation (10-73) is equivalent to applying the N-port maximum power transfer theorem to the active network containing the array, the test antenna, and the source I_t. This latter approach was used by Bloch [9], whose results can be summarized as follows: Maximum absorption area is obtained by a conjugate load, that is, when $[Z_L] = [Z_{aa}^*]$, and for any other load having the same terminal voltage and current.

In terms of terminal voltages, the maximum absorption area can be obtained from (10-71) by applying operations dual to (10-72). The result is

$$[V_a] = -\tfrac{1}{4}[Y_{aa} + \tilde{Y}_{aa}^*]^{-1}[Y_{at}]V_t \tag{10-74}$$

Again, this is consistent with the N-port maximum power-transfer theorem of network theory.

As long as all media are reciprocal, the numerical results for maximum A are identical to those for maximum G. Hence the examples for maximum gain of Section 10-3 serve also as examples for maximum absorption area.

10-5. Bandwidth and Q

As mentioned in the example of Section 10-3, optimization of the gain of an array of closely spaced elements results in what is known as a supergain antenna. A bibliography of the literature of supergain antennas is given by Bloch et al. [10]. It is known from theoretical studies that supergain antennas tend to be very frequency-sensitive (high Q), have high power losses on the antenna structure, and require extreme precision of excitation [11]. In large antennas, these undesirable characteristics rapidly become dominant, and large supergain antennas are usually considered impractical. However, significant improvement in the directive characteristics of small antennas is possible, and small supergain antennas have been constructed [6].

Since supergain antennas are frequency-sensitive, it is desirable to have a measure of their frequency sensitivity before their construction. From energy

considerations for an N-port network, the difference between the stored magnetic energy W_m and the stored electric energy W_e is given by [12]

$$W_m - W_e = \frac{1}{2\omega} \operatorname{Im}(P) \tag{10-75}$$

where P is the complex power, given by (10-34), and ω is the radian frequency. Defining the matrix

$$[X] = \tfrac{1}{2}[Z_{aa} - \tilde{Z}_{aa}^*] \tag{10-76}$$

which for reciprocal networks is the imaginary part of $[Z_{aa}]$, we can express (10-75) as

$$W_m - W_e = \tfrac{1}{2}[\tilde{I}_a^*][X][I_a] \tag{10-77}$$

For a loss-free network, we have the generalized form of Foster's reactance theorem [12]

$$W_m + W_e = \frac{1}{2}[\tilde{I}_a^*]\left[\frac{dX}{d\omega}\right][I_a] \tag{10-78}$$

Now, the stored electric and magnetic energies can be obtained from (10-77) and (10-78) as

$$\begin{aligned} W_m &= \frac{1}{4}[\tilde{I}_a^*]\left[\frac{dX}{d\omega} + \frac{X}{\omega}\right][I_a] \\ W_e &= \frac{1}{4}[\tilde{I}_a^*]\left[\frac{dX}{d\omega} - \frac{X}{\omega}\right][I_a] \end{aligned} \tag{10-79}$$

Although this result is exact only for loss-free networks, it is approximately valid for high-Q networks in the vicinity of resonance.

We now define the Q of an array excited by $[I_a]$ to be

$$Q = \frac{2\omega W}{P_{\text{in}}} \tag{10-80}$$

where $W = W_e$ or W_m, whichever is larger, and P_{in} is the input power to the array, given by (10-34). Substituting from (10-34) and (10-79), we have

$$Q = \frac{[\tilde{I}_a^*][\omega(dX/d\omega) \pm X][I_a]}{[\tilde{I}_a^*][Z_{aa} + \tilde{Z}_{aa}^*][I_a]} \tag{10-81}$$

where the + or − sign is chosen to give the higher Q. The term obtained from $[\omega\, dX/d\omega]$ is usually larger than that obtained from $[X]$, and it becomes dominant for supergain excitations.

If the Q is large, it is related to the frequency bandwidth of the array as follows. Consider the array to be resonated by a suitable reactance network at the frequency of interest ω_r. Define the frequency bandwidth of the array in the usual manner to be the fractional frequency increment between 0.707 points of the normalized input $|Z|$,

$$\beta = \frac{\Delta\omega}{\omega_r} \tag{10-82}$$

If the Q is high (say $Q > 10$), we have the relationship

$$Q \approx \frac{1}{\beta} \tag{10-83}$$

If the Q is small, the array is potentially broadband.

For some applications, it might be desirable to maximize the gain bandwidth product. From (10-38), (10-81), and (10-83), we have

$$G\beta = K_1 \frac{[\tilde{I}_a^*][\tilde{Z}_{ta}^*][Z_{ta}][I_a]}{[\tilde{I}_a^*][\omega(dX/d\omega) \pm X][I_a]} \tag{10-84}$$

which is again the ratio of Hermitian quadratic forms. Since energy cannot be negative, the matrix $[\omega\, dX/d\omega \pm X]$ is positive definite, and the maximization proceeds as in Section 10-2. From the theoretical studies [11], it is to be expected that frequency-sensitivity effects become dominant so rapidly that little improvement of the gain-bandwidth product over that obtainable from normal arrays can be expected.

For the dual case of voltage excitation, formulas dual to (10-75) to (10-84) apply. In particular, if we define

$$[B] = \tfrac{1}{2}[Y_{aa} - \tilde{Y}_{aa}^*] \tag{10-85}$$

then the Q of an array excited by terminal voltages $[V_a]$ is given by

$$Q = \frac{[\tilde{V}_a^*][\omega(dB/d\omega) \pm B][V_a]}{[\tilde{V}_a^*][Y_{aa} + \tilde{Y}_{aa}^*][V_a]} \tag{10-86}$$

which is dual to (10-81). In the high-Q case, the Q's from (10-81) and (10-86) will be the same, but they may differ in the low-Q case. A formula dual to (10-84) also applies for the gain-bandwidth product in terms of admittance parameters.

Computations of the Q of practical antennas are not available in the literature. An upper bound to the Q of antennas can be obtained by expanding the field external to the antenna in terms of spherical modes, and curves of these

results are available [11]. A different definition of Q was made by Lo et al. [8], and computations were performed for some particular cases. This reference [8] also considers the formulation of signal-to-noise ratio optimization, both with and without a constraint on the Q.

10-6. Experimental Gain Optimization

The parameters used in the optimization of antenna gain (Section 10-3) are terminal impedances and admittances, and hence, in principle, can be measured by circuit techniques. Procedures can be devised to systematically perform the required measurements. Possible procedures for transmitting arrays, receiving arrays, and reciprocal arrays are given in this section.

ANTENNA TRANSMITTING. For the impedance formulation, the array is excited with known input currents, and open-circuit voltages are measured at all ports. To be specific, we excite each port in turn with a known source I_0, obtaining a set of array excitations

$$[I_1] = \begin{bmatrix} I_0 \\ 0 \\ 0 \\ \vdots \\ 0 \end{bmatrix} \quad [I_2] = \begin{bmatrix} 0 \\ I_0 \\ 0 \\ \vdots \\ 0 \end{bmatrix} \quad \cdots \quad [I_N] = \begin{bmatrix} 0 \\ 0 \\ 0 \\ \vdots \\ I_0 \end{bmatrix} \tag{10-87}$$

For each $[I_i]$, we measure the open-circuit voltages at all array ports, obtaining the set of voltage matrices

$$[V_1] = \begin{bmatrix} V_{11} \\ V_{12} \\ \vdots \\ V_{1N} \end{bmatrix} \quad [V_2] = \begin{bmatrix} V_{21} \\ V_{22} \\ \vdots \\ V_{2N} \end{bmatrix} \quad \cdots \quad [V_N] = \begin{bmatrix} V_{N1} \\ V_{N2} \\ \vdots \\ V_{NN} \end{bmatrix} \tag{10-88}$$

where V_{ij} denotes the voltage at port j due to I_0 at port i. Now, applying the relationship $[V_a] = [Z_{aa}][I_a]$ to each $[V_i]$ and $[I_i]$, we have

$$\begin{aligned} [Z_{1a}] &= \frac{1}{I_0}[\tilde{V}_1] \\ [Z_{2a}] &= \frac{1}{I_0}[\tilde{V}_2] \\ &\cdots\cdots\cdots \\ [Z_{Na}] &= \frac{1}{I_0}[\tilde{V}_N] \end{aligned} \tag{10-89}$$

where $[Z_{ia}]$ is the ith row of $[Z_{aa}]$. From these measurements we can construct the matrix $[Z_{aa} + \bar{Z}_{aa}^*]$, which in the case of reciprocal media is twice the real part of $[Z_{aa}]$.

We now apply a reference current I_1 to one element of the array, say port 1, and excite each other port in turn such that no field is received by the test antenna. This gives a set

$$[\hat{I}_1] = \begin{bmatrix} I_1 \\ I_2 \\ 0 \\ \vdots \\ 0 \end{bmatrix} \quad [\hat{I}_2] = \begin{bmatrix} I_1 \\ 0 \\ I_3 \\ \vdots \\ 0 \end{bmatrix} \quad \cdots \quad [\hat{I}_{N-1}] = \begin{bmatrix} I_1 \\ 0 \\ 0 \\ \vdots \\ I_N \end{bmatrix} \tag{10-90}$$

which is equivalent to (10-43). The excitation which gives maximum gain must be the only $[I_a]$ linearly independent of the $[\hat{I}_i]$ and orthogonal to them according to the weighted product (10-41). The excitation for maximum gain $[\hat{I}_N]$ can, therefore, be obtained by the Schmidt process [1,2], or by solving the set of simultaneous equations (10-42).

An alternative method of determining the excitation for maximum gain is to measure $[Z_{ta}]$ and use (10-45). The ith element of $[Z_{ta}]$ is the open-circuit voltage at the test antenna when the ith array port is excited by a unit current, all other ports being open-circuited. This method is discussed further in the subsection on reciprocal arrays.

In terms of voltage excitation, the dual procedure is used. We excite the elements in turn with a voltage V_0 and measure the short-circuit currents at all ports. From this we can construct $[Y_{aa}]$. The ports are then excited in pairs such that no field is received by the test antenna. The voltage excitation for maximum gain can then be obtained by requiring it to be orthogonal to all excitations giving zero received field. Alternatively, we could measure the $[Y_{ta}]$ and use (10-48).

ANTENNA RECEIVING. For the receiving case, the test antenna is excited and the array terminal currents adjusted according to (10-73). The $[Z_{aa}]$ can, of course, be determined by the same set of measurements as in the transmitting case. However, since procedures which do not involve excitation of the array are of interest, we shall give an alternative procedure.

Consider the test antenna excited by a current I_t. The open-circuit voltages measured at the array ports are then the elements of the matrix

$$[V_a^0] = [Z_{at}]I_t \tag{10-91}$$

which determines $[Z_{at}]$. We now short-circuit one array port, say the ith port, and measure the short-circuit current I_i^s. Let $[V_i^s]$ denote the corresponding matrix of voltages at all array ports. By superposition, the voltage matrix

$[V_i^s - V_a^0]$ is precisely that which would be produced by a current source I_i^s at port i. This procedure can be repeated for each port, giving a set of excitations equivalent to (10-87), except that I_0 is replaced by I_i^s. Then, equivalent to (10-89), we have

$$\begin{aligned}
[\mathbf{Z}_{1a}] &= \frac{1}{I_1^s}[V_1^s - V_a^0] \\
[Z_{2a}] &= \frac{1}{I_2^s}[V_2^s - V_a^0] \\
&\cdots\cdots\cdots \\
[\mathbf{Z}_{Na}] &= \frac{1}{I_N^s}[V_N^s - V_a^0]
\end{aligned} \tag{10-92}$$

which determines $[Z_{aa}]$. The receiving current distribution for maximum absorption area is then found by substitution from (10-91) and (10-92) in (10-73).

For the determination of port voltages, the forementioned procedure applies in a dual sense. In this case we excite the test antenna with a voltage V_t, short-circuit all array ports, and measure the port currents. We then open-circuit one port at a time, measure its open-circuit voltage and the corresponding short-circuit currents at all other ports, and determine $[Y_{aa}]$ dual to (10-92). The port voltages for maximum absorption area are then calculated from (10-74).

If we wish to design a network to deliver the received power to a single load, we can use Bloch's procedure [9], modified as follows. Instead of using the field at each element, we must use the open-circuit voltage obtained at each element when the array is excited by the plane-wave field. With this correction, Bloch's derivation of a network for maximum absorption area becomes applicable to actual arrays.

RECIPROCAL ARRAYS. When the array and surrounding space contain only reciprocal media, the impedance and admittance matrices are symmetrical, and

$$[Z_{aa} + \tilde{Z}_{aa}^*] = 2[\text{Re } Z_{aa}] \tag{10-93}$$

This can be used to simplify measurement of Z_{aa} to some extent. Also, because of reciprocity,

$$[\mathbf{Z}_{at}] = [\tilde{Z}_{ta}] = \frac{1}{I_t}[V_a^0] \tag{10-94}$$

where $[V_a^0]$ is the matrix of open-circuit array voltages defined by (10-91). Letting $2C = I_t$, we have from (10-45) and (10-93),

$$[I_a] = [\text{Re } Z_{aa}]^{-1}[V_a^{0*}] \tag{10-95}$$

Experimentally $[V_a^0]$ is determined by open-circuiting all array ports, illuminating the array by a plane wave from the test antenna, and measuring the port voltages. For the case of point sources in empty space (10-95) corresponds to Bloch's traveling-wave theorem [6].

For maximum absorption area on receiving, we have from (10-73), (10-93), and (10-94),

$$[I_a] = -\tfrac{1}{2}[\text{Re } Z_{aa}]^{-1}[V_a^0] \tag{10-96}$$

Comparing this with (10-95), we see that the terminal currents for maximum A are proportional to the conjugate of the terminal currents for maximum G. This result can also be obtained from the reciprocity theorem applied to the array and test antenna network.

For the admittance formulation, the voltage excitation for maximum gain of a reciprocal transmitting antenna is

$$[V_a] = [\text{Re } Y_{aa}]^{-1}[I_a^{0*}] \tag{10-97}$$

which is dual to (10-95). Experimentally, the $[I_a^0]$ is found by short-circuiting all array ports, illuminating the array by a plane wave from the test antenna, and measuring the port currents. For a reciprocal receiving antenna, the maximum absorption area is obtained when

$$[V_a] = -\tfrac{1}{2}[\text{Re } Y_{aa}]^{-1}[I_a^0] \tag{10-98}$$

which is dual to (10-96). Hence the terminal voltages for maximum gain are proportional to the conjugate of those for maximum absorption area.

The crudest approximation used in array design is to neglect all mutual effects among array elements. In terms of (10-95), this is equivalent to assuming that $[Z_{aa}]$ is a diagonal matrix with elements equal to the input impedances of isolated antenna elements, and that $[V_a^0]$ is the matrix of voltages received by isolated elements. To this approximation (10-95) states that each element should be phased so that it contributes in phase to the main beam and is weighted in amplitude in proportion to its voltage pattern divided by its input resistance. For purposes of discussion, we shall call this *normal excitation* of an array. In the case of identical elements (identical input resistances and patterns), normal excitation is the usual uniform cophasal excitation.

A better approximation for maximizing gain can be obtained by simply neglecting all off-diagonal terms of $[\text{Re } Z_{aa}]$ in (10-95). This is equivalent to measuring the input impedance to each element, and the voltage received by each element, with all other elements present, but with their terminals open-circuited. It is interesting to note that the approximate current excitation obtained from (10-95) is not necessarily equal to the corresponding voltage approximation obtainable from (10-95). Note also that one no longer has an array of

identical elements even if the geometries of all elements are the same, because each element is in a different environment formed by the other elements.

Increasing the gain of an array over that obtained by normal excitation evidently depends upon the mutual effects among elements. If the off-diagonal terms of [Re Z_{aa}] are small compared to the diagonal terms, we can expect only small improvements in the gain over normal gain. Such is usually the case when elements are widely spaced, say more than a half wavelength between elements. If the off-diagonal elements of [Re Z_{aa}] are comparable in magnitude to the diagonal elements, considerable supergain effects can be obtained. Physically, this usually implies closely spaced elements. Hence, to design a supergain antenna, we consider (or construct) an array of closely spaced elements and calculate (or measure) its terminal impedance or admittance matrices. The excitation for maximum gain and the approximate Q of the antenna can then be determined from the formulas of this chapter. The resultant array will probably be a supergain array exhibiting the usual high Q and requiring precision excitation.

It is of interest to have some idea of how much supergaining is practicable to attempt. From previous studies on loss-free antennas [11], it has been found that, for large antennas, optimization techniques can give very little improvement over normal excitation. For arrays about two wavelengths in total length, it appears that the gain might be doubled by supergain techniques. For smaller arrays, even more improvement appears possible. Hence, although such techniques do not appear attractive for large arrays, they do become useful for small ones.

The procedures of this section are applicable to any antenna which has several input terminals; discrete elements do not have to be identifiable. For example, an aperture antenna fed in several places, or by several modes in a waveguide, can be optimized by these techniques. All measurements (or calculations) must, of course, be made with the ports open-circuited for the impedance formulation, or short-circuited for the admittance formulation. It might also be possible to use similar techniques to investigate changes in the structure of an antenna, by viewing the addition of a conductor as short-circuiting a port, or the removal of a conductor as open-circuiting a port.

References

[1] B. Friedman, *Principles and Techniques of Applied Mathematics*, John Wiley & Sons, Inc., New York, 1956.

[2] J. W. Dettman, *Mathematical Methods in Physics and Engineering*, McGraw-Hill Book Co., New York, 1962.

[3] F. R. Gantmacher, *The Theory of Matrices*, Vol. 1, translated by K. A. Hirsch, Chelsea Publ. Co., New York, 1959.

[4] R. F. Harrington, "Antenna Excitation for Maximum Gain," *IEEE Trans.*, Vol. **AP-13**, No. 6, Nov. 1965, pp. 896–903.